Review

Physics case for quarkonium studies at the Electron Ion Collider

Daniël Boer [1],[a], Chris A. Flett [2],[a], Carlo Flore [2,3,4],[a], Daniel Kikoła [5],[a], Jean-Philippe Lansberg [2],[*],[a], Maxim Nefedov [2],[a], Charlotte Van Hulse [2,6],[a], Shohini Bhattacharya [7], Jelle Bor [1,2], Mathias Butenschoen [8], Federico Ceccopieri [2,9], Longjie Chen [10,11], Vincent Cheung [12], Umberto D'Alesio [4], Miguel Echevarria [13], Yoshitaka Hatta [7,14], Charles E. Hyde [15], Raj Kishore [13,16], Leszek Kosarzewski [17], Cédric Lorcé [18], Wenliang Li [16,19], Xuan Li [20], Luca Maxia [1,4], Andreas Metz [21], Asmita Mukherjee [22], Carlos Muñoz Camacho [2], Francesco Murgia [4], Pawel Nadel-Turonski [19,23], Cristian Pisano [4], Jian-Wei Qiu [24], Sangem Rajesh [25], Matteo Rinaldi [26], Jennifer Rittenhouse West [27,28], Vladimir Saleev [29], Nathaly Santiesteban [30], Chalis Setyadi [1,31], Pieter Taels [32], Zhoudunmin Tu [7], Ivan Vitev [20], Ramona Vogt [12,33], Kazuhiro Watanabe [34,35], Xiaojun Yao [36,37], Yelyzaveta Yedelkina [2,38], Shinsuke Yoshida [10,11]

[1] Van Swinderen Institute for Particle Physics and Gravity, University of Groningen, 9747 AG Groningen, The Netherlands
[2] Université Paris-Saclay, CNRS, IJCLab, 91405 Orsay, France
[3] Dipartimento di Fisica, Università di Torino, and INFN Sezione di Torino, Via P. Giuria 1, I-10125 Torino, Italy
[4] Dipartimento di Fisica, Università di Cagliari, and INFN Sezione di Cagliari, Cittadella Univ., I-09042 Monserrato (CA), Italy
[5] Faculty of Physics, Warsaw University of Technology, plac Politechniki 1, 00-661, Warszawa, Poland
[6] University of Alcalá, Alcalá de Henares (Madrid), Spain
[7] Physics Department, Brookhaven National Laboratory, Bldg. 510A, Upton, NY 11973, USA
[8] II. Institut für Theoretische Physik, Universität Hamburg, Luruper Chaussee 149, 22761 Hamburg, Germany
[9] Université de Liège, B4000, Liège, Belgium
[10] Key Laboratory of Atomic and Subatomic Structure and Quantum Control (MOE), Guangdong Basic Research Center of Excellence for Structure and Fundamental Interactions of Matter, Institute of Quantum Matter, South China Normal University, Guangzhou 510006, China
[11] Guangdong-Hong Kong Joint Laboratory of Quantum Matter, Guangdong Provincial Key Laboratory of Nuclear Science, Southern Nuclear Science Computing Center, South China Normal University, Guangzhou 510006, China
[12] Nuclear and Chemical Sciences Division, Lawrence Livermore National Laboratory, Livermore, CA 94551, USA
[13] Department of Physics & EHU Quantum Center, University of the Basque Country UPV/EHU, Apartado 644, 48080 Bilbao, Spain
[14] RIKEN BNL Research Center, Brookhaven National Laboratory, Upton, NY 11973, USA
[15] Department of Physics, Old Dominion University, Norfolk, VA 23529, USA
[16] Center for Frontiers in Nuclear Science, Stony Brook University, Stony Brook, NY 11794, USA
[17] Faculty of Nuclear Sciences and Physical Engineering, Czech Technical University in Prague, Břehová 78/7, 115 19 Staré Město, Prague, Czech Republic
[18] CPHT, CNRS, Ecole polytechnique, Institut Polytechnique de Paris, 91120 Palaiseau, France
[19] Stony Brook University, Stony Brook, NY 11794, USA
[20] Los Alamos National Laboratory, Los Alamos, NM 87545, USA
[21] Department of Physics, Temple University, Philadelphia, PA 19122, USA
[22] Department of Physics, Indian Institute of Technology Bombay, Powai, Mumbai 400076, India
[23] University of South Carolina, Columbia, SC 29208, USA
[24] Theory Center, Jefferson Laboratory, Newport News, VA 23606, USA

---

* Corresponding author.
  E-mail address: Jean-Philippe.Lansberg@in2p3.fr (J.-P. Lansberg).
[a] Editors: D. Boer, C.A. Flett, C. Flore, D. Kikoła, J.P. Lansberg, M. Nefedov and C. Van Hulse.

[25] *Vellore Institute of Technology, Vellore, Tamil Nadu 632014, India*

[26] *Dipartimento di Fisica. Università degli studi di Perugia, and INFN Sezione di Perugia. Via A. Pascoli, Perugia, 06123, Italy*

[27] *Lawrence Berkeley National Laboratory, Berkeley, CA 94720, USA*

[28] *University of California at Berkeley, Berkeley, CA 94709, USA*

[29] *Joint Institute for Nuclear Research, Dubna, Russia*

[30] *University of New Hampshire, Durham, NH 03824, USA*

[31] *Department of Physics, Universitas Gadjah Mada, BLS 21 Yogyakarta, Indonesia*

[32] *Department of Physics, University of Antwerp, Groenenborgerlaan 171, 2020 Antwerpen, Belgium*

[33] *Department of Physics and Astronomy, University of California at Davis, Davis, CA 95616, USA*

[34] *SUBATECH UMR 6457 (IMT Atlantique, Université de Nantes, IN2P3/CNRS), 4 rue Alfred Kastler, 44307 Nantes, France*

[35] *Faculty of Science and Technology, Seikei University, Musashino, Tokyo 180-8633, Japan*

[36] *Center for Theoretical Physics, Massachusetts Institute of Technology, Cambridge, MA 02139, USA*

[37] *InQubator for Quantum Simulation, Department of Physics, University of Washington, Seattle, WA 98195, USA*

[38] *School of Physics, University College Dublin, Dublin 4, Ireland*

ARTICLE INFO

ABSTRACT

The physics case for quarkonium-production studies accessible at the US Electron Ion Collider is described.

Contents

1. Introduction

The Electron-Ion Collider (EIC) accelerator and detector systems are currently designed following the elaboration of an outstanding physics case aimed at further exploring the nucleon and nucleus partonic structure. The interested reader will find it useful to consult reviews of the EIC [1,2].

Bound states of heavy quark–antiquark pairs, $Q\bar{Q}$, *i.e.* quarkonia, allow for a detailed study of basic properties of quantum chromodynamics (QCD), the theory of the strong interaction. Indeed, charmonia and bottomonia have played a crucial role in the establishment of QCD as the theory of the strong interaction, given the clean signature they provide in different observables. On the theory side, the main origin of the simplifications is the hierarchy $m_Q \gg \Lambda_{\mathrm{QCD}}$, with m_Q the mass of a heavy quark, meaning that for processes occurring at this scale (or higher), a perturbative expansion in α_s of QCD is allowed. In parallel, the non-perturbative effects associated with the formation of the bound state can be factorised.

Heavy quarkonia are multiscale systems. Besides m_Q and Λ_{QCD}, one needs to consider, in addition, the scale of the typical momentum transfer between heavy constituent quarks ($m_Q v$), v being the velocity of the heavy quarks in the rest frame of the bound state, and the scale of their binding energy ($m_Q v^2$), all of which become widely separated in the limit $m_Q \to \infty$. At this point, the non-relativistic nature of the system comes into play, allowing for the development of different effective theories of QCD that attempt to more adequately describe the production of the bound state in the presence of different relevant scales as well as models such as the Colour-Singlet (CS) Model [3–6] or Colour-Evaporation Model (CEM) [7,8].

The multitude of existing theoretical approaches to describe quarkonium production reflects the fact that unfortunately, up to now, there is no universal physics picture of this process accepted by the community that would provide a satisfactory description of all available experimental data [9]. This complicates the use of quarkonia as tools for precision studies. Heavy quarkonia nevertheless remain useful to uncover new facets of the structure of nucleons and nuclei which we review in this document.

In this context, measurements of various quarkonium-production observables in electron–proton (ep) and electron–nucleus (eA) collisions at the EIC could provide crucial experimental clues to finally settle the quarkonium-production-mechanism debate.

Important targets for the EIC experimental programme are vector-quarkonium-polarisation observables and cross-section measurements of $C = +1$ states, like the η_c and $\chi_{c,b}$. These play a central role in the current debate about the heavy-quarkonium-production mechanism and yet corresponding precise data from ep collisions at HERA are simply lacking. Such measurements would hopefully clear up the quarkonium-production debate and allow one to fully employ quarkonium data at the EIC as tools.

Before discussing how quarkonia can be used as tools to study nucleons, let us recall that the multi-dimensional structure of nucleons is parametrised by different hadronic functions, which encode the dynamics of partons at different levels of complexity. These span from the one-dimensional (1D) parton distribution functions (PDFs), to the five-dimensional (5D) Wigner distributions –or generalised transverse-momentum-dependent distributions (GTMDs)–, to mention a few. These also incorporate a variety of spin and momentum correlations between the parton (or partons) participating in the hard subprocess and its (their) parent hadron. Depending on the considered scattering process and the measured kinematics, different hadronic functions enter the relevant cross sections. Among them, let us cite the transverse-momentum-dependent PDFs (TMD PDFs or TMDs), arising from TMD factorisation [10] and which provide information on the distribution of partons inside the nucleon as a function of both their longitudinal and transverse momentum. In the case of quarkonium production at transverse momenta, P_T, small compared to their mass and for specific other kinematical end-point regions, new TMD functions related to the produced quarkonium and referred to as shape functions, are expected to enter the cross-section formula besides the TMD PDFs of the initial-state hadron(s). This reflects the interplay between radiation of soft gluons and effects of the formation of the $Q\bar{Q}$ bound state. Their impact on the phenomenology remains at present unknown.

Much progress has been made in the determination of the above-mentioned PDFs, achieving different levels of success. Currently, the gluon distributions in general remain much less explored than their quark analogues. In this context, quarkonia arise as a

powerful handle to remedy this situation since, in the vast majority of situations, the $Q\bar{Q}$ pair at the origin of the quarkonium comes from photon–gluon (gluon–gluon) fusion in ep (resp. pp) collisions, whereas deep inelastic scattering (DIS) or Drell–Yan-pair production are sensitive to the gluon distribution only through radiative QCD corrections.

However, it has been shown [11,12] that factorisation of observables –cross sections, angular modulations, spin asymmetries,…– in terms of TMD PDFs is less universal than that in terms of standard (*collinear*) PDFs and that consequently such a factorisation could be violated in back-to-back-hadron production in proton–proton (pp) collisions. In ep and eA collisions, there is no anticipated violation of TMD factorisation, at least for inclusive single-hadron production, so quarkonium measurements will likely be easier to interpret in terms of gluon TMDs at the EIC rather than at hadron colliders.

Quarkonia are also key players in exclusive reactions. This is not surprising as exclusive meson production involving a hard scale is one of the main processes to access Generalised Parton Distributions (GPDs). Gluon GPDs are in particular accessible via exclusive heavy-quarkonium production [13,14]. These GPDs provide information on the distribution of gluons inside the nucleon simultaneously as a function of their longitudinal momentum and their transverse position. They also provide information on the angular momentum of the gluons inside the nucleon, about which very little is known to date. Furthermore, exclusive heavy-quarkonium production near the production threshold was suggested [15,16] as a tool for constraining the gluon condensate in the nucleon, itself linked to the nucleon mass, albeit with some unavoidable model dependence.

At small momentum fraction, x, the differential exclusive electro- and photoproduction cross sections of quarkonia can be expressed in terms of particular products of integrals of GTMDs. In single-quarkonium production, when a collinear expansion is applied, the cross section reduces to expressions in terms of GPDs, see for example [17,18].[1] However, in general, especially beyond single-particle production, it provides additional information on GTMDs and offers an opportunity to learn more about the combined three-momentum and spatial distributions of gluons inside a nucleon. Moreover, while there is a direct relation between exclusive photoproduction case in ep collisions and in ultra-peripheral pp and pPb collisions (UPCs), studies at the EIC would allow one to probe in more details the transverse-momentum dependence of the GTMDs.

To date, the detector simulations for the EIC physics case connected to quarkonium physics have been limited to J/ψ and Υ exclusive production as reported in the EIC Yellow report [2]. Whereas, as we discussed above, quarkonium production is still the object of intense debates within the community,[2] there is no doubt that it can play a crucial role in the scientific success of the EIC. As was recently done for the High Luminosity LHC phase [33], we gather in this review what we believe to be the most complete list of quarkonium studies that can be carried out at the EIC along with their motivation.

The document is organised as follows. In Section 2, the EIC accelerator system and the first EIC detector, ePIC, as currently envisioned are presented. Following a description of the kinematics of lepton–hadron collisions, the theoretical treatment of QED radiation and its significance will be discussed, concluding with a note on the impact of feed-down from b-quark production on charmonium studies. In Section 3, the different theoretical descriptions and measurements related to the production mechanism of quarkonia are presented. First, the various existing theoretical formalisms in collinear factorisation are discussed. Then, the legacy of existing measurements and the potential of future measurements at the EIC in constraining these formalisms are presented. It is subsequently demonstrated that TMD observables provide valuable insights into quarkonium formation and polarisation, with specific predictions presented for the EIC. Finally, the effect of final-state interactions on the production of quarkonium in lepton–nucleus collisions is touched upon. Section 4 focuses on the studies accessible in electron–proton collisions in order to advance our knowledge of the nucleon partonic structure. It then moves on to studies with nuclear beams, a unique feature of the EIC, which promises to drive a significant advancement into a new era of precision in exploring the partonic structure of nuclei. We underscore throughout this comprehensive review the diverse ways in which the EIC will utilise quarkonia to probe hadronic and nuclear physics and, conversely, will itself be a powerful tool for probing quarkonia.

2. Generalities about quarkonium studies at the EIC

2.1. The proposed EIC accelerator system

The EIC is an upcoming particle accelerator that will deliver intense beams of longitudinally polarised electrons and polarised light nuclei (p, d, ^{3}He) as well as unpolarised heavier ions, ranging up to uranium. It will produce electron-ion collisions at the highest energy and at the highest rate ever achieved.

The EIC will be constructed in Brookhaven National Laboratory using a few key elements of the currently operating Relativistic Heavy Ion Collider (RHIC) [34,35], such as the hadron ring and the RHIC Electron-Beam-Ion-Source (EBIS) [36]. The collider will be supplemented with a new electron ring (see Fig. 2.1), which will contain continuously injected, polarised electrons with an energy

---

[1] Strictly speaking, hard exclusive reactions admit a factorisation in terms of GPDs at small four-momentum transfer between the ingoing and outgoing hadrons, t (forward production). At small u (backward production), factorisation in terms of transition distribution amplitudes (TDAs) has been advocated [19,20]. As an example, hard exclusive reactions in the backward region for baryonic and mesonic exchanges in the u channel can be factorised in terms of TDAs. Phenomenological applications include backward pion electroproduction [21] observed by the CLAS collaboration at JLab [22], and more recently backward J/ψ photoproduction [23] extrapolating J/ψ photoproduction cross section over the full near-threshold kinematics measured by the GlueX collaboration at JLab [24].

[2] We guide interested readers to the following reviews [25–29] which address HERA and Tevatron results, to more recent ones [9,30] addressing progress made thanks to the RHIC and LHC data and to the HEPData database (https://www.hepdata.net/), a dedicated repository of quarkonium measurements up to 2012 (http://hepdata.cedar.ac.uk/review/quarkonii/ to [31] and to [32] for experimental quarkonium data.
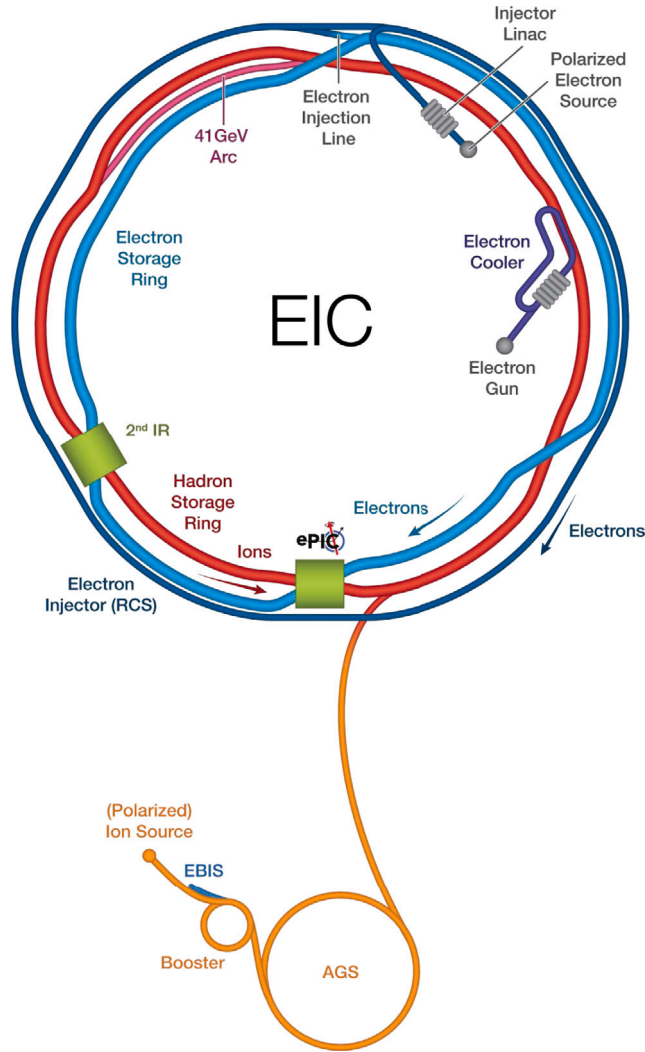
Fig. 2.1. A schematic drawing of the planned EIC [37].

from 5 GeV up to 18 GeV. The coverage in centre-of-mass energy will range from 28 GeV to 141 GeV for lepton–proton collisions, while for lepton–ion collisions an upper energy of 89 GeV/nucleon will be reached. The expected instantaneous luminosity depends on the centre-of-mass energy and will range from 10^{33} to 10^{34} cm^{-2}s^{-1} for electron–proton collisions, with a maximum value expected for $\sqrt{s_{ep}} = 105$ GeV. For electron-ion reactions, it will be on the order of 10^{34} cm^{-2}s^{-1}. Such figures will correspond to integrated luminosities of the order of 10 to 100 fb^{-1} per year. The designed average polarisation of electron, proton and ^{3}He beams is of the order of 70%.

At present, the installation of a first EIC detector is foreseen at interaction point 6 (IP6). A second interaction point (IP8) can, at any stage, host a second and complementary detector. The second interaction point could accommodate a design with a secondary focus, which in combination with forward spectrometry would allow for an extension of the acceptance towards the detection of particles at very small polar angles. The interaction points will re-use the existing large detector halls, currently occupied by the STAR and sPHENIX experiments. The first collisions at the EIC are expected in the early 2030s.

2.2. The proposed EIC detector

2.2.1. Requirements for an EIC detector in the context of quarkonium studies

The specification of an EIC detector is determined by the kinematics of the electron-ion scattering (see Fig. 2.2) and the observables and processes of interest. It should address the full range of physics outlined in the EIC White Paper [1], the NAS report [38] and the EIC Yellow Report [2]. The basic requirements include [2,39] 4π hermeticity with large acceptance in pseudorapidity, η, of about $-4 < \eta < 4$, very good momentum resolution both in the central, forward and backward regions, very
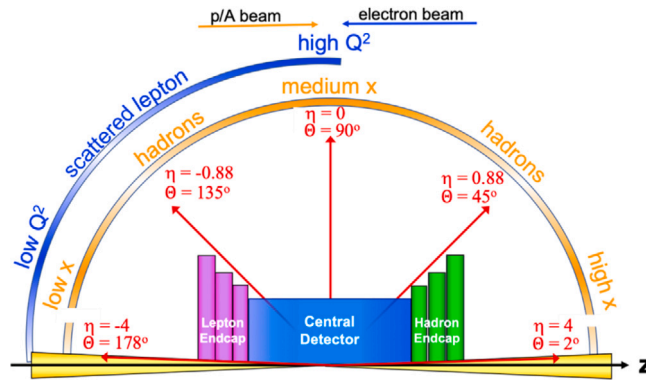
Fig. 2.2. A schematic of the expected lepton and hadron kinematic distributions in EIC reactions and related detector requirements. *Source:* Figure taken from [39].

good energy resolution in electromagnetic calorimeters and particle identification capabilities up to 50 GeV in momentum. Such a setup allows one to study processes over a wider range of four-momentum transfer Q. In addition, measurements of heavy-flavour hadron production demand a microvertexing detector that provides good impact-parameter resolution.

The detector technologies and configuration implementation will be known once the detector design is finalised. However, existing high-energy experiments (for example ALICE at the LHC and STAR at RHIC) indicate that an EIC detector that fulfils the aforementioned requirements will have capabilities for J/ψ and $Y(nS)$ measurements via their e^+e^- decay channel [40–45]. The precision of quarkonium reconstruction will strongly depend on the hardware configuration. For example, an internal silicon tracker could generate additional combinatorial background arising from conversions $\gamma \rightarrow e^+e^-$, limiting precision for low-mass quarkonia at low P_T. Moreover, the energy loss of electrons due to Bremsstrahlung in the detector material deteriorates the mass resolution. It may complicate, if not make impossible, separation of the $Y(1S)$, $Y(2S)$ and $Y(3S)$ states. Measurements of other quarkonium states (for instance χ_c or χ_b) add constraints for the experimental apparatus. Studies of decays involving photon radiation (e.g., $\chi_c(1P) \rightarrow J/\psi + \gamma$) would require an electromagnetic calorimeter able to isolate a soft photon and measure its energy with appropriate resolution. In addition, a muon detector would significantly extend capabilities for quarkonium studies. This is briefly discussed in Section 2.2.3.

Three different designs, ATHENA [46], CORE [47] and ECCE [48], were proposed. The main difference between the ATHENA and ECCE design consists of the magnet, providing respectively a 3.0 T and 1.4 T magnetic field. The distinguishing characteristic of the CORE detector is the compactness of the detector, obtained through exploitation of technological advances. From the proposed designs, the ECCE proposal was selected as baseline for the first EIC detector, with improvements to the proposal at present under development. This first EIC detector received the name electron–proton/ion collider (ePIC) detector. A description of the ePIC detector in its current design state is given below.

2.2.2. The ePIC detector

The central barrel of the ePIC detector, as currently envisioned, is depicted in Fig 2.3. Here, the hadron beam comes in from the left and defines the forward-going direction. The central barrel is around 10 m long and 5 m in diameter, providing a full coverage in azimuthal angle and a coverage in polar angle between 0° and 178°, corresponding to a pseudorapidity coverage between −4 and 4. In addition to the barrel detector, detectors in the far-forward and far-backward regions are foreseen. The far-backward region will contain a luminosity monitor and two detectors to tag low-Q^2 events. The far-forward region will contain a series of detectors aimed at detecting particles produced close to the beam line and as such will be instrumental to the reconstruction of an extensive set of diffractive processes and tagged measurements, such as proton reconstruction in exclusive processes, tagging of the two spectator protons when investigating the neutron structure through lepton-^{3}He interactions and tagging of respectively the neutron and Λ-baryon decay particles when probing the pion and kaon structure in lepton–proton interactions. The far-forward system will consist of a B0 spectrometer, containing an electromagnetic calorimeter and trackers for respectively the tagging of photons and reconstruction of charged particles, Roman Pots and off-momentum detectors, performing charged-particle reconstruction, as well as Zero-Degree Calorimeters, capable of detecting photons and neutrons.

In the central barrel, track and vertex reconstruction will be performed by silicon monolithic active pixel sensors placed close to the beam line and interaction point, while at a further distance micro-pattern gaseous detectors (micro-Resistive Well and Micro-Mesh Gaseous Structure) and AC-coupled low-gain avalanche diodes will contribute to track reconstruction. The tracking detectors will be embedded into a 1.7 T magnetic field. Such a setup will provide the momentum resolution needed to fulfil the EIC physics programme.

Electromagnetic calorimeters cover the backward, central and forward regions of the central barrel, providing electron and photon detection as well as hadron suppression. In the backward region, a high-precision lead-tungstate calorimeter read out by silicon photo-multipliers is foreseen. The detector will be critical to the reconstruction of (scattered) electrons, improving the reconstruction precision over that obtained from tracking detectors only, and in the identification of these electrons, by
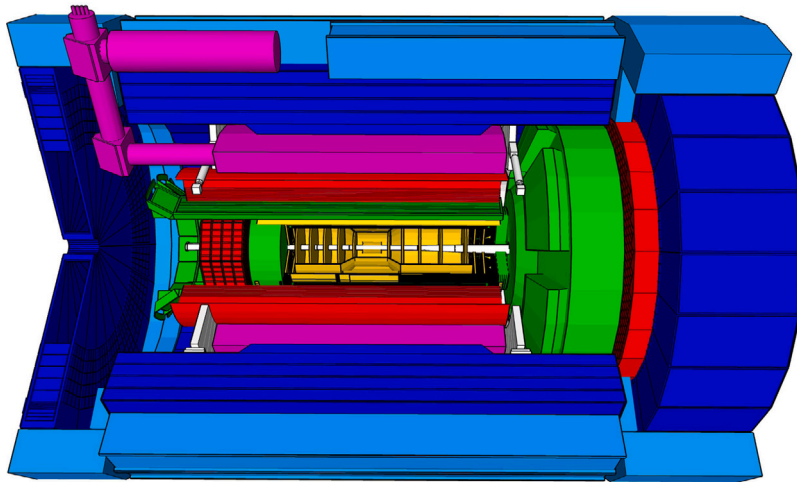
Fig. 2.3. Drawing of the ePIC detector as envisioned at present [37]. The hadron beam comes in from the left and defines the forward direction, while the lepton beam comes in from the right. The 1.7 *T* magnet is indicated in magenta; the tracking detectors are shown in yellow; the electromagnetic and hadronic calorimeters are represented, respectively, in red and darker blue, and the particle-identification Cherenkov detectors are drawn in green.

suppressing the background contribution strongly. This contribution originates mostly from charged pions. In the central region, a lead-scintillator imaging calorimeter is foreseen. For the forward region, an electromagnetic calorimeter will be integrated with the forward hadronic calorimeter. The system focuses on the containment of high-energetic particle showers while at the same time providing a good energy resolution for lower-energetic particles. Particle identification requires a good position resolution, in particular in the electromagnetic calorimeter. This will be provided by constructing the electromagnetic calorimeter out of segments, of scintillating fibres embedded in tungsten powder, smaller than the Molière radius. This will also result in a good shower separation at high pseudorapidity.

In the central region, a hadronic calorimeter will allow for the detection of neutral hadrons and as such will improve the resolution of jet reconstruction. Given the good momentum resolution of the central trackers, the central hadronic calorimeter system will not have an impact on the reconstruction of charged particles. The forward hadronic calorimeter, which forms an integrated system with the electromagnetic calorimeter, will consist of layers of alternating tiles of scintillating material and steel, while towards the end of the detector the steel is replaced by tungsten in order to serve as tail catcher of the shower and thus maximise the interaction length within the available space. Also in the backward region, a hadronic calorimeter will be installed, with the aim to serve as tail catcher of particle signals.

Detectors based on the detection of Cherenkov light will be used for the identification of charged pions, kaons and protons, while also contributing to electron identification. In addition, the aforementioned AC-coupled low-gain avalanche diodes will provide particle identification in the low-momentum region, below ~ 2 GeV, based on the detection of the time of flight of a particle. In the backward region, a proximity-focusing ring-imaging Cherenkov (RICH) detector with aerogel as radiator will be used. Because of the tight space constraints, a DIRC – detection of internally reflected Cherenkov light – detector will be incorporated in the central region. The forward region will contain a dual RICH detector, with an aerogel radiator for the low-momentum particles and C_2F_6 for the high-energetic ones, covering the momentum range up to 50 GeV.

No muon detectors are foreseen for the ePIC detector. While first studies, performed for the ATHENA and ECCE proposals, indicate that the reconstruction of J/ψ mesons from exclusive processes through their e^+e^- decay should be possible with the ePIC detector, there are neither studies for other quarkonium states nor for inclusive or semi-inclusive processes. Here, dedicated muon detectors might be needed. This is discussed in the following sub-section.

2.2.3. A case for a muon detector for quarkonium studies at the EIC

Measurement of vector-quarkonium production using their di-muon decay provides significant benefits. The energy loss of muons due to interactions with detector material is much smaller than that of electrons. This leads typically to a better momentum resolution of the muons than of the electrons, and therefore the resolution of the quarkonium mass reconstructed in the $\mu^+\mu^-$ channel is better compared to the e^+e^- one. The LHCb and CMS experiments provide a case in point as the performance of their muon detectors facilitated a rich and fruitful quarkonium physics program, which included that of $\Upsilon(1S)$, $\Upsilon(2S)$, $\Upsilon(3S)$ and other quarkonium states such as the χ_c and χ_b via their radiative decays into vector quarkonia. Additional measurements via the $\mu^+\mu^-$ decay channel would also essentially double the available statistics as the branching ratios into $\mu^+\mu^-$ and e^+e^- are nearly the same and enable analyses of rare decays (for example, $\chi_c \rightarrow J/\psi\mu\mu$). With a proper design, studies via the di-muon channel benefit from a lower combinatorial background, thus improving the statistical precision of the measurement. In addition, they provide a cross check of the e^+e^- results, which should in turn reduce systematic uncertainties.
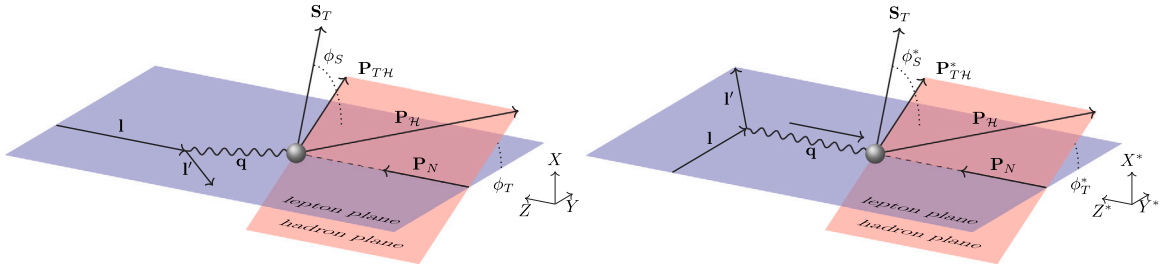
Fig. 2.4. Momenta and angles in two reference frames commonly used to describe the (SI)DIS process: *laboratory frame* (left) and *photon–hadron frame* (right).

In summary, a muon detector would significantly extend capabilities for quarkonium studies at the EIC. The present ePIC design does not consider muon-identification instrumentation, but possibilities for an enhanced muon identification can be investigated for ePIC. Moreover, the incorporation of dedicated muon-identification detectors in the design phase of the 2nd EIC detector can vastly extend quarkonium measurement capacities in the manner described above.

2.3. Kinematics and QED radiative corrections

2.3.1. Kinematics of electron–hadron reactions

In this section, we collect basic kinematical definitions useful for the description of lepton–hadron reactions. The next section is devoted to how QED radiative corrections on the lepton side can affect the resolution on various kinematic variables and to possible ways to address this problem.

Let us consider the inclusive production of an identified hadron $\mathcal{H}$, which in the context of this review is most likely to be a quarkonium, in electron-nucleon (eN) scattering:

$$e(\ell) + N(P_N) \rightarrow e(\ell') + \mathcal{H}(P_{\mathcal{H}}) + X. \tag{2.1}$$

For electron–nucleus (eA) scattering, the momentum P_N usually denotes the average momentum of a single nucleon. Depending on the experimental possibilities, one can tag the outgoing electron with the momentum ℓ' or consider the reaction inclusive w.r.t. the final-state electron. If the momentum ℓ' has been measured, one can define the momentum transfer $q = \ell - \ell'$ with $q^2 = -Q^2$ and the following Lorentz-invariant kinematic variables become experimentally accessible:

$$x_B = \frac{Q^2}{2 P_N \cdot q}, \qquad y = \frac{P_N \cdot q}{P_N \cdot \ell}, \qquad z = \frac{P_N \cdot P_{\mathcal{H}}}{P_N \cdot q}, \tag{2.2}$$

where z is referred to as the elasticity and y as the inelasticity that should not be confused with the rapidity.

Among frame-dependent variables, one usually distinguishes the transverse momentum of the hadron $\mathbf{P}_{T\mathcal{H}}$ in the *laboratory frame* (see Fig. 2.4 (left)), in which the initial electron $e(\ell)$ and nucleon $N(P_N)$ collide head on, defining the Z (collision) axis, from the transverse momentum $\mathbf{P}^*_{T\mathcal{H}}$ of the hadron $\mathcal{H}$ in the *photon–hadron frame* (see Fig. 2.4 (right)), where three-momenta $\mathbf{q}$ and $\mathbf{P}_N$ are aligned with the Z axis of this frame.[3] The word "photon" in the frame name specifically refers to the one-photon-exchange approximation between the electron and the hadronic part of the process. In this review, we will often use the simplified notation for the absolute value of the transverse momentum of the produced hadron: $P_T = |\mathbf{P}_{T\mathcal{H}}|$ or $P_T^* = |\mathbf{P}^*_{T\mathcal{H}}|$.

Even if the colliding particles are unpolarised, there could always be some dependence of the cross section on the azimuthal angle ϕ_T (or ϕ_T^*) formed by the vector $\mathbf{P}_{T\mathcal{H}}$ (or $\mathbf{P}^*_{T\mathcal{H}}$) and the plane spanned by the initial (ℓ) and final (ℓ') lepton three-momenta (Fig. 2.4), due to the exchanged-photon polarisation. If the initial nucleon and/or electron have transverse polarisation, *additional* angular modulations of the cross section, related to the direction(s) of the transverse spin vector(s) of the colliding particles, can be generated. The transverse polarisation vector of the initial nucleon is denoted as $\mathbf{S}_T$ and the angle of this vector with respect to the lepton plane in the photon–hadron (resp. laboratory) frame is generally indicated as ϕ_S^* (resp. ϕ_S).

If the recoil effects of the photons which can be emitted by the initial and final electrons during the scattering process (QED radiative corrections) are neglected, then the four-momentum of the exchanged photon is simply $q = \ell - \ell'$ as stated above. In such an approximation, the variables of Eq. (2.2) as well as the frame-dependent variables, such as $\mathbf{P}^*_{T\mathcal{H}}$, can be directly computed from the measured energy and momentum of the scattered electron. However, such a QED Born approximation might be insufficient for precision studies. Section 2.3.2 is devoted to this issue.

The regime of the process of Eq. (2.1), when the quasi-real-photon approximation can be applied to the exchanged photon, i.e. when Q is negligible compared to the hard scale (m_Q, P_T, P_T^*, ...), is commonly referred to as *photoproduction*, while the regime with Q being the hard scale, or among the potential hard scales, is called leptoproduction or *(semi-inclusive) deep inelastic scattering* (SIDIS). Experimentally, photoproduction is usually defined by a fixed cut on the photon virtuality, e.g. $Q < 1$ GeV.

---

[3] Different photon–hadron frames are related by a boost along the Z axis. In particular, one can adopt the *photon–nucleon centre-of-momentum frame* where $\mathbf{q} + \mathbf{P}_N = 0$. The transverse components of the momenta are the same in all photon–hadron frames.
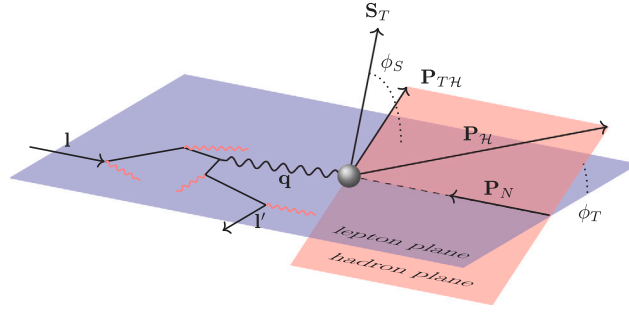
Fig. 2.5. Sketch of the kinematics of the process $e(\ell) + N(P_N) \rightarrow e(\ell') + \mathcal{H}(P_H) + X$ including collision-induced photon emissions from the initial and final-state leptons. Note that the lepton and hadron planes are not (by definition) affected by such radiations, unlike the off-shell-photon momentum q which is not any more in the lepton plane. Along the same lines, it is impossible to experimentally determine the photon–hadron frame (Fig 2.4 (right)), where q is aligned with the Z^* axis, by only measuring ℓ and ℓ'.

Beside the well-known regimes of photoproduction and leptoproduction (or SIDIS), which a priori require setting some constraints on Q^2, it appears very valuable for quarkonium studies to consider measurements where Q^2 is fully integrated over. Such yields then contain the contributions from both quasi-real and off-shell photons. This proposal is described in Section 3.2.3.

As it was mentioned in the introduction, polarisation observables play an important role in quarkonium physics. The polarisation parameters of a spin-1 heavy quarkonium λ_θ, $\mu_{\theta\phi}$ and $\nu_{\theta\phi}$ parametrise the angular distribution of decay leptons in the quarkonium rest frame:

$$\frac{\mathrm{d}\sigma}{\mathrm{d}\Omega} \propto 1 + \lambda_\theta \cos^2\theta + \mu_{\theta\phi} \sin 2\theta \cos\phi + \frac{\nu_{\theta\phi}}{2} \sin^2\theta \cos 2\phi. \tag{2.3}$$

These parameters depend on the orientation of the axes of the coordinate system chosen in the quarkonium rest frame with popular frame choices such as the Helicity, Collins–Soper, Gottfried–Jackson and target frames (see e.g. Section 2.3 of [30]). The same definition of polarisation parameters holds for the case of exclusive production of a vector quarkonium.

2.3.2. On the importance of QED corrections

The possibility to make a distinction between the photoproduction and electroproduction (or SIDIS) regimes, together with the rich phenomenology provided by measurements differential in the variables x_B, y, z as well as P_T^* and ϕ_T^*, has always been considered as an advantage of lepton–hadron reactions over hadron–hadron ones.

However, the emission of photons by initial- and final-state leptons modifies the relation between the momentum ℓ' of the final-state lepton *measured in the detector* and the four-momentum q of the photon exchanged between the leptonic and hadronic parts of the process in Eq. (2.1) (see Fig. 2.5) which in turn modifies the Lorentz-invariant variables (Eq. (2.2)) as well as $\mathbf{P}_{T\mathcal{H}}^*$ and ϕ_T^*. Beyond the Born approximation of QED, this relation is no longer simply $q = \ell - \ell'$ but includes the recoil from emitted photons. For strictly inclusive DIS measurements, as opposed to SIDIS, the application of QED radiative corrections boils down to an overall radiative correction factor to the cross section differential in x_B and the inelasticity y [49]. In the SIDIS case, fully differential Monte-Carlo computations have to be performed, using dedicated tools such as DJANGOH [50].

Recently, it has been shown [51] that QED radiative corrections fundamentally limit the accuracy of SIDIS measurements, in particular for the kinematic regime where the TMD factorisation is needed. In this context, a new approach to their treatment has been proposed. The QCD factorisation for the SIDIS cross section was historically discussed in the photon–hadron frame. However, as it was mentioned above, the collision-induced photon radiations change both the direction and magnitude of the exchanged virtual photon, making the photon–hadron frame and the quantities related to it only approximately defined. The ambiguities in the definition of kinematic variables in photon–hadron frame can impact our ability to extract the TMDs and, in particular, to use the angular modulation in ϕ_T^* to separate contributions of different TMD PDFs and fragmentation functions (FFs). Since the QED radiations differently affect the determination of the angles ϕ_T^* and ϕ_S^* (Fig. 2.4), this can affect the determination of various azimuthal (spin) asymmetries [51]. In addition to the uncertainty of the "photon–hadron" frame, the collision-induced photon radiations also change the true values of x_B and Q^2.

Although the effects of the QED radiations could be calculated perturbatively, the main point of concern are those QED radiative correction effects which are logarithmically enhanced due to the collinear and infrared sensitivity coming from the smallness of the electron mass m_e compared to all the other scales of the process. Omitting these effects may lead to significant uncertainties in some kinematic regimes where a wide phase space is available for collision-induced radiations, such as those relevant to the study of small-x physics or for two-scale observables described by TMD factorisation.

In Ref. [51], it has been argued that a combined QCD+QED factorisation can be performed such that the exchanged photon momentum q is not fixed by the *measured* $\ell - \ell'$, but rather has a range of values to be integrated over. The range is determined by the observed momentum of the scattered lepton for inclusive DIS and the momenta of both the scattered lepton and the observed final-state hadron for SIDIS. The approach consists of using collinear factorisation to take into account the collision-induced-QED-radiation effects which are enhanced by large logarithms of either Q/m_e, $|\mathbf{P}_{TH}|/m_e$ or $|\ell'_T|/m_e$, while either collinear or TMD factorisation can be used to account for QCD contributions depending on the hierarchy between the $|\mathbf{P}_{TH} - \ell'_T|$ and the hard scale Q. For the
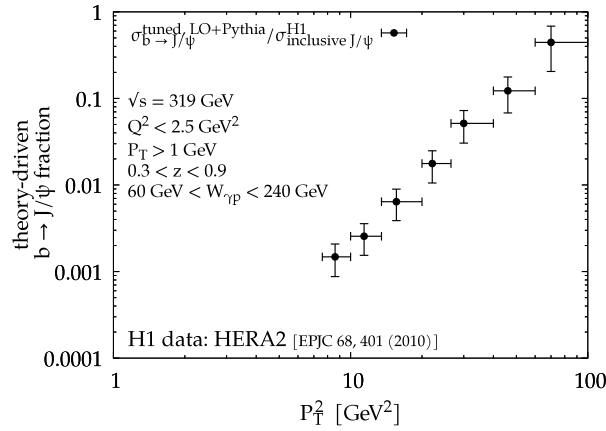
Fig. 2.6. Estimate for $b \to J/\psi$ feed-down fraction of the total cross-section for J/ψ photoproduction at HERA, based on the feed-down computed in Ref. [54] as a function of the square of the transverse momentum, P_T^2, of the J/ψ.

SIDIS process of Eq. (2.1) on a proton target, the hybrid factorisation formula is given by [51]:

$$E_{\ell'} E_{P_{\mathcal{H}}} \frac{d\sigma_{\text{SIDIS}}}{d^3\boldsymbol{\ell}' d^3\mathbf{P}_{\mathcal{H}}} \approx \sum_{a,b} \int_{\zeta_{\min}}^1 \frac{d\zeta}{\zeta^2} D_{e(\ell')/b(k')}(\zeta, \mu_F^2) \int_{\xi_{\min}}^1 d\xi \, f_{a(k)/e(\ell)}(\xi, \mu_F^2)$$
$$\times \left[E_{k'} E_{p_{\mathcal{H}}} \frac{d\sigma^{ap}[a(k) + p(P) \to b(k') + \mathcal{H}(p_{\mathcal{H}}) + X]}{d^3\mathbf{k}' d^3\mathbf{P}_{\mathcal{H}}} \right]_{k=\xi\ell, k'=\ell'/\zeta}, \tag{2.4}$$

where $a, b = e, \bar{e}, \gamma$, and where the active lepton/photon momenta entering or leaving the hard collision are defined as $k = \xi\ell$ and $k' = \ell'/\zeta$ with collinear momentum fractions ξ and ζ, and μ_F is the factorisation scale. The process-independent lepton distribution functions (LDFs) $f_{a/e}(\xi)$ and lepton fragmentation functions (LFFs) $D_{e/b}(\zeta)$ in Eq. (2.4) resum logarithmically-enhanced QED contributions in the limit when the hard scale, $\max(Q, |\mathbf{P}_{TH}|, |\boldsymbol{\ell}'_T|)$, is much larger than m_e. The non-logarithmically-enhanced part of QED radiative corrections can be included into $d\sigma^{ap}$ order by order in powers of α_{em}.

The differential cross section $d\sigma^{ap}$ in the second line of Eq. (2.4) can be further factorised by TMD or collinear factorisation in QCD depending on if the observed lepton and hadron are in the back-to-back regime or not. As it has been demonstrated in Refs. [51,52], the transverse-momentum broadening from the collision-induced QED radiations is much smaller than the TMD effects from QCD. Factorising out QED radiations using collinear LDFs and LFFs as done in the Eq. (2.4) is therefore a good approximation. Eq. (2.4) is valid up to Leading Power (LP), that is up to power corrections scaling as the inverse of the hard scale. Note that the same kind of equation holds in the case of $e - A$ collisions. Note also that Eq. (2.4) does not account for possible hadronic/resolved contributions from the photon.

Due to the smallness of α_{em}, σ^{ap} in Eq. (2.4) can be approximated by its QED Born order, $\sigma^{ap,(0)}$ with $a = b = e$. This lowest order cross section is the same as the SIDIS cross section without QED radiation which can be parametrised in terms of the usual SIDIS structure functions [53] but with different kinematics: $\ell \to k = \xi\ell$ and $\ell' \to k' = \ell'/\zeta$. Consequently, the exchanged-virtual-photon momentum between the scattered lepton and the colliding hadron is modified as $q = \ell - \ell' \to k - k' = \xi\ell - \ell'/\zeta$. By neglecting higher order QED contributions to σ^{ap} in Eq. (2.4), the SIDIS cross section *with* the collision-induced QED radiation can thus be obtained from the same SIDIS cross section *without* QED radiation plus the knowledge of the universal LDFs and LFFs.

2.4. On the importance of b feed down

An important and subtle concept needed to understand the quarkonium-production mechanism is the knowledge of feed downs. For instance, as shown in Ref. [54], in the case of J/ψ photoproduction at HERA, not all the J/ψ are produced by the hard scattering. Indeed, a non-negligible fraction of the J/ψ mesons produced at large P_T comes from the decay of a b quark. Fig. 2.6 shows the fraction of J/ψ coming from such a b feed down (also referred to as non-prompt yield) as a function of P_T^2 in the H1 kinematics. We guide the reader to Appendix A of Ref. [54] for more information about how it was estimated. One sees that the fraction of non-prompt J/ψ steadily grows to reach over 40% of the J/ψ yield at the highest reachable $P_T \lesssim 10$ GeV. Although the top energy of the EIC will be at most at $\sqrt{s_{ep}} = 140$ GeV, given the much higher luminosity of the EIC compared to HERA, the $W_{\gamma p}$ reach[4] might be such that, at high P_T, similarly large non-prompt fractions could be observed. With this respect, further dedicated studies are necessary.

---

[4] $W_{\gamma p} = \sqrt{s_{\gamma p}}$ designates the energy in the centre-of-mass of the photon–proton system.

3. EIC tools for quarkonium studies

3.1. Quarkonium-production mechanisms

As aforementioned, to justify the application of perturbative QCD to the studies of identified hadron production, the observables should involve some scale $\mu \gg \Lambda_{QCD}$, such that $\alpha_s(\mu) \ll 1$. In such cases, the cross section can be factorised (up to power-suppressed corrections in μ) into a product or convolution of a short-distance part, which is meant to be computed perturbatively as a series in $\alpha_s(\mu)$ and long-distance factors. The latter comprise (TMD-) PDFs of incoming hadrons and non-perturbative quantities which describe the hadronisation of partons produced at the short-distance/perturbative stage of the process into an observed final-state hadron.

The treatment of hadronisation differs for hadrons containing light quarks in the "naive" quark-model picture of these states as opposed to quarkonia, the primary component of which is expected to be a $Q\bar{Q}$ Fock state with the same quantum numbers as quarkonium. In the case of hadrons composed of light quarks or heavy-flavoured hadrons like D and B mesons, commonly denoted $\mathcal{H}_Q$ in this review, in which relativistic ("light") degrees of freedom play an important role, the hard-scale μ is $\sim p_T \gg m_{H_Q}$ and the "final-state" long-distance part of the cross section is usually encapsulated in a fragmentation function (FF). Due to the importance of light degrees of freedom, the FFs of such hadrons cannot be computed perturbatively and they are *parametrised* at some starting scale μ_0, on the order of 1 GeV, with parameters fitted to reproduce experimental data, see e.g. [55–60] for fits of respectively light and heavy-flavoured hadrons. For hadrons containing two tightly-bound heavy quarks, such as "standard" charmonia (η_c, J/ψ, χ_c, $\psi(2S)$, …) and bottomonia (η_b, $\Upsilon(nS)$, χ_b, …), denoted hereafter by $\mathcal{Q}$, a deeper understanding of hadronisation is believed to be possible.

The overall success of non-relativistic potential models in the description of the mass spectrum of these states implies that the contributions of QCD Fock states containing gluons or light quarks is suppressed by the powers of the average velocity v of the heavy quarks in the bound state compared to that of the simplest Fock state with only one heavy $Q\bar{Q}$ pair. The typical squared velocity v^2 is estimated in potential models to be ~ 0.3 for charmonia and ~ 0.1 for bottomonia, which turns it into a useful small parameter with respect to which the observables can be expanded. The different existing models of quarkonium production [9] follow more or less closely the above observation which yields to somehow disparate predictions for some production observables. We review below the main features of three of the most popular ones which will follow us throughout this review.

3.1.1. NRQCD & CSM

In the non-relativistic QCD (NRQCD) factorisation formalism [61], the cross sections and decay rates are expanded in powers of $\alpha_s(\mu)$ and v^2. At each order of the v^2 expansion, the short-distance part of the observable describes the production or annihilation of the $Q\bar{Q}$-pair in a colour-singlet or colour-octet state with a particular value of spin, orbital and total angular momentum. The hard scale, μ, for the short-distance part can be the heavy-quark mass m_Q, or any other larger scale not comparable to Λ_{QCD}, justifying the perturbative calculation of this factor. The corresponding long-distance part of the cross section is a number called the Long-Distance Matrix Element (LDME) which, for the production case, can be written up to conventional colour and spin normalisation factors, omitted for the sake of clarity, as:

$$\langle \mathcal{O}^{\mathcal{Q}}[i] \rangle \propto \sum_{X_s} \langle 0| \left(\mathcal{O}_i^\dagger \mathcal{Y}_n^\dagger \right)^{ab} (0) \left| \mathcal{Q} + X_s \right\rangle \left\langle \mathcal{Q} + X_s \right| \left(\mathcal{Y}_n \mathcal{O}_i \right)^{ba} (0) |0\rangle, \tag{3.1}$$

where it is implied that any final state X_s containing light quarks and gluons can be produced together with the quarkonium $\mathcal{Q}$. The factors $\mathcal{Y}_n$ in Eq. (3.1) contain Wilson lines along the light-like direction n needed for the gauge invariance of the Colour-Octet (CO) LDMEs. The structure of the colour indices, ab, connecting the amplitude and complex-conjugate amplitude in Eq. (3.1) reflects the process-dependent configuration of the Wilson lines in the factors $\mathcal{Y}_n$. The local NRQCD operators $\mathcal{O}_i$ contain heavy-quark and antiquark fields[5] and are labelled in the same way as the simplest Fock state $|Q\bar{Q}[i] + X_s\rangle$ which this operator can excite from the vacuum. The spectroscopic notation of the label $i = {}^{2S+1}L_J^{[1,8]}$ is used to denote the total spin S, the orbital angular momentum L, the total angular momentum J and the singlet (CS, [1]) or octet (CO, [8]) colour quantum numbers of the heavy-quark pair. With these conventions, the complete traditional notation for the LDME becomes: $\langle \mathcal{O}^{\mathcal{Q}} \left[{}^{2S+1}L_J^{[1,8]} \right] \rangle$.

NRQCD velocity-scaling rules [61–63] lead to the assignment of the $O(v^m)$ suppression to LDMEs, thus allowing us to truncate the velocity expansion at some fixed order in v^2. Usually the contributions associated with the LDMEs up to Next-to-Next-to-Leading Order (NNLO) in v^2 ($O(v^4)$ relative to the LDME of the ${}^3S_1^{[1]}$ state) are taken into account in phenomenological studies. This means that, besides the colour-singlet $Q\bar{Q}$ states, the colour-octet states ${}^1S_0^{[8]}$, ${}^3S_1^{[8]}$ and ${}^3P_J^{[8]}$ can contribute to J/ψ production, for example.

For S-wave quarkonia, the expansion limited to the leading order of v^2 corresponds to the colour-singlet $Q\bar{Q}$-state with the same quantum numbers as those of $\mathcal{Q}$. The *colour-singlet model* (CSM) [3–5] for the production of these states is nothing but the truncation of the v^2 expansion at this order. The CS LDMEs can be estimated from potential-model wave functions [64], while their accurate estimation from $\ell^+\ell^-$ decay rates of $\mathcal{Q}$ is rendered complicated by large NNLO QCD corrections [65] to the decay width. However, the CSM is not sufficient theoretically [61,66,67] for the description of the production of the P-wave quarkonia, such as $\chi_{c,b}$, beyond LO in α_s and cannot describe inclusive hadroproduction P_T spectra of charmonia and bottomonia at high P_T [68,69]. Nevertheless, the NNLO corrections in α_s to the short-distance part of the CSM cross section, only partially computed so far, may

---

[5] Denoted as χ and ψ in NRQCD.

decrease the existing large discrepancy between the CSM and the data from Tevatron and the LHC [70–73]. This point is still under debate [9,74,75].

In contrast to the hadroproduction case described above, in (prompt) *inclusive* photo- and electroproduction of heavy quarkonia, which are relevant for the EIC experimental program, the CSM has been expected [25,76] and proven to be able to account for a large fraction of the observed cross section [54,77] even up to the highest reachable P_T. Estimates varying from 50% [77] to almost 100% [54] can be found in literature.

For the *exclusive* photo- and electroproduction of single J/ψ or $\Upsilon(nS)$, the CS contribution is also expected to be strongly dominating. In such exclusive reactions, no final-state radiation (X_s) is allowed and the NRQCD operators containing a CO $Q\bar{Q}$ pair can only couple to the higher Fock-state contributions in the expansion of the physical quarkonium eigenstate, which are velocity-suppressed, e.g. $|J/\psi\rangle = O(1)|c\bar{c}[^3S_1^{[1]}]\rangle + O(v)|c\bar{c}[^3P_J^{[8]}] + g\rangle + \cdots$ The matrix elements of the gauge-invariant CO operators which in principle can contribute to exclusive photoproduction, e.g. $\psi^\dagger(g_s\mathbf{E}\cdot\mathbf{D})\chi$ where $\mathbf{E}$ is the chromoelectric field and $\mathbf{D}$ is the QCD covariant derivative, can be estimated[6] to scale at least as $O(v^5)$ at the level of the amplitude using the velocity scaling rules [62]. In Ref. [78], the same conclusion has been made about the CO contributions to the matrix elements of the operator $\psi^\dagger\mathbf{D}^2\chi = \psi^\dagger\nabla^2\chi + \psi^\dagger(g_s\mathbf{A}\cdot\nabla)\chi + \cdots$, which are more suppressed than the CS relativistic corrections $\langle J/\psi|\psi^\dagger\nabla^2\chi|0\rangle \sim \nabla^2\Psi(0) \sim O(v^2)$. Therefore, taking into account CS relativistic corrections to exclusive vector-quarkonium photoproduction is currently considered to be more important [78–80] than taking into account the CO corrections.

Another success [81] of the CSM at NLO in α_s is the description of the prompt η_c hadroproduction, measured by LHCb [82,83]. However, such a success of the CSM to describe this data set, both at moderate $P_T \sim m_{\eta_c}$ and for $P_T \gg m_{\eta_c}$ is problematic for NRQCD. Indeed, from heavy-quark-spin-symmetry (HQSS) arguments, one expects the CO contributions to η_c cross section at $P_T \gg m_{\eta_c}$ to be on the same order of magnitude as that previously found to describe J/ψ data at similar P_T.

As aforementioned, at higher orders in the v^2 expansion, the CO LDMEs contribute, but at present they are treated as free parameters and are adjusted to describe experimental data. Besides order-of-magnitude constraints from $O(v^n)$ scaling and HQSS constraints, the progress on their theoretical calculation has been limited so far. Recently new expressions for LDMEs in terms of potential-model quarkonium wave functions and certain chromoelectric-field correlators have been proposed in the potential-NRQCD (pNRQCD) formalism in the strongly coupled regime [84,85]. These relations can be used to reduce number of free parameters in the fit under the assumption $m_Q v^2 \ll \Lambda_{\text{QCD}}$. Currently, the advantage of using pNRQCD compared to conventional NRQCD fits is still under debate as well as its applicability, since $m_Q v^2$ is naively not much smaller than Λ_{QCD}.

In Section 3.2.1, we describe existing phenomenological fits of LDMEs within collinear factorisation, commenting on their successes and shortcomings in more details. Unfortunately at present time there is no single set of LDMEs which can satisfactorily describe the charmonium e^+e^- annihilation, $\gamma\gamma$ fusion, hadro- and photoproduction data together with polarisation observables in the framework of NRQCD factorisation at NLO in α_s, which is a serious problem for the NRQCD factorisation approach. For the case of bottomonia, we lack photoproduction, e^+e^- annihilation and $\gamma\gamma$ fusion data, which prevents us from checking the process-independence of LDMEs for the $b\bar{b}$ family. Another important task for the EIC, in connection with the clarification of the quarkonium-production mechanism, is to perform the first measurement of $\chi_{c0,1,2}$ and η_c inclusive photoproduction cross sections. In this context, we discuss corresponding phenomenological predictions in Section 3.2.3. Such measurements will be complementary to those of χ_c and η_c hadroproduction to check the process-independence of the corresponding LDMEs.

Data at high $P_T \gg m_Q$, where CS and CO contributions behave differently, are potentially very discriminant for LDME fits. This calls for improvement of the perturbative accuracy of the short-distance part since, at large P_T, terms proportional to $\alpha_s^{n+k}\ln^n P_T/m_H$ appearing in the perturbative series for the short-distance part of the cross section both at LP in P_T and in power-suppressed corrections at $P_T \gg m_Q$ need to be tackled. These potentially large terms can be resummed using the formalism of FFs, perturbatively evolving with the scale $\mu \sim P_T$. At LP, this formalism is analogous to the FFs for light hadrons mentioned in the beginning of this section, with a sole but important difference, namely that at the starting scale $\mu_0 \sim m_Q$ the FF is assumed to be factorised into a short distance part and a LDME. We refer to e.g. [86] as an example of the NLO study of this type as well as Refs. [87–89] at LO. At Next-to-Leading Power (NLP), new contributions with the $Q\bar{Q}$ pair as a whole participating in the fragmentation process appear [90]. These corrections seem to influence not only the cross section but also the evolution of leading-power FFs [91]. However, the effect of this corrections on cross sections and the polarisation is still under investigation in particular for the EIC phenomenology where the P_T reach, limited to roughly 15-20 GeV, might not be large enough for these to be relevant.

3.1.2. CEM & ICEM

Given the above mentioned phenomenological problems along with others which we review later, NRQCD factorisation at fixed order in v^2 and α_s is not completely satisfactory. Due to its simplicity, the *Colour Evaporation Model* (CEM), introduced in Refs. [7,8] remains an attractive alternative mechanism to explain the formation of quarkonium. As the CEM is inspired from quark–hadron duality, one postulates that any $Q\bar{Q}$ pair produced at short distance with invariant mass $M_{Q\bar{Q}}$ less than the invariant mass of a pair of lightest mesons (H_Q) with open-heavy flavour Q (e.g. D^0 mesons in the case of charmonia) has to hadronise into one of the quarkonia below this heavy-flavour-production threshold with some universal probability. In the CEM, this probability, commonly denoted as F_Q for the quarkonium state Q, is taken to be independent of spin, orbital momentum and colour quantum numbers of the pair, and is fit as a free parameter.

---

[6] The scaling for $\mathbf{D}$ is $O(v)$ and the scaling for $g_s\mathbf{E}$ is $O(v^3)$ so together with the $O(v)$ suppression of the $|c\bar{c}[^3P_J^{[8]}] + g\rangle$ component of $|J/\psi\rangle$), one obtains $O(v^5)$.

In the improved CEM (ICEM) [92–94], the kinematic effects arising from the mass difference between the $Q\bar{Q}$-pair produced at short distance and the final-state quarkonium is taken into account, which roughly models the effects of soft-gluon emissions at hadronisation stage. This is done through the rescaling of the three-momentum of the pair by the mass ratio, so that the direct quarkonium-production cross section in pp collisions in the ICEM is given by [92]:

$$\sigma = F_Q \sum_{i,j} \int_{M_Q}^{2m(\mathcal{H}_Q)} dM_{Q\bar{Q}} dx_i dx_j \ f_i(x_i, \mu_F) f_j(x_j, \mu_F) \cdot \hat{\sigma}_{ij \to Q\bar{Q}}(x_i, x_j, \mathbf{p}_{Q\bar{Q}}, \mu_R, \mu_F)\Big|_{\mathbf{p}_{Q\bar{Q}} = \frac{M_{Q\bar{Q}}}{M_Q}\mathbf{P}_Q} , \tag{3.2}$$

where i and j are $q, \bar{q}$ and g such that $ij = q\bar{q}, qg, \bar{q}g$ or gg, $x_{i,j}$ is the momentum fraction of the parton, $f(x_{i,j}, \mu_F)$ is the parton distribution function (PDF) in the proton as a function of $x_{i,j}$ at the factorisation scale μ_F. Finally, $\hat{\sigma}_{ij \to Q\bar{Q}}$ are the parton-level cross sections for the initial states ij to produce a $Q\bar{Q}$ pair of momentum $\mathbf{p}_{Q\bar{Q}}$ at the renormalisation scale μ_R. In the ICEM, the invariant mass of the $Q\bar{Q}$ pair, $M_{Q\bar{Q}}$, is integrated from the physical mass of quarkonium M_Q to two times the mass of the lightest open heavy Q-flavour meson $m(\mathcal{H}_Q)$. In the traditional CEM, see e.g. [95], the value of $2m_Q$ is used as the lower limit of mass-integration instead of M_Q and the momentum-shift due to the mass-difference between the $Q\bar{Q}$-pair and the quarkonium is neglected.

We emphasise that the physical picture of the (I)CEM is opposite to NRQCD in the sense that the CS contributions play no special role at all. This assumption makes CEM incapable of describing observables where CS states are clearly dominating, e.g. the prompt hadroproduction of J/ψ pairs [95] and the $e^+e^- \to J/\psi + c\bar{c}$ cross section [96]. However, the (I)CEM still provides a reasonable description of single inclusive prompt quarkonium hadroproduction [92–94] although the model is not capable to describe $P_T \sim m_Q$ and $P_T \gg m_Q$ simultaneously even at NLO [95,97].

Recent ICEM calculations [94,98] have considered the polarisation in hadroproduction. Polarised production of quarkonium in these calculations restricts the final state quark–antiquark pair to be in the desired spin state, thus implicitly assuming that soft gluons are decoupled from heavy-quark spin. The polarisation parameters are then calculated in terms of the spin matrix elements σ_{i_z, j_z}. In these matrix elements, the quarkonium is assumed to have $J_z = i_z$ when calculating the scattering matrix element, $\mathcal{M}$. The quarkonium is assumed to take $J_z = j_z$ in calculating the conjugate, $\mathcal{M}^*$. The polar anisotropy (λ_θ), defined in the Eq. (2.3), is given in this model by [99]

$$\lambda_\theta = \frac{\sigma_{+1,+1} - \sigma_{0,0}}{\sigma_{+1,+1} + \sigma_{0,0}} . \tag{3.3}$$

As the ICEM is an alternative to NRQCD in hadroproduction, developments to extend it into other collision systems are still in progress. The authors of [94,98,100] anticipate that the value of λ_θ for J/ψ production in ep collisions will also be very similar to the pp case, which they found to be compatible with the existing Tevatron and LHC data. In addition, they also find the free parameter F_Q in photoproduction to be consistent with that in hadroproduction. The description of HERA H1 data [101] on J/ψ photoproduction in the ICEM [100] is illustrated in Fig. 3.1. However, the (I)CEM prediction introduces a parameter to keep the propagator at some minimum distance of M_ψ^2 from the pole. Thus, its prediction of the z-differential spectrum in photoproduction is likely to be complicated by large radiative corrections at $1 - z \ll 1$ if the parameter is removed, which was seen already in the LO analysis of Ref. [102,103] where the agreement with data at $z \to 1$ was reached only after introduction of an *ad-hoc* cut $|\hat{t}| > 4m_c^2$ on the partonic $\hat{t}$ variable.

The observation that the CEM leads to unpolarised heavy-quarkonium hadroproduction at high-P_T [98], a result which is non-trivial to achieve with NRQCD fits, perhaps means that, in cases where CO LDMEs dominate, the dynamics of soft-gluon emissions should be taken into account more accurately than it is done in the fixed-order NRQCD factorisation approach. The recently proposed soft-gluon factorisation approach represents a progress in this direction [104,105], whose phenomenological implications, however, remain to be investigated.

3.2. Legacy from HERA, the tevatron and the LHC, and predictions for the EIC for cross-section and polarisation observables

3.2.1. Status of NRQCD LDME fits
A side note on the positivity of the LDMEs beyond LO. Before discussing the NLO LDME fits, let us make a comment about the positivity of LDMEs. At LO in α_s, the LDMEs have a simple interpretation as "probabilities" of the transition of the $Q\bar{Q}$-pair in a certain colour, spin and angular-momentum state into an observed quarkonium. This physical interpretation follows from the operator definition of LDMEs (3.1) in terms of "bare" fields [61,106] if QCD loop corrections are not taken into account and Wilson-line factors are ignored. Consequently, in LO calculations, LDMEs are typically assumed to be positive-definite. This is similar to the situation with LO (TMD)PDFs.

Already at NLO in α_s, both ultraviolet (UV) and infrared (IR) divergences appear in the operator definitions of LDMEs, see e.g. Appendix B of Ref. [61] as well as Section 6 of Ref. [107] and references therein. If NRQCD factorisation holds – which is yet to be proven beyond NNLO in α_s [106,108] – the IR divergences of the hard-scattering coefficients should cancel against the corresponding IR divergences of the LDMEs at all orders of the v^2 and α_s expansions, while the UV divergences appearing in LDMEs are removed by the operator renormalisation. The *renormalised* LDMEs then become non-perturbative fit parameters. Therefore, these parameters do not necessarily have to be positive. Their definition involves the subtraction of the divergent part. In addition, the finite renormalised LDMEs are scheme- and scale-dependent, and mix with each other due to the NRQCD-scale evolution. The relation between the short-distance cross section and LDMEs, described above, is similar to the relation between NLO short-distance cross sections and QCD PDFs and/or fragmentation functions, which are also not necessarily positive-definite, at least if the calculation is truncated to a fixed order in α_s. This is the reason why there are usually no positivity constraints imposed in NLO LDME fits. One
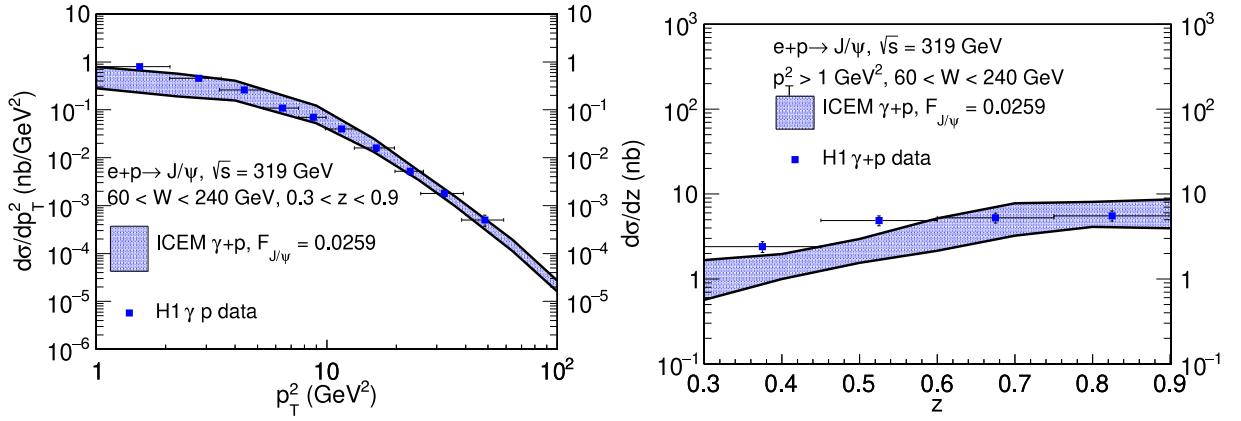
Fig. 3.1. Description of the HERA H1 data [101] on P_T^2-differential (left) and z-differential (right) cross section of inclusive J/ψ photoproduction in ep scattering by the ICEM calculation in collinear factorisation. The combined mass and scale uncertainties are shown in the band. Feed down contributions are not included. *Source:* Taken from Ref. [100].

Table 3.1

Phenomenological comparison of a selection of existing J/ψ-η_c LDME extractions at NLO in α_s. The cut on the J/ψ transverse momentum, applied in each fit, is indicated in parentheses in the third column. This cut is applied because all but the first fit badly fail to account for the low-P_T data.

Acronym	Reference	J/ψ hadropr.	J/ψ photopr. and e^+e^-	J/ψ polar. in hadropr.	η_c hadropr. ($P_T > 6.5$ GeV)
BK11	Butenschön et al. [110–113]	✓($P_T > 3$ GeV)	✓	✗	✗
H14	Chao et al. + η_c [120]	✓($P_T > 6.5$ GeV)	✗	✓	✓
Z14	Zhang et al. [121]	✓($P_T > 6.5$ GeV)	✗	✓	✓
G13	Gong et al. [115]	✓($P_T > 7$ GeV)	✗	✓	✗
C12	Chao et al. [114]	✓($P_T > 7$ GeV)	✗	✓	✗
B14	Bodwin et al. [86]	✓($P_T > 10$ GeV)	✗	✓	✗
pNRQCD′	Brambilla et al. [116,122]	✓($P_T > 9$ GeV)	✗	✓	✗
pNRQCD	Brambilla et al. [116,122]	✓($P_T > 15$ GeV)	✗	✓	✓

of the consequences of this is that the numerical values of LDMEs obtained in fits at NLO in α_s have limited physical significance outside the NLO context and should only cautiously be used in LO calculations, because this could create unjustifiable cancellation between some contributions.

In general though, it is not clear that negative NLO LDMEs would yield positive NLO cross sections for all possible measurable processes one could think of. Let us for instance mention the case of quarkonium–photon associated production for which it was shown [109] that some of the NLO LDME fits which we discuss below would yield negative NLO cross sections. Such a physical constraint on LDMEs at NLO has however not been systematically investigated as it requires the complete NLO computation of the hard scatterings for all the processes one wishes to consider.

Survey of existing NLO LDME fits. Several groups have performed fits of CO LDMEs for charmonia [86,110–116] and bottomonia [117–119] at NLO in α_s for the short-distance parts. We emphasise that the computation at NLO in α_s of short-distance cross sections for the production of NRQCD states ($Q\bar{Q}[i]$) is done in exactly the same framework of collinear factorisation by most of the groups with the exception of the fit of Bodwin et al. [86]. The latter computation includes, beside corrections at NLO in α_s, the resummation of logarithms of P_T/m_Q which become important at $P_T \gg m_Q$. Therefore the difference of the fits boils down mostly to the choice of different experimental data to fit and approximate (up to higher-orders in v^2) relations between different LDMEs which are assumed or not to hold exactly in the fitting procedure. For a detailed discussion, we refer to the recent review [9]. Table 3.1 briefly compares phenomenological results of each fit for the case of charmonia using benchmark observables such as the cross sections and polarisation of inclusive prompt J/ψ produced in pp collisions as a function of P_T as well as photoproduction in ep collisions and the total cross section of charmonium production in e^+e^- annihilation. We also indicate in Table 3.1 whether the corresponding set of LDMEs for J/ψ allows one to describe the prompt η_c hadroproduction P_T-spectrum measured by LHCb [82,83] using heavy-quark-spin-symmetry relations between η_c and J/ψ LDMEs which hold up to v^2 corrections. As the experimental data are a crucial ingredient for these fits, we have collected the complete list of experimental results that are used for these fits in Appendix A.

The P_T spectra of the prompt inclusive quarkonia produced in pp and $p\bar{p}$ collisions at mid and large P_T at the Tevatron and the LHC are well described by all the fits mentioned in Table 3.1; this is the major phenomenological success of NRQCD factorisation at NLO. Note, however, that hadroproduction data with $P_T \lesssim m_Q$ (or integrated in P_T [123,124]) cannot be simultaneously described by NLO NRQCD fits of large P_T data. In fact, most of the fits have been performed with even stronger P_T cuts, as indicated in Table 3.1.
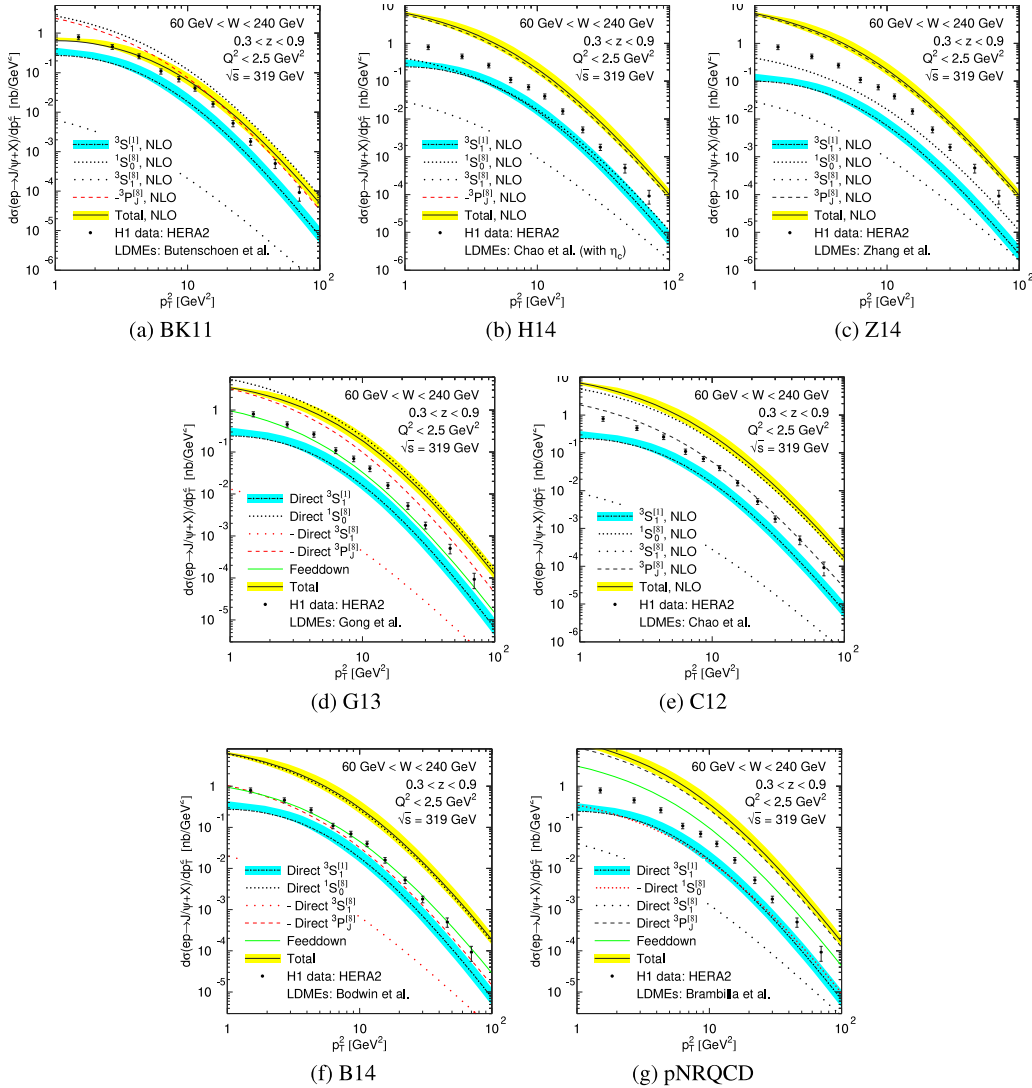
Fig. 3.2. Description of the HERA H1 data [101] for the P_T^2-differential cross section of inclusive J/ψ photoproduction by NLO NRQCD fits in collinear factorisation for the LDMEs listed in Table 3.1. In each plot the sum of CS and CO contributions is plotted by the solid line with the yellow scale-variation band. The dash-dotted line with blue scale-variation band corresponds to the CSM contribution at NLO. Other curves in each plot correspond to the contributions to the "total NLO" curve from various CO states (with negative contributions being plotted in red) and to the feed down contribution, as indicated by the legend of each of the plots.

The only existing global NLO LDME fit [110–113], BK11, beyond hadroproduction, also provides a reasonable description of unpolarised charmonium production cross sections in e^+e^-, pp, $p\bar{p}$ and ep collisions. The description of HERA H1 data [101] on J/ψ photoproduction by the BK11 fit is illustrated in the Fig. 3.2(a) and Fig. 3.3(a). However, this fit is not able [112,113] to describe charmonium-polarisation observables, measured in hadroproduction at high-P_T, see e.g. Ref. [30] for a global survey of heavy-quarkonium-polarisation data. This situation is often referred to as the "heavy-quarkonium-polarisation puzzle" in the literature. Polarisation observables relevant for J/ψ production at the EIC will be discussed in Section 3.2.3.

Two of the fits in Table 3.1, H14 and Z14, turned out to be able to simultaneously describe J/ψ and η_c hadroproduction data using heavy-quark-spin-symmetry relations between LDMEs. Remarkably, the J/ψ-polarisation observables in hadroproduction are also reasonably well reproduced by these fits but they significantly overestimate the HERA photoproduction cross section as can be seen in Fig. 3.2(b,c). The same holds for all the other LDME fits (with the exception of BK11 discussed above), see Fig. 3.2(d-g). The discrepancies between the NRQCD NLO predictions with these fits range from 2 at $P_T \simeq 10$ GeV up to 10 at $P_T \simeq 1-2$ GeV in the case of pNRQCD and B14. This means that the yield predictions at the EIC using these LDMEs can be overestimated by up to one order of magnitude. Since the discrepancies remain at $P_T = 10$ GeV, which roughly corresponds to the maximum values which would be reached at the EIC, this should be kept in mind when considering predictions with CO contributions (except for the BK11 LDMEs) for the EIC case at any P_T.
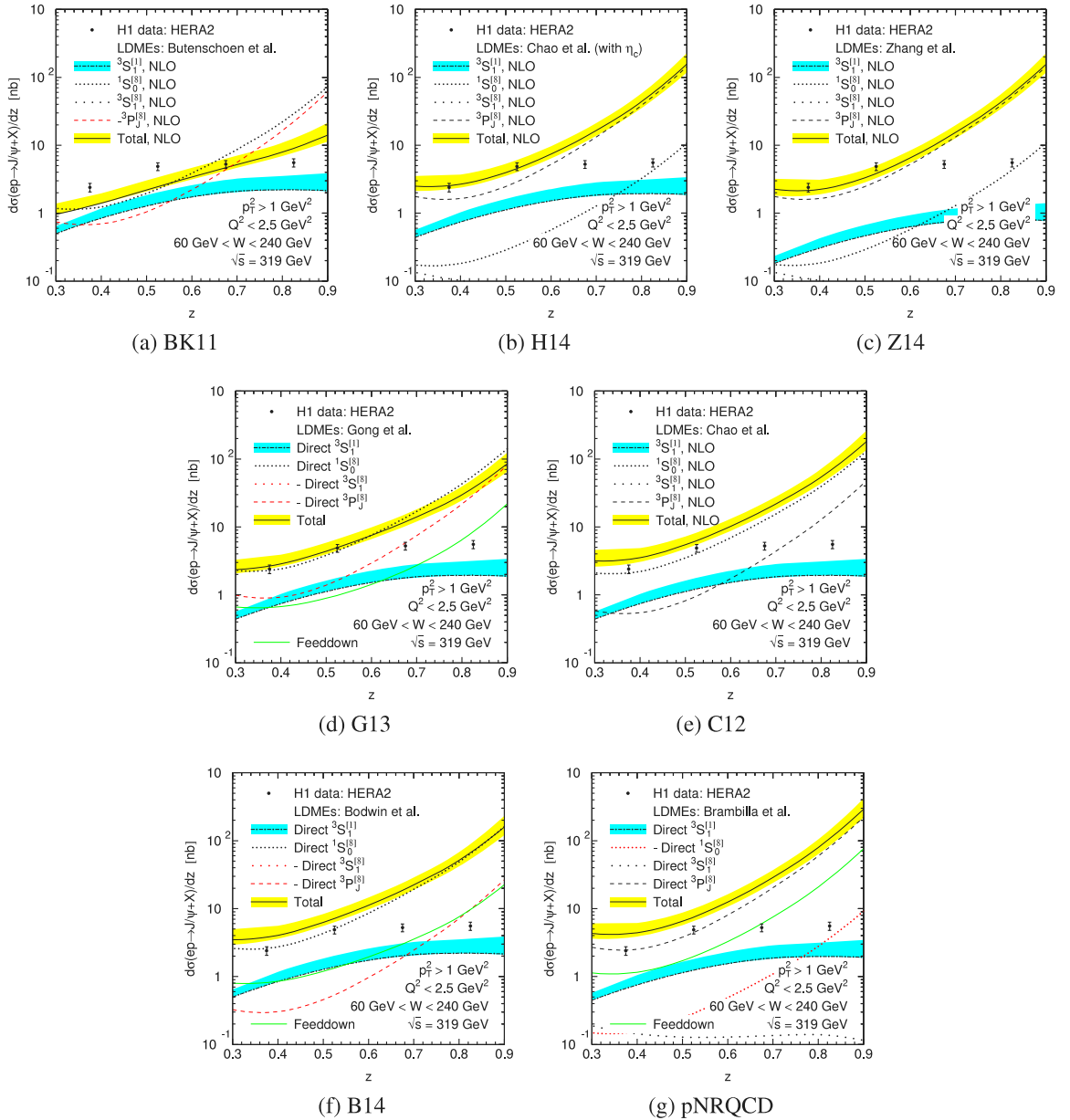
Fig. 3.3. Description of the HERA H1 data [101] for the z-differential cross section of inclusive J/ψ photoproduction by the NLO NRQCD fits in collinear factorisation for the LDMEs taken listed in Table 3.1. The notation for the curves is the same as in the Fig. 3.2.

As one can seen from Fig. 3.3, all LDME fits except BK11 also strongly overestimate the z-differential cross section for $z > 0.6$. The BK11 fit is consistent with the photoproduction data due to the cancellation between $^1S_0^{[8]}$ and $^3P_J^{[8]}$ channels. Other fits use this degree of freedom to accommodate the polarisation and/or η_c production data and therefore lose flexibility which is needed to achieve a global fit across different collision systems.

In a recent study [125], the NRQCD cross sections of $J/\psi + Z$ and $J/\psi + W$ hadroproduction have been completely calculated at NLO. Interestingly, the only set of LDMEs found to be marginally capable of reproducing the $J/\psi + Z$ hadroproduction data from the LHC is the set of Refs. [116,122], referred to in the Table 3.1 as "pNRQCD". This fit uses potential-NRQCD relations between LDMEs to reduce the number of free parameters in the fit of the J/ψ P_T spectrum in hadroproduction and which also describes polarisation observables. However, this set of LDMEs is not able to describe J/ψ photoproduction and e^+e^- annihilation data and is consistent with η_c hadroproduction data only within large uncertainties and with a P_T threshold for the J/ψ data large than for
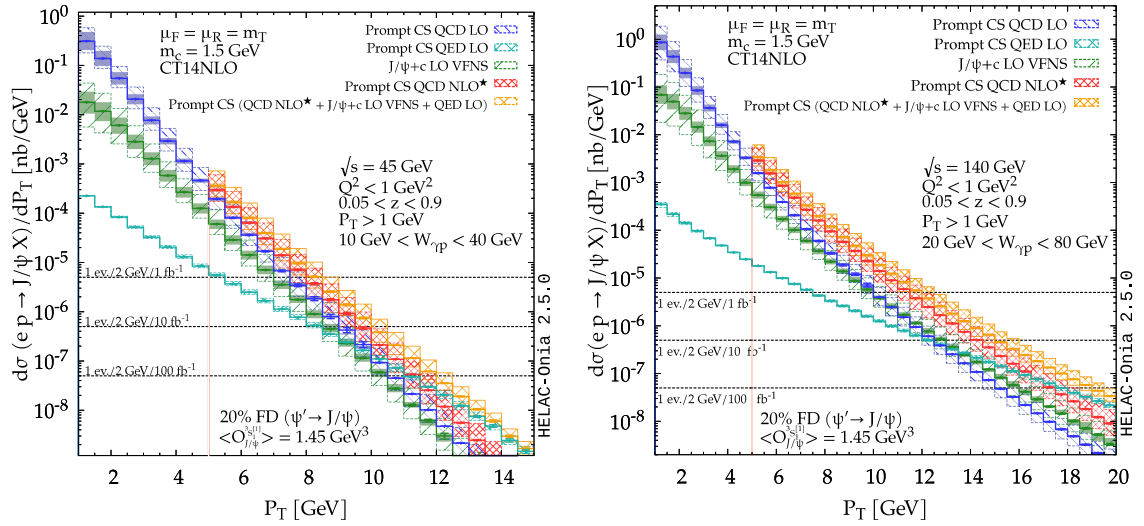
Fig. 3.4. Predictions for the future EIC at $\sqrt{s_{ep}} = 45$ GeV (left) and $\sqrt{s_{ep}} = 140$ GeV (right) as a function of the J/ψ transverse momentum, P_T. The solid bands indicate the mass uncertainty while the patterns display the scale uncertainty.
Source: Figure taken from Ref. [54].

the η_c data. As just discussed, the pNRQCD fit, like all the hadroproduction, badly fails to account for the J/ψ-photoproduction data from the H1 collaboration at HERA as shown on Fig. 3.2(g) and Fig. 3.3(g) which cast doubts on its relevant for EIC predictions.[7]

Several fits of CO LDMEs for bottomonia have also been performed at NLO [117–119]. Only the most recent one [119] considered the $\Upsilon(1, 2, 3S)$ and $\chi_{bJ}(1, 2P)$ LDMEs independently and systematically included the feed-down contributions from $\Upsilon(nS)$ and $\chi_{bJ}(nP)$ states with larger masses. These feed-down contributions constitute $\sim 40\%$ of the $\Upsilon(1S, 2S)$ cross section, which is significant. In the case of $\Upsilon(3S)$, the feed down from $\chi_b(3P)$ states, which were discovered by ATLAS [127] and which lie just below the $B\bar{B}$-threshold, also turns out to be significant (see [9] for a more detailed discussion of the feed-down impact). This was, however, not taken into account in [119]. This may explain the difficulties of the corresponding fit to account for the $\Upsilon(3S)$ polarisation. The polarisation observables for $\Upsilon(1S, 2S)$ states came out to be about consistent with data in this fit. We guide the reader to the recent Ref. [128] for a detailed discussion of the agreement with various polarisation observables. Note that there is no bottomonium data from inelastic photoproduction nor from e^+e^- annihilation. Hence, future measurements of $\Upsilon(nS)$ inclusive electro- and photoproduction at the EIC will serve as an excellent test of the LDME process-independence in the b-quark case, where it has more chances to hold due to smaller $\mathcal{O}(v^2)$ corrections.

3.2.2. Recent developments regarding inclusive J/ψ photoproduction within the CSM

New P_T-enhanced contributions. The recent study of Ref. [54], performed within the CSM, is interesting regarding corrections which were not included in the NLO NRQCD analyses presented above, although they could become important at $P_T \gg M_{J/\psi}$. The study focused on the leading-P_T leading-v next-to-leading-α_s corrections, within the NLO* approximation [70,71]. The latest HERA data from the H1 Collaboration [101] was first revisited, by including new contributions such as the pure QED one ($\gamma + q \rightarrow \gamma^\star + q \rightarrow J/\psi + q$ at $\mathcal{O}(\alpha^3)$ where the off-shell photon $\gamma^\star$ fluctuates into a J/ψ) and the associated J/ψ+ charm production ($\gamma + g \rightarrow J/\psi + c + \bar{c}$ and $\gamma + \{c, \bar{c}\} \rightarrow J/\psi + \{c, \bar{c}\}$). The former involves quark PDFs in the initial state, while the latter is described within a LO Variable Flavour Number Scheme (LO-VFNS) [129,130]. It was shown that the CSM at $\mathcal{O}(\alpha\alpha_s^3)$ and $\mathcal{O}(\alpha^3)$ is able to describe the latest HERA data at large P_T. The NLO corrections to $\gamma + g \rightarrow J/\psi + c + \bar{c}$ were recently computed [131] and were found to increase the cross section a factor close to 2 in the HERA kinematics.

The corresponding predictions for the $P_T(J/\psi)$ spectrum in photoproduction at the EIC are shown in Fig. 3.4 with kinematical cuts on Q^2, the elasticity, z, and $W_{\gamma p} \equiv \sqrt{s_{\gamma p}}$ inspired from the latest H1 measurements. The CT14NLO proton PDF set [132] was used. The factorisation and renormalisation scales were taken to be $\mu_F = \mu_R = m_T = \sqrt{M_{J/\psi}^2 + P_T^2}$, the transverse mass of the J/ψ, later this is called $m_{TJ/\psi}$ and the corresponding uncertainties were evaluated by varying them in the interval $\mu_F, \mu_R \in [1/2, 2] \times m_T$. The charm mass m_c was set to 1.5 GeV and the corresponding mass uncertainty was evaluated by varying it by ± 0.1 GeV. Moreover, the CS LDME $\langle \mathcal{O}^{J/\psi} [^3S_1^{[1]}] \rangle$ was taken to be 1.45 GeV^3. Finally, a 20% feed-down $\psi' \rightarrow J/\psi$ was taken into account.

In Fig. 3.4, predictions for two energy configurations are presented. At $\sqrt{s_{ep}} = 45$ GeV (Fig. 3.4, left), as P_T increases, one enters the valence region. This makes the QED contribution become the dominant one at the largest measurable $P_T \simeq 11$ GeV, with an integrated luminosity of $\mathcal{L} = 100$ fb^{-1}. Furthermore, $\gamma + q$ fusion contributes more than 30% for $P_T > 8$ GeV and the $J/\psi +$

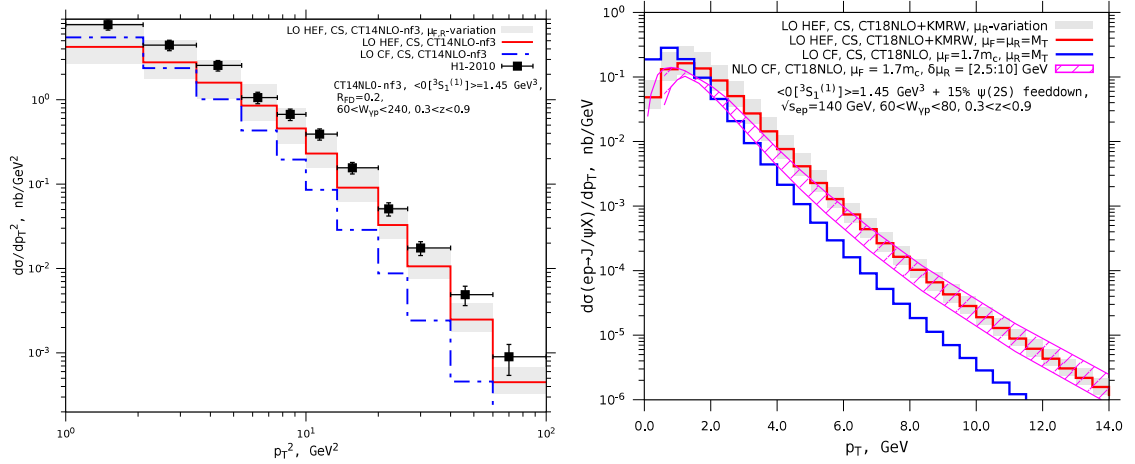[7] For recent updates and more discussions, see [126].

Fig. 3.5. Left panel: LO HEF results (solid histogram) for the H1-2010 [101] prompt J/ψ photoproduction $P_T{}^2(J/\psi)$ spectrum within the CSM compared to LO CF results (dash-dotted histogram). See the main text for details. Right panel: Comparison between the LO HEF prediction (solid histogram with μ_R-variation band) for the prompt $P_T(J/\psi)$ spectrum at the EIC with the NLO CF prediction (shaded μ_R-variation band) evaluated at the optimal value of factorisation scale proposed in Ref. [147].

unidentified charm contribution is comparable to the $\gamma + g(q)$ fusion subprocesses. Hence, these so far overlooked contributions are going to be relevant at the EIC. At $\sqrt{s_{ep}} = 140$ GeV (right panel in Fig. 3.4), the yield is measurable up to $P_T \sim 18$ GeV. The QED contribution is the leading one at the largest reachable P_T, while $\gamma + g$ fusion is the dominant contribution up to $P_T \sim 15$ GeV. More generally, it turns out that the production of $J/\psi + 2$ hard partons (i.e. $J/\psi + \{gg, qg, c\bar{c}\}$) is dominant for $P_T \sim 8 - 15$ GeV. This could lead to the observation of $J/\psi + 2$ jets with moderate P_T, with the leading jet_1 recoiling on the $J/\psi + \mathrm{jet}_2$ pair.

High-energy-enhanced contributions. In order to study the possible effects of higher-order QCD corrections enhanced by logarithms of the partonic centre-of-mass energy ($\hat{s}$), the Leading-Twist (LT) High-Energy Factorisation [133–136] (HEF) can be used. In many phenomenological studies, it is generalised to include, not only the resummation of $\ln(\hat{s}/M_Q^2)$-enhanced effects in the leading-logarithmic approximation, but also the resummation of the "Sudakov" $\ln(M_Q/P_T)$ large logarithms at $P_T \ll M_Q$ in the next-to-leading logarithmic approximation, assuming CS state production, through the use of the Kimber-Martin-Ryskin-Watt (KMRW formula) [137–139]. However, the systematic study of the overlap between LT HE factorisation and the TMD factorisation usually employed to resum such transverse-momentum logarithms has been initiated only very recently [140,141]. The KMRW formula converts the set of usual collinear PDFs to the so-called unintegrated PDFs (uPDFs) of the LT HEF formalism. uPDFs depend not only on the longitudinal momentum fraction, x, but also on the transverse momentum of the parton. These objects can yield transverse momenta comparable to, or even larger than, M_Q to the final state. This is indeed possible in the Regge limit $\hat{s} \gg m_{TQ}$. For a more detailed review of the LT HEF and its connection to quarkonium physics, see Section 4.3 of Ref. [33].

It has been shown earlier [142,143] that the phenomenological framework based on HEF with KMRW uPDF is capable of reproducing the J/ψ photoproduction data from HERA. This is already the case with the HEF coefficient function computed at LO in α_s and in the CS approximation of NRQCD, as illustrated by the left panel of Fig. 3.5 obtained with the version of KMRW uPDF introduced in the Ref. [144]. We note that the transverse-momentum integral of the uPDF exactly reproduces the input gluon PDF. The precise fulfilment of this normalisation condition both at $x \ll 1$ and $x \sim 1$ is important to avoid contradictions between LT HEF and NLO Collinear Factorisation (CF) predictions for the J/ψ prompt hadroproduction P_T spectrum in pp collisions at low energies, in particular at $\sqrt{s_{pp}} = 24$ GeV for the planned Spin-Physics-Detector experiment at the NICA facility [145,146].

From Fig. 3.5 (left), one can see that there is still some room for additional contributions on top of the LO CS contribution from the fusion of a photon and a Reggeon $\gamma(q) + R(x_1, \mathbf{q}_{T1}) \to c\bar{c}[^3S_1^{[1]}] + g$. These could be from $c\bar{c}[^3S_1^{[1]}] + c$ considered above (see Fig. 3.4) and from CO contributions. The large scale uncertainty of the LO HEF prediction, shown in the Fig. 3.5, comes from the variation of μ_R and μ_F around their default value of $m_{TJ/\psi}$. Clearly, the uncertainty has to be reduced via the inclusion of the NLO corrections to make such predictions more precise.

The comparison between LT HEF predictions for the EIC energy $\sqrt{s_{ep}} = 140$ GeV and the full NLO CF CSM predictions (computed using FDC [148]) is shown in Fig. 3.5 (right). The latter prediction is evaluated at a special value of the factorisation scale, $\mu_F = 1.7m_c$, chosen [147] to minimise the NLO correction coming from the region of $\hat{s} \gg M_{J/\psi}^2$ (see Section 4.1.1). There is a good agreement between these NLO predictions at the optimal scale and LO HEF predictions at the default scale $\mu_R = \mu_F = m_{T,J/\psi}$: this indicates that the effects of the $\ln(\hat{s}/M_{J/\psi}^2)$ resummation can be reproduced by the optimal factorisation scale choice at EIC energies and that the NLO CF prediction with the optimal scale is robust. At higher photon–nucleon collision energies, a matched calculation between LL HEF and NLO CF predictions, similar to that done in Ref. [149], is necessary [150] to correctly capture the high-energy resummation effects at $\hat{s} \gg M_{J/\psi}^2$ while staying at NLO accuracy for $\hat{s} \sim M_{J/\psi}^2$.
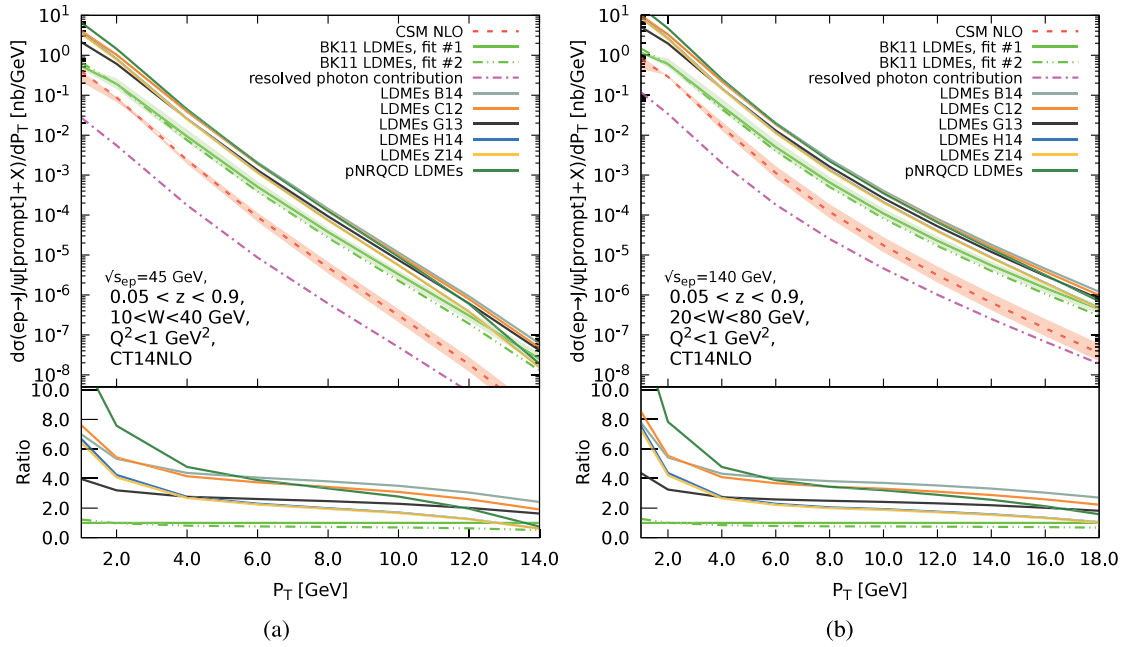
Fig. 3.6. Predictions using NRQCD at NLO for the J/ψ transverse momentum (P_T) differential prompt-J/ψ photoproduction cross section in the EIC kinematic conditions: (a) $\sqrt{s_{ep}}$ = 45 GeV and (b) $\sqrt{s_{ep}}$ = 140 GeV for the various LDME sets listed in Table 3.1 as well as of the CSM (dashed line, $\langle \mathcal{O}^{J/\psi} \left[{}^3S_1^{[1]} \right] \rangle$ = 1.45 GeV^3) are shown. The scale-variation uncertainty bands are only plotted for the prediction of the BK LDME set [111] as well as for the CSM. The resolved-photon contribution also refers to the BK LDME set. The AGF [153] photon PDF set has been used. The calculation of the short-distance cross sections is based on [77,110].

3.2.3. Testing NRQCD factorisation at the EIC

Prompt J/ψ yields in inclusive photoproduction. We plot in Figs. 3.6 and 3.7 the NLO NRQCD factorisation predictions for the P_T- and z-differential photoproduction cross section of prompt J/ψ mesons in the EIC kinematic conditions. These predictions have been calculated using the short-distance cross sections of Refs. [77,110] and the LDME sets listed in Table 3.1. All LDME sets fitted only to the hadroproduction data predict a significantly (factor 3 to 6) higher J/ψ photoproduction cross section than the LDME set of Table 1 of Ref. [111], denoted as "LDMEs Kniehl, Butenschön, fit # 1" in Figs. 3.6 and 3.7, which includes the photoproduction data from HERA. We also plot the predictions performed with another set of LDMEs from the same paper, denoted as "LDMEs Kniehl, Butenschön, fit # 2". The latter set of LDMEs had been fitted to the prompt J/ψ hadro- and photoproduction data corrected approximately for feed-down contributions from heavier charmonium states using constant feed-down fractions. For this fit, we calculate the feed-down contributions from $\chi_{c0,1,2}$ and $\psi(2S)$ decays to J/ψ using the χ_c LDMEs from Ref. [151] and the fit for $\psi(2S)$ LDMEs performed in Ref. [152]. Calculating the feed-down contribution in this way is consistent with the treatment of feed-down in Ref. [111].

As expected, the predictions from both Kniehl–Butenschön LDMEs are reasonably close to each other. Yet, they differ from those obtained with the other LDME sets fit to hadroproduction data. This is mostly because the latter sets predict a more pronounced $z \to 1$ growth of the cross section (see Fig. 3.7) than the global fit LDME sets of Ref. [111] which, when integrated over z, translates into larger P_T differential cross sections. This increase is due to both the ${}^1S_0^{[8]}$ and ${}^3P_J^{[8]}$ CO states.

It is important to note that such a rapid increase of the spectrum towards $z \to 1$ is not a feature of the HERA data. Including these data in LDME fits calls for a compensation between contributions of $\langle \mathcal{O}^{J/\psi} \left[{}^1S_0^{[8]} \right] \rangle$ and $\langle \mathcal{O}^{J/\psi} \left[{}^3P_J^{[8]} \right] \rangle$ LDMEs resulting in different signs for these as in the LDME sets of Ref. [111]. Therefore the photoproduction data essentially fix the latter LDMEs and do not allow anymore to adjust them to describe the polarisation observables in hadroproduction, which leads to the polarisation puzzle discussed above. The EIC measurements will allow us to check the robustness of this feature of NRQCD predictions against variation of collision energy, since larger radiative corrections at $z \to 1$ could be expected at higher energies of the HERA collider.

The resolved-photon contribution manifests itself in the opposite region $z \ll 1$ (Fig. 3.7) and EIC data are less sensitive to it than HERA data, again due to lower collision energies. Therefore the cleaner test of process-independence of LDMEs can be performed with EIC photoproduction data rather than with HERA data.

Prompt J/ψ yields in Q^2-integrated lepton–nucleon interactions. Another possibility to study the contributions of various LDMEs is to consider *single-inclusive* production of J/ψ in ep collisions, without detecting the final-state electron, as was pioneered recently in Ref. [154]: $e(\ell) + h(p) \to J/\psi(P_{J/\psi}) + X$. The rapidity ($y$) and transverse momentum (P_T) distributions of J/ψ inclusive production at the EIC are promising observables for both studying the production mechanism of heavy quarkonia and extracting PDFs, in particular, the gluon PDF, complementary to other observables described in Section 4.1.
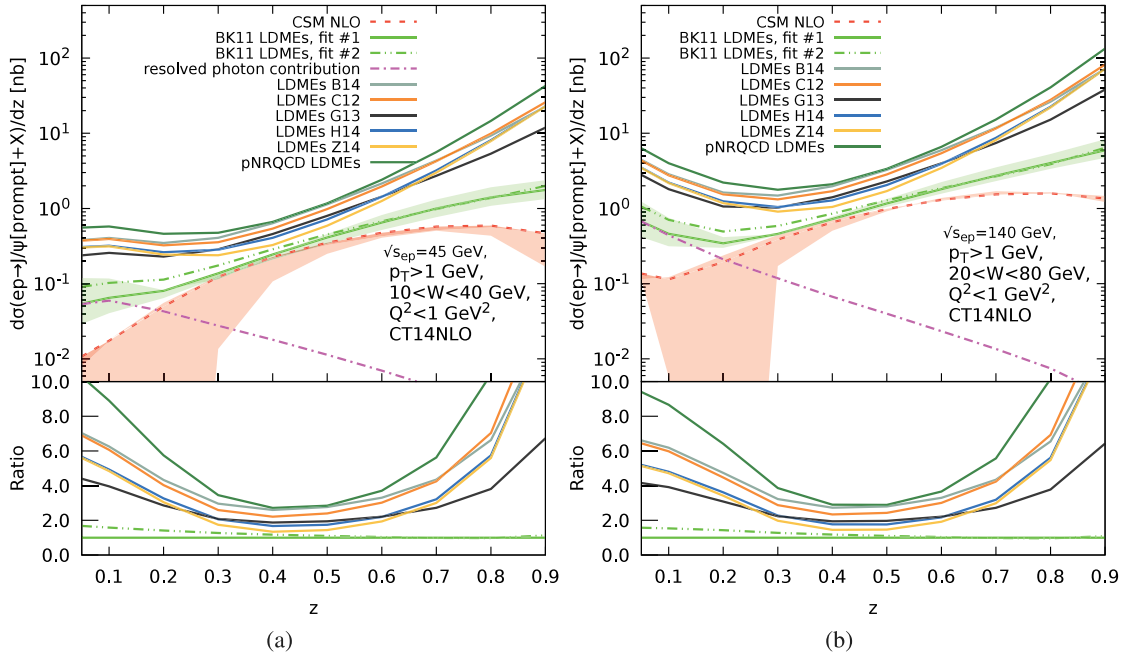
Fig. 3.7. Same as Fig. 3.6 but for the z-differential cross section.

When the transverse momentum of J/ψ defined relatively to the lepton–hadron collision axis P_T is much larger than m_c, the perturbative hard coefficient functions for producing the $c\bar{c}$ pair receive large higher-order QCD corrections that are enhanced by powers of $\ln(P_T^2/m_c^2)$. Such logarithmically-enhanced higher-order corrections can be systematically resummed and factorised into FFs [106,155–158]. On the other hand, when $P_T \gtrsim m_c$, the perturbative hard coefficients at a fixed order in α_s should be sufficient.

In addition, the occurrence of a hard partonic collision producing the J/ψ with large transverse momentum $P_T \gg m_e$ necessarily induces multiple photon emissions from the incoming lepton, leading to large higher-order QED corrections enhanced by powers of $\ln(P_T^2/m_e^2)$. As we discussed in Section 2.3.2, these QED corrections can also be systematically factorised and resummed into universal LDFs [51,52]. In order to predict the production rate of J/ψ at the EIC, a new factorisation formalism, which takes into account both collision-induced QCD and QED radiation and provides a systematic transition from $P_T \gtrsim m_c$ to $P_T \gg m_c$, was introduced [91,159]. The factorisation formula for the inclusive production cross section is given by:

$$
E_{J/\psi} \frac{d\sigma_{eh\to J/\psi(P_{J/\psi})X}}{d^3\mathbf{P}_{J/\psi}} = \sum_{a,b} \int dx_a\, f_{a/e}(x_a, \mu_F^2) \int dx_b\, f_{b/h}(x_b, \mu_F^2)
$$
$$
\times \left[E_{J/\psi} \frac{d\tilde{\sigma}_{ab\to J/\psi(P_{J/\psi})X}^{\mathrm{Resum}}}{d^3\mathbf{P}_{J/\psi}} + E_{J/\psi} \frac{d\tilde{\sigma}_{ab\to J/\psi(P_{J/\psi})X}^{\mathrm{NRQCD}}}{d^3\mathbf{P}_{J/\psi}} - E_{J/\psi} \frac{d\tilde{\sigma}_{ab\to J/\psi(P_{J/\psi})X}^{\mathrm{Asym}}}{d^3\mathbf{P}_{J/\psi}} \right],
\tag{3.4}
$$

where indices a, b, in principle, run, respectively, over all lepton and parton flavours, but in practice, as an approximation, a takes into account only $(e, \gamma, \bar{e})$. The functions $f_{a/e}(x_a, \mu_F^2)$ and $f_{b/h}(x_b, \mu_F^2)$ are the LDFs of an electron and the usual parton PDFs respectively, depending on partonic momentum fractions, x_a and x_b. The LDFs satisfy the DGLAP-like μ_F-evolution equations mixing the QED and QCD splittings [159]. In Eq. (3.4), the partonic cross sections $\tilde{\sigma}_{ab\to J/\psi(P_{J/\psi})X}$ are computed with all the perturbative collinear singularities along the direction of colliding lepton (a) and parton (b) removed. These singularities are absorbed into $f_{a/e}$ and $f_{b/h}$, respectively.

The cross section $d\tilde{\sigma}^{\mathrm{Resum}}$ in Eq. (3.4) represents the partonic cross section with the $\ln(P_T^2/m_c^2)$ contributions being resummed to describe the J/ψ production rate for $P_T \gg m_c$, as we have mentioned above. In $\tilde{\sigma}^{\mathrm{NRQCD}}$, the production of $c\bar{c}[^{2S+1}L_J^{[1,8]}]$-state at the perturbative stage is computed at fixed order in α_s and the corresponding non-perturbative formation of a J/ψ from a produced $c\bar{c}$ pair is taken care using the NRQCD velocity expansion and universal NRQCD LDMEs. This part of the cross section should provide a good description of the J/ψ production rate when $P_T \sim m_c$. Finally, $\tilde{\sigma}^{\mathrm{Asym}}$ is equal to a fixed-order expansion of $\bar{\sigma}^{\mathrm{Resum}}$ to the same order in α_s as in $\tilde{\sigma}^{\mathrm{NRQCD}}$. The latter part is needed to remove the double counting between $\tilde{\sigma}^{\mathrm{Resum}}$ and $\tilde{\sigma}^{\mathrm{NRQCD}}$. By including all these three terms, this factorisation formalism can be applied to both lepton–hadron and hadron–hadron collisions, as well as e^+e^- collisions [91,160], providing a smooth transition when observed $P_T \sim m_c$ increases to $P_T \gg m_c$.
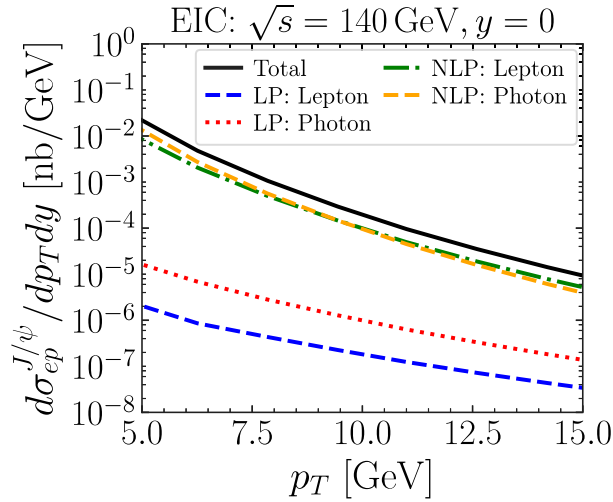
Fig. 3.8. The J/ψ transverse momentum (P_T) distribution of the inclusive J/ψ production cross section in electron–proton collisions in the electron–hadron centre-of-mass frame without tagging the scattered electron, computed by using the new factorisation formalism in Eq. (3.4) [159]. The solid black line (overlap with the dashed orange line) is for the total contribution, which is dominated by the subprocess: $\gamma + g \to [c\bar{c}] + g$ (NLP Photon) and $e + g \to [c\bar{c}] + e$ (NLP Lepton) with the $c\bar{c}$ pair fragmenting to J/ψ, while others represent contributions from other subprocesses, see the text for details.

The predictive power of Eq. (3.4) relies on the factorisation of each term and our ability to calculate them. Up to next-to-leading power corrections in m_c/P_T, the $\tilde{\sigma}^{\text{Resum}}$ can be factorised as [106,156–158],

$$
E_{J/\psi} \frac{d\tilde{\sigma}^{\text{Resum}}_{ab \to J/\psi(P_{J/\psi})X}}{d^3 \mathbf{P}_{J/\psi}} \approx \sum_k \int \frac{dz}{z^2} D_{k \to J/\psi}(z, \mu_F^2) E_k \frac{d\hat{\sigma}_{ab \to k(p_k)X}}{d^3 \mathbf{p}_k}(z, p_k = P_{J/\psi}/z, \mu_F^2) \tag{3.5}
$$
$$
+ \sum_\kappa \int \frac{dz}{z^2} D_{[c\bar{c}(\kappa)] \to J/\psi}(z, \mu_F^2) E_k \frac{d\hat{\sigma}_{ab \to [c\bar{c}(\kappa)](p_k)X}}{d^3 \mathbf{p}_c}(z, p_k = P_{J/\psi}/z, \mu_F^2),
$$

where $k = q, g, \bar{q}$ and $\kappa = v, a, t$ for $c\bar{c}$ pairs respectively in a vector, axial–vector or tensor spin state [157,158]. The first and second terms are the factorised leading power (LP) and next-to-leading power (NLP) contributions to the cross section in its $1/P_T$ expansion. The corrections to Eq. (3.5) are suppressed by $1/P_T^4$ and cannot be further factorised [161]. The universal single-parton and double-parton ($c\bar{c}$) FFs, $D_{c \to J/\psi}(z, \mu_F^2)$ and $D_{[c\bar{c}(\kappa)] \to J/\psi}(z, \mu_F^2)$, respectively, satisfy a closed set of evolution equations with respect to changes of the factorisation scale μ_F [157,158]. Solving these evolution equations one resums the logarithmic contributions scaling like $\ln(P_T^2/m_c^2)$ to these FFs. The universal FFs at an input scale $\mu_F = \mu_0 \simeq 2m_c$ can be calculated assuming NRQCD factorisation [61] in terms of universal NRQCD LDMEs,

$$
D_{c \to J/\psi}(z, \mu_0^2) \approx \sum_{c\bar{c}[^{2S+1}L_J]} \hat{d}_{c \to c\bar{c}[^{2S+1}L_J]}(z, \mu_0^2) \langle O^{J/\psi}_{c\bar{c}[^{2S+1}L_J]}(0) \rangle, \tag{3.6}
$$

$$
D_{[c\bar{c}(\kappa)] \to J/\psi}(z, \mu_0^2) \approx \int_{-1}^1 du \int_{-1}^1 dv \, \mathcal{D}_{[c\bar{c}(\kappa)] \to J/\psi}(z, u, v, \mu_0^2) \tag{3.7}
$$
$$
\approx \sum_{c\bar{c}[^{2S+1}L_J]} \hat{d}_{[c\bar{c}(\kappa)] \to c\bar{c}[^{2S+1}L_J]}(z, \mu_0^2) \langle O^{J/\psi}_{c\bar{c}[^{2S+1}L_J]}(0) \rangle.
$$

Eq. (3.7) involves further approximations, neglecting possible differences between the momentum fractions carried by the $c\bar{c}$ pair in the amplitude, u, and its complex-conjugate, v, which can be taken into account through the more general FF $\mathcal{D}_{[c\bar{c}(\kappa)] \to J/\psi}$, defined in [157]. The approximation in the second line of Eq. (3.7) reflects the fact that the integral of this function is dominated by the vicinity of $u = v = 1/2$ [91,160].

The formalism described above has been already tested partially in the case of pp collisions, where instead of LDFs in Eq. (3.4) one substitutes the proton PDFs. With perturbatively calculated short-distance matching coefficients for both single-parton and $c\bar{c}$-pair FFs at the input scale [162,163] and solving the coupled evolution equations for these FFs, the factorised and resummed cross section in Eq. (3.5) describes the P_T distribution of J/ψ production at the LHC and Tevatron [91,160] for $P_T > 10$ GeV, as we note in Table 3.1. At the LHC energies, the LP contributions, namely the first term in Eq. (3.5), dominate when $P_T \gg 20$ GeV, while the NLP contributions, namely the second term in Eq. (3.5), are comparable at $P_T \sim 20$ GeV and become dominant when P_T further decreases, which is critically important to describe the shape of the observed P_T distribution.

Making predictions of the P_T distribution of inclusive J/ψ production at the EIC requires the knowledge of the universal LDFs. In Fig. D.1 of Appendix D, the scale dependence of the LDFs with and without the mixing of QED and QCD evolution is shown. Like in any factorisation approach, the perturbatively calculated short-distance partonic cross section, such as $\hat{\sigma}_{ab \to k(p_k)X}$ in Eq. (3.5), does not depend on the details of the hadronic state produced. It has been calculated for single hadron production at LO [164], at

NLO [165,166], and at NNLO [167,168]. The fixed-order calculation for $\bar{\sigma}^{\text{NRQCD}}$ has been carried out in NRQCD up to NLO [154].

In Fig. 3.8, we present the predictions of the P_T distribution of inclusive J/ψ production in ep collisions at the EIC for $\sqrt{s_{ep}} = 140$ GeV. For these predictions, only the $\bar{\sigma}^{\text{Resum}}$ term in Eq. (3.4) is used and the same LDMEs that we used for describing the J/ψ production at the LHC and Tevatron energies [91] are taken here. These LDMEs are close to those from the Chao et al. [114] fit (H14) mentioned in Table 3.1. The CT18ANLO PDF central set [169] was used for the proton PDFs. Unlike J/ψ production at the LHC and the Tevatron, the reach in the J/ψ P_T defined with respect to the lepton–hadron axis, is much smaller due to the smaller collision energy. The solid line in Fig. 3.8 refers to the total contribution, which is dominated by the subprocess $\gamma + g \rightarrow [c\bar{c}] + g$ (NLP Photon) and $e + g \rightarrow [c\bar{c}] + e$ (NLP Lepton) with the $c\bar{c}$ pair fragmenting into J/ψ. The lepton or photon initiated LP contribution to the production cross section, namely the first term in Eq. (3.5), is dominated by the lowest-order subprocesses, such as $e + q \rightarrow e + q$ or $\gamma + q \rightarrow g + q$, respectively, with a produced parton fragmenting into the observed J/ψ, and is strongly suppressed by the single-parton FFs at the EIC energy. In summary, the LP contributions are essentially irrelevant in the EIC kinematics. Therefore, a matching to the fixed-order calculations (described above in this section), including the second and third terms in Eq. (3.4), is awaited for.

Polarisation of J/ψ in inclusive photoproduction. Since the prediction [170] in 1994 of a transversely-polarised J/ψ hadroproduction yield at high P_T, much hope has been put in polarisation measurements to advance our understanding of quarkonium production, with a very limited success though [9]. For charmonium hadroproduction, a dozen of measurements of J/ψ polarisation (also referred to as spin-alignment) have been carried out at the Tevatron [171,172], RHIC [42,173–175] and the LHC [176–181], half a dozen for $\psi(2S)$ [171,172,178,179,181,182] while the relative polarisation of χ_{c1} and χ_{c2} has been measured by CMS [183]. For bottomonia, half a dozen of $\Upsilon(1S)$ polarisation hadroproduction studies have been carried out [184–188], four for $\Upsilon(2S)$ [185–188] and three for $\Upsilon(3S)$ [185,187,188]. As regards photoproduction, NLO CSM computations of polarisation observables were performed in 2009 [189,190] and subsequently completed with the COM NRQCD contributions in 2011 [191] without clear conclusions owing to the large uncertainties in the H1 [101] and ZEUS [192] data and in the theory.

In Figs. 3.9 and 3.10, we show the NLO NRQCD predictions for the P_T and z dependence of the polarisation parameter λ_θ of promptly photoproduced J/ψ mesons in the EIC kinematic conditions. These predictions include CS and CO contributions using the LDME sets discussed in Section 3.2.1 as well as direct and resolved-photon interaction contributions (see Figs. 3.6 and 3.7 for the corresponding differential cross-section plots). As one can see from Fig. 3.9, the P_T-dependent NRQCD predictions for all LDME sets are roughly consistent with unpolarised production ($\lambda_\theta = 0$ in all frames), unlike the predictions of the CSM, which leads to significant polarisation of photo produced J/ψ mesons. In the z-dependent case, the region of $z \rightarrow 1$ has the most discriminating power between different LDME sets. We however have reasons to doubt the relevance of these predictions given that all but the BK11 LDMEs are unable to describe the corresponding HERA data. From Figs. 3.9 and 3.10, one also observes that the detailed behaviour of λ_θ for different LDME sets is significantly different for different polarisation frames, which could be an important tool for additionally constraining the theory.

Polarisation of J/ψ in electroproduction. The HERA collider experiments provided some results on the J/ψ polarisation, mostly for photoproduction [193,194], but unfortunately these data do not allow to favour or disfavour different models and/or approaches. The reasons behind this are twofold: data were not precise enough and they were collected in regions where theoretical predictions are very close to each other [191,193]. Furthermore in Ref. [195], Yuan and Chao showed that the estimates for the λ_θ parameter in SIDIS, within both the CSM and NRQCD approaches, are overlapping for most of the values of the variable z. In this respect EIC could play a crucial role: highly precise data are expected and other/extended kinematical regions could be explored.

In the following, we present some predictions at LO, both in the CSM and NRQCD frameworks, adopting different NLO LDME sets. Some comments are therefore in order: (i) as previously discussed, the combined usage of NLO hard scattering with NLO LDMEs is subject to great caution. As of now, only the CSM part of the electroproduction cross section has been computed at NLO [197]. The only full NRQCD analysis has been performed at LO [198] and show mixed agreements between the different NRQCD predictions and HERA data; (ii) a number of quarkonium-production processes exhibit very large QCD corrections to polarisation observables [70,72,112,128,189,190,199]. The following LO results should therefore only be considered as a simple guidance for future measurements and certainly not as quantitative predictions to which future measurements should be confronted to. In this context, a NLO NRQCD analysis of electroproduction is eagerly awaited for.

Fig. 3.11 shows some estimates for the λ_θ parameter at the centre-of-mass energy $\sqrt{s_{ep}} = 45$ GeV together with their uncertainty bands, visible mostly for the CSM and obtained by varying the factorisation scale in the range $\mu_0/2 < \mu_F < 2\mu_0$, with $\mu_0 = \sqrt{M_{J/\psi}^2 + Q^2}$. The integration regions are detailed in the legend box. No uncertainty bands from LDMEs are included, instead predictions for different sets are presented: C12 [114], BK11 [111] and G13 [115]. This illustrates their impact on the results. From Fig. 3.11, it is clear that the λ_θ value can be significantly different if we consider different frames. In particular, the *Gottfried–Jackson* frame provides the better overall separation between CSM and NRQCD curves.

Another possibility offered by the EIC experiment is the collection of data at different energies. In Fig. 3.12, the impact coming from the energy variation on CSM and NRQCD predictions is shown. In this case, only the central values are presented ($\mu_F = \mu_0$); for the lower energy, $\sqrt{s_{ep}} = 45$ GeV, the integration region is the same as in Fig. 3.11, while for $\sqrt{s_{ep}} = 140$ GeV a wider W integration is considered (see legend). Even focusing on one specific frame, like the helicity frame in Fig. 3.12, one clearly sees that the CSM is more affected by the energy shift. Note that moving to higher energies allows one to access contributions with higher virtuality, with an interesting effect: in the CSM these contributions are opposite to the lower virtuality ones (reducing the size of the estimates), while in NRQCD this phenomenon is less important. It however remains to be shown that such discriminant effects remain at NLO.
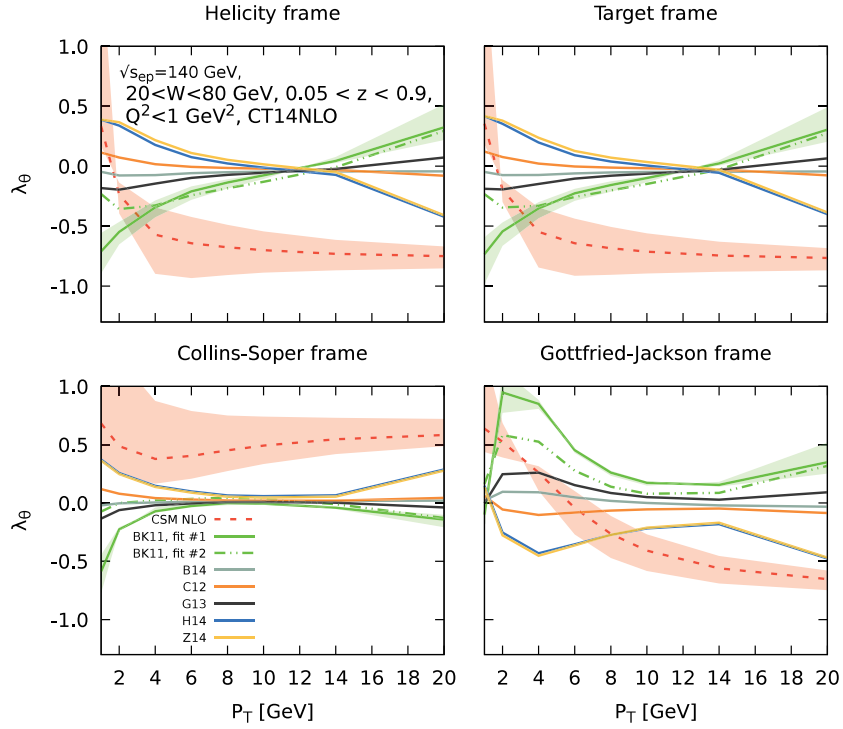
Fig. 3.9. The NLO NRQCD factorisation predictions for the J/ψ transverse momentum (P_T) dependence of the λ_θ polarisation parameter in prompt-J/ψ photoproduction for the EIC kinematic conditions. Central predictions using the LDME sets listed in Table 3.1 as well as for the CSM are shown. The scale-variation uncertainty bands are plotted for the prediction of the LDME set of Kniehl and Butenschön [111] as well as for the CSM. The calculation of the short-distance cross sections is based on [191].
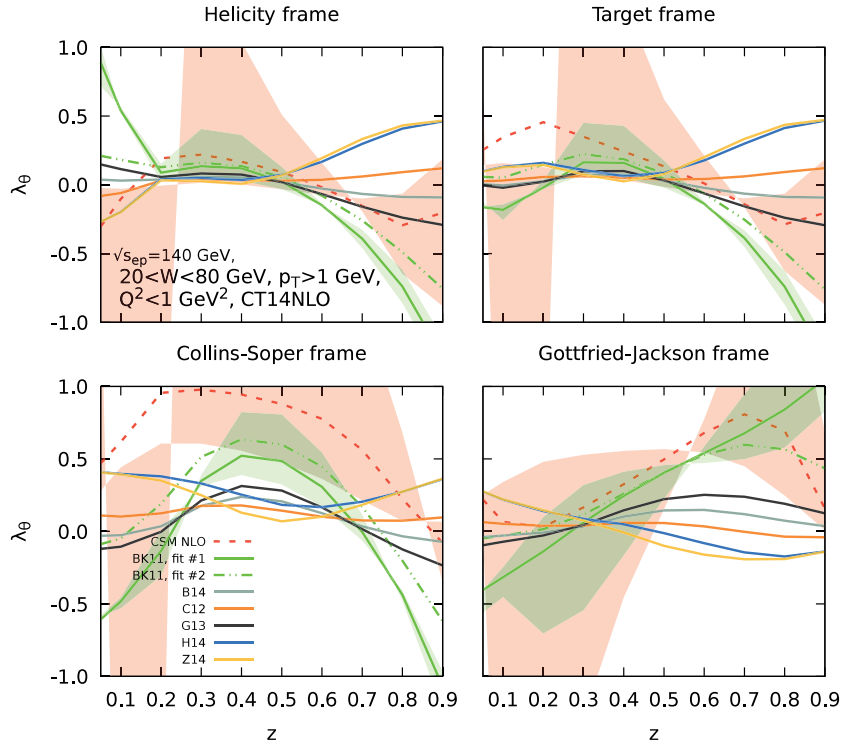
Fig. 3.10. Same as Fig. 3.9 but for the z-differential cross section.
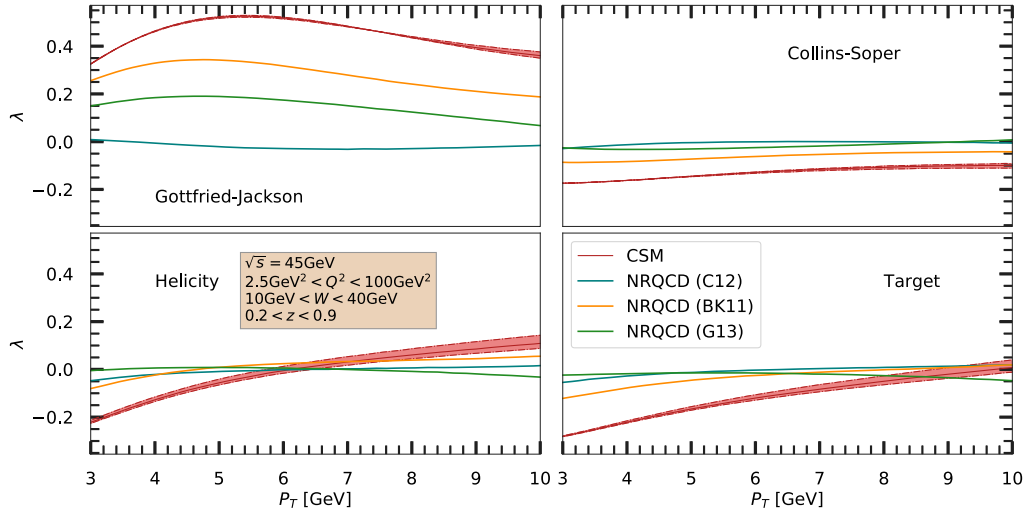
Fig. 3.11. Predictions for the λ_θ parameter for J/ψ electroproduction (or SIDIS) at $\sqrt{s_{ep}} = 45$ GeV as a function of the J/ψ transverse momentum, P_T, for different frames and models; bands refer to the variation of the scale $\mu_0/2 \leq \mu_F \leq 2\mu_0$. Kinematic cuts are given in the legend. Plot based on Ref. [196].
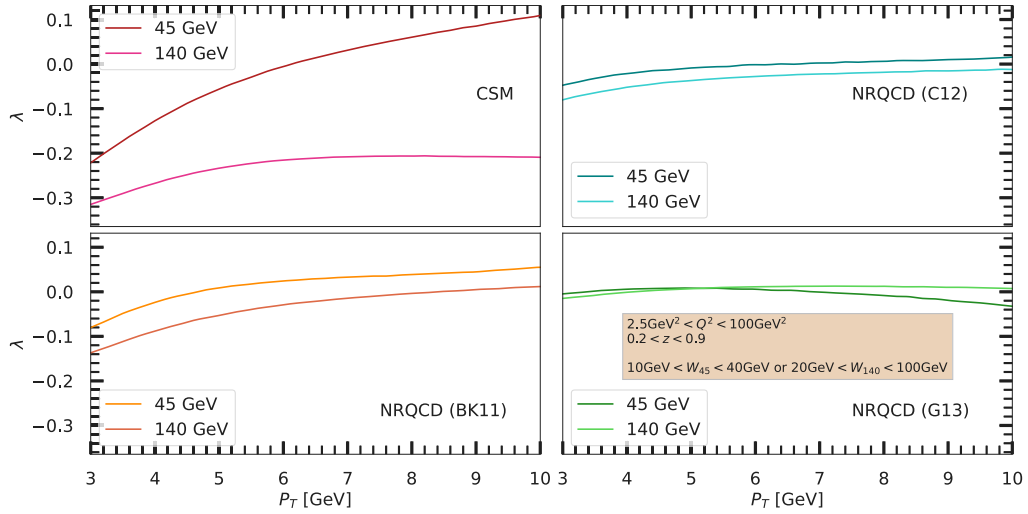
Fig. 3.12. Predictions for the $\lambda \equiv \lambda_\theta$ parameter in the helicity frame in J/ψ electroproduction (or SIDIS) as a function of the J/ψ transverse momentum, P_T, for different LDME fits at $\sqrt{s_{ep}} = 45$ GeV and 140 GeV. Only central value estimates ($\mu_F = \mu_0$) are shown. Kinematic cuts are given in the legend.

Prompt η_c and χ_c yields. As mentioned in Section 3.1.1, the dominance of the CS mechanism in prompt-η_c hadroproduction at $P_T \gtrsim M_{\eta_c}$ was not expected by NRQCD factorisation. Therefore, from the point of view of studies of the heavy-quarkonium production mechanism, it is important to understand if this feature of η_c production persists also in ep collisions. If it is indeed the case, then η_c hadro-, photo- and leptoproduction can be used as a tool for hadron-structure studies with a reduced uncertainty stemming from the CO mechanism compared to production of other charmonium states.

In recent works [200,201], η_c photo- and electroproduction cross sections were computed including all the CO and CS contributions at LO in α_s. In the case of photoproduction [200], both direct-photon and resolved-photon interactions were taken into account. The CS contribution had been assumed to be negligible in earlier studies [202,203], because the corresponding direct-photon interaction subprocess appears at $\mathcal{O}(\alpha\alpha_s^3)$ due to the necessity of two-gluon radiation in the final state to produce a $c\bar{c}[^1S_0^{[1]}]$ pair and because resolved-photon contributions were assumed to be small. However, it was found [200] that the resolved-photon subprocesses make the CS contribution to the photoproduction cross section non-negligible. These predictions, updated with the use of CT14LO PDFs, are shown in Figs. 3.13 and 3.14. The CO contributions were computed by converting the J/ψ CO LDME sets listed in Table 3.1 to the η_c LDMEs through HQSS relations valid up to v^2 corrections. As one can see from these figures, the CO contributions are still important and the cross section at $z > 0.5$ strongly depends on the LDME choice.

For electroproduction [203], the CS contribution is also sizeable, but for a different reason, namely an additional Q^2-dependent term appearing in the short-distance cross section. Of course, the main problem of the predictions for η_c production in ep collisions
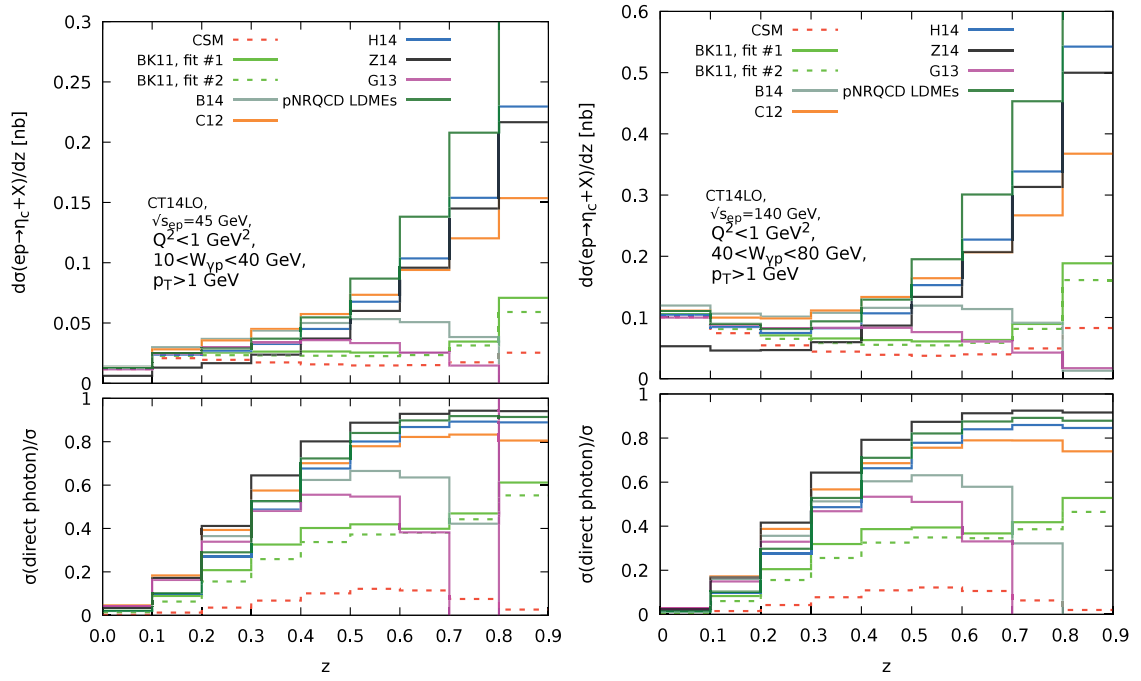
Fig. 3.13. LO CF predictions for η_c inclusive photoproduction distributions as a function the elasticity z in the EIC kinematics using HQSS and the LDME sets mentioned in Table 3.1. The calculation of the short-distance cross sections is based on Refs. [200,201]. The bottom plots show the fraction of direct-photon interaction contributions.
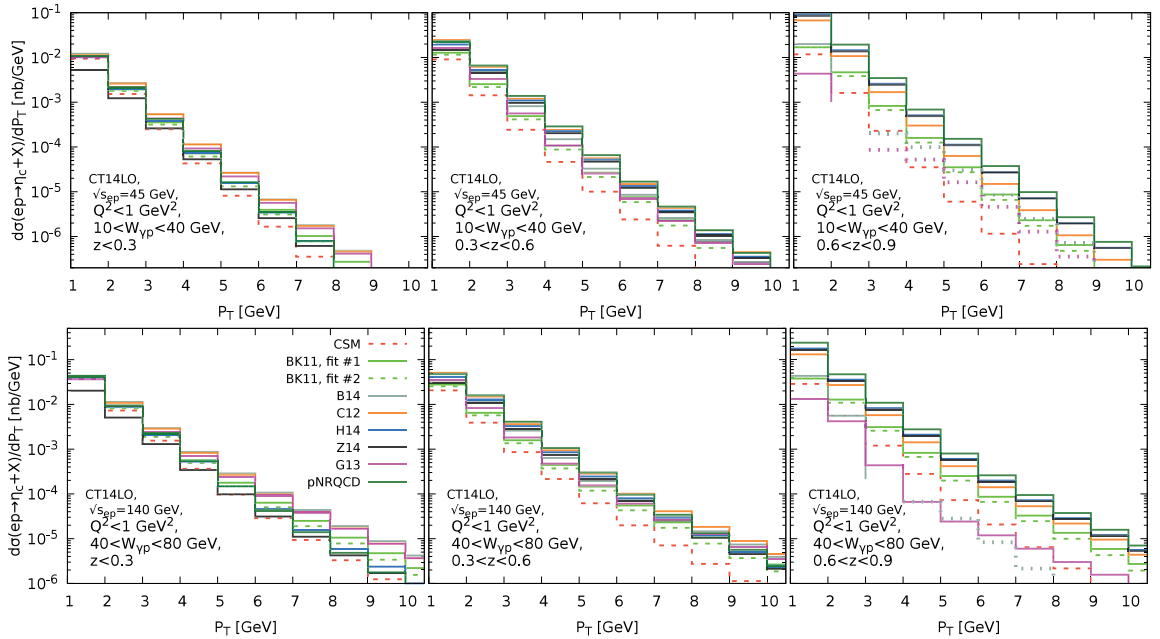

Fig. 3.14. LO CF predictions for η_c inclusive photoproduction distributions in the η_c transverse momentum P_T in the EIC kinematics using the LDME sets mentioned in Table 3.1. The calculation of short-distance cross sections is based on Refs. [200,201]. The negative values of the cross sections are plotted with the dotted histograms.

is that they so far have been done only at LO in α_s. The NLO corrections could be particularly important for the CS $^1S_0^{[1]}$ state whose LO contribution is highly suppressed at $P_T \gtrsim M_{\eta_c}$ in photo- and leptoproduction in comparison to CO states, especially $^3S_1^{[8]}$. As
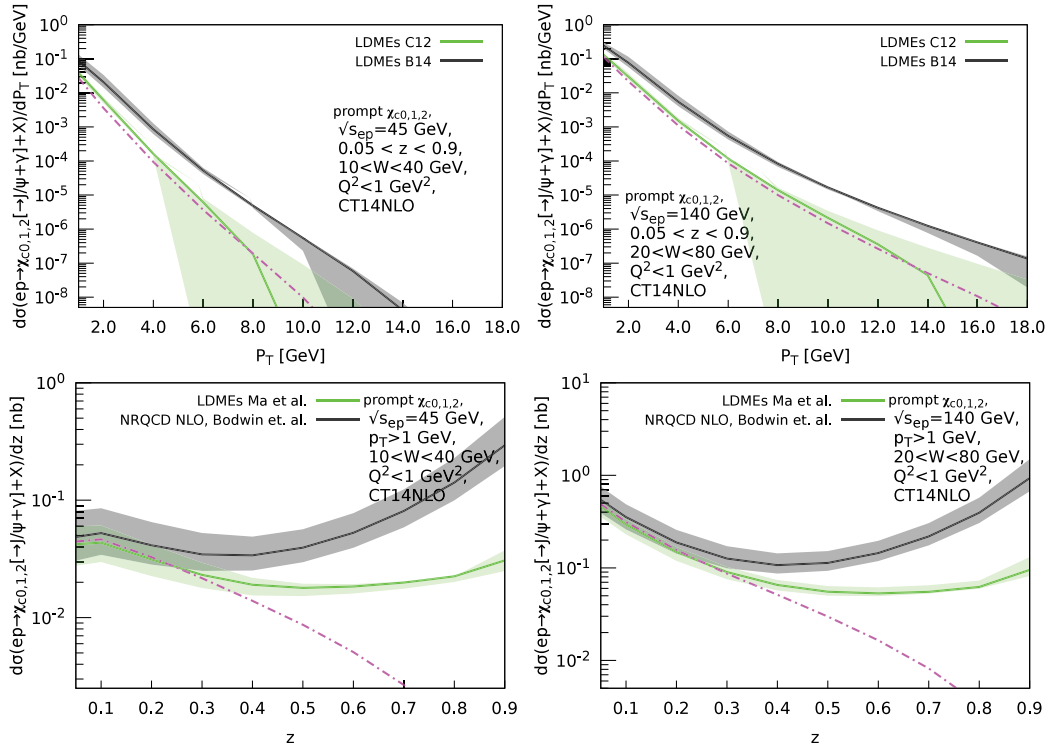
Fig. 3.15. NLO NRQCD factorisation predictions for cross sections differential in the χ_c transverse momentum (P_T) and the elasticity (z) for the photoproduction of prompt $\chi_{c0,1,2}$ mesons at the EIC using the LDMEs obtained by Ma et al. [151] (which is compatible with the treatment of feed down to J/ψ of Ref. [111]) and by Bodwin et al. [86]. Only these sets lead to positive photoproduction cross sections. The resolved-photon contribution for the LDME set of Ma et al. is shown by the dash-dotted line. The AGF [153] photon PDF set has been used. The calculation of the short-distance cross sections is based on [77,110]. The $\psi(2S) \to \chi_c$ feed down has been included.

known from J/ψ production, this suppression will be lifted by large NLO corrections [68,76]. The NLO calculation, at least in the CS channel, should be done before drawing conclusions about the importance of the CS mechanism in η_c production at the EIC.

Besides J/ψ and η_c production, it is also essential to study $\chi_{c0,1,2}$ states at the EIC. Indeed, the measurements of inclusive hadroproduction of χ_c and χ_b at the Tevatron, RHIC and the LHC [204–212] have been instrumental to uncover the various quarkonium-production puzzles [9,27,28,30]. Photo- or electroproduction of these mesons has not been observed experimentally yet. NLO NRQCD predictions for the photoproduction cross sections of $\chi_{c0,1,2}$ radiatively decaying to J/ψ are shown in Fig. 3.15. They are based on known calculations of short-distance cross sections for J/ψ photoproduction [77,110] and the χ_{c0} LDME values obtained in hadroproduction fits by Ma et al. [151], respectively Bodwin et al. [86]. We remark that the former χ_{c0} LDME values are also those used by Gong et al. in Ref. [119] and in the LDME set denoted "Kniehl, Butenschoen, fit #2" in Figs. 3.6 and 3.7. We remind the reader that for P−wave production at NLO in NRQCD, one cannot make a clear distinction between CO and CS contributions as they directly depend on the NRQCD factorisation scale, μ_Λ.

It is an expected feature that resolved photon contributions dominate photoproduction at low z. Interestingly, however, the predictions of Fig. 3.15 are dominated by the resolved-photon contribution already for z below 0.5. Moreover, it is only due to the resolved photons that the χ_c cross sections are positive at low z after all. This feature of the theoretical predictions may indicate our poor understanding of χ_c photoproduction, but if confirmed, the photoproduction of these mesons could serve as a useful source of information about the poorly known gluon component of photon PDFs.

3.3. Learning about quarkonia from TMD observables

3.3.1. LDME constraints from TMD observables

One important reason to investigate quarkonium production at the EIC is the possibility to probe TMDs that have not been extracted from experiments yet. The semi-inclusive heavy vector quarkonium production process, $e\,p \rightarrow e'\,J/\psi\,(\Upsilon)\,X$ at small transverse momentum, P_T, is expected to offer a promising probe of gluon TMDs,[8] as will be discussed extensively in Section 4.

---

[8] Due to the presence of the large scale given by the quarkonium mass $M_Q \approx 2m_Q$ one can consider not only electroproduction, but in principle also the photoproduction case ($Q^2 \approx 0$). A large photon virtuality is expected to suppress background from diffraction and higher-twist effects [213]. To our knowledge, at present there are no studies of the numerical impact of such background on the photoproduction process $\gamma\,p \to J/\psi\,(\Upsilon)\,X$ in the TMD regime.

Besides gluon TMD extractions, this process may also allow for improved determinations of certain LDMEs. In this way EIC can also improve our knowledge on NRQCD.

At small P_T, the differential cross section is expected to be described in terms of TMDs. As will be discussed in detail in the next subsection, for quarkonium production, this involves TMD shape functions [214,215], rather than TMD FFs like for light hadron production. At the lowest order, $\alpha^2 \alpha_s$, the process $e\, p \to e'\, J/\psi\, (Y)\, X$ at small transverse momentum is described by photon–gluon scattering producing a heavy quark–antiquark pair in the CO state. The transition from the heavy-quark pair into the bound state is then described by a shape function. If one assumes the shape function to be a delta function in transverse momentum, one can connect to the standard NRQCD expressions for this transition. To lowest order in the strong coupling, but with the inclusion of the NNLO in v^2 $^1S_0$ and ^3P_J ($J = 0, 1, 2$) CO intermediate states [216], the resulting expression for the cross section involves two of the CO LDMEs which were discussed above, $\langle \mathcal{O} \left[^1S_0^{[8]} \right] \rangle$ and $\langle \mathcal{O} \left[^3P_0^{[8]} \right] \rangle$, for which constraints from new types of observables are clearly welcome. In this way, measurements of the transverse-momentum spectrum of $e\, p \to e'\, J/\psi\, (Y)\, X$ in the TMD regime can lead to improved determinations of these CO LDMEs. However, inclusion of higher-order corrections, in particular from the leading v CS NRQCD contributions at $\alpha^2 \alpha_s$, and the proper shape functions will be required for a robust extraction of these LDMEs.

3.3.2. TMD effects from quarkonia: shape functions

The NRQCD factorisation approach can only be applied *for transverse-momentum spectra* when the quarkonium state is produced with a relatively large transverse momentum compared to its mass, i.e. $P_T \gtrsim 2m_Q$. This is because the emissions of soft gluons from the heavy-quark pair cannot modify the large transverse momentum of the bound state. The large P_T is generated in the hard process through recoil off unobserved particles, while the infrared divergences are parametrised in terms of the well-known LDMEs, collinear PDFs and FFs, depending on the particular process under consideration.

On the contrary, when the quarkonium is produced with a small transverse momentum, all soft gluon effects can no longer be factorised in terms of standard TMD PDFs. In order to properly deal with soft-gluon radiation at small P_T in a transverse-momentum spectrum of quarkonium, it has recently been found that one needs to promote the LDMEs to the so-called TMD shape functions (TMD ShFs) [214,215]. Earlier, similar shape functions had been introduced in quarkonium photo-/leptoproduction in the endpoint region [217–219], which however are functions of z, but a more general form was discussed in [220]. On the other hand, the role of single-parton quarkonium TMD FFs, as an additional production mechanism, introduced in Refs. [221,222] needs further studies.

The newly introduced non-perturbative TMD ShFs encode the two soft mechanisms present in the process at low P_T: the formation of the bound state and the radiation of soft gluons. As a consequence, they parametrise the transverse-momentum smearing of the bound state, and carry a dependence on the factorisation and rapidity scale.

Schematically, for the production of a single quarkonium state $\mathcal{Q}$ at the EIC, with mass $M_{\mathcal{Q}}$, we have [223]:

$$d\sigma \sim F_{g/P}(b_T; \mu, \zeta) \sum_{i \in \{^1S_0^{[1]}, \dots\}} H^{[i]}(M_{\mathcal{Q}}, Q; \mu)\, \Delta^{[i]}(b_T, \mu, \zeta), \tag{3.8}$$

where $F_{g/P}$ stands for any of the eight leading-twist gluon TMDs [224], $H^{[i]}$ are the process-dependent hard scattering coefficients and $\Delta^{[i]}$ are the quarkonium TMD ShFs [214,215]. The above formula is written down in coordinate space where b_T is Fourier-conjugate to the quarkonium transverse momentum P_T^* (to be specific, in the virtual photon–proton centre of mass frame). Moreover, μ and ζ are the factorisation/resummation and rapidity scales, respectively. The summation is performed over the various colour and angular-momentum configurations (i) of the $Q\bar{Q}$ pair. Similarly to LDMEs, the TMD ShFs are of a specific order in the relative velocity v of the heavy quark–antiquark pair in the quarkonium rest frame. Therefore, the factorisation formula is a simultaneous expansion in v and $\lambda = P_T^*/M_{\mathcal{Q}}$. The operator definition of a bare[9] TMD ShF with NRQCD quantum numbers i is:

$$\Delta^{[i]}(b_T, \mu, \zeta) \propto \sum_{X_s} \langle 0| \left(\mathcal{O}_i^\dagger \mathcal{Y}_n^\dagger \right)^{ab}(b_T) |X_s\, \mathcal{Q}\rangle \langle \mathcal{Q}\, X_s| \left(\mathcal{Y}_n \mathcal{O}_i \right)^{ba}(0) |0\rangle, \tag{3.9}$$

which is just the TMD generalisation of the LDME operator definition in Eq. (3.1). On the r.h.s., the usual LDME operators $\mathcal{O}$ are evaluated at positions b_T and 0 and sandwiched between the vacuum $|0\rangle$ and the state $|\mathcal{Q}X_s\rangle$ of the produced quarkonium together with possible soft radiation carrying away colour. Moreover, these operators are multiplied by Wilson lines $\mathcal{Y}_n$ parametrising the resummation of gluons exchanged between the hard part and the state $|\mathcal{Q}X_s\rangle$.

The operator definition in Eq. (3.9) can be related to the NRQCD LDMEs by the first term in an operator product expansion (OPE) for $b_T \to 0$ [223]:

$$\Delta^{[i]}(b_T, \mu, \zeta) = \sum_n C_n^{[i]}(b; \mu, \zeta) \times \langle \mathcal{O}^{\mathcal{Q}}[n] \rangle(\mu) + \mathcal{O}(b_T). \tag{3.10}$$

In order to extend this expression to larger b_T, one can introduce a prescription like $b_T \to b_T^* \equiv b_T/\sqrt{1 + \left(b_T/b_{T,\max} \right)^2} \le b_{T,\max}$ to ensure validity of this perturbative expression and include a nonperturbative overall factor $\Delta^{[i]NP}$:

$$\Delta^{[i]}(b_T, \mu, \zeta) \equiv \Delta^{[i]NP}(b_T) \sum_n C_n^{[i]}(b_T^*; \mu, \zeta) \times \langle \mathcal{O}^{\mathcal{Q}}[n] \rangle(\mu). \tag{3.11}$$

---

[9] It is understood that the TMD ShF in the factorised cross section in Eq. (3.8) is free from rapidity divergences, i.e. it has been divided by the relevant soft factor which has also been used to properly subtract rapidity divergences in the gluon TMD $F_{g/P}$.

This expression involves the usual "collinear" LDMEs, multiplied by perturbatively calculable Wilson coefficients $C_n^{[i]}(b_T; \mu, \zeta)$ to match the expansion on pQCD, and a non-perturbative part $\Delta^{[i]NP}$ that needs to be modelled or extracted from experimental data. Note that, in principle, at higher orders in α_s, there might be operator mixing: e.g. the $^1S_0^{[8]}$ TMD ShF could become dependent on the $^3P_0^{[8]}$ LDME, hence the sum over NRQCD states n in Eq. (3.10).

In Ref. [225], the OPE of Eq. (3.10) is implemented in a practical way by studying single-inclusive J/ψ electroproduction. In the regime $P_T^{*2} \sim Q^2 \sim M_Q^2$, with P_T^* being the transverse momentum of the quarkonium in the virtual photon–proton centre-of-mass frame and μ either given by Q or by the quarkonium mass M_Q, the cross section is computed as usual in collinear factorisation. On the other hand, when $P_T^{*2} \ll \mu^2$, TMD factorisation Eq. (3.8) applies. By comparing both cross sections in the kinematical regime $\Lambda_{QCD}^2 \ll P_T^{*2} \ll \mu^2$, one can match the relevant TMD ShF onto the collinear LDMEs, confirming the need for introducing shape functions. The analysis of Ref. [225] was revised in Ref. [226], modifying the obtained expression for the shape function, but not its necessity.

To summarise, the factorisation theorem in Eq. (3.8) contains a convolution of two non-perturbative hadronic quantities at low transverse momenta: the gluon TMD PDFs and the TMD ShFs. It is therefore possible to perform a phenomenological extraction of gluon TMDs from quarkonium production processes. However, to do so, one also needs to model or extract the involved TMD ShFs. This is analogous to SIDIS where one observes a light hadron, where one needs information on the light-hadron TMD FFs in order to extract quark TMD PDFs.

3.3.3. Azimuthal $\cos 2\phi_T^*$ modulation in J/ψ electroproduction

In (semi-inclusive) quarkonium electroproduction on an unpolarised proton target, an azimuthal $\cos 2\phi_T^*$ modulation (see Section 2.3.1 for our kinematic definitions) of the differential cross section will arise from linearly polarised gluons inside the unpolarised proton. These are described by the TMD $h_1^{\perp g}$ [216,227–229].[10] In many studies the shape functions of the quarkonium are assumed and then the differential cross section can be written as:

$$d\sigma = \frac{1}{2s} \frac{d^3 l'}{(2\pi)^3 2E_l'} \frac{d^3 P_Q}{(2\pi)^3 2E_{P_Q}} \int dx \, d^2\mathbf{k}_\perp (2\pi)^4 \delta(q + k - P_Q)$$
$$\times \frac{1}{Q^4} \mathcal{L}^{\mu\mu'}(l, q) \Phi^{\nu\nu'}(x, \mathbf{k}_\perp) \, \mathcal{M}_{\mu\nu}(\mathcal{M}_{\mu'\nu'})^*, \tag{3.12}$$

where $\mathcal{M}_{\mu\nu}$ is the amplitude of production of the quarkonium $\mathcal{Q}$ in the subprocess $\gamma^* + g \to \mathcal{Q}$, $\mathcal{L}^{\mu\mu'}$ is the leptonic tensor, and the gluon correlator is given by [230–232]:

$$\Phi^{\nu\nu'}(x, \mathbf{k}_\perp) = -\frac{1}{2x} \left\{ g_\perp^{\nu\nu'} f_1^g(x, \mathbf{k}_\perp^2) - \left(\frac{k_\perp^\nu k_\perp^{\nu'}}{M_p^2} + g_\perp^{\nu\nu'} \frac{\mathbf{k}_\perp^2}{2M_p^2} \right) h_1^{\perp g}(x, \mathbf{k}_\perp^2) \right\}. \tag{3.13}$$

Here, $g_\perp^{\nu\nu'} = g^{\nu\nu'} - P^\nu n^{\nu'}/P \cdot n - P^{\nu'} n^\nu/P \cdot n$, x and $\mathbf{k}_\perp$ are the light-cone momentum fraction and transverse momentum of the gluon. The asymmetry is defined as:

$$\langle \cos(2\phi_T^*) \rangle = \frac{\int d\phi_T^* \cos(2\phi_T^*) d\sigma}{\int d\phi_T^* d\sigma}, \tag{3.14}$$

where ϕ_T^* is the azimuthal angle of the production plane of J/ψ with respect to the lepton scattering plane.

In a more complete picture of the $P_T^{*2} \ll M_{J/\psi}^2 \sim Q^2$ region, as explained in 3.3.2, the TMD factorisation applies and LDMEs are promoted to TMD ShFs. Hence, the differential cross section for this process can be recast in the following form:

$$\frac{d\sigma^{UP}}{dy \, dx_B \, d^2\mathbf{P}_T^*} = \mathcal{N} \left[\sum_n A_{UP}^{[n]} C \left[f_1^g \Delta^{[n]} \right] + \sum_n B_{UP}^{[n]} C \left[w h_1^{\perp g} \Delta_h^{[n]} \right] \cos 2\phi_T^* \right], \tag{3.15}$$

where the subscript UP on the amplitudes $A_{UP}^{[n]}$ and $B_{UP}^{[n]}$ denotes the polarisation state of the proton (U, since it is unpolarised) and of the quarkonium ($P = U, L, T$), respectively, and $\mathcal{N}$ denotes an overall normalisation factor. Here, the quarkonium polarisation is defined with respect to the direction of the quarkonium three-momentum in the virtual photon–proton centre-of-mass frame. Measurements of the transverse-momentum dependence of the above cross section at the EIC would allow one to gather information on the so-far unknown quarkonium shape functions. In particular, the $\cos 2\phi_T^*$-weighted cross section would give access to a linear combination of the convolutions $C \left[w h_1^{\perp g} \Delta_h^{[n]} \right]$, with $n = {}^1S_0^{[8]}$ or $n = {}^3P_0^{[8]}$. Here the weight in the convolution expression

$$C \left[w h_1^{\perp g} \Delta_h^{[n]} \right](q_T) \equiv \int d^2\mathbf{p}_T \int d^2\mathbf{k}_T \, \delta^2(\mathbf{p}_T + \mathbf{k}_T - \mathbf{q}_T) \, w(\mathbf{p}_T, \mathbf{q}_T) \, h_1^{\perp g}(x, \mathbf{p}_T^2) \Delta_h^{[n]}(\mathbf{k}_T^2), \tag{3.16}$$

is given by (in standard TMD notation, note however that $\mathbf{q}_T$ will correspond to $\mathbf{P}_T^*$ used here)

$$w(\mathbf{p}_T, \mathbf{q}_T) = \frac{1}{M_p^2 q_T^2} \left[2(\mathbf{p}_T \cdot \mathbf{q}_T)^2 - p_T^2 q_T^2 \right]. \tag{3.17}$$

On the other hand, integrating over ϕ_T^* would single out a combination of the convolutions $C \left[f_1^g \Delta^{[n]} \right](P_T^*)$ for the same octet S- and P-waves, which could be in principle disentangled by looking at different values of the inelasticity y. Measurements of these

---

[10] Note that, in the photoproduction regime, one cannot determine the angle ϕ_T^* because the lepton plane is not defined, hence, also not the $\cos 2\phi_T^*$ modulation. In photoproduction, azimuthal modulations can only be seen for two-particle observables.
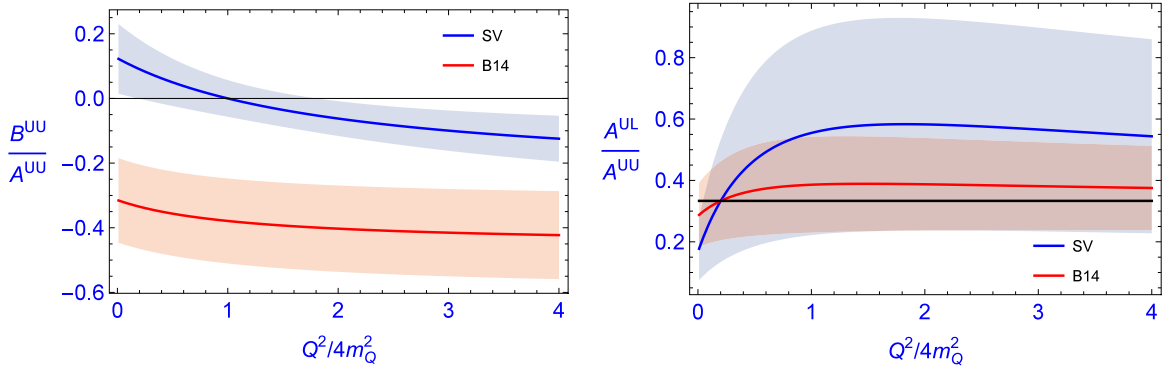
Fig. 3.16. (Left plot) The ratio B_{UU}/A_{UU} of the asymmetry $\langle \cos 2\phi_T^* \rangle$ (Eq. (3.18)) as a function of $\hat{Q}^2 = Q^2/(4m_Q^2)$ for the LDMEs at LO by Sharma and Vitev (SV) [233] and at NLO B14 [86] and for the inelasticity value $y = 0.1$; (Right plot) The ratio A_{UL}/A_{UU} Eq. (3.21) as a function of $Q^2/(4m_Q^2)$ for the same LDMEs and $y = 0.1$. The line at $1/3$ corresponds to unpolarised production. These plots are obtained from results presented in [216,229].

observables should help to establish the relevance of smearing effects and, in case they turn out to be sizeable, to even perform a first extraction of the shape functions. In this way, it would be possible to compare $\Delta^{[n]}$ and $\Delta_h^{[n]}$ as well as determine some other properties, like their relations with the LDMEs and their dependence on n.

For unpolarised quarkonium production ($P = U$), applying the above expressions gives the following normalised asymmetry ratio:

$$\langle \cos 2\phi_T^* \rangle \equiv \frac{\int d\phi_T^* \cos 2\phi_T^* \frac{d\sigma^{UU}}{dy\,dx_B\,d^2\boldsymbol{P}_T^*}}{\int d\phi_T^* \frac{d\sigma^{UU}}{dy\,dx_B\,d^2\boldsymbol{P}_T^*}} = \frac{1}{2} \frac{\sum_n B_{UU}^{[n]}\, \mathcal{C}\left[wh_1^{\perp g}\,\Delta_h^{[n]}\right]}{\sum_n A_{UU}^{[n]}\, \mathcal{C}\left[f_1^g\,\Delta^{[n]}\right]}. \tag{3.18}$$

As the matching analysis mentioned in Section 3.3.2 suggests, it is expected that the shape functions are proportional to the LDMEs belonging to the $[n]$ state, at least at LO: $\Delta^{[n]}(k_T^2;\mu^2) \simeq \langle \mathcal{O}^Q[n] \rangle \Delta(k_T^2;\mu^2)$ and $\Delta_h^{[n]}(k_T^2;\mu^2) \simeq \langle \mathcal{O}^Q[n] \rangle \Delta_h(k_T^2;\mu^2)$, for some $\Delta(k_T^2;\mu^2)$ and $\Delta_h(k_T^2;\mu^2)$. In this case the above asymmetry expression reduces to:

$$\langle \cos 2\phi_T^* \rangle = \frac{1}{2} \frac{B_{UU}}{A_{UU}} \frac{\mathcal{C}\left[wh_1^{\perp g}\,\Delta_h\right]}{\mathcal{C}\left[f_1^g\,\Delta\right]}, \tag{3.19}$$

where $A_{UU} = \sum_n A_{UU}^{[n]}\,\langle \mathcal{O}^Q[n] \rangle$ and $B_{UU} = \sum_n B_{UU}^{[n]}\,\langle \mathcal{O}^Q[n] \rangle$. At LO, the coefficients appearing in this expression are [229] :

$$A_{UU}^{[^1S_0^{[8]}]} = 1 + \bar{y}^2, \quad A_{UU}^{[^3P_0^{[8]}]} = \left[2\bar{y}\frac{7+3\hat{Q}^2}{1+\hat{Q}^2} + y^2\frac{7+2\hat{Q}^2+3\hat{Q}^4}{(1+\hat{Q}^2)^2}\right]\frac{1}{m_Q^2}, \quad B_{UU}^{[^1S_0^{[8]}]} = -\bar{y}, \quad B_{UU}^{[^3P_0^{[8]}]} = \frac{3-\hat{Q}^2}{1+\hat{Q}^2}\frac{\bar{y}}{m_Q^2}. \tag{3.20}$$

Here, we defined $\bar{y} = 1 - y$, with y being the inelasticity variable (see Eq. (2.2)), and $\hat{Q}^2 \equiv Q^2/(4m_Q^2)$ and we approximated $m_Q \simeq 2m_Q$, where m_Q denotes the heavy-quark mass.

At the EIC, one could try to determine the LDMEs together with the gluon TMDs. The Q^2 and y dependence of the P_T^*-independent pre-factor B_{UU}/A_{UU} can then be exploited, as it makes the observable dependent on different linear combinations of the LDMEs. This is similar to the slight rapidity dependence of the LDME linear combination appearing in the polarisation of the hadroproduction yield [9]. Another option is to consider ratios in which the gluon TMDs cancel out [216,229], although that may only hold at LO in certain cases. An example of this will be discussed in Section 3.3.4 where the quarkonium polarisation is used to cancel out the gluon TMDs.

A further constraint on the LDMEs comes from the bound on the above asymmetry. At leading order, the bound $q_T^2|h_1^{\perp g}(x,q_T^2)|/(2M_p^2) \leq f_1^g(x,q_T^2)$ [230] and the fact that $|\langle \cos 2\phi_T^* \rangle| \leq 1$ leads to the condition $|B_{UU}/A_{UU}| \leq 1$. The LDMEs that determine the ratio B_{UU}/A_{UU} will have to respect this bound. In this way one can find for instance that the CO LDMEs from Ref. [110] do not respect this bound at LO (and A_{UU} which should be positive becomes negative below the central value within the 1σ uncertainty range), but it has to be noted that these LDMEs were obtained at NLO from hadro- and photoproduction data.

The ratio B_{UU}/A_{UU} at LO is shown in Fig. 3.16 (left plot) for two different CO LDME sets: one obtained at LO [233] (SV), which is very similar to the NLO fit [114], denoted C12 in Table 3.1, and another obtained at NLO with FF [86] (BCKL), denoted B14 in Table 3.1. The uncertainty bands are obtained assuming uncorrelated uncertainties on the $\langle \mathcal{O}^Q\left[^1S_0^{[8]}\right]\rangle$ and $\langle \mathcal{O}_8^Q\left[^3P_0^{[8]}\right]\rangle$ determinations. The ratio is shown as a function of $\hat{Q}^2$. Here $\hat{Q}^2 = 0.01$ is considered to be the minimum achievable value. Indeed, in order for ϕ_T^* to be determined, one needs to be in the electroproduction regime where $Q^2 \geq 1$ GeV^2. In the bottomonium case, $\hat{Q}^2$ should thus be larger than 1 GeV$^2/(4m_b^2) \approx 0.01$.

The figure indicates that there is much uncertainty in the LO result. It also indicates the precision needed at the EIC in order to differentiate among the various fits and to improve on them. A determination of B_{UU}/A_{UU} at the 10% level would be an improvement of the current situation. Assuming $h_1^{\perp g}$ is 10% of its maximal value at EIC energies (for a more detailed analysis,

see Section 4.2.2), this translates into a percent level accuracy requirement on the measurement of $\langle \cos 2\phi_T^* \rangle$. For other y values, similar conclusions hold. Needless to say, an NLO analysis of the asymmetry will be needed in order to arrive at more accurate predictions for the EIC and for a fully coherent NLO computation with NLO LDMEs.

For these measurements, a good P_T^*-resolution at small P_T^* is an important requirement. Small P_T^* applies to the range up to a few GeV for the EIC energies. Therefore, the transverse-momentum resolution in the small transverse-momentum region should be on the order of a few hundred MeV, such that sufficient bins can be selected to map out this region. For the determination of $\langle \cos 2\phi_T^* \rangle$, a sufficient angular resolution is needed.

3.3.4. Quarkonium polarisation in electroproduction within TMD factorisation

If the polarisation state P (L or T) of the produced quarkonium can be determined in the semi-inclusive quarkonium production process, $e\,p \to e'\,J/\psi\,(Y)\,X$ at small transverse momentum, P_T^*, then that may offer a further possibility to improve our knowledge on LDMEs. As an illustration, here we consider the example of the ratio of the ϕ_T^*-integrated cross sections:

$$\frac{\int d\phi_T^* \frac{d\sigma^{UP}}{dy\,dx_B\,d^2\boldsymbol{P}_T^*}}{\int d\phi_T^* \frac{d\sigma^{UU}}{dy\,dx_B\,d^2\boldsymbol{P}_T^*}} = \frac{\sum_n A_{UP}^{[n]}\,C\left[f_1^g\,\Delta^{[n]}\right]}{\sum_n A_{UU}^{[n]}\,C\left[f_1^g\,\Delta^{[n]}\right]} = \frac{A_{UP}}{A_{UU}}. \tag{3.21}$$

Let us stress that Eq. (3.21) relies on the assumption that the shape functions are equal to the corresponding LDMEs times a universal shape function that is also polarisation independent. If so, the ratios A_{UL}/A_{UU} and A_{UT}/A_{UU} are independent of the value of $P_T^* \equiv |\boldsymbol{P}_T^*|$ to all orders and hence not affected by TMD evolution. The ratio will only receive contributions from higher orders through modification of the amplitudes. Thus far only the LO expressions are known [216,229]: A_{UU} was already given in Section 3.3.1, and

$$A_{UL} = \frac{1}{3}\left[1 + (1-y)^2\right]\langle \mathcal{O}^{\mathcal{Q}}\left[{}^1S_0^{[8]}\right]\rangle + \left[2(1-y)\frac{1 + 10\hat{Q}^2 + \hat{Q}^4}{(1+\hat{Q}^2)^2} + y^2\frac{1 + 2\hat{Q}^2 + \hat{Q}^4}{(1+\hat{Q}^2)^2}\right]\frac{\langle \mathcal{O}^{\mathcal{Q}}\left[{}^3P_0^{[8]}\right]\rangle}{m_Q^2}, \tag{3.22}$$

where $A_{UT} = A_{UU} - A_{UL}$. Compared to A_{UU}, the $\langle \mathcal{O}^{\mathcal{Q}}\left[{}^3P_0^{[8]}\right]\rangle$ term in A_{UL} has different inelasticity y and $\hat{Q}^2$ dependences. This implies that there can be a significant deviation of A_{UL} from $A_{UU}/3$ (and of A_{UT} from $2A_{UU}/3$), signalling the production of polarised quarkonia. Likewise, one could consider the ratios B_{UL}/B_{UU} or B_{UT}/B_{UU} which are similar, but different linear combinations of LDMEs.

In Fig. 3.16 (right plot) the ratio A_{UL}/A_{UU} at LO is shown for the LDME fits [233] at LO (SV) and [86] (here denoted BCKL, B14 in Table 3.1) at NLO, including uncertainty bands, assuming again uncorrelated uncertainties on the $\langle \mathcal{O}^{\mathcal{Q}}\left[{}^1S_0^{[8]}\right]\rangle$ and $\langle \mathcal{O}^{\mathcal{Q}}\left[{}^3P_0^{[8]}\right]\rangle$ determinations. In reality the uncertainties are correlated, which means that the bands are expected to be overestimations. The difference between the central values of the two different LDME sets could be viewed as another measure for the size of the involved uncertainties. Although both fits are compatible with unpolarised production, both fits also allow, within their uncertainties, for values considerably different from $1/3$. It is important to recall that quarkonium-polarisation observables are very sensitive to radiative corrections [70,72,112,128,189,190,199]. Computations of the NLO corrections to the hard parts entering the ratio A_{UL}/A_{UU} are therefore necessary to perform a reliable extraction of the LDMEs from these ratios.

In Ref. [154], the fit C12 [114] is used to demonstrate the dominance of the ${}^1S_0^{[8]}$ $c\bar{c}$ state in the inclusive process $e\,h \to J/\psi\,X$ (which is dominated by $Q^2 \approx 0$) described in collinear factorisation. As a result, it is concluded that the J/ψ will be approximately produced in an unpolarised state. However, the above results show that due to the large uncertainties in the CO LDMEs, one cannot draw the same conclusion for semi-inclusive J/ψ electroproduction *in the TMD regime* (where P_T^{*2} is much smaller than the two hard scales $M_{J/\psi}^2$ and Q^2). Observation of a non-zero polarisation of the J/ψ yield would signal the relevance of the P-wave LDME $\langle \mathcal{O}^{\mathcal{Q}}\left[{}^3P_0^{[8]}\right]\rangle$ or of higher-order contributions.

Again a 10% level precision of the determination of the ratio A_{UL}/A_{UU} at EIC would be sufficient to improve on the present situation. For this the polarisation state L or T of the quarkonium needs to be determined with sufficient precision of course.

3.4. On the importance of final-state effects on quarkonium formation in electron–nucleus collisions

Interest in quarkonium formation in reactions with nuclei goes back more than 30 years in the context of heavy-ion reactions. The colour interaction between heavy quarks immersed in a high temperature quark–gluon plasma (QGP), produced in such reactions, was predicted to be screened, preventing quarkonium states from forming as well as dissociating [234]. Excited, weakly-bound-state solutions to the Schrödinger equation, such as $Y(2S)$, $\psi(2S)$, χ_c, were expected to melt first in the QGP and provide a "thermometer" for determining the plasma temperature. Since their introduction, these ideas have evolved significantly. It was realised that dissociation and formation suppression of hadrons in QCD matter is not limited to quarkonia. Open heavy- flavour mesons have short formation times and can also be destroyed by collisional interactions in the nuclear medium [235,236], reducing the experimentally measured cross sections. Importantly, the breakup of J/ψs and Ys is not exclusive to the QGP and can take place in different forms of strongly-interacting matter, for example a hadron gas or a large nucleus. Measurements of the modification of charmonium and bottomonium production in dAu, pAu, pAl and pPb collisions at RHIC [237–239] and at the LHC [240], respectively, showed that production suppression increases with the multiplicity of hadrons recorded in a reaction [30,241]. Moreover, recent measurements of bottomonium yields in pPb collisions showed [242] that excited Y states are more suppressed than the ground state,
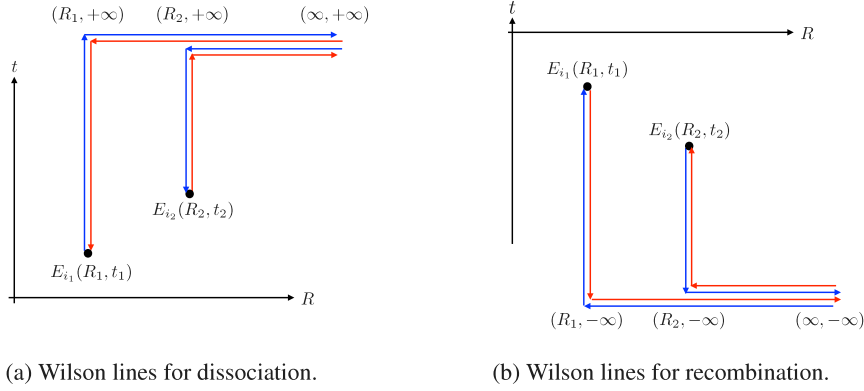
(a) Wilson lines for dissociation.   (b) Wilson lines for recombination.

Fig. 3.17. Staple-shape Wilson lines in the definition of the chromoelectric correlator of Eq. (3.23). Here we set $i_1 = i_2$, $y = (\boldsymbol{R}_1, t_1)$ and $x = (\boldsymbol{R}_2, t_2)$.
Source: The plots are taken from Ref. [250].

and the hierarchical pattern becomes more manifest in the negative rapidity region, which is the direction of the lead nucleus [243]. Studies indicate that final-state interactions can play a significant role in reducing the rates of quarkonium production at the EIC. This quenching effect has been demonstrated for light and heavy mesons (containing a single heavy quark) [244] and inclusive and heavy flavour-tagged jets [245,246]. At forward rapidities and, especially at lower centre-of-mass energies, suppression in cold nuclear matter can be as large as a factor of two and serves as a strong motivation to investigate these effects for quarkonium final states.

These observations and predictions indicate that final-state effects (interaction of quarkonium with co-moving hadrons as well as the remnant of the nucleus) require careful treatment in order to extract information about nuclear PDFs and transport properties of the nuclear matter. This can be addressed from both experimental and theoretical perspectives.

Experimentally, one can approach this concern by studying femtoscopic correlations (two-particle correlations at low relative momentum) between quarkonium and hadron in ep and eA reactions. Such observables are sensitive to interactions in the final state and strong interaction parameters can be measured directly (the scattering length and effective range) [247–249]. Quarkonium–hadron elastic and inelastic scattering cross sections can be evaluated as a function of event multiplicity. Such information can be used to calculate the modification of the quarkonium yield in the hadronic environment.

From the theory point of view, in order to extract nuclear PDFs and constrain the transport properties of large nuclei using quarkonium production in eA collisions, we need to develop a theoretically well-controlled framework capable of describing final-state interactions. Below, we briefly present an example of such an attempt.

Since the remnant of the nucleus is a cold nuclear environment, we expect the energy transferred between the nucleus remnant and the heavy-quark pair traversing the nucleus to be small. With this assumption, one can use the open quantum system framework and the Boltzmann equation developed in Refs. [250–256] to study final-state interactions. In this approach the physical quantity that encodes the essential information of the nuclear remnant relevant for a final-state interaction is the chromoelectric field correlator, which is defined in a gauge-invariant way:

$$g_E^>(q) = \sum_{i=1}^{3} \int \mathrm{d}^4(y-x)\, e^{iq\cdot(y-x)}\, \mathrm{Tr}_N\left(E_i(y) W\, E_i(x) \rho_N \right), \tag{3.23}$$

where ρ_N is the density matrix of the remnant nucleus and W denotes a staple-shape Wilson line in the adjoint representation that connects the spacetime points y and x such that the correlator is defined gauge invariantly. For quarkonium dissociation and formation, the two time-like Wilson lines are connected at positive and negative infinite times separately, as shown in Fig. 3.17. The Wilson lines involved here are similar to those involved in the definition of proton TMDs, with a difference in the orientation of the Wilson lines.

In a nutshell, quarkonium production in eA collisions involves both initial-state and final-state effects. It will be important for the community to develop strategies for how to best separate these distinct contributions. The combination of both eA and pA experimental data will be useful to determine quarkonium–hadron interaction parameters, nuclear PDFs, and properties of the remnant nucleus such as the chromoelectric correlator strength.

4. Quarkonia as tools to study the parton content of the nucleons

The goal of the present section is to show that quarkonium production in lepton–hadron collisions can be an excellent observable to probe the partonic content of the nucleon.

First, we discuss how quarkonium-production measurements at the EIC can contribute to our knowledge of collinear PDFs of the nucleon. Section 4.1.1 is dedicated to accessing the gluon PDF from inclusive-quarkonium-photoproduction processes. In Section 4.1.2, we emphasise how measurements of exclusive J/ψ and Υ electroproduction at the EIC, by extension of those from

the HERA collider, can be used as an indirect probe of the gluon PDF at moderate values of the momentum fraction over a wide range of scales. Section 4.1.3 is devoted to the sensitivity to light quark PDFs of inclusive J/ψ photoproduction, while Section 4.1.4 focuses on the charm PDF and the potential detection of intrinsic charm at the EIC. We then move to the multidimensional imaging of the partonic structure of nucleons through quarkonium-related measurements at the EIC.

Sections 4.2 and 4.3 are devoted to the possibility to extract information on TMD PDFs of unpolarised and polarised nucleons, respectively, from quarkonium electroproduction data at the EIC. The systematic description of exclusive production processes is done in terms of GPDs (Section 4.4) and GTMDs (Section 4.5). We stress that the relation between GPDs and PDFs used in Section 4.1.2 is only an approximation, albeit a good one at the moderate and low values of the momentum fraction that we consider here. Furthermore, in Section 4.6, we touch on the possibility to access the QCD trace anomaly through the measurement of exclusive J/ψ electroproduction at the threshold.

Finally, in Section 4.7, we concentrate on double-parton scattering (DPS), which is another interesting probe of nucleon structure. First estimates for J/ψ-pair electroproduction at the EIC, which include DPS contributions, are presented.

4.1. Unpolarised-nucleon PDFs

4.1.1. Gluon PDF from inclusive quarkonium photoproduction

Inclusive J/ψ photoproduction, when an almost real photon hits and breaks the proton producing a J/ψ, is a useful tool to study the quarkonium-production mechanism and to probe the gluon PDF. This process has been the object of several studies at HERA [101,257–262], and, in the future, it could be studied at the EIC.

In Ref. [147] the inclusive photoproduction up to NLO in QCD for J/ψ and $Y(1S)$ at lepton–proton colliders was revisited, focusing on the P_T- and z-integrated yields. Like for other charmonium-production processes [124,263,264], the appearance of negative hadronic cross sections was observed at increasing energies, due to large negative *partonic* cross sections. There can only be two sources of negative partonic cross sections: the interference of the loop amplitude with the Born amplitude or the subtraction of the IR poles from the initial-emission collinear singularities to the real-emission amplitude. Here, the latter subtraction is the source of the negative cross sections. Conventionally, such divergences are removed by subtraction and included in the PDFs via Altarelli-Parisi counterterms (AP-CT). In principle, the negative term from the AP-CT should be compensated by the evolution of the PDFs according to the DGLAP equation. Yet, for the μ_F values on the order of the natural scale of these processes, the PDFs are not evolved much and can sometimes be so flat for some PDF parametrisations that the large $\hat{s}$ region still significantly contributes. This results in negative values of the hadronic cross section.

To solve the negative cross-section issue, the $\hat{\mu}_F$ prescription proposed in [264] was used, which, up to NLO, corresponds to a resummation of such collinear divergences in HEF [149]. According to this prescription, one needs to choose μ_F such that for the partonic cross section $\hat{\sigma}_{\gamma i}$ ($i = q, \bar{q}, g$), $\lim_{\hat{s}\to\infty} \hat{\sigma}_{\gamma i}^{\mathrm{NLO}} = 0$. It was found that, for $z < 0.9$, the optimal factorisation scale is $\hat{\mu}_F = 0.86 M_Q$ [147] which falls well within the typical ranges of used values. Like for η_c hadroproduction, such a factorisation-scale prescription indeed allows one to avoid negative NLO cross sections, but it of course in turn prevents one from studying the corresponding factorisation-scale uncertainties. The NLO μ_R uncertainties become reduced compared to the LO ones but slightly increase around $\sqrt{s_{\gamma p}} = 50$ GeV , because of rather large (negative[11]) interferences between the one-loop and Born amplitudes. At NNLO, a further reduction of the μ_R uncertainties is expected. This is particularly relevant especially around $\sqrt{s_{\gamma p}} = 50 - 100$ GeV, which corresponds to the EIC region. This would likely allow us to better probe gluon PDFs using photoproduction data. Going further, differential measurements in the elasticity or the rapidity could provide a complementary leverage in x to fit the gluon PDF, even in the presence of the v^4 CO contributions. Indeed, these would likely exhibit a very similar dependence on x.

The possibility to constrain PDFs using future J/ψ and $Y(1S)$ photoproduction data [147] was investigated by comparing the PDF and μ_R uncertainties. Unsurprisingly, the PDF uncertainties get larger than the (NLO) μ_R uncertainties with the growth of the γp centre-of-mass energy, in practice from around 300 GeV, i.e. for x below 0.01. Although this is above the reach of the EIC, with NNLO predictions at our disposal in the future, with yet smaller μ_R uncertainties, one could set novel constraints on PDFs with such EIC measurements. Following the estimated counting rates for 100 fb^{-1} of ep collisions given in [147], a number of differential measurements (in P_T, z and/or y) will be possible to reduce the impact of highly- or even partially-correlated theoretical uncertainties, including the contamination of higher-v^2 corrections, such as the CO contributions.

Table 4.1 gathers estimates of the expected number of J/ψ and $Y(1S)$ possibly detected at the different ep centre-of-mass energies at the EIC. For $Y(1S)$, the yields should be sufficient to extract cross sections even below the nominal EIC luminosities.

One can also estimate the expected number of detected ψ', $Y(2S)$ and $Y(3S)$ using the following relations

$$
\begin{aligned}
N_{\psi'} &\simeq 0.08 \times N_{J/\psi}, \\
N_{Y(2S)} &\simeq 0.4 \times N_{Y(1S)}, \\
N_{Y(3S)} &\simeq 0.35 \times N_{Y(1S)},
\end{aligned}
\tag{4.1}
$$

derived from the values of[12] $|R_Q(0)|^2$ (the quarkonium radial wave function at the origin, that is related to the $^3S_1^{[1]}$ LDME) and of the branching fractions to leptons. Using the values in Table 4.1 and Eq. (4.1) [147], one can see that the yield of ψ' should be measurable and the yields of $Y(2S)$ and $Y(3S)$ are close to about half of that of $Y(1S)$ and should be measurable as well at the EIC.

---

[11] Let us stress that unless μ_R is taken very small with a large $\alpha_s(\mu_R)$, these negative contributions are not problematic, unlike the oversubtraction by the AP-CT.

[12] These contributions were estimated using $|R_{\psi'}(0)|^2 = 0.8$ GeV^3, $|R_{Y(2S)}(0)|^2 = 5.0$ GeV^3 and $|R_{Y(3S)}(0)|^2 = 3.4$ GeV^3 and the corresponding measured branching fractions to J/ψ and $Y(1S)$ [266].

Table 4.1

Expected event rates for quarkonium photoproduction at NLO at different $\sqrt{s_{ep}}$ (in GeV) of the EIC for $\mu_R = 5$ GeV for J/ψ and $\mu_R = 16$ GeV for $Y(1S)$, setting $\mu_F = \hat{\mu}_F$ and applying the cut $z < 0.9$. We assumed a detector efficiency of $\epsilon_{detect} = 85\%$ for both $\mu^+\mu^-$ and e^+e^- channels. Combined with branching fractions, this yields $\epsilon_{\ell^+\ell^-}^{J/\psi} \approx 0.1$, and $\epsilon_{\ell^+\ell^-}^{Y(1S)} \approx 0.04$. The CT18NLO PDFs [265] are used.

Source: Table from [147].

$\sqrt{s_{ep}}$	$\mathcal{L}$ (fb^{-1})	$N_{J/\psi}$	$N_{Y(1S)}$
45	100	$8.5^{+0.5}_{-1.0} \cdot 10^6$	$6.1^{+0.7}_{-0.8} \cdot 10^2$
140	100	$2.5^{+0.1}_{-0.4} \cdot 10^7$	$7.6^{+0.3}_{-0.7} \cdot 10^3$
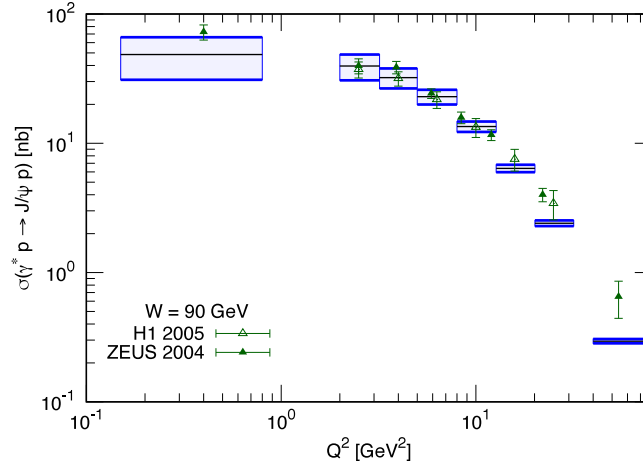
Fig. 4.1. The exclusive J/ψ electroproduction cross section as a function of Q^2 for a fixed centre-of-mass energy $W = 90$ GeV and compared to the data from H1 [278] and ZEUS [271], using results in [277] and Shuvaev-transformed MSHT20 input NLO PDFs [279]. The black lines represent the central prediction in each bin, while the upper and lower blue lines are indicative of the propagation of the PDF error only. The discrepancy of the prediction from the data at the largest Q^2 is indicative of the need for resummation effects, see text for details. The current data in this regime are, however, sparse and we anticipate the EIC will be able to provide more resolving power in the shape of further statistics to discern if such effects are already needed.

4.1.2. Gluon PDFs from exclusive quarkonium photo- and electroproduction

Forward exclusive production of heavy vector mesons has long been a fascinating observable to study, functioning as an enticing avenue to unravelling the small-x behaviour of the gluon PDF from low to moderate scales. Measured in the first instance in the fixed-target mode [267–269] and in DIS events at HERA, see e.g. [270–273], and then more recently in ultra-peripheral collisions at the LHC [274–276], they provide a means to explore the quarkonium production mechanism and act as sensitive probes at the frontier of small-x saturation physics.

The exclusive J/ψ electroproduction, $\gamma^* p \to J/\psi p$, has been measured via dilepton decays at HERA in a narrow range of photon virtualities, extending up to $\langle Q^2 \rangle = 22.4$ GeV^2. The corresponding photoproduction has also been determined in ultraperipheral events at the LHC. There are not, as of yet however, any data from HERA and the LHC for exclusive Y electroproduction, $\gamma^* p \to Y p$, away from the photoproduction limit. Going forward, the EIC will extend the kinematic reach in Q^2, providing a lever arm up to larger virtualities and, moreover, allow for a measurement of the Y electroproduction with off-shell photon kinematics for the first time, albeit with a projected lower $Q^2 + M_Q^2$ bin coverage and event count rates due to its heavier mass [2].

Recently, in Ref. [277], the coefficient functions for exclusive heavy vector meson electroproduction were derived at NLO within the framework of collinear factorisation, with the transition from an open heavy quark–antiquark pair to a bound heavy vector meson made within LO NRQCD.

Based on the above derivation of the coefficient functions, predictions for the exclusive J/ψ electroproduction cross section have been made. They are shown in Fig. 4.1 in bins of Q^2 at a fixed centre-of-mass energy, $W = 90$ GeV, of the $\gamma^* p$ pair. We use the Shuvaev transform [280,281] as a reliable means to obtain the GPD, see Section 4.4, from input PDFs in the kinematic regions shown. We construct GPDs in such a way using MSHT20 [279], NNPDF3.1 [282] and CT18 [265] input NLO PDFs and the predictions based on the former are shown in the figure. The choice of input PDF has the largest effect at the lowest Q^2, where the choice of the initial condition of the DGLAP evolution is felt, while for larger Q^2, this effect washes out and the predictions based on each PDF set agree at or below the percent level. The central values of the prediction for low to moderate Q^2 are in good agreement with the experimental data from H1 and ZEUS, but for larger Q^2 there appears to be a downward shift of the prediction from the data. The prediction in the highest Q^2 bin exhibits a small factorisation-scale dependency and is essentially independent of the choice of the input PDF but, as shown, the deviation from the data is sizeable. Interestingly, in the large Q^2 limit, the gluon
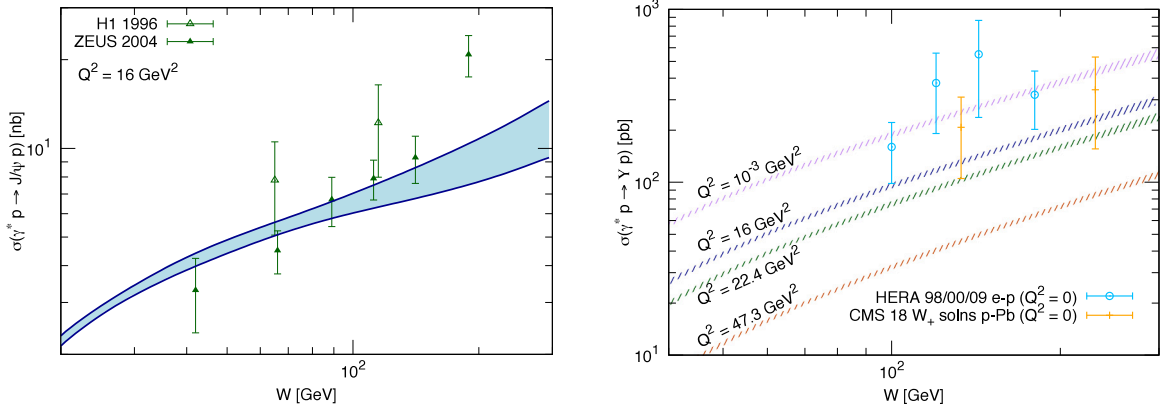
Fig. 4.2. (Left panel): The EIC will provide increased statistics for the J/ψ electroproduction at current and new and unexplored virtualities. Shown is a postdiction for the exclusive J/ψ electroproduction as a function of W for fixed $\langle Q^2 \rangle = 16$ GeV^2. (Right panel): Prediction for the exclusive Υ electroproduction as a function of W for a selection of scale choices accessible by the EIC, as well as current photoproduction data from HERA and LHC in the given W range.

amplitude $\propto \ln(Q^2/m_Q^2)^2$ while the quark amplitude $\propto \ln(Q^2/m_Q^2)$. This observation seems to necessitate a program of resummation for the exclusive electroproduction of heavy vector mesons for virtualities $Q^2 \gg m_Q^2$, *i.e.* those relevant for EIC kinematics, and may provide for the reconciliation of the theory prediction and experimental data at large scales.

The data statistics are currently limited for larger Q^2 and, in particular, there is a wide range where the EIC can provide a first coverage. This will help to ascertain on which front the difference between this prediction and the data at large Q^2 lies and if resummation effects are already needed. Other numerical effects in this framework such as the so-called 'Q_0 subtraction' [283], crucial for a fruitful description of the photoproduction data [284–289], are not surmised to be important for electroproduction kinematics because the corresponding power correction $\mathcal{O}(Q_0^2/\mu_F^2)$ is no longer of $\mathcal{O}(1)$. See also [290,291] for a recent baseline study of exclusive J/ψ photoproduction in heavy-ion collisions in the collinear factorisation framework to NLO.

Simulated event count projections were given for the exclusive electroproduction of the J/ψ and Υ in bins of $Q^2 + M_Q^2$ as a function of x in [2]. In Fig. 4.2 (left panel), we show predictions for the exclusive J/ψ electroproduction cross section as a function of W at a fixed scale $\langle Q^2 \rangle = 16$ GeV^2 using Shuvaev-transformed MSHT20 input NLO PDFs, as well as the exclusive J/ψ electroproduction HERA data that lie in this bin for comparison purposes. The prediction agrees most favourably with the more up-to-date dataset, however the EIC will be able to provide more statistics and resolve the slight tension between (and discrepancies within) the datasets. In particular, the data point at $W = 189$ GeV is around a factor of two larger than other data lying in this bin. We also show predictions for the exclusive Υ electroproduction cross section as a function of W (right panel) for $\langle Q^2 \rangle = 0.001, 16, 22.4$ GeV^2 and 47.3 GeV^2, which may ultimately be compared with data from the EIC.[13] In each case the quark contribution to the total amplitude is negligible and so the forthcoming enhanced statistics and increased data coverage from the EIC will allow for refined and improved constraints on the gluon PDF at low to moderate scales.

4.1.3. Light quarks

At EIC energies, we also expect to be sensitive to quark-initiated partonic subprocesses. As shown in Ref. [54], in inclusive quarkonium photoproduction, the quark-induced subprocesses $\gamma + q \rightarrow J/\psi + q (+g)$ will be a relevant contribution to the cross section. Therefore, through quarkonium photoproduction, the EIC will also be partially sensitive to the light-quark PDFs.

To highlight the quark-induced contribution, we show in Fig. 4.3 the ratio to the CSM cross section for every partonic subprocess (up to $\mathcal{O}(\alpha\alpha_s^3)$) depicted in Fig. 3.4, at two different centre-of-mass energies, $\sqrt{s_{ep}} = 45$ GeV (left panel) and $\sqrt{s_{ep}} = 140$ GeV (right panel), as a function of J/ψ transverse momentum. It is clear that the pure QED quark-initiated process at $\mathcal{O}(\alpha^3)$ becomes dominant at high P_T, accounting for over half of the cross section at $P_T \sim 12\,(16)$ GeV at $\sqrt{s_{ep}} = 45\,(140)$ GeV. The effect is larger at $\sqrt{s_{ep}} = 45$ GeV, where the valence region of the PDF is probed. The $\mathcal{O}(\alpha\alpha_s^3)$ contribution ($\gamma + q \rightarrow J/\psi + q + g$) is roughly $5 - 15\%$ and $10 - 15\%$ of the cross section at $\sqrt{s_{ep}} = 45$ GeV and $\sqrt{s_{ep}} = 140$ GeV, respectively. We then expect that, in J/ψ photoproduction processes at the EIC, the J/ψ produced at large P_T will be recoiling off of at least one quark jet. The significant contribution of quark-induced subprocesses at high P_T of the J/ψ is also observed in the NLO NRQCD calculation, as shown in Fig. 4.4. Moreover, this conclusion depends only mildly on the NRQCD LDMEs that were used.

---

[13] Admittedly, the expected event count rate is a lot lower than that of the corresponding J/ψ production, even by three orders of magnitude in the photoproduction bin containing the most counts [2]. Any data will therefore likely be sparse and exhibit large uncertainties, but nonetheless complement those already existing from HERA and LHC, shown in the right panel of Fig. 4.2.
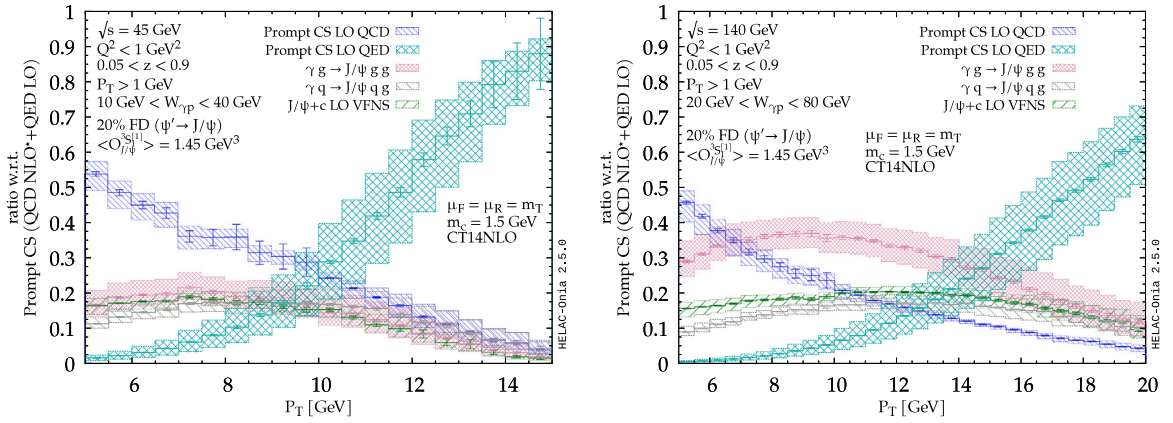
Fig. 4.3. Ratio of the different contributions to the cross section of Fig. 3.4 at the EIC at $\sqrt{s_{ep}} = 45$ GeV (left) and $\sqrt{s_{ep}} = 140$ GeV (right) as a function of the J/ψ transverse momentum, P_T.
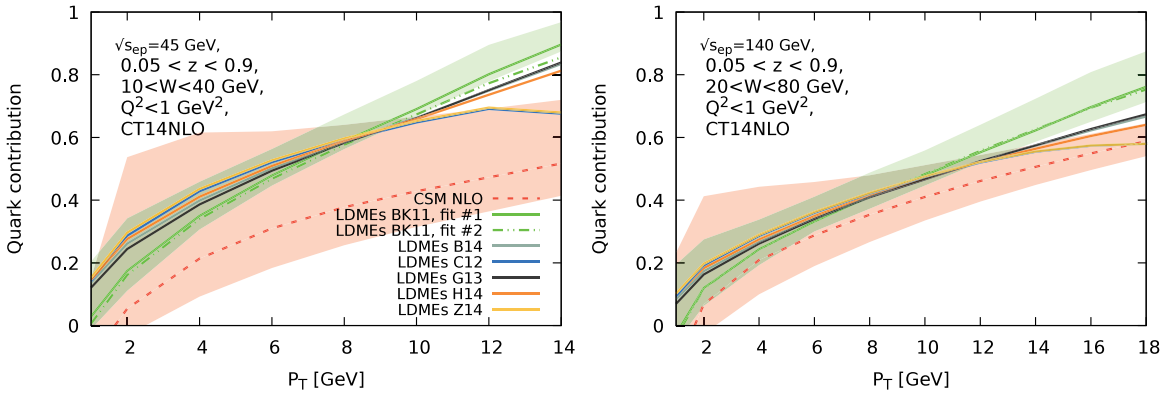*Source:* Figure taken from Ref. [54].

Fig. 4.4. Plots of the fraction of light-quark-induced subprocesses in the P_T spectra of J/ψ photoproduction at the EIC shown in Fig. 3.6 at NLO in NRQCD factorisation for different LDME sets.

4.1.4. Charm quark and intrinsic charm

The existence of a nonperturbative charm-quark content in the proton, referred to as intrinsic charm (IC), has long been postulated [292,293]. Intrinsic charm states are a fundamental property of hadronic bound-state wave functions [292,293]. They differ from extrinsic charm in perturbative QCD that arises from gluon splitting and contributes to the heavy-quark PDFs (i.e., radiatively generated). The "intrinsic" label is due to the fact that a $c\bar{c}$ pair formed by gluons from more than one quark line forces the $c\bar{c}$ parameters to be dependent upon (i.e., reflective of) the hadron that creates it. Therefore the c and $\bar{c}$ distributions are "intrinsic" to the identity of the proton, or the meson, or whichever hadron contains the bound quarks that emit gluons. "Extrinsic" means that the sea quark pairs come from a single quark line gluon and therefore do not reflect the bound state structure they exist in, at least not in the clear way that IC of the proton does, peaking at $\sim x_B = 0.4$ and imparting a difference in c and $\bar{c}$ distributions, according to recent lattice calculations [294].

Since extrinsic charm contributions are due to a gluon emitted by a single quark line which then splits into a $c\bar{c}$ pair, these charm distributions are soft, appear at low x and depend logarithmically on the mass of the heavy quark m_Q. On the other hand, IC contributions dominate at higher x and have a $1/m_Q^2$ dependence. They come from five-quark (and higher) Fock-state configurations of the proton, $|uudc\bar{c}\rangle$, and are kinematically dominated by the regime where the state is minimally off-shell, leading to equal-rapidity constituent quarks. Thus, the charm quarks are manifested at large x. When the proton in this state interacts with its collision partner, whether a hadron or a lepton, the coherence of the Fock components is broken and the fluctuations can hadronise [292,293,295]. In hadroproduction, the state can be broken up by a soft gluon from the target interacting with the proton. In ep interactions, instead of a soft gluon, a low-energy photon can play the same role and bring the state on mass shell.

Several formulations of intrinsic charm in the proton wave function have been proposed. The first was proposed by Brodsky and collaborators in [292,293]:

$$\frac{dP_{\mathrm{ic}\,5}}{dx_1 dx_2 dx_3 dx_c dx_{\bar{c}}} = P_{\mathrm{ic}\,5}^0 N_5 \int dk_{x1} \cdots dk_{x5} \int dk_{y1} \cdots dk_{y5} \frac{\delta(1 - \sum_{i=1}^5 x_i)\delta(\sum_{i=1}^5 k_{xi})\delta(\sum_{i=1}^5 k_{yi})}{(m_p^2 - \sum_{i=1}^5 (\hat{m}_i^2/x_i))^2}, \tag{4.2}$$

where $i = 1, 2, 3$ are the light quarks (u, u, d) and $i = 4$ and 5 are the c and $\bar{c}$ quarks. Here, N_5 normalises the $|uudc\bar{c}\rangle$ probability to unity and $P^0_{\text{ic}5}$ scales the unit-normalised probability to the assumed intrinsic-charm content of the proton. The delta functions conserve longitudinal and transverse momentum. The denominator of Eq. (4.2) is minimised when the heaviest constituents carry the dominant fraction of the longitudinal momentum, $\langle x_Q \rangle > \langle x_q \rangle$. In the first papers, the c and $\bar{c}$ distributions were treated equally, but later studies showed an asymmetry in c and $\bar{c}$ distributions [294]. The asymmetry is caused by QCD diagrams where, for example, two gluons from two different valence quarks in the nucleon couple to a heavy-quark pair $gg \to Q\bar{Q}$ with charge conjugation value $C = +1$ [296]. This amplitude interferes with QCD diagrams where an odd number of gluons attach to the heavy-quark pair, e.g. $g \to Q\bar{Q}$ and $ggg \to Q\bar{Q}$ with $C = -1$. The interference of amplitudes with the same final state but different charge conjugation symmetry for the $Q\bar{Q}$ produces the asymmetric distribution functions. The analogous interference term is seen in the electron and positron distributions in e^+e^- pair production [297].

At leading order, the charm-quark structure function from this state can be written as

$$F^{\text{ic}}_{2c}(x_c) = \frac{8}{9} x_c \, c(x_c) = \frac{8}{9} \int dx_1 dx_2 dx_3 dx_{\bar{c}} \frac{d P_{\text{ic}5}}{dx_1 dx_2 dx_3 dx_c dx_{\bar{c}}} \,. \tag{4.3}$$

Intrinsic-charm models. Intrinsic-charm distributions in the proton have also been calculated using meson-cloud models where the proton fluctuates into a $\bar{D}(u\bar{c})\Lambda_c(udc)$ state [298,299]. A further development of this model examined all possible charm meson–baryon combinations in the $|uudc\bar{c}\rangle$ state [300], finding that charm mesons would predominantly be produced through D^* mesons. In these models the charm sea contribution would be asymmetric $xc(x) \neq x\bar{c}(x)$. In both the Brodsky et al. and the meson-cloud formulations, the intrinsic-charm contributions appear as an enhancement at large x. On the other hand, a sea-like distribution [301,302] has also been considered. In this case, the intrinsic-charm distribution is represented simply as an overall enhancement to the light-quark-mass sea. These distributions are symmetric, $xc(x) = x\bar{c}(x)$.

Intrinsic-charm distributions from these models have been included in global analyses of the parton densities [301–305]. Earlier analyses [306,307] focused specifically on the European Muon Collaboration (EMC) high-x and high-Q^2 data [308]. A range of values of $P^0_{\text{ic}5}$ were extracted, from 0.1% to 1%. For more details of these analyses, see [309]. See also the recent review in [310] for more applications of intrinsic-heavy-quark states. New evidence for a finite charm-quark asymmetry in the nucleon wave function from lattice gauge theory, consistent with intrinsic charm, was published in [294]. Further evidence for unequal c and $\bar{c}$ distributions in the proton has recently been presented along with proposed experimental tests with the EIC using flavour-tagged structure functions [311].

Note that only the 5-particle intrinsic-charm state of the proton has been discussed. However, one can also consider higher Fock components such as $|uudc\bar{c}q\bar{q}\rangle$. These will reduce the average momentum fraction of the charm quark and also have lower probability. See e.g. [312] for examples of charm hadron distributions from higher Fock states. Finally, the possibility for an enhanced IC component in the deuteron was studied in [313].

Recent hints from the LHC. A number of experimental measurements [308,314,315] over the last several decades have provided tantalising hints of intrinsic charm. Recently LHCb announced that their measurement of $Z + $ charm jets relative to all $Z + $ jets is consistent with an intrinsic-charm component of the proton as large as 1% at large Z rapidity [316]. These results were recently confirmed by a phenomenological analysis made by the NNPDF Collaboration [317]. Measurements at lower scales than the Z-boson mass are therefore eagerly awaited for to advance our understanding of this higher-Fock-state phenomenon.

Intrinsic charm at the EIC. The EIC will offer the possibility to probe the nonperturbative charm-quark content in the proton. Recent studies show that the EIC will be capable of precision studies of intrinsic-charm as well as gluon distribution functions in the nucleus and in the nucleon [318].

Quarkonium associated production has been measured by experiments at the LHC and at Tevatron in the past.[14] The associated production of a J/ψ and a charmed particle is an additional potential probe of intrinsic-charm related effects. A leading order Variable-Flavour-Number Scheme (VFNS) study, first made in [130] for quarkonium hadroproduction, has been extended in [54] to the case of J/ψ photoproduction. Such a scheme allows a proper merging of different partonic contributions, namely $\gamma + g \to J/\psi + c + \bar{c}$ and $\gamma + \{c, \bar{c}\} \to J/\psi + \{c, \bar{c}\}$, respectively calculated with 3 and 4 flavours in the proton, using a counter term, $d\sigma^{\text{CT}}$, that avoids double counting. When the charm-tagging efficiency ε_c is taken into account, the corresponding VFNS cross section is given by:

$$d\sigma^{\text{VFNS}} = d\sigma^{\text{3FS}} \left[1 - \left(1 - \varepsilon_c \right)^2 \right] + \left(d\sigma^{\text{4FS}} - d\sigma^{\text{CT}} \right) \varepsilon_c. \tag{4.4}$$

Based on such computations, the J/ψ+charm yield has been calculated for two different EIC configurations: $\sqrt{s_{ep}} = 45(140)$ GeV, taking into account a 10% charm-tagging efficiency [329]. The calculation has been done with the CT14NNLO PDF set [330], which includes different eigensets with some IC effects: a "sea-like" (in green in the following), a "valence-like" (in red) also called "BHPS", and a central eigenset with no IC effects which we refer to as "no IC" (in blue).

Fig. 4.5 shows the result for the J/ψ+charm yield at the EIC. First, we note that, at $\sqrt{s_{ep}} = 45$ GeV (left panel in Fig. 4.5), the yield is limited to low P_T values even with the largest estimated integrated luminosity. Nonetheless, it is clearly observable if

---

[14] See [319–328] for experimental studies of J/ψ and Y associated production at the LHC and the Tevatron. For a theory review, see [9].
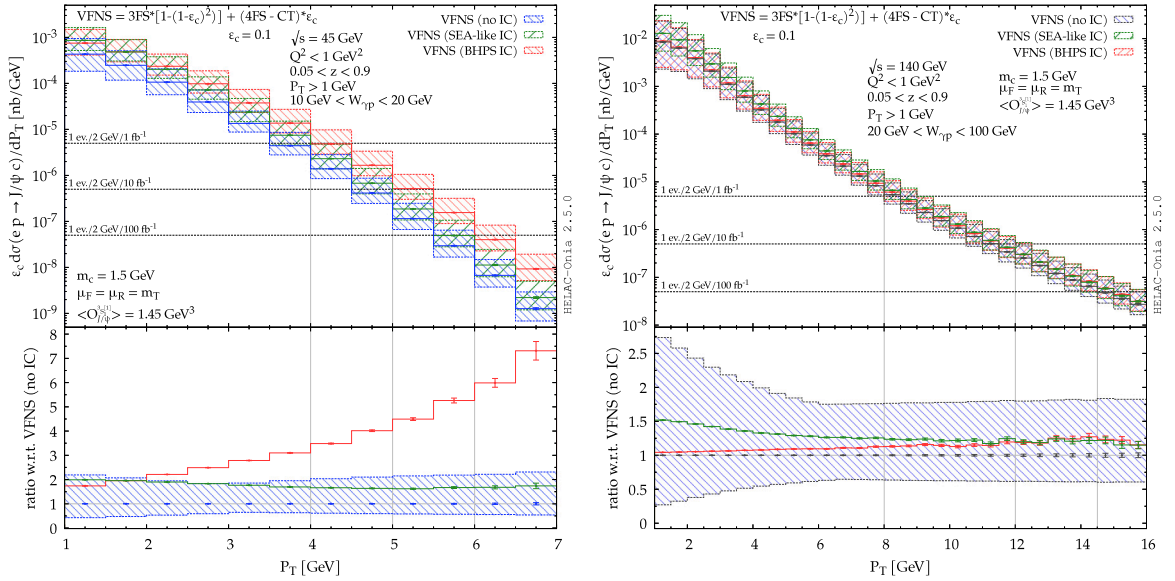
Fig. 4.5. Predictions for the J/ψ+charm yield at the EIC at $\sqrt{s_{ep}} = 45$ GeV (left) and $\sqrt{s_{ep}} = 140$ GeV (right) as a function of the J/ψ transverse momentum, P_T. The solid bands indicate the mass uncertainty while the patterns display the scale uncertainty.
Source: Figure taken from Ref. [54].

$\epsilon_c = 0.1$ with $\mathcal{O}(5000, 500, 50)$ events for $\mathcal{L} = (100, 10, 1)$ fb^{-1}. On the other hand, at $\sqrt{s_{ep}} = 140$ GeV (Fig. 4.5, right panel), the P_T range extends to ~ 14 GeV and we expect $\mathcal{O}(10000)$ events at $\mathcal{L} = 100$ fb^{-1}. Such events could be observed by measuring a charmed jet. Finally, we note that, at $\sqrt{s_{ep}} = 140$ GeV, where the valence region is not probed, no clear IC effect is visible, while at $\sqrt{s_{ep}} = 45$ GeV we expect a measurable effect, where the BHPS valence-like peak is visible with a yield enhancement as large as $5 - 6$ times the "no IC" yield. The EIC at $\sqrt{s_{ep}} = 45$ GeV will thus be the place to probe the nonperturbative charm content of the proton via associated J/ψ+charm production.

4.2. Unpolarised-nucleon TMDs

4.2.1. Unpolarised gluons

Quark TMDs have now been extracted from data with reasonable precision [331–334]. On the contrary, phenomenological studies of gluon TMDs are still very much at the beginning stage. In Ref. [335], a gluon TMD description of the Higgs-production transverse-momentum spectrum was compared to data, which, however, suffers from very large uncertainties. In Refs. [336,337], a gluon TMD description of the LHCb J/ψ-pair-production data [338] was obtained. Like for Higgs-boson production, the experimental errors are large and require the subtraction of double parton scattering contributions (see [9,339] and Section 4.7.2), which adds an additional uncertainty. In Ref. [340], it was discussed that back-to-back production of a heavy quarkonium, in particular of an Υ, and an isolated photon in proton–proton collisions at the LHC is a promising way to access the distribution of both the transverse momentum and the polarisation of gluons inside unpolarised protons. In a wide range of invariant masses of the quarkonium and photon system, gluon–gluon scattering into a photon plus a quarkonium in the CS state dominates.

In the aforementioned processes, one however probes a convolution of two gluon TMDs. At the EIC, one can probe gluon TMDs more directly through the P_T^* distribution, although upon the inclusion of ShFs (see Section 3.3.2); this also deals with convolutions. At the LHC, with the consideration of such ShFs, one even folds three transverse-momentum-dependent distributions. Another possibility to study gluon TMDs at the EIC using quarkonia is to consider the transverse-momentum imbalance between the scattered lepton and the observed J/ψ in the electron–hadron centre-of-mass frame $\bar{\mathbf{p}}_T = |\boldsymbol{\ell}'_T + \boldsymbol{P}_T|$. If large $|\boldsymbol{\ell}'_T| \simeq |\boldsymbol{P}_T| \gg |\bar{\mathbf{p}}_T|$ determines the hard scale of the process, then in quarkonium production at the EIC the leading subprocess is $e + g \rightarrow (c\bar{c})^{[8]} + e$ with the octet $c\bar{c}$ pair hadronising into an observed J/ψ. Within the hybrid factorisation formalism for SIDIS discussed in Section 2.3.2, the $\bar{\mathbf{p}}_T$ should be determined by the transverse momentum k_T of the colliding gluon (or its TMD distribution) and the quarkonium TMD ShF. Since gluon radiation from a heavy quark should be strongly suppressed compared to a light quark or a gluon, the observed momentum imbalance $\bar{\mathbf{p}}_T$ is expected to be dominated by the k_T of the colliding gluon [52]. Therefore, the $\bar{\mathbf{p}}_T$-distribution of J/ψ production in SIDIS could be a more direct observable for the gluon TMD [159].

It would be very interesting to compare the gluon TMD obtained at EIC to that from the $J/\psi + J/\psi$ or $\Upsilon + \gamma$ process at LHC in the future. In principle, gluon TMDs are process dependent, even in the unpolarised case (see e.g. [341,342]). However, provided that the CS final state dominates in $J/\psi + J/\psi$ and $\Upsilon + \gamma$ production at the LHC, these processes involve the same gluon TMD. This then would provide a nice test of TMD factorisation in combination with NRQCD and of TMD evolution, if the processes are probed at different scales. Another comparison that seems worthwhile is the extraction of gluon TMDs from open heavy-quark pair

production at the EIC [342] or from inclusive η_c or η_b production in proton–proton collisions [343,344]. Note that inclusive CS J/ψ or Υ production from two gluons is forbidden by the Landau–Yang theorem, while inclusive CO J/ψ or Υ production does not involve the same gluon TMD and may not even factorise to begin with.

4.2.2. Linearly polarised gluons

As discussed in Section 3.3.3, linearly polarised gluons lead to a $\cos 2\phi_T^*$ asymmetry in semi-inclusive electroproduction of J/ψ in unpolarised ep collisions [216,227–229,345,346]. In this section, we present some predictions for this asymmetry at low transverse momenta P_T^*.

Within NRQCD, contributions to the asymmetry comes through the fusion of a virtual photon and a gluon [227] already at Born order, i.e. $\alpha_s\alpha$, but at NNLO in v^2 via CO contributions. Such $\alpha_s\alpha$ contributions however only sit at $z = 1$. As soon as $z \neq 1$, a recoiling particle against the quarkonium is needed and Born-order contributions are at $\alpha_s^2\alpha$ both from CS and CO states. From a simple counting in v^2 the CS contributions [197] should be dominant at $z \neq 1$. However, the current LDME fits seem not to obey such a simple v^2 counting and, as a matter of fact, sometimes leads to an excess[15] in describing the scarce data available from HERA [198]. In principle, the asymmetry thus receives contributions from both CS and CO states.

The first estimate we present here is based on a model expression for the cross section [346]:

$$
d\sigma = \frac{1}{2s} \frac{d^3 l'}{(2\pi)^3 2E_l'} \frac{d^3 P_Q}{(2\pi)^3 2E_{P_Q}} \int \frac{d^3 p_g}{(2\pi)^3 2E_g} \int dx\, d^2\mathbf{k}_\perp (2\pi)^4 \delta(q + k - P_Q - p_g)
$$
$$
\times \frac{1}{Q^4} \mathcal{L}^{\mu\mu'}(l,q) \Phi^{\nu\nu'}(x,\mathbf{k}_\perp)\, \mathcal{M}_{\mu\nu}(\mathcal{M}_{\mu'\nu'})^*.
\tag{4.5}
$$

This expression is akin to the Generalised Parton Model employed to describe single-spin asymmetries in polarised proton collisions (to be discussed in Section 4.3). It is not of TMD-factorisation form and differs from Eq. (3.12) by considering the subprocess $\gamma^* + g \to Q + g$, where the additional hard gluon in the final state generates larger transverse momenta and elasticity z values below 1, while the dependence on the initial gluon transverse momentum is kept everywhere. In other words, no collinear expansion is performed and the obtained expression is thus not a CF expression either.

In Fig. 4.6, we show the $\cos 2\phi_T^*$ asymmetry as a function of P_T for $\sqrt{s_{ep}} = 140$ GeV, for fixed values of z and Q^2. Both CS and CO contributions are included. We show the results for two different models for the TMDs, the Gaussian [343] and the McLerran–Venugopalan model [347], and for two different sets of LDMEs, CMSWZ [114] and BK [111]. The asymmetry is small and depends on the chosen LDME set. Details of the calculation may be found in [345,346].

A second estimate – only relevant for $z \simeq 1$ – is based on the TMD formalism involving shape functions. Although the semi-inclusive quarkonium electroproduction is naturally described in TMD factorisation at small quarkonium transverse momentum ($P_T^* \ll M_{J/\psi} \sim Q$), there is large uncertainty due to the non-perturbative part of the TMD description and due to the lack of knowledge on the TMD shape functions. However, using the leading-order shape functions in terms of LDMEs and including leading-order TMD evolution, it is nevertheless possible to obtain rough predictions for the EIC (details on the shape function can be found in Ref. [226]). Using this approach, estimates for the $\cos 2\phi_T^*$ asymmetry in J/ψ production as a function of P_T^* can be obtained. The results are shown in Fig. 4.7 for several LDME sets (for more predictions see Ref. [348]) and for kinematics similar to that of Fig. 4.6 (to be precise, for the same $\sqrt{s_{ep}}$ and Q^2, and comparable x_B, but different values of z). Despite the large uncertainties in these TMD results (the uncertainty bands reflect the uncertainty in the non-perturbative Sudakov factor), it is clear that within these uncertainties it allows for significantly (by more than an order of magnitude) larger asymmetries than in Fig. 4.6. Its measurement may thus be feasible at EIC such that further constraints on the LDMEs, and more generally on the TMD shape functions, can be obtained in this way.

Observing a nonzero asymmetry would be a signal of linear polarisation of the gluons inside an unpolarised proton, which is expected theoretically but not established experimentally thus far. The range of predictions is currently too large to draw a definite conclusion about its observability at EIC, but that makes it all the more important to obtain first data on the $\cos 2\phi_T^*$ asymmetry. It would provide information on the distribution of linearly polarised gluons as well as on LDMEs.

4.3. Polarised-nucleon TMDs

Among the observables that can be measured at the EIC to access polarised nucleon TMDs (e.g. the Sivers function), the most common are probably the Single Transverse Spin Asymmetries (STSA), denoted A_N, or A_{UT}. Two theory approaches have been pushed forward to explain STSAs observed on polarised protons [349]. Both of them can in principle be extended to quarkonium production.

The first approach is referred to as collinear twist-3 (CT3) formalism [350–354] and, like CF, applies to single-scale processes. The STSA then arises from quark–gluon–quark or triple-gluon correlators, which are the sub-leading (in the scale) twist-3 extensions of the usual collinear PDFs (putting aside for this discussion FF contributions). Some CT3 analyses for A_N in ep collisions have been performed in the past, see e.g. [355], and only very recently this approach has been extended to STSAs in quarkonium production in polarised ep collisions [356].

---

[15] It should be clear to the reader that such computations are as of now only carried at LO whereas the LDMEs are extracted at NLO. We refer to our introductory discussion at the beginning of Section 3.2.1 regarding potential issues in doing so.
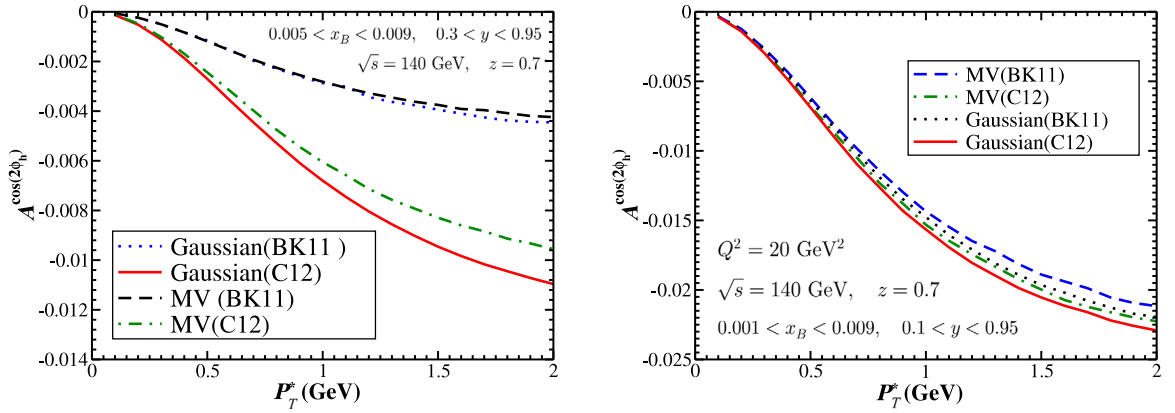
Fig. 4.6. $\cos(2\phi_h) \equiv \cos(2\phi_T^*)$ asymmetry in $e + p \to e + J/\psi + X$ process as function of the J/ψ transverse momentum P_T^* at $\sqrt{s} = 140$ GeV and $z = 0.7$. Left plot: asymmetry obtained by integrating over $x_B \in [0.005 : 0.009]$ and the inelasticity $y \in [0.3 : 0.95]$; right plot: asymmetry obtained at fixed $Q^2 = 20$ GeV^2, integrated over $x_B \in [0.001 : 0.009]$ with the corresponding y range determined from $y = Q^2/(sx_B)$. The curves are obtained using a Gaussian parametrisation for the TMDs [343] as well as McLerran–Venugopalan (MV) model [347] in the small-x region. Two sets of LDMEs are used: C12 [114] and BK11 [111].
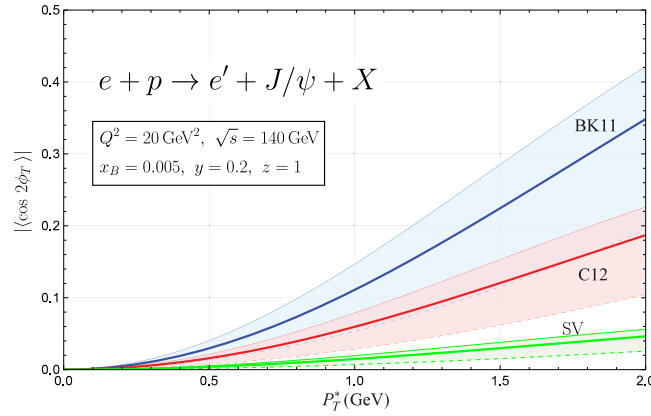
Fig. 4.7. Estimates for the $\cos 2\phi_T \equiv \cos(2\phi_T^*)$ asymmetry in J/ψ production as a function of the J/ψ transverse momentum $P_{h\perp} = P_T^*$ for three different LDME sets (central values) and including the uncertainties from the nonperturbative Sudakov factor.

The second approach is TMD factorisation, thus applicable when two very different momenta are measured, or when a small (yet perturbative) momentum is measured in a process involving a large mass (e.g. $(\Lambda_{\text{QCD}} \lesssim P_T^* \ll Q$ in SIDIS, where P_T^* is the transverse momentum of the hadron in the final state and Q^2 is the photon virtuality). The STSA arises from the Sivers TMD PDF $f_{1T}^\perp$ [357], i.e. the distribution of unpolarised partons inside the transversely-polarised hadron. In the case of quarkonium production in ep collisions, TMD factorisation has been assumed and used to compute the Sivers asymmetry in several cases [358,359].

In addition, a phenomenological approach, called the Generalised Parton Model (GPM) [360], encapsulates the Sivers mechanism via the aforementioned TMD Sivers function, assumed to be universal, but also applied in single-scale processes. This is done by keeping track of the transverse-momentum exchanges in the partonic scattering. As such, it can be considered as a hybrid approach between strict CT3 and TMD factorisation. Its extension, called Colour Gauge Invariant GPM (CGI-GPM) [361,362], allows one to recover the modified universality of the quark Sivers function between SIDIS and Drell–Yan [363–365]. Moreover, for the gluon Sivers effect, similarly to the CT3 approach case, two independent gluon Sivers functions (GSFs) appear [366], dubbed as f- and d-type. This approach has proven to be quite successful in phenomenological analyses [367–370]. One should however be careful if one wishes to draw any conclusion about the properties of the used TMDs and the underlying phenomena. In any case, it is useful to get estimates of STSAs in single-scale processes where a CT3 analysis becomes challenging, like for quarkonium production, due to still unconstrained twist-3 functions appearing in its computation. It has been applied to the quarkonium cases in several studies [362,367,371–373].

Below STSAs in different quarkonium-production processes are discussed, in the context of the EIC, which could perform these measurements by polarising a target. In general, it is believed that quarkonium-related STSA would be key player to underpin the Sivers mechanism for gluons.

Experimentally, one defines the so-called transverse STSA as

$$A_N = \frac{1}{\mathcal{P}} \frac{\sigma^\uparrow - \sigma^\downarrow}{\sigma^\uparrow + \sigma^\downarrow}, \tag{4.6}$$
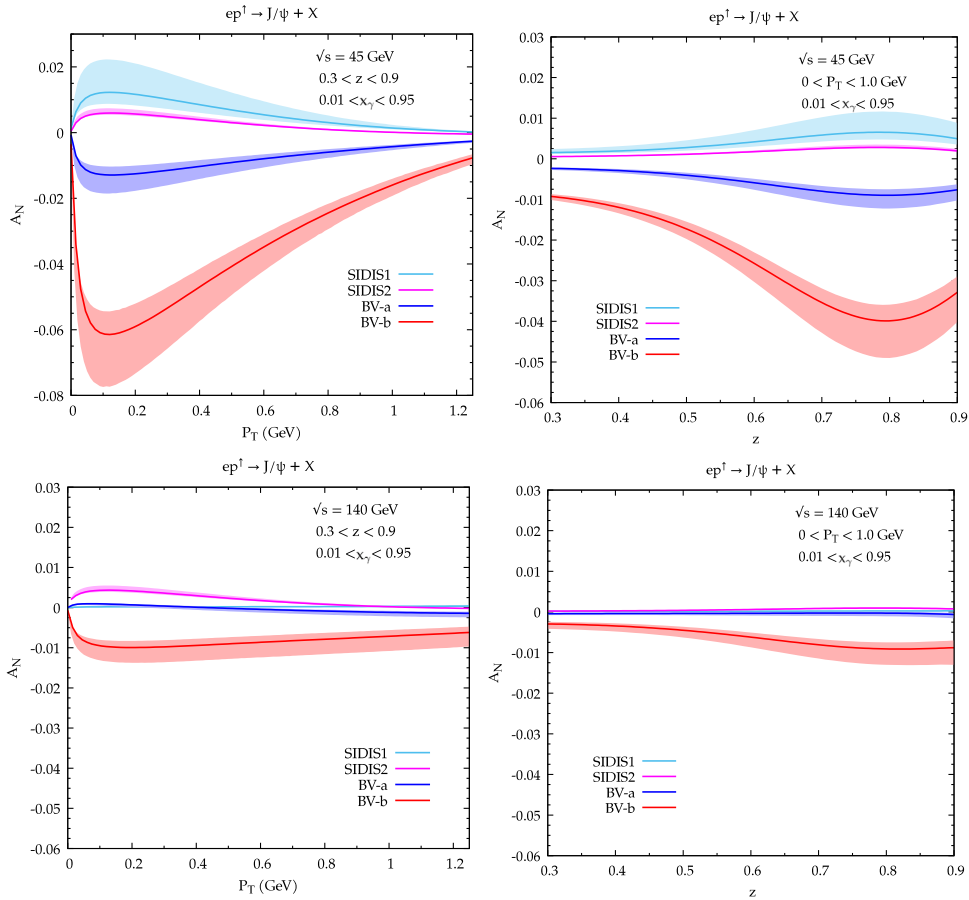
Fig. 4.8. STSA in inclusive J/ψ photoproduction ($ep^\uparrow \to J/\psi X$) as a function of the J/ψ transverse momentum, P_T (left) and z (right) at $\sqrt{s_{ep}} = 45$ GeV (top) and $\sqrt{s_{ep}} = 140$ GeV (bottom). The integration ranges are $0.3 < z < 0.9$ and $0 < P_T \leq 1$ GeV, respectively. The uncertainty bands are obtained by varying the factorisation scale by a factor 2 around $\mu_0 = \sqrt{M_{J/\psi}^2 + P_T^2}$.

where $\sigma^{\uparrow(\downarrow)}$ is the cross section of particles produced with the target nucleon spin orientation upwards (downwards), and $\mathcal{P}$ is the average nucleon polarisation. In what follows, we present predictions and projections for STSA in J/ψ inclusive photoproduction and for azimuthal weighted Sivers asymmetries in J/ψ leptoproduction in SIDIS processes.

4.3.1. EIC reach for $A_N^{J/\psi}$ for inclusive photoproduction

In this section, we study how to probe the GSF via the GPM approach by measuring the STSA in inclusive J/ψ photoproduction ($\gamma + p^\uparrow \to J/\psi + X$) [371]. In such a process, only the f-type GSF contributes to the Sivers asymmetry.

In photoproduction, there are contributions from direct and resolved photons. Resolved photons mainly contribute in the region of low elasticity z. At z close to unity, diffractive contributions become significant. In inclusive photoproduction, the variable z can be measured using the Jacquet–Blondel method. The differential cross section of inclusive J/ψ production in unpolarised ep collisions can be written as

$$E_{\mathcal{Q}} \frac{d\sigma}{d^3 \boldsymbol{P}_{\mathcal{Q}}} = \frac{1}{2(2\pi)^2} \int dx_\gamma dx_g d^2 \boldsymbol{k}_{\perp g} f_{\gamma/e}(x_\gamma) f_{g/p}(x_g, \boldsymbol{k}_{\perp g}) \delta(\hat{s} + \hat{t} + \hat{u} - M_{\mathcal{Q}}^2)$$
$$\times \frac{1}{2\hat{s}} |\mathcal{M}_{\gamma+g \to \mathcal{Q}+g}|^2. \tag{4.7}$$

Here, x_γ and x_g are the light-cone momentum fractions of the photon and gluon, respectively; $\hat{s}, \hat{t}, \hat{u}$ are the partonic Mandelstam variables; $\mathcal{M}_{\gamma+g \to \mathcal{Q}+g}$ is the matrix element for the partonic subprocess $\gamma + g \to \mathcal{Q} + g$; $f_{g/p}(x_g, \boldsymbol{k}_{\perp g})$ is the unpolarised gluon TMD, while $f_{\gamma/e}(x_\gamma)$ is the Weizsäcker–Williams distribution, giving the density of photons inside the electron [374]. For theory predictions of measurements on a transversely polarised nucleon, the STSA, as introduced in Eq. (4.6), is generally used.

Some GPM predictions for STSA in inclusive J/ψ photoproduction at the EIC for $\sqrt{s_{ep}} = 45(140)$ GeV are shown in Fig. 4.8, as a function of the J/ψ transverse momentum, P_T, as well as a function of the elasticity z. The amplitude for the J/ψ production is calculated in NRQCD. Details of the calculation can be found in Ref. [371]. The dominating channel of J/ψ production is γg fusion. The contribution to the numerator of the STSA comes mainly from the GSF [367], while the linearly polarised gluons do
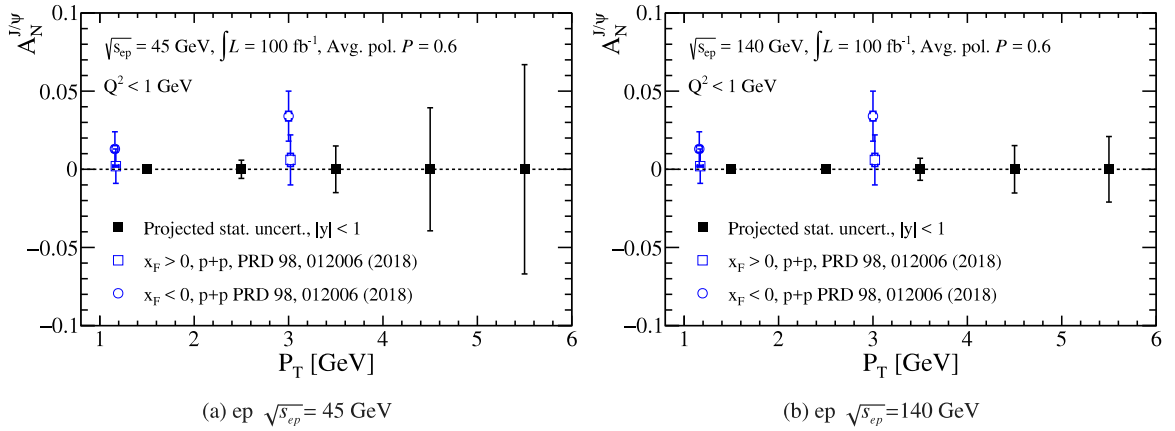
Fig. 4.9. Statistical projections for J/ψ A_N as a function of the J/ψ transverse momentum for electron+proton collisions at $\sqrt{s_{ep}}$ = 45 GeV and $\sqrt{s_{ep}}$ =140 GeV, compared to existing results from pp interactions reported by the PHENIX experiment [382].

not contribute to the denominator for this specific process. Moreover, the numerator of the asymmetry only receives contributions from CO states [375], whereas in the denominator, both CO and CS contributions are included.

We have used the GSF parametrisations (SIDIS1, SIDIS2) from Ref. [376]. BV-a and BV-b are parametrisations of the GSF in terms of up and down quark Sivers functions [377], where parameters from Ref. [378] are used. The effect of TMD evolution is not incorporated in the plot. The PDF set MSTW2008 [379] is used; the uncertainty bands have been obtained by varying the factorisation scale $\mu_F \in \left[\frac{1}{2}\mu_0, 2\mu_0\right]$, with $\mu_0 = m_T = \sqrt{M_{J/\psi}^2 + P_T^2}$ being the J/ψ transverse mass. The value of α_s is calculated at the scale μ_0 and is taken from the MSTW set. The cuts used are the following: $Q^2 < 1$ GeV^2 and $0.3 < z < 0.9$. Note that, in the photoproduction case, y coincides with x_γ. The corresponding cut is $0.01 < x_\gamma < 0.95$. As shown in Fig. 4.8, we expect A_N to be small and positive in the SIDIS1 and SIDIS2 cases, while it is larger (in size) but negative when the GSF is parametrised in terms of the up- and down-quark Sivers functions.

Another estimate is shown in Fig. 4.9. Here, projections for statistical uncertainties for the J/ψ A_N measurement as a function of transverse momentum for ep collisions at $\sqrt{s_{ep}}$ =45 GeV and $\sqrt{s_{ep}}$ = 140 GeV for an integrated luminosity $\int \mathcal{L} = 100$ fb^{-1} are presented. We consider the J/ψ reconstruction via its electron decay channel ($J/\psi \to e^+e^-$, $\mathcal{B} = 5.94 \pm 0.06\%$), and we assume the single-electron measurement efficiency to be 80% and constant with respect to its transverse momentum and in the pseudorapidity interval $|\eta| < 2$. The J/ψ measurement efficiency is calculated using decay kinematics simulated with PYTHIA8 [380] (see Appendix B for details). Based on these results, we assume the J/ψ measurement efficiency to be 64%. Furthermore, we assume the signal-to-background ratio S/B = 1, and use the same method as in Ref. [381] to estimate statistical uncertainties on A_N. For the expected cross section for prompt J/ψ production in ep collisions at the EIC, we consider the CSM predictions from Ref. [54], which were shown to approximately reproduce HERA data. For illustration, the projections are compared to results from pp collisions reported by the PHENIX experiment [382]. At low P_T, the statistical precision is at the per-cent level, exceeding the quality of the corresponding pp data. In this range, the final uncertainty will be dominated by systematic effects. The uncertainties increase fast with increasing P_T of J/ψ because the P_T spectrum is predicted to be rather steep. Nonetheless, such a measurement would be valuable for constraining gluon TMDs at low transverse momentum.

Finally, we suggest that the associated photoproduction of J/ψ and a jet, having them back-to-back, can also probe the GSF [227,358]. In this case the produced J/ψ can have large transverse momentum, and need not be in the forward region. A wide kinematical region can be covered by varying the invariant mass of the J/ψ-jet pair.

4.3.2. Azimuthal asymmetries for J/ψ production in SIDIS at the EIC

In this section we consider the Sivers effect in the SIDIS process, $e(l) + p^\uparrow(P_N) \to e(l') + J/\psi(P_{J/\psi}) + X$, that represent a promising tool to probe the GSF. The weighted Sivers asymmetry for such a process is defined as

$$A_N^{\sin(\phi_T^* - \phi_S^*)} \equiv 2 \frac{\int d\phi_S^* d\phi_T^* \sin(\phi_T^* - \phi_S^*)(d\sigma^\uparrow - d\sigma^\downarrow)}{\int d\phi_S^* d\phi_T^* (d\sigma^\uparrow + d\sigma^\downarrow)} \equiv \frac{\int d\phi_S^* d\phi_T^* \sin(\phi_T^* - \phi_S^*) d\Delta\sigma(\phi_S^*, \phi_T^*)}{\int d\phi_S^* d\phi_T^* d\sigma}, \qquad (4.8)$$

where $d\sigma^{\uparrow(\downarrow)} = d\sigma^{\uparrow(\downarrow)}/dQ^2 dy d^2 P_T^* dz$ is the differential cross section with the initial proton polarised along the transverse direction $\uparrow$ ($\downarrow$) with respect to the lepton plane in the $\gamma^* p$ centre-of-mass frame (at an angle ϕ_S^*).

We start by presenting the predictions in the CT3 formalism. In Ref. [356], the twist-3 contributions to the unpolarised and polarised cross sections (respectively denominator and numerator of Eq. (4.8)) were computed in the CSM. Among the different contributions, one has access to the gluon Sivers effect via the CT3 gluon Qiu–Sterman function, which at LO is related via an integral relation to the GSF first $k_\perp$ moment. Predictions for the gluon Sivers asymmetry at the EIC at $\sqrt{s_{ep}}$ = 45 GeV are presented in Fig. 4.10. They are computed at $Q^2 = 10$ GeV^2, $x_{(B)} = 0.005$ and $P_T = 2$ GeV, and are presented as a function of z for two different
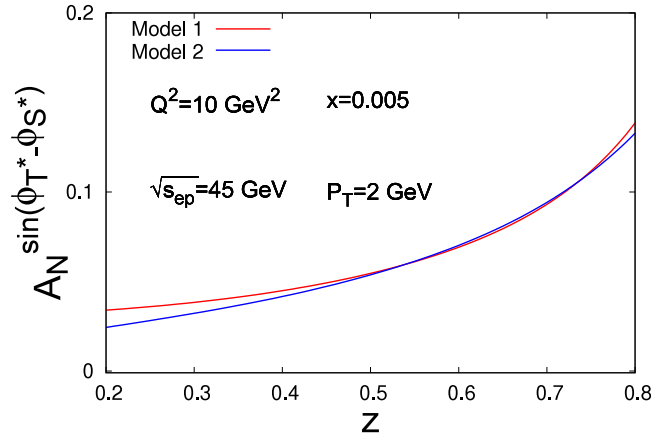
Fig. 4.10. CSM predictions for the gluon Sivers asymmetry in the CT3 formalism for the $ep^\uparrow \to e + J/\psi + X$ process as a function of z at $\sqrt{s_{ep}} = 45$ GeV. Predictions for two different models are given.
Source: Figure adapted from Ref. [356].

models of the gluon Qiu–Sterman function. Both models are proportional to $f_{g/p}(x)$, the unpolarised collinear gluon PDF, and read

$$\text{Model 1:} \quad 0.002\, x f_{g/p}(x), \tag{4.9}$$

$$\text{Model 2:} \quad 0.0005\, \sqrt{x} f_{g/p}(x). \tag{4.10}$$

Notice that, as these CSM predictions are ratios of cross sections, they do not depend on the value of the CS LDME. Both models predict a sizeable Sivers asymmetry, with a steady increase as a function of z, reaching up to $\sim 13 - 14\%$ at $z = 0.8$.

Another prediction for the Sivers asymmetry is performed within the GPM at $\alpha \alpha_s^2$. In order to study the effects of initial- and final-state interactions (ISIs and FSIs) on the Sivers asymmetry, the CGI-GPM approach [361,362] is employed. In Ref. [227], the same observable was studied at $\mathcal{O}(\alpha \alpha_s)$ within the GPM, which implies $z = 1$. Here the analysis is extended to the region $z < 1$.

Assuming TMD factorisation within the GPM framework, the unpolarised differential cross section, entering the denominator of Eq. (4.8), can be written as

$$\frac{d\sigma}{dQ^2 \, dy \, d^2\boldsymbol{P}_T^* \, dz} = \frac{1}{(4\pi)^4 zs} \sum_a \int \frac{dx_a}{x_a} d^2\boldsymbol{k}_{\perp a} \delta\left(\hat{s} + \hat{t} + \hat{u} - M_{J/\psi}^2 + Q^2\right) \sum_n \frac{1}{Q^4} f_{a/p}(x_a, k_{\perp a}) L^{\mu\nu} H_{\mu\nu}^{a,U}[n] \langle \mathcal{O}^{J/\psi}[n] \rangle, \tag{4.11}$$

where $a = g, q, \bar{q}$ and $H_{\mu\nu}^{a,U}[n]$ is calculated at the perturbative order $\alpha \alpha_s^2$ using NRQCD. More precisely, it is the squared amplitude of the partonic process $\gamma^* + a \to c\bar{c}[n] + a$, averaged/summed over the spins and colours of the initial/final parton, with $n = {}^3S_1^{[1,8]}, {}^1S_0^{[8]}, {}^3P_J^{[8]}$, $J = 0, 1, 2$. $L^{\mu\nu}$ is the standard leptonic tensor and $\langle \mathcal{O}^{J/\psi}[n] \rangle$ represents the LDME of the state indicated by n. The numerator in Eq. (4.8) is directly sensitive to the Sivers function and within the GPM reads

$$d\Delta\sigma^{\text{GPM}} = \frac{1}{(4\pi)^4 zs} \sum_a \int \frac{dx_a}{x_a} d^2\boldsymbol{k}_{\perp a} \delta\left(\hat{s} + \hat{t} + \hat{u} - M_{J/\psi}^2 + Q^2\right) \sin(\phi_S^* - \phi_a^*)$$

$$\times \sum_n \frac{1}{Q^4} \left(-2\frac{k_{\perp a}}{M_p}\right) f_{1T}^{\perp a}(x_a, k_{\perp a}) L^{\mu\nu} H_{\mu\nu}^{a,U}[n] \langle \mathcal{O}^{J/\psi}[n] \rangle, \tag{4.12}$$

where $f_{1T}^{\perp a}(x_a, k_{\perp a})$ is the Sivers function.

The numerator of the asymmetry in the CGI-GPM is given by

$$d\Delta\sigma^{\text{CGI}} = \frac{1}{2s} \frac{2}{(4\pi)^4 z} \int \frac{dx_a}{x_a} d^2\boldsymbol{k}_{\perp a} \delta\left(\hat{s} + \hat{t} + \hat{u} - M_{J/\psi}^2 + Q^2\right) \sin(\phi_S^* - \phi_a^*) \left(-2\frac{k_{\perp a}}{M_p}\right)$$

$$\times \sum_n \frac{1}{Q^4} L^{\mu\nu} \left\{ \sum_q f_{1T}^{\perp q}(x_a, k_{\perp a}) H_{\mu\nu}^{q,\text{Inc}}[n] + f_{1T}^{\perp g(f)}(x_a, k_{\perp a}) H_{\mu\nu}^{g,\text{Inc}(f)}[n] \right\} \langle \mathcal{O}^{J/\psi}[n] \rangle, \tag{4.13}$$

where $H_{\mu\nu}^{a,\text{Inc}}[n]$ is the perturbative squared amplitude calculated by incorporating the FSIs within the CGI-GPM approach. Note that, in Eq. (4.13), there is no contribution from the d-type GSF. In fact, in ep collisions, ISIs are absent due to the colourless nature of the virtual photon and only the f-type GSF is contributing to the Sivers asymmetry [373]. This means that quarkonium production in ep collisions is a powerful tool to directly access the process-dependent f-type GSF. Moreover, the modified colour factor associated with the ${}^3S_1^{[1]}$ state is zero in the CGI-GPM approach, which leads to a vanishing Sivers asymmetry in the CSM.

By adopting a Gaussian factorised form for the unpolarised TMD distribution, a Gaussian-like Sivers distribution and by maximising the latter we can give estimates for the upper bounds of the Sivers asymmetry (Eq. (4.8)) at the EIC. Results are presented in Fig. 4.11, and are computed using the following kinematical cuts: $2.5\,\text{GeV}^2 < Q^2 < 100\,\text{GeV}^2$, $10\,\text{GeV} < W_{\gamma p} < 40\,\text{GeV}$, $0.3 < z < 0.9$
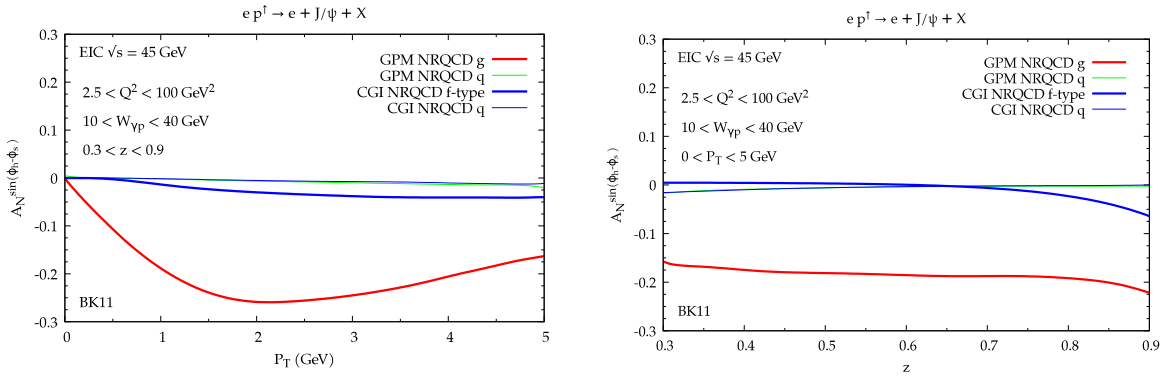
Fig. 4.11. Maximised contributions to the Sivers asymmetry for the $ep^\uparrow \to e + J/\psi + X$ process as a function of the J/ψ transverse momentum P_T (left) and z (right) obtained with the BK11 LDME set [111] at $\sqrt{s_{ep}} = 45$ GeV: GSF contribution in NRQCD for the GPM (red solid thick line) and CGI-GPM (blue, dashed, thick line); quark Sivers contribution in NRQCD for the GPM (green, dashed, thin line) and CGI-GPM (blue, dotted, thin line).
Source: Figure adapted from Ref. [383].

and $P_T < 5$ GeV. The BK11 LDMEs set [111] is adopted.

The asymmetry is mostly dominated by the GSF, while the quark contribution is negligible. This indicates that such an observable is a powerful tool to probe the unknown GSF. The GPM predicts negative values around 20%. The asymmetry is drastically reduced in size in the CGI-GPM due to colour-factor relative cancellations and the absence of the $^3S_1^{[1]}$-state contribution and is essentially driven by the f-type GSF.

4.4. Generalised parton distributions

Information on the three-dimensional structure of the nucleon, correlating the transverse position of partons with their longitudinal momentum, is provided by GPDs. Processes to access GPDs include Deeply Virtual Compton Scattering (DVCS) and Deeply Virtual Meson Production (DVMP). A factorisation theorem has been proven for DVCS in the Bjorken limit [384,385]. It allows one to compute the DVCS amplitude as the product of some GPDs and corresponding coefficient functions that can be calculated perturbatively. GPDs are in very solid theoretical footing: at leading-twist level, all-order QCD-factorisation theorems directly relate the GPDs to particular hard exclusive scattering processes. GPDs are thus process-independent, universal quantities. In the case of DVMP, factorisation applies in the case of longitudinally polarised photons. The hard-scattering process includes the exchange of hard quarks and gluons, involving the strong coupling constant α_s and a meson distribution amplitude, which is not completely understood to date.

The GPDs do not uphold a probabilistic interpretation like PDFs do, but are well-defined in quantum field theory as matrix elements of bilocal quark and gluon operators at a light-like separation. In the light-cone gauge at leading twist, the quark GPD is

$$
\begin{aligned}
F^q(x,\xi,t) &= \frac{1}{2} \int \frac{dz^-}{2\pi} e^{ixP^+ z^-} \langle p' | \bar{\psi}^q \left(-\frac{z}{2}\right) \gamma^+ \psi^q \left(\frac{z}{2}\right) | p \rangle |_{z^+ = z_\perp = 0} \\
&= \frac{1}{2P^+} \left[H^q(x,\xi,t) \bar{u}(p') \gamma^+ u(p) + E^q(x,\xi,t) \bar{u}(p') \frac{i\sigma^{+\mu} \Delta_\mu}{2m_N} u(p) \right]
\end{aligned}
\tag{4.14}
$$

and the gluon GPD,

$$
\begin{aligned}
F^g(x,\xi,t) &= \frac{1}{P^+} \int \frac{dz^-}{2\pi} e^{ixP^+ z^-} \langle p' | F^{+\mu} \left(-\frac{z}{2}\right) F_\mu^+ \left(\frac{z}{2}\right) | p \rangle |_{z^+ = z_\perp = 0} \\
&= \frac{1}{2P^+} \left[H^g(x,\xi,t) \bar{u}(p') \gamma^+ u(p) + E^g(x,\xi,t) \bar{u}(p') \frac{i\sigma^{+\mu} \Delta_\mu}{2m_N} u(p) \right],
\end{aligned}
\tag{4.15}
$$

where $z = (z^+, z_\perp, z^-)$ are the light-cone coordinates, P^+ is the light-cone plus-component of the average of the incoming- and outgoing-nucleon momenta, x is he fractional parton plus-component momentum of the nucleon, ξ the skewness variable and t the Mandelstam variable, which represents the four-momentum transfer squared to the nucleon. The symbols γ and σ are the Dirac matrices, u and $\bar{u}$ are nucleon spinors and m_N is the mass of the nucleon. Here, F^q and F^g are both expressed as a Fourier transform of a matrix element of a chiral-even operator formed from either quark fields ψ^q or the gluon-field strength tensor $F^{\mu\nu}$. The result is a decomposition into twist-2 parton-helicity conserving GPDs H and E.

GPDs cannot be directly extracted from experimental data. Indeed, in the expression of the cross section of exclusive electroproduction processes, GPDs appear in convolution integrals known as Compton Form Factors (CFFs). These CFFs are complex quantities, the real and imaginary parts of which provide complementary constraints on GPDs. The DVCS CFF $\mathcal{H}$, at leading-twist and leading-order (and at fixed momentum transfer t and skewness ξ), for example, is given by

$$
\mathcal{H} = \int_{-1}^{1} dx \frac{F^q(x,\xi,t)}{x - \xi + i\epsilon} = \mathcal{P} \int_{-1}^{1} dx \frac{F^q(x,\xi,t)}{x - \xi} - i\pi F^q(\pm\xi,\xi,t),
\tag{4.16}
$$
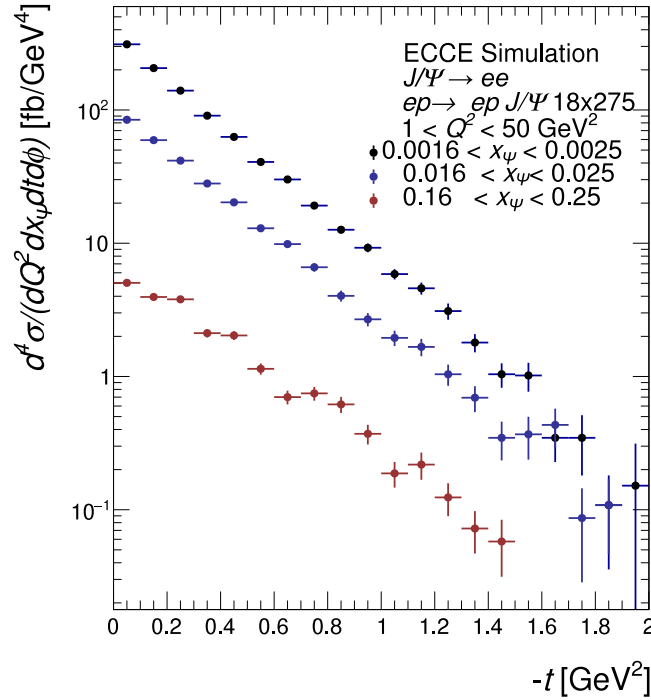
Fig. 4.12. Simulation of the J/ψ exclusive electroproduction cross section as a function of the four-momentum transfer squared t for different bins in x_Q, at the EIC, for lepton–proton beam energies of 18x275 GeV^2. The integrated luminosity is assumed to be 10 fb^{-1}.

and with

$$\sigma(\gamma^* p \to \gamma p) \propto |\mathcal{H}|^2. \tag{4.17}$$

In addition, there are also spin-dependent GPDs and are probed in measurements in which the spin or polarisation state is fully defined. If the spin states are averaged over, as in the description of an unpolarised measurement, then there is no way to have a direct dependence on, or be sensitive to, these objects. Moreover, there are also parton-helicity-flip GPDs (chiral odd), in which the initial- and final-state hadrons have different polarisations.

GPDs are also connected to the distribution of pressure and shear forces inside the nucleon [386,387] and, furthermore, the second moment of a particular combination of GPDs is related to the angular momenta of quarks and gluons via Ji's relation [388]. A comprehensive review on the phenomenology of GPDs in DVCS can be found in [389].

4.4.1. Gluons

DVCS is sensitive to quarks and, at higher order and/or higher twist, also to gluons. On the other hand, the production of light mesons in DVMP probes quarks and gluons, depending on the energy scale at which the process is measured. However, J/ψ production in exclusive photoproduction (or electroproduction) reactions is a golden channel for gluon GPDs. Indeed, in this case the quark exchange plays only a minor role and due to the large scale provided by the heavy-quark mass, perturbative calculations are expected to be applicable even for photoproduction [14].

At the EIC, precise measurements of exclusive cross sections will be possible in order to map out the dependence on the squared momentum transfer to the nucleon $t = (P_N - P'_N)^2$ for J/ψ, ϕ and K, among others. EIC will cover the region of $0 < |t| < 1.5$ GeV^2, down to an impact parameter of ~ 0.1 fm.

Fig. 4.12 shows the projected precision obtainable at the EIC in the exclusive J/ψ electroproduction cross section as a function of the momentum transfer t to the proton, for different bins in $x_Q = (Q^2 + M_Q^2)/(2\,p \cdot q)$, the x-Bjorken equivalent scale variable for heavy mesons. The projections are produced using the LAGER [390] event generator and are based on the calculations presented in [391]. LAGER is described as a modular accept–reject generator, capable of simulating both fixed-target and collider kinematics, and has previously been used for vector-meson studies at EIC kinematics, with significant recent developmental effort in support of DVMP studies. The transverse spatial distribution of partons can be obtained by a Fourier-transform of the cross section as a function of t.

The key experimental feature of hard exclusive channels such as J/ψ electroproduction is the detection of the recoil protons in the far-forward detectors, in particular in the B0 spectrometer and the Roman Pots. This allows for accurate computation of the momentum transfer t, which is the Fourier conjugate variable to the impact parameter. A wide and continuous acceptance that extends to low-t is essential for a precision extraction of transverse-position distributions of partons.

On the other hand, far-forward detectors can also help in detecting the process where the proton does not stay intact but breaks up. The dominance of this process over exclusive J/ψ production increases with increasing t. In [392], it has been shown that the cross-section measurement of dissociative diffractive J/ψ photoproduction at large t as a function of the rapidity gap between the produced J/ψ and the dissociated proton is possible at the EIC. The interest of this process lies in the presence of two comparable hard scales, the charm mass and the large t, and hence the possibility to probe the presence of Balitsky–Fadin–Kuraev–Lipatov (BFKL) dynamics.

4.4.2. Light quarks

In [290,291,393–396], it was shown that the rapidity differential cross section for exclusive J/ψ photoproduction in heavy-ion ultra-peripheral collisions at NLO decomposes into a complicated interplay of contributions from both the quark and gluon sectors as well as their interference, over the whole region of rapidities accessible at the LHC. In particular, at mid-rapidities the quark contribution was shown to be the dominant player. While such a picture remains in place under a conservative factorisation and renormalisation scale variation, and is reflected in the original work of Ivanov et al. [14] in the context of the underlying hard scattering process, $\gamma p \to J/\psi p$, which drives the ultra-peripheral collisions, and indeed the eA collisions at the EIC, care must be taken to interpret such results. Indeed, it was shown that such a hierarchy arises from a coincidental cancellation of LO and NLO gluon contributions together with the positive-definite quark contribution at NLO. At NNLO, when there are also interference contributions wholly within the quark sector, one may anticipate a different final picture. Υ photoproduction on the other hand, sitting at a higher scale, does not exhibit such a complicated interplay of contributions at NLO, see [397], with the gluon contribution dominating over all rapidities. The J/ψ results are therefore indicative of the long-standing problem of the scale dependence and perturbative instability exhibited by low-scale processes. Indeed, after the so-called Q_0 subtraction' [283] discussed in Section 4.1.2, the quark contribution to the amplitude becomes negligible. A new study [398] which includes the high-energy resummation effects in the coefficient function of exclusive J/ψ photoproduction in the HEF formulism similar to one applied in the inclusive case [149,150] supports this conclusion.

4.5. Generalised TMDs

The non-perturbative structure of the hadrons can be described in terms of parton correlation functions such as form factors, 1D PDFs and their 3D generalisations in terms of TMDs and GPDs. All these functions can be derived from more general objects called GTMDs [399–402]. Hence, GTMDs are also known as the "mother distributions". There are several compelling reasons to study GTMDs . Firstly, GTMDs contain physics that outmatches the content encoded in the TMDs and GPDs. Secondly, via Fourier transformation, GTMDs can be related to Wigner functions, a concept that spans across other branches of physics as well. Partonic Wigner functions may allow for a hadron tomography in 5D phase-space [403,404]. Thirdly, certain GTMDs can unravel unique correlations between parton orbital motion and spin inside hadrons [405–409]. In particular, the Wigner distribution can be used for a gauge-invariant definition of the canonical orbital angular momentum [407,410–415], which makes this quantity also accessible for calculations in lattice QCD [416,417]. Fourthly, there is a particular GTMD that is related to the Sivers TMD. By establishing a relation between GTMDs and the QCD odderon at small x, the authors in Ref. [418] have shown that one can access the gluon Sivers TMD through exclusive π^0 production in unpolarised ep scattering. This finding goes against our traditional belief that the Sivers function can only be measured with a transversely polarised target.

For a long time, it was questionable whether GTMDs could be measured at all. The authors in Ref. [419] were the first to propose addressing gluon GTMDs through exclusive diffractive dijet production in lepton–nucleon/nucleus collisions at small x (see left panel of Fig. 4.13). The GTMDs depend on the average transverse parton momentum $\vec{k}_\perp$ and the transverse momentum transfer to the target $\vec{\Delta}_\perp$, and it is possible to decompose the angular correlation between these two vectors into a Fourier series. The leading angular dependent term, known as the elliptic distribution, has a characteristic $\cos(2\phi)$ angular modulation similar to the observed elliptic flow phenomenon in relativistic heavy-ion collisions [420–422]. It was shown that the cross section of this diffractive dijet process also exhibits such a $\cos(2\phi)$ behaviour where ϕ is now the angle between the dijet total and relative momenta. The pioneering work in Ref. [419] gave impetus to the field of GTMDs and subsequently many other interesting ideas were put forward; see, for instance, Refs. [423–428].

An alternative idea [420,429] is to exclusively produce a single particle (instead of two jets) such as a J/ψ. The role of the second jet is now played by the scattered electron which must be detected. It has been shown that in this process the elliptic $\cos 2\phi$ correlation of the gluon GTMD manifests itself in the angular correlation between the scattered electron and the J/ψ [429] (or the recoiling proton/nucleus [420]). For a proton target, a sizable v_2 of a few percent or larger has been predicted [429]. The same effect can also be seen in DVCS, but J/ψ production is more promising since there is no contamination from the Bethe–Heitler process. In the GPD-based approach to DVCS, the same angular correlation is known to be generated by the so-called gluon transversity GPD. The elliptic gluon GTMD is the mother distribution of the gluon transversity GPD [17].

Quarkonium production processes are also useful to study other aspects of GTMDs. In Ref. [430], it was shown that exclusive double production of pseudo-scalar quarkonia ($\eta_{c/b}$) in hadronic collisions could serve as a direct probe of GTMDs for gluons at
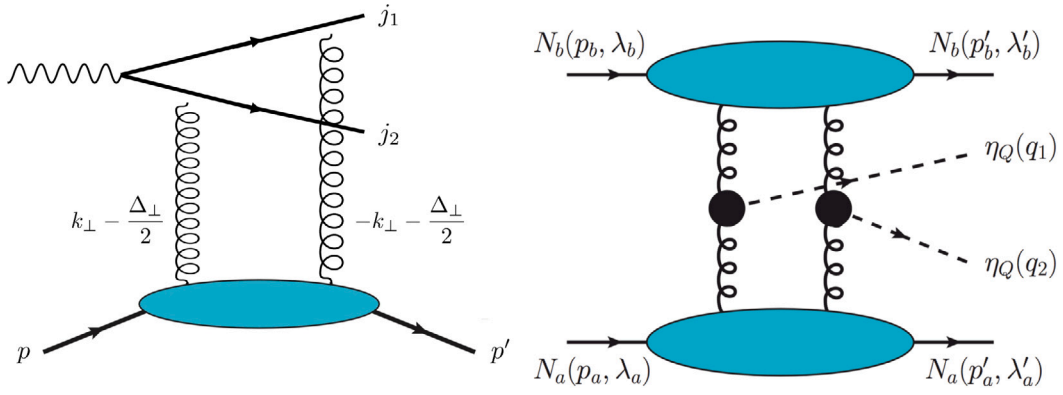
Fig. 4.13. Left panel: leading-order Feynman graph for the exclusive dijet production in lepton–nucleon/nucleus scattering. Right panel: leading-order Feynman graph for the exclusive double-quarkonium production in nucleon–nucleon collisions. The perturbative subprocess $gg \to \eta_Q$ is computed in the colour-singlet model in NRQCD.
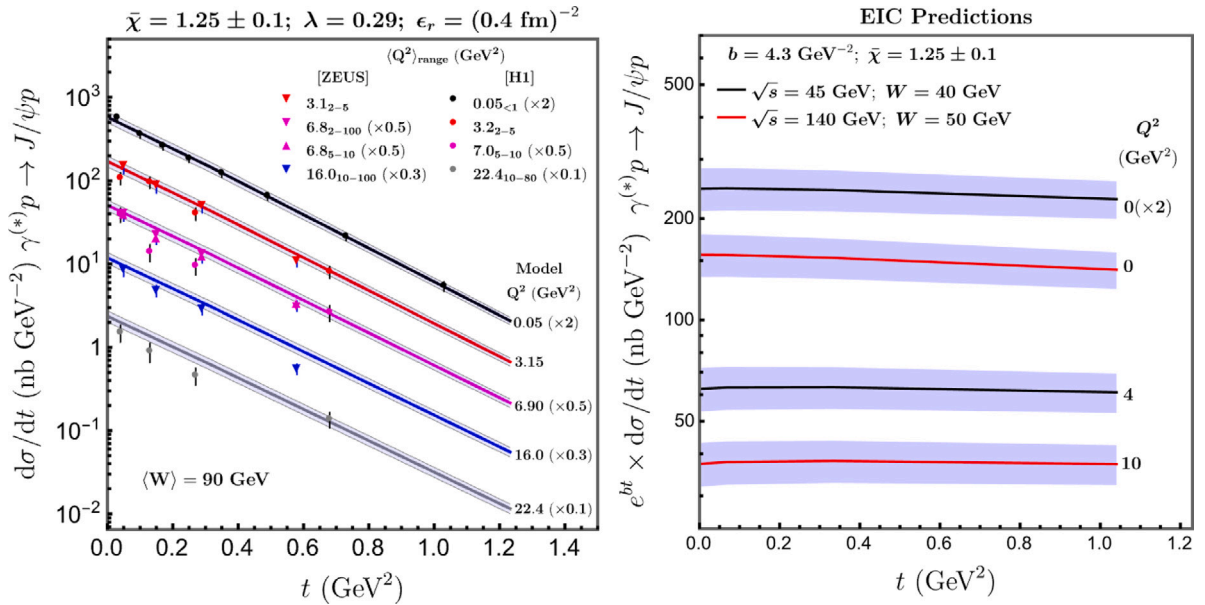
Fig. 4.14. Left: fit of exclusive diffractive J/ψ data from H1 [278] and ZEUS [271] using a gluon GTMD model [432] with boosted Gaussian wave functions from [433]. Right: EIC predictions with the same parametrisations for $W_{\gamma^*p} = 40$ GeV at $\sqrt{s_{ep}} = 45$ GeV and for $W_{\gamma^*p} = 50$ GeV at $\sqrt{s_{ep}} = 140$ GeV.

moderate x (see right panel of Fig. 4.13). A similar idea came out in Ref. [431] where the authors proposed to access the Weizsäcker–Williams gluon GTMD at small x via double χ_{cJ} or η_c meson production in diffractive pp/pA collisions where (one of) the proton(s) stays intact.

At the EIC, the primary process to look for gluon GTMDs is exclusive diffractive dijet production, as mentioned above. A challenge, however, is that due to the limited centre-of-mass energy, the transverse momenta of diffractively produced particles in the forward rapidity region are often not large enough to cleanly reconstruct jets. As a first step to test the underlying GTMD picture of exclusive diffractive production processes, like dijet or J/ψ electro- and photoproduction at small x, a GTMD model can be fitted to existing HERA data. Predictions can then be obtained for EIC in different kinematic regions. This has been considered for dijet production in [432], where it was shown that a gluon GTMD model based on the impact-parameter-dependent McLerran–Venugopalan model can give a reasonably good description of diffractive dijet production data from H1 [432]. The same framework (slightly extended) can be applied to exclusive diffractive J/ψ production to describe the H1 and ZEUS data, as shown in Fig. 4.14 on the left ($\sqrt{s_{ep}} = 319$ GeV). With the resulting GTMD parametrisation, predictions for exclusive diffractive J/ψ production at EIC can be obtained. These are shown for $\sqrt{s_{ep}} = 45$ and 140 GeV in Fig. 4.14 on the right. Generally, at small x, and in particular for nuclear targets, a GTMD-based description becomes more appropriate for exclusive and diffractive processes. Exclusive quarkonium production at the EIC could be used to systematically study the transition between the collinear and $k_\perp$-dependent frameworks.

4.6. Exclusive quarkonium production near threshold and the trace anomaly

It has been noticed long ago that the mass M of a hadronic system can be expressed in terms of the forward matrix element of the trace of the QCD energy–momentum tensor as [434,435]

$$2M^2 = \langle p| \frac{\beta}{2g} F^2 + (1 + \gamma_m)\overline{\psi}m\psi \,|p\rangle, \tag{4.18}$$

where β and γ_m are anomalous dimensions and the operator $\beta/(2\,g)\,F^2 + \gamma_m \overline{\psi}m\psi$ is the QCD trace anomaly [436,437]. The decomposition of the r.h.s. of Eq. (4.18) into quark and gluon contributions has been discussed in detail [438,439]. Other mass decompositions, based this time on the QCD Hamiltonian, have also been proposed in the literature [440–446]. The latter all require the knowledge of the same four quantities, combined in different ways for the physical interpretation [447]. Two of these quantities, namely the quark momentum fraction $A_q(0) = \langle x \rangle_q$ and the gluon momentum fraction $A_g(0) = \langle x \rangle_g$, are already well known. The other two numbers $\bar{C}_q(0)$ and $\bar{C}_g(0)$ can be determined by measuring the quark and gluon contributions to Eq. (4.18). While the quark condensate $\langle p|\overline{\psi}m\psi|p\rangle$ has already received a lot of attention over the last decades (see [448] and references therein), little is known so far about the gluon condensate $\langle p|F^2|p\rangle$ from the experimental side.

Four-momentum conservation implies that $A_q(0) + A_g(0) = 1$ and $\bar{C}_q(0) + \bar{C}_g(0) = 0$. From a phenomenological point of view, the knowledge of $A_q(0)$ and the quark condensate is therefore sufficient for specifying all the contributions to the various mass decompositions (see [444,449] for recent estimates). Measuring the gluon condensate is not expected to change much the current phenomenology of the nucleon mass, but it will provide a fundamental sanity check of the mass sum rules and the virial theorem [447]. Another motivation for measuring the gluon condensate is that it could shed light on the existence and nature of the recently discovered LHCb "pentaquark" states [450].

More than two decades ago, exclusive heavy-quarkonium production near the production threshold, was suggested as a promising tool for constraining the gluon condensate in the nucleon [15,16]. This development together with the prospect to obtain through this process further information about the gravitational structure of the nucleon, which is contained in the form factors of the energy–momentum tensor (such as the mass radius and mechanical pressure distributions [386,387,451]), as well as the measurement of exclusive J/ψ photoproduction near threshold at Jefferson Lab [24,452,453] has stimulated a significant amount of activities in this area [296,391,454–474]. Recently, it was argued that the extraction of the gravitational form factors through exclusive quarkonium photoproduction will necessarily retain model dependence [469,473]. Generally, access to the gravitational structure of the nucleon is expected to be cleaner for electroproduction [458,466]. At the EIC, one would have the unique opportunity to explore photo- and electroproduction of both J/ψ and Y close to threshold [450].

4.7. Probing double parton scattering at the EIC with quarkonium pairs

4.7.1. A word of context

In this section, we study the possibility to observe double-J/ψ production at the EIC. In particular, we discuss both the single-parton-scattering (SPS) and the double-parton-scattering (DPS) mechanisms, which could lead to the observation of a pair of J/ψ. In fact, the cross section for the latter case would allow one to access new information on the so-called proton double-parton-distribution functions (dPDFs), which encode novel information on the partonic structure of the proton.

Let us recall the analysis of four-jet photoproduction at HERA, which pointed out the relevance of multi-parton interactions (MPIs) to account for the measured total cross section [475]. In Ref. [476], the DPS cross section for four-jet photoproduction was calculated. DPS are initiated by a quasi-real photon [477] splitting into a $q\bar{q}$ pair. The same strategy as for pp collisions [478–488] has been used to evaluate the photoproduction cross section. At this stage, the only missing quantity was $\sigma_{eff}^{\gamma p}$, the effective size of the photon–proton interaction, which is expected to be process independent. It was estimated for the first time [476] and compared to that of the pp case from Refs. [33,339,489–491]. The four-jet DPS cross section has then been calculated for the HERA kinematics [492] to be $\sigma_{DPS}^{4j} \geq 30$ pb, while the total one was inferred from [492] to be $\sigma_{tot}^{4j} \sim 135$ pb at $x_\gamma < 0.75$. This indicated that the DPS contribution is sizeable even in photon-induced reactions for the production of four jets and that it could also be so for other processes like quarkonium-pair production. Further analyses of the HERA data could lead to the extraction of $\sigma_{eff}^{\gamma p}$ and, in turn, provide a first access to the mean transverse distance between two partons in the proton, an unknown property of the proton structure. To this aim, the needed luminosity was evaluated to be $\mathcal{L} \sim 200$ pb^{-1} [476]. Double-J/ψ production from DPS at EIC will be presented below along the same lines.

4.7.2. DPS at the EIC and J/ψ-pair production

Here we discuss J/ψ-pair photoproduction at the EIC. In ep collisions, the radiated quasi-real photon can interact with the partons within the proton in two ways, namely as a "pointlike" particle and via its "resolved" hadronic content. In the first case, the photon "directly" interacts with the target while, in the latter case, the photon splits into (colour charged) partons, which subsequently interact with partons in the proton.

The treatment of the interaction between a proton and such a resolved photon is carried out by using a PDF describing the momentum distributions of these partons inside the photon. One of these is the GRV [493,494] set, which is adopted here. For what regards the quarkonium-production mechanisms, the CSM (i.e. the leading v^2 contribution of NRQCD) is used. Fig. 4.15 shows different Feynman graphs for SPS and DPS photoproduction. In the SPS case, the contributing channels at leading order, i.e. $\alpha\alpha_s^4$, are shown in Fig. 4.15(a-c), namely $\gamma q \to J/\psi + J/\psi + q$, $gg \to J/\psi + J/\psi$ and $q\bar{q} \to J/\psi + J/\psi$. However, the graph in Fig. 4.15(d) contributes at order $\alpha\alpha_s^5$, i.e. via the SPS $\gamma g \to J/\psi + J/\psi + g + g$. The gluon-initiated channel in DPS for di-J/ψ
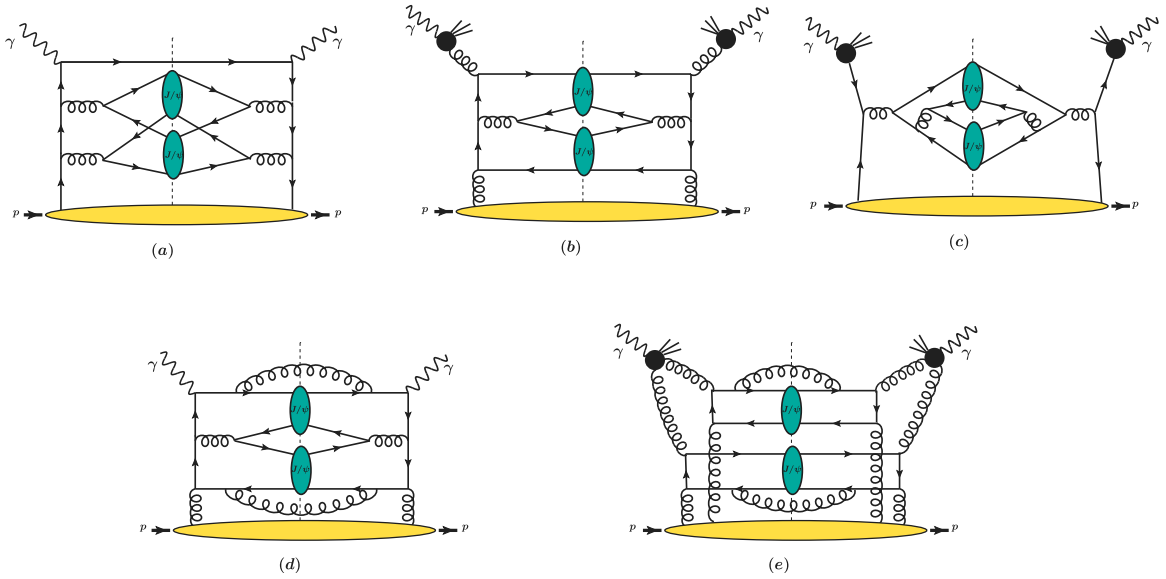
Fig. 4.15. Di-J/ψ photoproduction at the EIC via SPS $\mathcal{O}(\alpha_s^4)$ (a-c), $\mathcal{O}(\alpha_s^5)$ (d) and DPS $\mathcal{O}(\alpha_s^6)$ (e).

production at α_s^6 is shown in Fig. 4.15(e), while the quark-initiated channel does not contribute in the CSM at order α_s^6. The partonic channel $gg \to J/\psi + g$ dominates for single-J/ψ production. The SPS cross section, i.e. the squared matrix elements convoluted with single-parton PDFs, can be calculated using HELAC-Onia [495,496]. In order to estimate the DPS cross section, we need to use the poorly known proton dPDFs, which provide the number densities of a parton pair with a given transverse distance $b_\perp$ and carrying the longitudinal momentum fractions (x_1, x_2) of the parent hadron [497–502]. Assuming that dPDFs can be factorised in terms of ordinary 1D PDFs and a transverse part, the DPS cross section can be expressed in terms of two SPS cross sections for the production of each of the observed particles among the pair:

$$\sigma_{DPS}^{(J/\psi, J/\psi)} = \frac{1}{2} \frac{\sigma_{SPS}^{(J/\psi)} \sigma_{SPS}^{(J/\psi)}}{\sigma_{eff}^{\gamma p}}, \tag{4.19}$$

which is the so-called "DPS pocket formula", valid under the assumption of totally uncorrelated kinematics between both parton scatterings. The $\sigma_{SPS}^{(J/\psi)}$ is the SPS contribution for single J/ψ production. In the present study, within the mentioned assumptions, one gets:

$$\sigma_{eff}^{\gamma p} = \left[\int \frac{\mathrm{d}^2 \vec{k}_\perp}{(2\pi)^2} F_2^\gamma(\vec{k}_\perp, Q^2) F_2^p(\vec{k}_\perp) \right]^{-1} \tag{4.20}$$

where here $F_2^{p(\gamma)}(k_\perp)$ parametrises the transverse structure of the proton (photon) [476]. For the photon, the only available calculation is that of Ref. [476] while, for the proton, there are several models based on the data for DPS in pp collisions. Recently, several experimental analyses on DPS have been carried out for the production of $J/\psi + W$ [503], $J/\psi + Z$ [504], J/ψ+charm [505] in pp and $J/\psi + J/\psi$ [506] in $p\bar{p}$ processes. A comprehensive comparison between theory and experiments for di-J/ψ production at the Tevatron and the LHC has been presented in [9,339], and it was observed that DPS dominates the yield at large J/ψ-rapidity difference. DPS has been also studied for J/ψ-pair production for the LHC fixed-target (also referred to as AFTER@LHC) kinematics in [491].

At the EIC, LO computations using HELAC-Onia show that measurements are possible at $\sqrt{s_{ep}} = 140$ GeV with SPS contributions generally dominant over the DPS ones, but there are certain regions (low z and large Δy) in the phase space where DPS cannot be disregarded. If $\sigma_{eff}^{\gamma p}$ is not too small, DPS events could be measured. In these regions, there is thus a compelling opportunity to distinguish between the resolved and unresolved contributions in the cross section and thereby to gain valuable insight into the internal structure of photons and protons.

5. Quarkonia as tools to study the parton content of nuclei

5.1. Nuclear PDFs

Decades of experimental and theoretical studies showed that the distributions of partons in a nucleus are considerably modified compared to the nucleon ones. While significant progress has been made since the initial observation of the modification of PDFs in bound nucleons by the EMC Collaboration [507], our understanding of nuclear PDFs (nPDFs) is still not satisfactory, most notably in the case of gluons. Measurements of quarkonium production in eA reactions can bridge this knowledge gap.

One of the main EIC goals is a high-precision survey of the partonic structure of the nucleus to significantly advance our quantitative understanding of nPDFs. The EIC will offer the possibility to study nPDFs over a broad range of momentum transfers [2]. An improved knowledge of nPDFs will enable more precise theoretical calculations for nuclear effects and increase the scientific benefit of already successful heavy-ion programmes at RHIC and LHC.

A widely accepted approach to quantify nuclear effects in PDFs is to start with proton PDFs and use a function $R(x, Q^2)$ that captures the modification of a given PDF in a nucleus. Experimentally, such a modification could be studied by a ratio of structure functions F_2 or by the so-called nuclear modification factor as done by RHIC and LHC experiments. In the case of eA collisions, $R(x, Q^2)$ is defined as

$$R_{eA} = \frac{1}{A} \frac{(d)\sigma_{eA}}{(d)\sigma_{ep}}, \tag{5.1}$$

where $(d)\sigma_{eA}$ and $(d)\sigma_{ep}$ are the cross sections for the process under consideration, respectively, in eA and ep reactions, while mass number A serves as a normalisation factor. Note that these cross sections can be differential in different kinematical variables. With the definition of Eq. (5.1), $R_{eA} = 1$ in the absence of nuclear effects. In the following, we review and quantify prospects for nuclear-PDF determination at EIC via R_{eA} measurements.

5.1.1. Gluons

In order to give an estimate of the potential impact of the EIC on nPDF determination, the nuclear modification factor R_{eAu}, which can be measured in inclusive J/ψ photoproduction in eAu reactions, is compared with projected statistical uncertainties. Such a prediction is shown in Fig. 5.1 and Fig. 5.2 at two different values of the centre-of-mass energy, $\sqrt{s_{eN}}$, namely 45 GeV and 90 GeV, as a function of the J/ψ rapidity in the $N\gamma$ centre-of-mass frame[16] and as a function of $W_{\gamma N}$. Kinematical cuts are applied on the elasticity ($0.2 < z < 0.9$) and on the pseudorapidity of the electron pair coming from the $J/\psi \rightarrow e^+ e^-$ decay ($|\eta_{ee}| < 3.5$). Different cuts on $W_{\gamma N}$ are applied for the rapidity spectra at the two different $\sqrt{s_{eN}}$ energies.

The nuclear-modification-factor predictions are calculated using HELAC-Onia [495,496], adopting the CT14nlo set [132] as a proton PDF baseline and using two different nuclear PDF sets for the gold nucleus, namely EPPS16nlo [508] and nCTEQ15FullNuc [509]. Factorisation and renormalisation scales are taken to be the J/ψ transverse mass, $\mu_F = \mu_R = m_T = \sqrt{M_{J/\psi}^2 + P_T^2}$. Note also that, since these predictions are calculated at LO in the CSM, where the only partonic subprocess is $\gamma + g \rightarrow J/\psi + g$, they can be directly interpreted as R_g, the nuclear modification factor for the gluon nPDF. The statistical projections are calculated assuming $R_{eAu} = 1$ (using the central value of CT14nlo) and assuming an integrated luminosity of $10\,\text{fb}^{-1}/A$. The branching ratio for the $J/\psi \rightarrow e^+ e^-$ decay was taken to be 5.94% and a J/ψ reconstruction efficiency of 64% was assumed (considering an average identification efficiency of the electrons from the J/ψ decay to be approximately 80%).

Some comments are in order. First, as can be seen in Fig. 5.1 and Fig. 5.2, J/ψ is expected to be mostly produced in the backward region in the γN centre-of-mass frame as the yield essentially vanishes at positive rapidities (see the increase of the statistical uncertainties of our projections). This happens for both energy configurations. Second, the regions where shadowing (relative parton depletion at x smaller than 0.01), antishadowing (relative parton excess at x around 0.11) and the EMC effect (relative parton depletion for $0.3 < x < 0.7$) take place can be probed at the EIC via J/ψ photoproduction. The antishadowing peak is expected to be observed at moderate backward rapidity in the γN centre-of-mass frame, while the shadowing region would be probed at larger negative rapidities. Such regions are also those where the projections point to a smaller statistical uncertainty compared to the PDF and scale uncertainties, *i.e.* the gluon nPDFs would be the most constrained. The $W_{\gamma N}$ dependence of the nuclear modification factor would also be a very interesting tool to probe gluon nPDFs. A large shadowing tail is expected to be probed for larger values of $W_{\gamma N}$, while clear antishadowing peaks are expected in the region $W_{\gamma N} \in [10 : 20]$ GeV, in both energy configurations. The projected uncertainties are also small, and seem to have an interesting constraining power for the gluon nPDFs. More detailed dedicated studies are surely required and would help in motivating new measurements to probe gluon nPDFs at the EIC.

Fig. 5.3 presents predictions for the P_T dependence of R_{eAu} at $\sqrt{s_{eN}} = 100$ GeV by using the same factorisation formalism in Eq. (3.4), with proton PDFs replaced by nuclear PDFs for the eA collision. The total, LP and NLP contributions are shown. The EPPS21nlo central set [510] is used as nPDF. Since the production rate is dominated by the $\gamma + g \rightarrow [c\bar{c}] + g$ subprocess, this ratio is directly sensitive to the nuclear dependence of the gluon PDF. At EIC energies, the P_T distribution of J/ψ production is sensitive to the gluon at a relatively large momentum fraction due to the soft-photon distribution in the incoming electron. The enhancement of the J/ψ production rate in eAu over ep collisions in Fig. 5.3 is a direct consequence of the "antishadowing" behaviour of the nuclear gluon distribution from the EPPS21nlo nuclear PDF set. Since the quark-initiated subprocesses dominate the LP contribution, the ratio of the LP contribution (blue dashed and red dotted lines) shows the well-known EMC-type effect from nuclear quark PDFs. However, this feature of the LP contribution does not have a real impact on the observed nuclear dependence of the P_T dependence of J/ψ production at the EIC energies (the solid line), since the LP contribution is strongly suppressed; that is, the P_T distribution of J/ψ production at the EIC should also be an excellent observable for probing the nuclear gluon PDF.

---

[16] Note that we adopt the same kinematical configuration as the EIC Yellow Report, with the proton(ion) moving along $+\hat{z}$ and the electron along $-\hat{z}$ (see also Fig. 2.2).
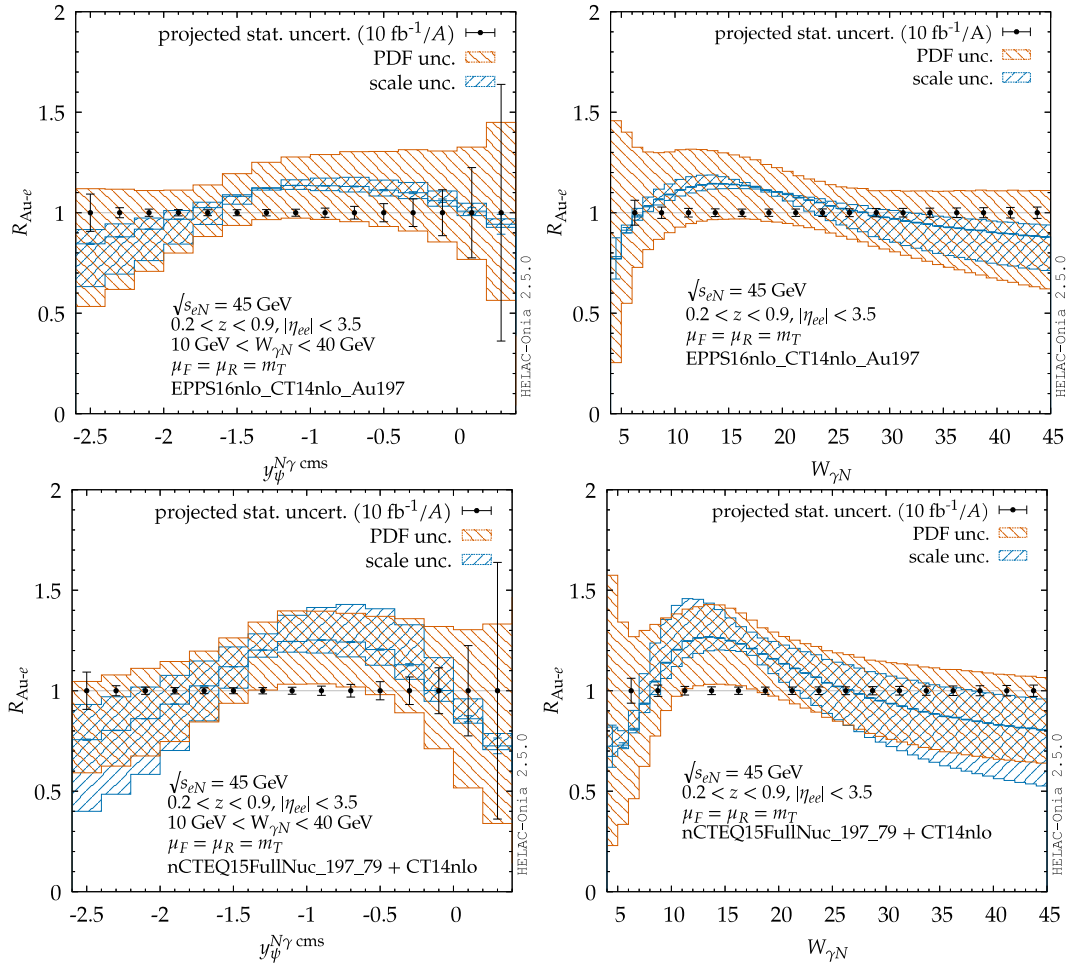
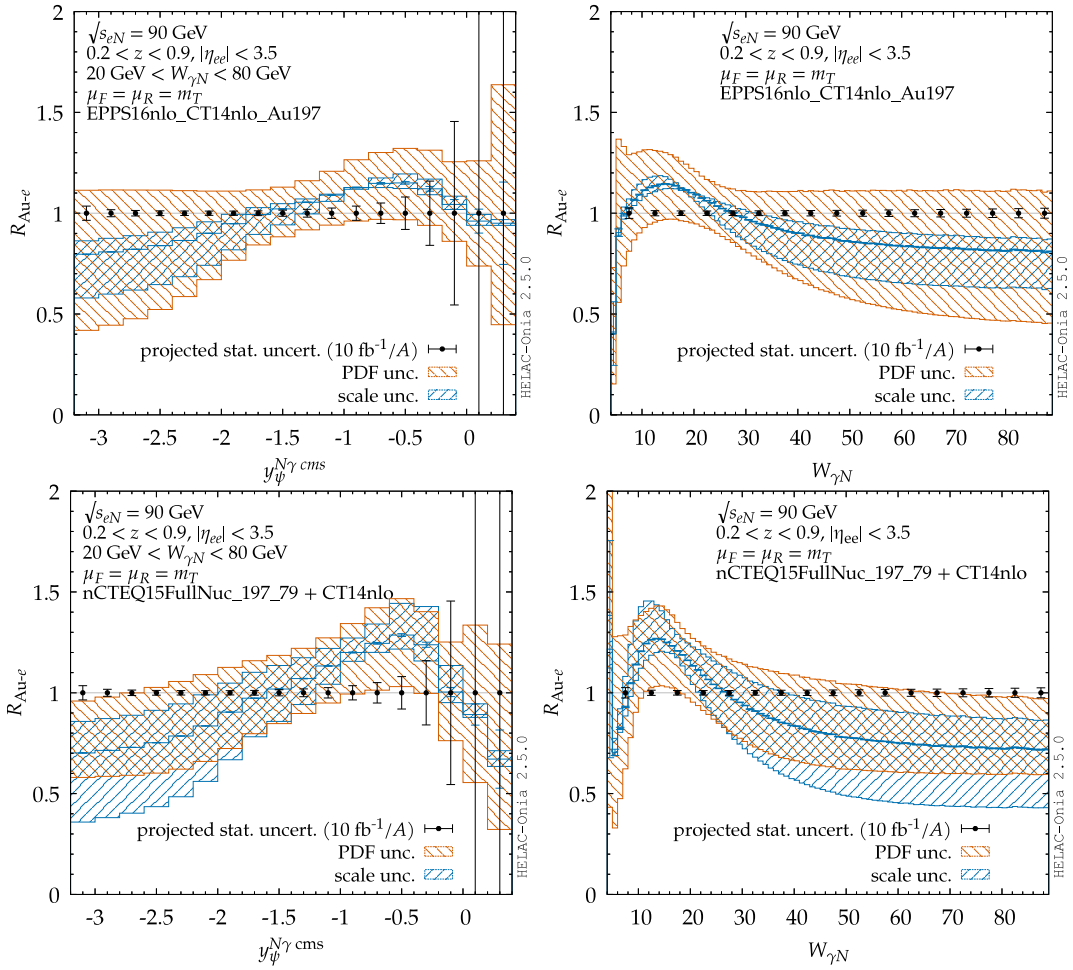**Fig. 5.1.** R_{eAu} LO CSM prediction at $\sqrt{s_{eN}} = 45$ GeV as a function of the J/ψ rapidity in the γN centre-of-mass frame (left panels) and as a function of $W_{\gamma N}$ (right panels). Calculations are based on HELAC-Onia [495,496] with the cuts $0.2 < z < 0.9$, $|\eta_{ee}| < 3.5$ and the nPDFs EPPS16NLO+CT14nlo (top plots) and nCTEQ15FullNuc+CT14nlo (lower plots). Projections are calculated assuming $R_{eAu} = 1$ and for an integrated luminosity of 10 fb^{-1}/A.

5.2. Nuclear GPDs

In coherent diffractive production of vector mesons off a nucleus, the light (photon) generated by the electron interacts, similarly to optical experiments of diffraction, with the nucleus as a whole, resulting in the production of a vector meson in the final state. This process has been proposed as a tool to investigate gluon saturation dynamics [511]. Here, the production of lighter vector mesons, such as the ϕ meson, is expected to be sensitive to saturation effects. On the other hand, because of the heavier quarkonium mass (and thus smaller size of the dipole formed by the quark–anti-quark pair that evolves into the vector meson) the production of quarkonia would not be optimal to study gluon saturation, but rather serve as a baseline free from saturation effects. Diffractive production also gives access to the spatial distribution of partons inside the nucleus. While coherent diffractive production provides information on the average spatial distribution of partons, incoherent production, where the nucleus does not stay intact, probes local fluctuations of this spatial distribution [512]. For the study of the spatial distribution of gluons in heavy nuclei, in particular, the diffractive production of a quarkonium, such as a J/ψ, is most adequate. For the coherent process, the momentum transfer distribution $\sqrt{|t|}$ from the photon to the target nucleus is expected to exhibit a diffractive pattern, where the details of the shape of this pattern encode information on the gluon GPD [433,511,513,514]. An example of such a diffractive pattern is shown in Fig. 5.4, as represented by the square symbols. The data points have been simulated using the Sartre Monte-Carlo event generator [515]. Results including (filled symbols) and excluding (open symbols) saturation effects are shown. In addition to the diffractive coherent production, the expected incoherent contribution (circles) is shown. As can be seen, apart from the very low $|t|$ region, the incoherent contribution dominates the coherent one.

Elastic and inelastic diffractive quarkonium production off the proton has been studied at the HERA lepton–proton collider experiments H1 [278,516,517] and ZEUS [271,516,518,519], while a first measurement of exclusive J/ψ photoproduction at threshold has been performed in the fixed-target experiment GlueX at Jefferson Lab [452]. At hadron-collider experiments, diffractive

Fig. 5.2. R_{eAu} LO CSM prediction at $\sqrt{s_{eN}} = 90$ GeV as a function of the J/ψ rapidity in the γN centre-of-mass frame (left panels) and as a function of $W_{\gamma N}$ (right panels). Calculations are based on HELAC-Onia [495,496] with the cuts: $0.2 < z < 0.9$, $|\eta_{ee}| < 3.5$ and the nPDFs EPPS16NLO+CT14nlo (top plots) and nCTEQ15FullNuc+CT14nlo (lower plots). Projections are calculated assuming $R_{eAu} = 1$ and for an integrated luminosity of 10 fb^{-1}/A.

quarkonium production has been investigated in $p\bar{p}$ collisions [520] at the Tevatron, in pp [274–276,521], pPb [522] and PbPb [523–526] collisions at the LHC and in dAu [527] and AuAu [528] collisions at RHIC. The existing measurements off nuclei are at present restricted in statistical precision, while only offering a rough determination of the momentum transfer $\sqrt{|t|}$ and in general a limited separation of coherent and incoherent production. Hence, the knowledge on the gluonic structure of nuclei is at present poor, with many fundamental questions unanswered.

The EIC is expected to perform measurements of diffractive vector-meson production off light and nuclear ions with unprecedented precision. The two experimental challenges consist in determining t with high precision and in distinguishing coherent from incoherent events [530]. Recently, the capability of proposed EIC detectors in reconstructing t and their ability to suppress incoherent production have been examined [46,48,530]. The variable t needs to be reconstructed from the scattered lepton and reconstructed vector meson, since in coherent production the trajectory of the ion after the interaction is nearly unmodified and thus the ion cannot be detected, while in the case of incoherent production not all fragments from the nuclear break up can be detected. The distribution in $|t|$ for coherent diffractive J/ψ production off gold ions is shown in Fig. 5.5, left. Here, $|t|$ is reconstructed as the squared sum of the transverse momenta of the scattered lepton and of the lepton pair originating from the J/ψ decay. It forms a good approximation for the true $-t$. The data have been simulated again with Sartre and subsequently passed through a full simulation of the ePIC detector. The histogram represented by the continuous line is the generated distribution, while the other curves represent the reconstructed distribution, with beam effects. The latter include an angular divergence originating from the focussing and defocussing quadrupoles in the interaction region and a small angular kick from the crab cavities. The crossing angle from the beams in principle also influences the t distribution, but contrary to the other effects it can be corrected for. For the curve indicated by the open, blue circles only information from tracking detectors is used for the reconstruction of the scattered lepton, while for the curve indicated by the black, closed circles only information from the backward electromagnetic calorimeter is used for the reconstruction of the scattered lepton. The curve indicated by the red, open circles selects the best of the two methods. As
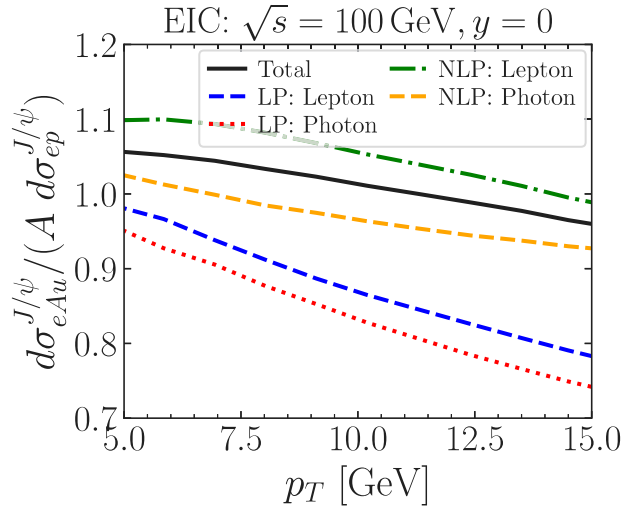
Fig. 5.3. R_{eAu} as a function of the J/ψ transverse momentum, P_T, for inclusive production in electron–gold collisions without tagging the scattered electron, computed by using the new factorisation formalism in Eq. (3.4) [159]. The solid black line represents the total contribution, which is dominated by the subprocess $\gamma + g \to [c\bar{c}] + g$ (NLP Photon) and $e + g \to [c\bar{c}] + e$ (NLP Lepton) with the $c\bar{c}$ pair hadronising to J/ψ, while others represent contributions from other subprocesses, see the text for details.
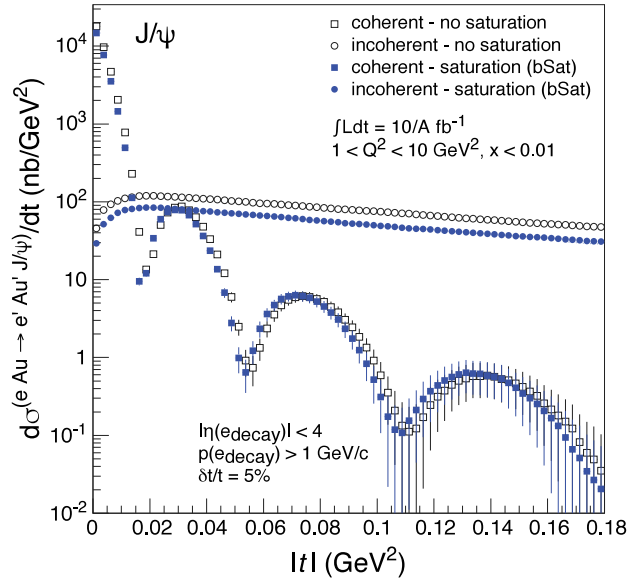
Fig. 5.4. Simulation of the differential cross section of coherent (squares) and incoherent (circles) J/ψ production in eAu collisions at the EIC [513], where a 5% resolution effect from experimental conditions is included. Predictions without saturation (open symbols) and with saturation (closed symbols) are shown.

can be seen, the quality of the reconstruction in t is strongly dependent on the quality of the reconstruction of the scattered beam lepton. In the diffractive process the beam lepton generally is scattered under a small angle and covers a region where the tracking performance is degraded. Using in addition the electromagnetic calorimeter in the backward region for the reconstruction of the scattered lepton improves the reconstruction in t vastly.

The spatial distribution of partons in impact-parameter space is related to a Fourier transformation, with t going from 0 to infinity [531]. Experimentally, one is limited by a maximal momentum transfer, which preferably extends as far as possible. In practice, studies have shown that it is necessary to resolve the minima up to the third one for the evaluation of the spatial distribution [2]. This dictates the needed level of suppression of the incoherent contribution. The suppression of incoherent events includes the requirement of exactly three reconstructed lepton tracks with the correct charge in absence of any other signal in the main detector and various criteria corresponding to the absence of signal in a series of far-forward detectors, which can tag protons (Roman Pots for protons with energy close to the beam energy and the B0 spectrometer and off-momentum detectors for nuclear-breakup protons), neutrons (Zero-Degree Calorimeters) and photons (B0 and Zero-Degree Calorimeters). The capability to suppress
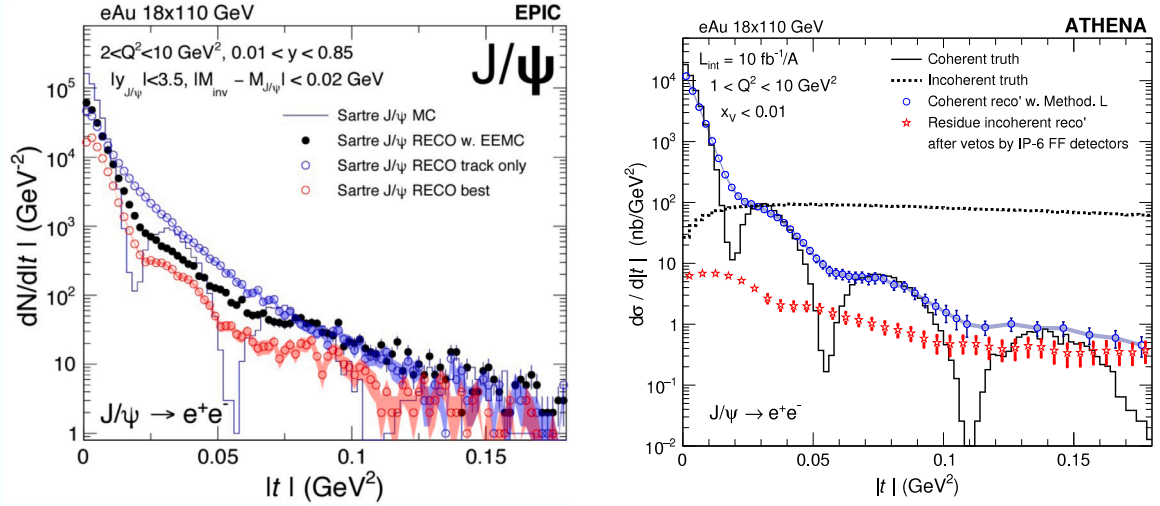
Fig. 5.5. The distribution in generated and reconstructed $-t$, with the reconstructed $-t$ being the squared sum of the transverse momenta of the scattered beam lepton and of the lepton pair originating from J/ψ decay, in diffractive production off gold nuclei. The panel on the left-hand side illustrates the influence of the quality of the scattered-lepton reconstruction on the determination of $-t$, as studied by ePIC. The panel on the right-hand side shows the level of suppression of incoherent production (see text), as studied by ATHENA. Figs. taken from Ref. [529] and from the supplementary material provided in the evaluation process of [46], respectively.

incoherent production is illustrated in Fig. 5.5, right, which shows the $-t$ distribution for coherent and incoherent production off gold nuclei. The former is again simulated using Sartre, while for the latter the BeAGLE generator [532] is used. The generated coherent (incoherent) contribution is represented by the continuous (dotted) line. The generated data are passed through a full simulation of the ATHENA detector. The effect of data selection requirements on the event activity in the main detector and on the absence of activity in the far-forward detectors, based on the studies in Ref. [530], is represented by the blue, open circles. As can been seen, the obtained distribution lies close to the distribution from coherent events simulated by Sartre. The remaining contribution from incoherent events is given by the red, star symbols. The largest suppression of the incoherent process comes from the requirement on the absence of any neutron signal in the Zero-Degree Calorimeter, while the requirement on the absence of photon signals in this Zero-Degree Calorimeter also has an impact. Ways to further improve the reconstruction of t and the suppression of incoherent production are at present under investigation.

The study of light nuclei can offer additional insights into the internal structure of the nuclear medium. In contrast to measurements with heavy nuclei, the total final state in incoherent diffractive production off light nuclei can be unambiguously identified through tagging of the spectator nucleons. Such measurements are of interest when studying the short-range correlation (SRC) of a nucleon pair, which is the temporal fluctuation of two nucleons into a strongly interacting pair in close proximity and large measured relative momentum [533,534]. SRC pairs are suggested as a possible explanation for the nuclear modification of the momentum distribution of high-x partons, known as the EMC effect, with a strong correlation between the two phenomena suggested by measurements by the CLAS experiment at Jefferson Lab [535] and a quark-level QCD basis for SRC has been proposed for the lightest nuclei [536] and $A \geq 4$ nuclei [537].

The simplest nuclear system consists of deuteron and the first measurement of incoherent diffractive production with spectator tagging was performed in the measurement of incoherent diffractive J/ψ production in ultra-peripheral dAu collisions by the STAR experiment at RHIC [527], with tagging of the spectator neutron in the Zero-Degree Calorimeter. At the EIC, similar measurements can be performed with enhanced precision, and studies of incoherent diffractive J/ψ production off the deuteron at the EIC have been proposed to study the nuclear modification of the gluon distribution and its possible link with the SRC [538,539]. For the proposed measurement, the scattered lepton and J/ψ decay leptons are reconstructed in the main detector, while both the leading and spectator nucleon (neutron and proton) can be detected in the far-forward detectors. The detection of both nucleons instead of only one offers certain advantages in the reconstruction of the event and some kinematic variables [539].

In Fig. 5.6, the three-momentum distribution of the tagged neutron (left) and tagged proton (right) in the deuterium rest frame is illustrated for incoherent diffractive production of J/ψ in the scattering of 18 GeV electrons off 110 GeV deuterons at the EIC, as simulated with BeAGLE [539]. The star symbols represent the generated distribution, the open circles represent the distribution including acceptance effects of the main and far-forward detectors, and the open squares also take the finite detector resolution and beam effects into account. The momentum distribution of the tagged nucleon reflects the initial-state momentum of the nucleons inside the deuteron. The region above 300 MeV corresponds to the region of the SRC, and as visible in the figures, the EIC will be able to provide a good reconstruction of the tagged-nucleon momentum. A similar statement holds for the reconstruction of other variables of interest [539].
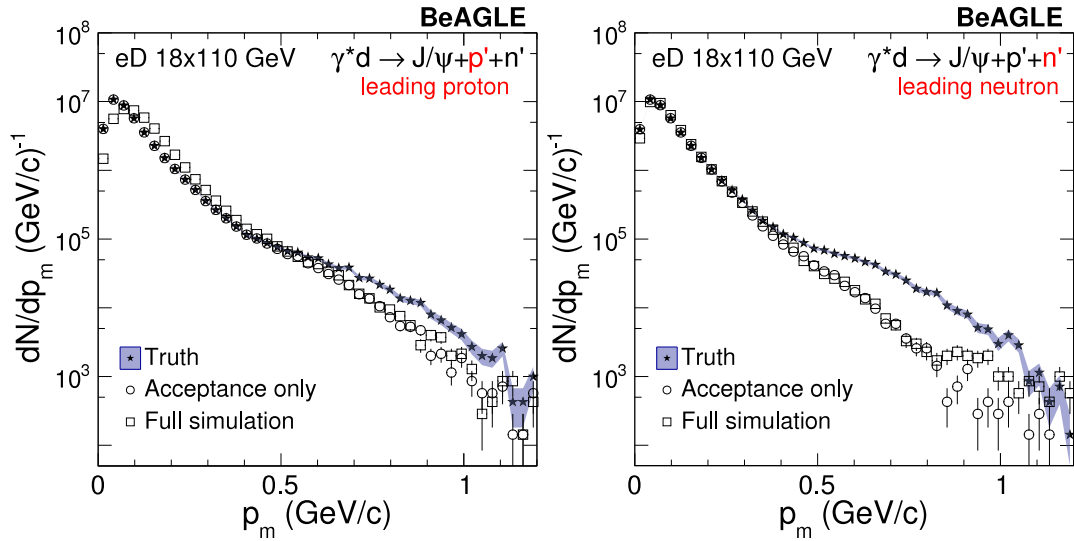
Fig. 5.6. The three-momentum distribution in the deuteron rest frame of the spectator neutron (left) and spectator proton (right) for the incoherent diffractive production of J/ψ in lepton–deuteron collisions at the EIC. The distribution is generated with BeAGLE. The star symbols represent the generated distribution, the open circles represent the distribution including acceptance effects of the main and far-forward detectors, and the open squares take in addition the finite detector resolution and beam effects into account.
Source: Figures are taken from Ref. [539].

5.3. Study of transport properties of nuclear matter

The vital element of portraying nuclear matter is to get information on how the medium responds to a parton traversing the matter. It is characterised by transport coefficients, e.g. a diffusion coefficient or $\hat{q}$, which is the mean squared momentum transfer between the propagating particle and the medium per unit length. Transport coefficients are an essential ingredient in the modelling of nuclear reactions , and determining these parameters is one of the main goals of high-energy nuclear physics experimental and phenomenological efforts [540].

Measurements of hadron production in pA collisions have shown a broadening of the transverse momentum distribution at intermediate hadron transverse momentum compared to pp reactions. This phenomenon is visible over a wide range of hadronic collision energies, starting from collisions at $\sqrt{s_{NN}} \approx 20$ GeV [541,542] up to 200 GeV at RHIC [543]. The Cronin effect is also anticipated for quarkonium production in pA collisions [30]. A similar effect was observed also in semi-inclusive deep-inelastic scattering off nuclei by the HERMES experiment [544]. One possible source of this effect is the multiple scattering of the struck parton while traversing the nucleus, which broadens the parton momentum k_T. Under this assumption, the modification of k_T can be related to the transport properties of matter, expressed by the transport coefficient $\hat{q}$. Other effects, like nuclear absorption and parton energy loss, are also expected to contribute when studying particle production in nuclear matter.

Additional measurements of the P_T spectrum in ep and eA at the EIC can help to discriminate between models and constrain their parameters, including the relative role of multiple scattering and nuclear absorption. Such a programme will greatly extend the studies pioneered by the HERMES collaboration.

We present here an example of the calculation of the expected modification of the quarkonium energy spectrum in eA collisions due to multiple scattering of the parton in the medium. The study is based on an earlier work [545], where a microscopic approach was adopted for the calculation of the decay of J/ψ and Υ in the QGP. Here the QGP medium is replaced with cold nuclear matter, specifically with a large gold nucleus, and its properties are constrained taking into account various nuclear effects: nuclear shadowing [546,547], coherent QCD multiple scattering [548], initial- and final-state parton-energy loss [549,550], and initial- and final-scattering effects (including multiple scatterings) [551,552].

To study the nuclear modification, the ratio of cross sections for quarkonium production in reactions that involve a nucleus and a proton baseline is used:

$$R_{AA} = \frac{1}{\langle N_{\text{bin}} \rangle} \frac{d\sigma_{AA}}{d\sigma_{pp}}, \qquad R_{eA} = \frac{1}{A} \frac{d\sigma_{eA}}{d\sigma_{ep}}. \tag{5.2}$$

Here, A and the average number of nucleon–nucleon collisions $\langle N_{\text{bin}} \rangle$ provide the relevant normalisation factors such that in the absence of nuclear modification the ratios are unity. The R_{AA} presents suppression from QGP, including thermal dissociation in the QGP, while R_{eA} offers the cold nuclear-matter counterpart.

A preliminary study demonstrates that most quarkonium states show a larger R_{eA} compared to R_{AA}, and thus a decreased suppression, with the exception of the J/ψ state, which sees an increase in suppression by roughly 20%, and of the $\chi_b(1P)$ state, which sees a relatively low increase in suppression of roughly 10%. The χ_c state experiences a significant decrease of about 50% in

the suppression factor. The Y states follow an analogous trend, with decreased suppression of around 25% for $Y(1S)$ and $Y(2S)$ and 90% for $Y(3S)$. Finally, $\chi_b(2P)$ and $\chi_b(3P)$ show decreases in their suppression factors of roughly 55% and > 95%, respectively. The overall trend seems to indicate that highly suppressed states see the largest decrease in suppression, while the least suppressed states show either a small decrease or a slight increase in their suppression factors. All states retain a similar amount of E dependence, which is not surprising given that it is assumed that the time for the onset of the interaction is $\tau_{\text{form.}} = 1$ fm. We direct an interested reader to C for more details.

These preliminary results show that one can expect a significant modification due to cold nuclear-matter effects, which should allow for experimental investigation of these effects at the EIC. Thus, quarkonium studies in eA collisions at the EIC will help to understand the impact of different transport coefficients on quarkonium production in reactions that involve heavy nuclei and, in turn, help to calibrate quarkonium as a probe of the properties of matter created in high-energy pA and AA collisions.

6. Summary

Quarkonium is an extremely useful tool to probe the internal structure of matter, namely one of the main goals of the Electron Ion Collider. In this review, we argue that studies of quarkonium production and correlations in (polarised) electron–proton and electron–nucleus collisions can produce unprecedented insights into the 3D structure of the nucleon and into the partonic content of the nuclei as well as help to settle the long-lasting debate on how quarkonia form.

Section 2 briefly introduced the EIC project, its key parameters, and requirements for an EIC detector. We also defined conventions and basic kinematical quantities useful for describing lepton–hadron reactions. Finally, we made a case for a muon detector for quarkonium studies at the EIC.

Studies of collinear PDFs, form factors, TMD PDFs, GPDs, GTMDs and even double-parton distribution functions can be done at EIC using quarkonium production on a nucleon. In Sections 3–5, we reviewed physics cases for quarkonium measurements at the EIC. Quarkonium production at large transverse momenta in proton–proton and electron–proton collisions has been studied extensively within the frameworks of NRQCD and collinear factorisation. As discussed in Sections 3.1 and 3.2, it remains a challenge to obtain a simultaneous description of all HERA, LHC and Tevatron data for J/ψ photo- and hadroproduction, η_c hadroproduction, $J/\psi + Z$ hadroproduction, J/ψ polarisation as well as inclusive production in e^+e^- annihilation at B factories.

Further data from the EIC can help but its p_T reach is limited to 10–15 GeV for charmonia and much less for bottomonia. The focus would then be on low-p_T data. The latter needs to be described within the framework of transverse momentum dependent parton distributions (TMDs) and requires the inclusion of so-called shape functions, which are the subjects of Section 3.3. In this way the EIC will provide new data to further unravel the quarkonium production mechanism, while at the same time offer new ways to employ quarkonium production as a tool to study TMDs and other parton distributions (the subjects of Section 4). This applies especially to gluon TMDs about which currently very little is known. Analogous studies can be performed in electron–nucleus collisions (including, among others, insights into transport properties of nuclear matter), which is the subject of Section 5. J/ψ polarisation studies can be done, as well as various spin asymmetry measurements, where the electron, proton and light nuclei can be polarised. All these observables can contribute to our understanding of hadron structure and hadron formation, in particular those involving heavy quarks.

Overall, the physics case for quarkonium physics at the EIC is very extensive and promising.

CRediT authorship contribution statement

Daniël Boer: Writing – review & editing, Writing – original draft, Validation, Supervision. **Chris A. Flett:** Writing – review & editing, Writing – original draft. **Carlo Flore:** Writing – review & editing, Writing – original draft, Validation, Supervision. **Daniel Kikoła:** Writing – review & editing, Writing – original draft, Validation, Supervision. **Jean-Philippe Lansberg:** Writing – review & editing, Writing – original draft, Validation, Supervision. **Maxim Nefedov:** Writing – review & editing, Writing – original draft, Validation, Supervision. **Charlotte Van Hulse:** Writing – review & editing, Writing – original draft, Validation, Supervision. **Shohini Bhattacharya:** Writing – original draft. **Jelle Bor:** Writing – original draft. **Mathias Butenschoen:** Writing – original draft. **Federico Ceccopieri:** Writing – original draft. **Longjie Chen:** Writing – original draft. **Vincent Cheung:** Writing – original draft. **Umberto D'Alesio:** Writing – original draft. **Miguel Echevarria:** Writing – original draft. **Yoshitaka Hatta:** Writing – original draft. **Charles E. Hyde:** Writing – original draft. **Raj Kishore:** Writing – original draft. **Leszek Kosarzewski:** Writing – original draft. **Cédric Lorcé:** Writing – original draft. **Wenliang Li:** Writing – original draft. **Xuan Li:** Writing – original draft. **Luca Maxia:** Writing – original draft. **Andreas Metz:** Writing – original draft. **Asmita Mukherjee:** Writing – original draft. **Carlos Muñoz Camacho:** Writing – original draft. **Francesco Murgia:** Writing – original draft. **Pawel Nadel-Turonski:** Writing – original draft. **Cristian Pisano:** Writing – original draft. **Jian-Wei Qiu:** Writing – original draft. **Sangem Rajesh:** Writing – original draft. **Matteo Rinaldi:** Writing – original draft. **Jennifer Rittenhouse West:** Writing – original draft. **Vladimir Saleev:** Writing – original draft. **Nathaly Santiesteban:** Writing – original draft. **Chalis Setyadi:** Writing – original draft. **Pieter Taels:** Writing – original draft. **Zhoudunmin Tu:** Writing – original draft. **Ivan Vitev:** Writing – original draft. **Ramona Vogt:** Writing – original draft. **Kazuhiro Watanabe:** Writing – original draft. **Xiaojun Yao:** Writing – original draft. **Yelyzaveta Yedelkina:** Writing – original draft. **Shinsuke Yoshida:** Writing – original draft.

Declaration of competing interest

The authors declare that they have no known competing financial interests or personal relationships that could have appeared to influence the work reported in this paper.

Acknowledgements

Appendix A. Experimental data used in the CO LDME fits

See Table A.1

Table A.1

Compilation of the experimental data used in the CO LDME fits at NLO listed in Table 3.1.

Acronym	Reference	Experimental data used in the fit
BK11	Butenschön et al. [110–113]	• J/ψ photoproduction at DESY HERA by H1 [553,554] and ZEUS [555]; • J/ψ hadroproduction at Tevatron by CDF [556,557]; • J/ψ hadroproduction at RHIC by PHENIX [173]; • J/ψ hadroproduction at the LHC by ATLAS [558], CMS [559] and LHCb [560]; • e^+e^- annihilation at LEP by DELPHI [561] and at KEK-B by Belle [562]
H14	Chao et al. + η_c [120]	• J/ψ hadroproduction at the Tevatron by CDF [556,557], • η_c hadroproduction at the LHC by LHCb [82]. **Predictions:** • J/ψ hadroproduction at the LHC by CMS [563] and LHCb [560]; • J/ψ polarisation in hadroproduction at the LHC by ALICE [176], CMS [178] and LHCb [177]

Table A.1 (*continued*).

Acronym	Reference	Experimental data used in the fit
Z14	Zhang et al. [121]	• J/ψ hadroproduction at the Tevatron by CDF [556,557] and at the LHC by LHCb [560]; • J/ψ polarisation in hadroproduction at the LHC by LHCb [177] and the Tevatron by CDF [171,172]; • η_c hadroproduction at the LHC by LHCb [82]
G13	Gong et al. [115]	• J/ψ hadroproduction at the Tevatron by CDF [557] and at the LHC by LHCb [560]; • J/ψ polarisation in hadroproduction at the LHC by LHCb [177] and at the Tevatron by CDF [171,172]
C12	Chao et al. [114]	• J/ψ hadroproduction at the Tevatron by CDF [557]; • J/ψ polarisation in hadroproduction at the Tevatron by CDF [172]. **Predictions:** • J/ψ hadroproduction at the LHC by ATLAS [564] and CMS [563]
B14	Bodwin et al. [86]	• J/ψ hadroproduction at the Tevatron by CDF [557] and at the LHC by CMS [563]; • J/ψ polarisation in hadroproduction at the Tevatron by CDF [172] and at the LHC by CMS [178]
pNRQCD	Brambilla et al. [116,122]	• J/ψ and $\psi(2S)$ hadroproduction at the LHC by CMS [178,179,565]; • Υ hadroproduction at the LHC by ATLAS [566] and CMS [565]

Appendix B. Estimation of J/ψ measurement efficiency

The J/ψ measurement efficiency is calculated using the decay kinematics simulated with PYTHIA8 [380] and two cases for the minimum transverse momentum of the electron measurable in the experiment: $P_T^{ele} > 0.2$ GeV for a detector with a magnetic field
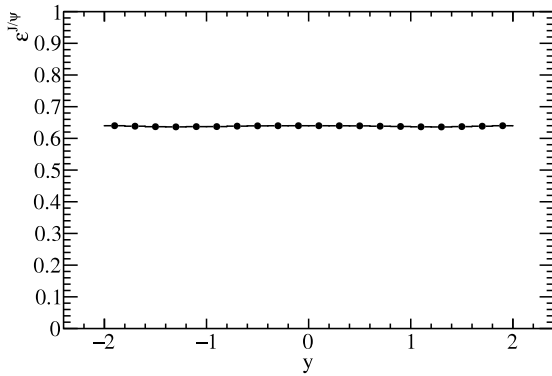
(a) magnetic field $B = 1.5$ T, $P_T^{ele} > 0.2$ GeV
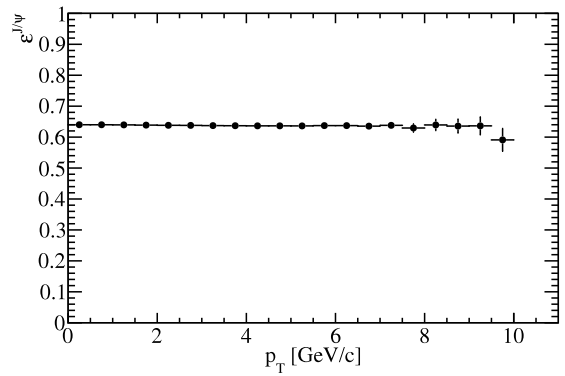
(b) magnetic field $B = 1.5$ T, $P_T^{ele} > 0.2$ GeV
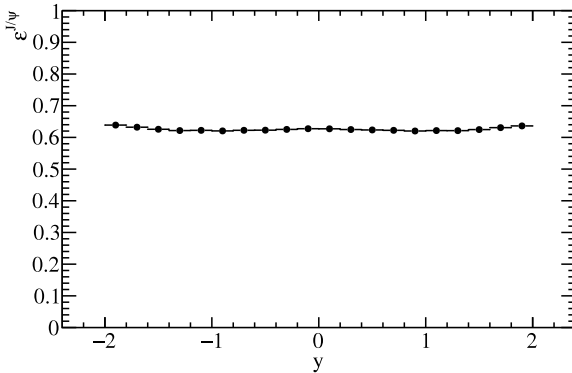
(c) magnetic field $B = 3$ T, $P_T^{ele} > 0.4$ GeV
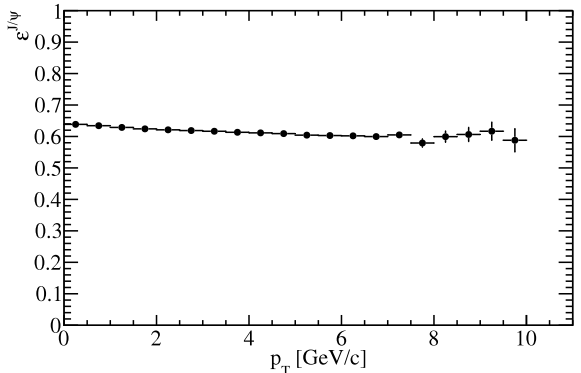
(d) magnetic field $B = 3$ T, $P_T^{ele} > 0.4$ GeV

Fig. B.1. J/ψ measurement efficiency as a function of J/ψ rapidity and transverse momentum for a generic EIC detector using as magnetic field $B = 1.5$ T or $B = 3$ T.
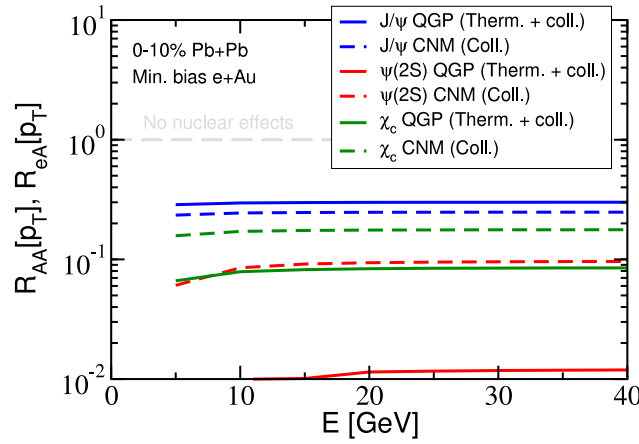
Fig. C.1. Nuclear modification of the J/ψ, $\psi(2S)$ and χ_c states as a function of their respective energy E in the hadron centre-of-mass frame. The solid lines indicate that the calculation was done using thermal wave-function effects while traversing the QGP and correspond to R_{AA} in the centrality class 0%–10% in PbPb LHC collisions. The dashed lines indicate that the calculation was done without thermal effects (only Cold Nuclear Matter (CNM) effects) and correspond to R_{eA} for minimum bias eAu collisions. J/ψ curves are shown in blue, $\psi(2S)$ states are shown in red, and χ_c states are shown in green. All calculations are done using direct production and ignoring feed-down effects.
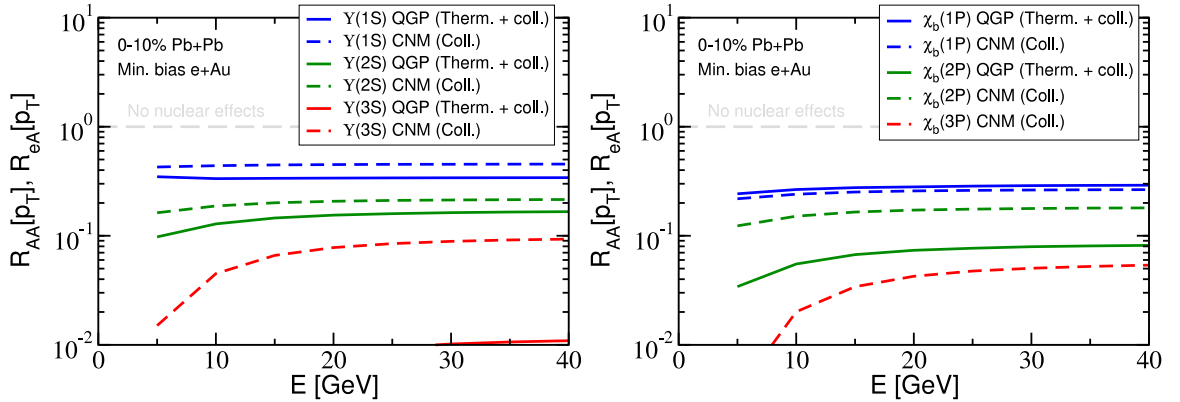
Fig. C.2. Left: nuclear modification of the Y states as a function of the Y energy E in the hadron centre-of-mass frame. The solid lines indicate that the calculation was done using thermal wave-function effects while traversing the QGP and correspond to R_{AA} in the centrality class 0%–10% in PbPb LHC collisions. The dotted lines indicate that the calculation was done without thermal effects (only Cold Nuclear Matter (CNM) effects) and correspond to R_{eA} for minimum bias eAu collisions. Results for $1S$ states are shown in blue, $2S$ states are shown in green, and $3S$ states are shown in red. Right: the same ratios but for χ_b states. The colour coding is similar but for $1P$, $2P$ and $3P$ states. All calculations were done using direct and ignoring feed-down effects. The initial suppression of $\chi_b(3P)$ is not shown because it has a very low R_{AA} value, far lower than any other state pictured.

$B = 1.5$ T, and $P_T > 0.4$ GeV for $B = 3$ T [2]. The single electron tracking efficiency is assumed to be 80%. Fig. B.1 shows the efficiency as a function of J/ψ rapidity and P_T: it is approximately constant, and for the $B = 3$ T case, there is a mild decrease of efficiency with increasing P_T due to decay kinematics. For high-P_T J/ψ, one of the electrons tends to carry the majority of the momentum; thus the P_T of the other falls below the reconstruction threshold. Based on these results, we assume the J/ψ measurement efficiency to be 64%.

Appendix C. Numerical results for nuclear modification R_{AA} and R_{eA} for quarkonium production within the microscopic model presented in Section 5.3

See Figs. C.1 and C.2.

Appendix D. The lepton, photon and parton distribution in an unpolarised electron

See Fig. D.1.
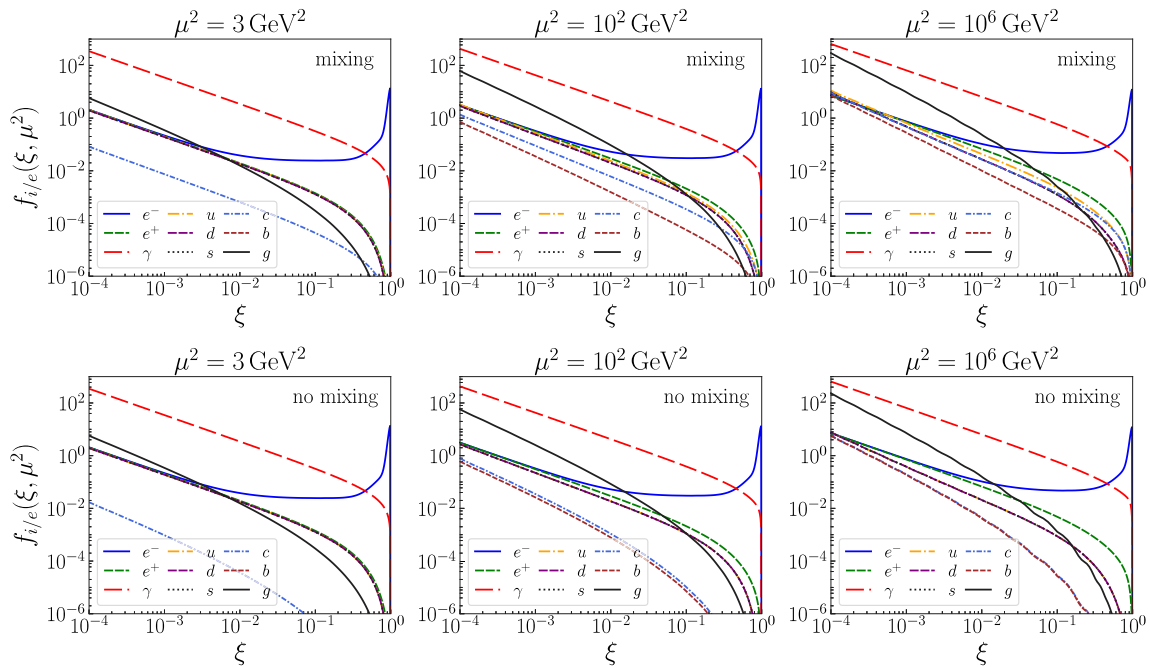
Fig. D.1. The lepton, photon and parton distribution in an unpolarised electron at $\mu^2 = 3\,\mathrm{GeV}^2$, $10^2\,\mathrm{GeV}^2$, and $10^6\,\mathrm{GeV}^2$ are presented as a function of the longitudinal momentum fraction ξ [159]. The upper (lower) figures represent LDFs with (without) the mixing of QED and QCD evolution.

References

[1] A. Accardi, et al., Eur. Phys. J. A 52 (9) (2016) 268, http://dx.doi.org/10.1140/epja/i2016-16268-9, arXiv:1212.1701.
[2] R. Abdul Khalek, et al., Nucl. Phys. A 1026 (2022) 122447, http://dx.doi.org/10.1016/j.nuclphysa.2022.122447, arXiv:2103.05419.
[3] C.-H. Chang, Nuclear Phys. B 172 (1980) 425–434, http://dx.doi.org/10.1016/0550-3213(80)90175-3.
[4] E.L. Berger, D.L. Jones, Phys. Rev. D 23 (1981) 1521–1530, http://dx.doi.org/10.1103/PhysRevD.23.1521.
[5] R. Baier, R. Ruckl, Phys. Lett. B 102 (1981) 364–370, http://dx.doi.org/10.1016/0370-2693(81)90636-5.
[6] R. Baier, R. Ruckl, Z. Phys. C 19 (1983) 251, http://dx.doi.org/10.1007/BF01572254.
[7] F. Halzen, Phys. Lett. B 69 (1977) 105–108, http://dx.doi.org/10.1016/0370-2693(77)90144-7.
[8] H. Fritzsch, Phys. Lett. B 67 (1977) 217–221, http://dx.doi.org/10.1016/0370-2693(77)90108-3.
[9] J.-P. Lansberg, Phys. Rep. 889 (2020) 1–106, http://dx.doi.org/10.1016/j.physrep.2020.08.007, arXiv:1903.09185.
[10] J.C. Collins, Foundations of Perturbative QCD, vol. 32, Cambridge University Press, 2013.
[11] J. Collins, J.-W. Qiu, Phys. Rev. D 75 (2007) 114014, http://dx.doi.org/10.1103/PhysRevD.75.114014, arXiv:0705.2141.
[12] T.C. Rogers, P.J. Mulders, Phys. Rev. D 81 (2010) 094006, http://dx.doi.org/10.1103/PhysRevD.81.094006, arXiv:1001.2977.
[13] M. Diehl, Phys. Rep. 388 (2003) 41–277, http://dx.doi.org/10.1016/j.physrep.2003.08.002, http://dx.doi.org/10.3204/DESY-THESIS-2003-018. arXiv:hep-ph/0307382.
[14] D. Yu. Ivanov, A. Schafer, L. Szymanowski, G. Krasnikov, Eur. Phys. J. C 34 (3) (2004) 297–316, http://dx.doi.org/10.1140/epjc/s10052-015-3298-8, http://dx.doi.org/10.1140/epjc/s2004-01712-x. arXiv:hep-ph/0401131; Eur. Phys. J.C 75 (2) (2015) 75, Erratum:.
[15] D. Kharzeev, Proc. Int. Sch. Phys. Fermi 130 (1996) 105–131, http://dx.doi.org/10.3254/978-1-61499-215-8-105, arXiv:nucl-th/9601029.
[16] D. Kharzeev, H. Satz, A. Syamtomov, G. Zinovjev, Eur. Phys. J. C 9 (1999) 459–462, http://dx.doi.org/10.1007/s100529900047, arXiv:hep-ph/9901375.
[17] Y. Hatta, B.-W. Xiao, F. Yuan, Phys. Rev. D 95 (11) (2017) 114026, http://dx.doi.org/10.1103/PhysRevD.95.114026, arXiv:1703.02085.
[18] D. Boer, C. Setyadi, Eur. Phys. J. C 83 (10) (2023) 890, http://dx.doi.org/10.1140/epjc/s10052-023-12040-6, arXiv:2301.07980.
[19] B. Pire, L. Szymanowski, Phys. Lett. B 622 (2005) 83–92, http://dx.doi.org/10.1016/j.physletb.2005.06.080, arXiv:hep-ph/0504255.
[20] B. Pire, K. Semenov-Tian-Shansky, L. Szymanowski, Phys. Rep. 940 (2021) 1–121, http://dx.doi.org/10.1016/j.physrep.2021.09.002, arXiv:2103.01079.
[21] J.P. Lansberg, B. Pire, K. Semenov-Tian-Shansky, L. Szymanowski, Phys. Rev. D 85 (2012) 054021, http://dx.doi.org/10.1103/PhysRevD.85.054021, arXiv:1112.3570.
[22] K. Park, et al., Phys. Lett. B 780 (2018) 340–345, http://dx.doi.org/10.1016/j.physletb.2018.03.026, arXiv:1711.08486.
[23] B. Pire, K.M. Semenov-Tian-Shansky, A.A. Shaikhutdinova, L. Szymanowski, AAPPS Bull. 33 (1) (2023) 26, http://dx.doi.org/10.1007/s43673-023-00094-3, arXiv:2212.07688.
[24] S. Adhikari, et al., Phys. Rev. C 108 (2) (2023) 025201, http://dx.doi.org/10.1103/PhysRevC.108.025201, arXiv:2304.03845.
[25] Michael Krämer, Prog. Part. Nucl. Phys. 47 (2001) 141–201, http://dx.doi.org/10.1016/S0146-6410(01)00154-5, arXiv:hep-ph/0106120.
[26] N. Brambilla, et al., 2004. http://dx.doi.org/10.5170/CERN-2005-005, arXiv:hep-ph/0412158.
[27] J.P. Lansberg, Internat. J. Modern Phys. A 21 (2006) 3857–3916, http://dx.doi.org/10.1142/S0217751X06033180, arXiv:hep-ph/0602091.
[28] N. Brambilla, et al., Eur. Phys. J. C 71 (2011) 1534, http://dx.doi.org/10.1140/epjc/s10052-010-1534-9, arXiv:1010.5827.
[29] Z. Conesa del Valle, et al., Nucl. Phys. Proc. Suppl. 214 (2011) 3–36, http://dx.doi.org/10.1016/j.nuclphysbps.2011.03.053, arXiv:1105.4545.
[30] A. Andronic, et al., Eur. Phys. J. C 76 (3) (2016) 107, http://dx.doi.org/10.1140/epjc/s10052-015-3819-5, arXiv:1506.03981.
[31] A. Andronic, et al., 2013. arXiv:1304.2224.
[32] Z.-B. Tang, W.-M. Zha, Y.-F. Zhang, Nucl. Sci. Tech. 31 (8) (2020) 81, http://dx.doi.org/10.1007/s41365-020-00785-8.
[33] E. Chapon, et al., Prog. Part. Nucl. Phys. 122 (2022) 103906, http://dx.doi.org/10.1016/j.ppnp.2021.103906, arXiv:2012.14161.

[34] https://www.bnl.gov/rhic/complex.php.

[35] P. Jacobs, X.-N. Wang, Prog. Part. Nucl. Phys. 54 (2005) 443–534, http://dx.doi.org/10.1016/j.ppnp.2004.09.001, arXiv:hep-ph/0405125.

[36] E. Beebe, J. Alessi, S. Binello, T. Kanesue, D. McCafferty, J. Morris, M. Okamura, A. Pikin, J. Ritter, R. Schoepfer, AIP Conf. Proc. 1640 (1) (2015) 5–11, http://dx.doi.org/10.1063/1.4905394.

[37] ePIC Collaboration, 2014. http://dx.doi.org/10.5281/zenodo.11522461.

[38] National Academies of Sciences, Engineering, and Medicine, An Assessment of U.S.-Based Electron-Ion Collider Science, The National Academies Press, Washington, DC, 2018, http://dx.doi.org/10.17226/25171, URL https://www.nap.edu/catalog/25171/an-assessment-of-us-based-electron-ion-collider-science.

[39] F. Willeke, 2021. http://dx.doi.org/10.2172/1765663.

[40] J. Adam, et al., Phys. Rev. D 100 (5) (2019) 052009, http://dx.doi.org/10.1103/PhysRevD.100.052009, arXiv:1905.06075.

[41] J. Adam, et al., Phys. Lett. B 786 (2018) 87–93, http://dx.doi.org/10.1016/j.physletb.2018.09.029, arXiv:1805.03745.

[42] J. Adam, et al., Phys. Rev. D 102 (9) (2020) 092009, http://dx.doi.org/10.1103/PhysRevD.102.092009, arXiv:2007.04732.

[43] S. Acharya, et al., Eur. Phys. J. D 81 (2021) 1121, http://dx.doi.org/10.1140/epjc/s10052-021-09873-4, arXiv:2108.01906.

[44] B. Abelev, et al., J. High Energy Phys. 11 (2012) 065, http://dx.doi.org/10.1007/JHEP11(2012)065, arXiv:1205.5880.

[45] L. Kosarzewski, PoS ICHEP 2020 (2021) 545, http://dx.doi.org/10.22323/1.390.0545.

[46] ATHENA Collaboration, 2021. http://dx.doi.org/10.5281/zenodo.6539707.

[47] CORE Proto-Collaboration, 2021. http://dx.doi.org/10.5281/zenodo.6536630.

[48] ECCE consortium, 2022. http://dx.doi.org/10.5281/zenodo.6537588.

[49] A.A. Akhundov, D.Y. Bardin, L. Kalinovskaya, T. Riemann, Fortsch. Phys. 44 (1996) 373–482, http://dx.doi.org/10.1002/prop.2190440502, arXiv:hep-ph/9407266.

[50] K. Charchula, G.A. Schuler, H. Spiesberger, Comput. Phys. Comm. 81 (1994) 381–402, http://dx.doi.org/10.1016/0010-4655(94)90086-8.

[51] T. Liu, W. Melnitchouk, J.-W. Qiu, N. Sato, J. High Energy Phys. 11 (2021) 157, http://dx.doi.org/10.1007/JHEP11(2021)157, arXiv:2108.13371.

[52] T. Liu, W. Melnitchouk, J.-W. Qiu, N. Sato, Phys. Rev. D 104 (9) (2021) 094033, http://dx.doi.org/10.1103/PhysRevD.104.094033, arXiv:2008.02895.

[53] A. Bacchetta, M. Diehl, K. Goeke, A. Metz, P.J. Mulders, M. Schlegel, J. High Energy Phys. 02 (2007) 093, http://dx.doi.org/10.1088/1126-6708/2007/02/093, arXiv:hep-ph/0611265.

[54] C. Flore, J.-P. Lansberg, H.-S. Shao, Y. Yedelkina, Phys. Lett. B 811 (2020) 135926, http://dx.doi.org/10.1016/j.physletb.2020.135926, arXiv:2009.08264.

[55] B.A. Kniehl, G. Kramer, B. Potter, Nuclear Phys. B 582 (2000) 514–536, http://dx.doi.org/10.1016/S0550-3213(00)00303-5, arXiv:hep-ph/0010289.

[56] D. de Florian, R. Sassot, M. Stratmann, Phys. Rev. D 76 (2007) 074033, http://dx.doi.org/10.1103/PhysRevD.76.074033, arXiv:0707.1506.

[57] V. Bertone, N.P. Hartland, E.R. Nocera, J. Rojo, L. Rottoli, Eur. Phys. J. C 78 (8) (2018) 651, http://dx.doi.org/10.1140/epjc/s10052-018-6130-4, arXiv:1807.03310.

[58] V.G. Kartvelishvili, A.K. Likhoded, V.A. Petrov, Phys. Lett. B 78 (1978) 615–617, http://dx.doi.org/10.1016/0370-2693(78)90653-6.

[59] C. Peterson, D. Schlatter, I. Schmitt, P.M. Zerwas, Phys. Rev. D 27 (1983) 105, http://dx.doi.org/10.1103/PhysRevD.27.105.

[60] J. Binnewies, B.A. Kniehl, G. Kramer, Phys. Rev. D 58 (1998) 034016, http://dx.doi.org/10.1103/PhysRevD.58.034016, arXiv:hep-ph/9802231.

[61] G.T. Bodwin, E. Braaten, G. Lepage, Phys. Rev. D 51 (1995) 1125–1171, http://dx.doi.org/10.1103/PhysRevD.55.5853, arXiv:hep-ph/9407339; Phys. Rev. D 55 (1997) 5853, Erratum:.

[62] G.P. Lepage, L. Magnea, C. Nakhleh, U. Magnea, K. Hornbostel, Phys. Rev. D 46 (1992) 4052–4067, http://dx.doi.org/10.1103/PhysRevD.46.4052, arXiv:hep-lat/9205007.

[63] G.T. Bodwin, E. Braaten, J. Lee, Phys. Rev. D 72 (2005) 014004, http://dx.doi.org/10.1103/PhysRevD.72.014004, arXiv:hep-ph/0504014.

[64] E.J. Eichten, C. Quigg, Phys. Rev. D 52 (1995) 1726–1728, http://dx.doi.org/10.1103/PhysRevD.52.1726, arXiv:hep-ph/9503356.

[65] M. Beneke, A. Signer, V.A. Smirnov, Phys. Rev. Lett. 80 (1998) 2535–2538, http://dx.doi.org/10.1103/PhysRevLett.80.2535, arXiv:hep-ph/9712302.

[66] G.T. Bodwin, E. Braaten, G.P. Lepage, Phys. Rev. D 46 (1992) R1914–R1918, http://dx.doi.org/10.1103/PhysRevD.46.R1914, arXiv:hep-lat/9205006.

[67] P.L. Cho, A.K. Leibovich, Phys. Rev. D 53 (1996) 150–162, http://dx.doi.org/10.1103/PhysRevD.53.150, arXiv:hep-ph/9505329.

[68] J.M. Campbell, F. Maltoni, F. Tramontano, Phys. Rev. Lett. 98 (2007) 252002, http://dx.doi.org/10.1103/PhysRevLett.98.252002, arXiv:hep-ph/0703113.

[69] B. Gong, J.-X. Wang, Phys. Rev. D 78 (2008) 074011, http://dx.doi.org/10.1103/PhysRevD.78.074011, arXiv:0805.2469.

[70] P. Artoisenet, J.M. Campbell, J. Lansberg, F. Maltoni, F. Tramontano, Phys. Rev. Lett. 101 (2008) 152001, http://dx.doi.org/10.1103/PhysRevLett.101.152001, arXiv:0806.3282.

[71] J. Lansberg, Eur. Phys. J. C 61 (2009) 693–703, http://dx.doi.org/10.1140/epjc/s10052-008-0826-9, arXiv:0811.4005.

[72] J.P. Lansberg, Phys. Lett. B 695 (2011) 149–156, http://dx.doi.org/10.1016/j.physletb.2010.10.054, arXiv:1003.4319.

[73] J.P. Lansberg, J. Phys. G 38 (2011) 124110, http://dx.doi.org/10.1088/0954-3899/38/12/124110, arXiv:1107.0292.

[74] Y.-Q. Ma, K. Wang, K.-T. Chao, Phys. Rev. D 84 (2011) 114001, http://dx.doi.org/10.1103/PhysRevD.84.114001, arXiv:1012.1030.

[75] H.-S. Shao, J. High Energy Phys. 01 (2019) 112, http://dx.doi.org/10.1007/JHEP01(2019)112, arXiv:1809.02369.

[76] M. Krämer, Nuclear Phys. B 459 (1996) 3–50, http://dx.doi.org/10.1016/0550-3213(95)00568-4, arXiv:hep-ph/9508409.

[77] M. Butenschoen, B.A. Kniehl, Phys. Rev. Lett. 104 (2010) 072001, http://dx.doi.org/10.1103/PhysRevLett.104.072001, arXiv:0909.2798.

[78] P. Hoodbhoy, Phys. Rev. D 56 (1997) 388–393, http://dx.doi.org/10.1103/PhysRevD.56.388, arXiv:hep-ph/9611207.

[79] H. Mäntysaari, J. Penttala, Phys. Lett. B 823 (2021) 136723, http://dx.doi.org/10.1016/j.physletb.2021.136723, arXiv:2104.02349.

[80] H. Mäntysaari, J. Penttala, J. High Energy Phys. 08 (2022) 247, http://dx.doi.org/10.1007/JHEP08(2022)247, arXiv:2204.14031.

[81] M. Butenschoen, Z.-G. He, B.A. Kniehl, Phys. Rev. Lett. 114 (9) (2015) 092004, http://dx.doi.org/10.1103/PhysRevLett.114.092004, arXiv:1411.5287.

[82] R. Aaij, et al., Eur. Phys. J. C 75 (7) (2015) 311, http://dx.doi.org/10.1140/epjc/s10052-015-3502-x, arXiv:1409.3612.

[83] R. Aaij, et al., Eur. Phys. J. C 80 (3) (2020) 191, http://dx.doi.org/10.1140/epjc/s10052-020-7733-0, arXiv:1911.03326.

[84] N. Brambilla, H.S. Chung, A. Vairo, Phys. Rev. Lett. 126 (8) (2021) 082003, http://dx.doi.org/10.1103/PhysRevLett.126.082003, arXiv:2007.07613.

[85] N. Brambilla, H.S. Chung, A. Vairo, J. High Energy Phys. 09 (2021) 032, http://dx.doi.org/10.1007/JHEP09(2021)032, arXiv:2106.09417.

[86] G.T. Bodwin, H.S. Chung, U.-R. Kim, J. Lee, Phys. Rev. Lett. 113 (2) (2014) 022001, http://dx.doi.org/10.1103/PhysRevLett.113.022001, arXiv:1403.3612.

[87] E. Braaten, T.C. Yuan, Phys. Rev. Lett. 71 (1993) 1673–1676, http://dx.doi.org/10.1103/PhysRevLett.71.1673, arXiv:hep-ph/9303205.

[88] M. Cacciari, M. Greco, Phys. Rev. Lett. 73 (1994) 1586–1589, http://dx.doi.org/10.1103/PhysRevLett.73.1586, arXiv:hep-ph/9405241.

[89] E. Braaten, M.A. Doncheski, S. Fleming, M.L. Mangano, Phys. Lett. B 333 (1994) 548–554, http://dx.doi.org/10.1016/0370-2693(94)90182-1, arXiv:hep-ph/9405407.

[90] Z.-B. Kang, J.-W. Qiu, G. Sterman, Phys. Rev. Lett. 108 (2012) 102002, http://dx.doi.org/10.1103/PhysRevLett.108.102002, arXiv:1109.1520.

[91] K. Lee, J.-W. Qiu, G. Sterman, K. Watanabe, SciPost Phys. Proc. 8 (2022) 143, http://dx.doi.org/10.21468/SciPostPhysProc.8.143, arXiv:2108.00305.

[92] Y.-Q. Ma, R. Vogt, Phys. Rev. D 94 (11) (2016) 114029, http://dx.doi.org/10.1103/PhysRevD.94.114029, arXiv:1609.06042.

[93] V. Cheung, R. Vogt, Phys. Rev. D 96 (5) (2017) 054014, http://dx.doi.org/10.1103/PhysRevD.96.054014, arXiv:1706.07686.

[94] V. Cheung, R. Vogt, Phys. Rev. D 98 (11) (2018) 114029, http://dx.doi.org/10.1103/PhysRevD.98.114029, arXiv:1808.02909.

[95] J.-P. Lansberg, H.-S. Shao, N. Yamanaka, Y.-J. Zhang, C. Noûs, Phys. Lett. B 807 (2020) 135559, http://dx.doi.org/10.1016/j.physletb.2020.135559, arXiv:2004.14345.

[96] D. Kang, J.-W. Lee, J. Lee, T. Kim, P. Ko, Phys. Rev. D 71 (2005) 094019, http://dx.doi.org/10.1103/PhysRevD.71.094019, arXiv:hep-ph/0412381.

[97] J.-P. Lansberg, H.-S. Shao, J. High Energy Phys. 10 (2016) 153, http://dx.doi.org/10.1007/JHEP10(2016)153, arXiv:1608.03198.

[98] V. Cheung, R. Vogt, Phys. Rev. D 104 (9) (2021) 094026, http://dx.doi.org/10.1103/PhysRevD.104.094026, arXiv:2102.09118.
[99] P. Faccioli, C. Lourenco, J. Seixas, H.K. Wohri, Eur. Phys. J. C 69 (2010) 657–673, http://dx.doi.org/10.1140/epjc/s10052-010-1420-5, arXiv:1006.2738.
[100] V. Cheung, R. Vogt, 2024. arXiv:2406.00070.
[101] F. Aaron, et al., Eur. Phys. J. C 68 (2010) 401–420, http://dx.doi.org/10.1140/epjc/s10052-010-1376-5, arXiv:1002.0234.
[102] O.J.P. Eboli, E.M. Gregores, F. Halzen, 23rd Brazilian National Meeting on Particle and Fields, 2002, arXiv:hep-ph/0211161.
[103] O.J.P. Eboli, E.M. Gregores, F. Halzen, Phys. Rev. D 67 (2003) 054002, http://dx.doi.org/10.1103/PhysRevD.67.054002.
[104] Y.-Q. Ma, K.-T. Chao, Phys. Rev. D 100 (9) (2019) 094007, http://dx.doi.org/10.1103/PhysRevD.100.094007, arXiv:1703.08402.
[105] R. Li, Y. Feng, Y.-Q. Ma, J. High Energy Phys. 05 (2020) 009, http://dx.doi.org/10.1007/JHEP05(2020)009, arXiv:1911.05886.
[106] G.C. Nayak, J.-W. Qiu, G.F. Sterman, Phys. Rev. D 72 (2005) 114012, http://dx.doi.org/10.1103/PhysRevD.72.114012, arXiv:hep-ph/0509021.
[107] A. Petrelli, M. Cacciari, M. Greco, F. Maltoni, M.L. Mangano, Nuclear Phys. B 514 (1998) 245–309, http://dx.doi.org/10.1016/S0550-3213(97)00801-8, arXiv:hep-ph/9707223.
[108] G.T. Bowdin, H.S. Chung, J.-H. Ee, U.-R. Kim, J. Lee, Phys. Rev. D 101 (9) (2020) 096011, http://dx.doi.org/10.1103/PhysRevD.101.096011, arXiv:1910.05497.
[109] B. Gong, J.-P. Lansberg, C. Lorcé, J. Wang, J. High Energy Phys. 03 (2013) 115, http://dx.doi.org/10.1007/JHEP03(2013)115, arXiv:1210.2430.
[110] M. Butenschoen, B.A. Kniehl, Phys. Rev. Lett. 106 (2011) 022003, http://dx.doi.org/10.1103/PhysRevLett.106.022003, arXiv:1009.5662.
[111] M. Butenschoen, B.A. Kniehl, Phys. Rev. D 84 (2011) 051501, http://dx.doi.org/10.1103/PhysRevD.84.051501, arXiv:1105.0820.
[112] M. Butenschoen, B.A. Kniehl, Phys. Rev. Lett. 108 (2012) 172002, http://dx.doi.org/10.1103/PhysRevLett.108.172002, arXiv:1201.1872.
[113] M. Butenschoen, B.A. Kniehl, Modern Phys. Lett. A 28 (2013) 1350027, http://dx.doi.org/10.1142/S0217732313500272, arXiv:1212.2037.
[114] K.-T. Chao, Y.-Q. Ma, H.-S. Shao, K. Wang, Y.-J. Zhang, Phys. Rev. Lett. 108 (2012) 242004, http://dx.doi.org/10.1103/PhysRevLett.108.242004, arXiv:1201.2675.
[115] B. Gong, L.-P. Wan, J.-X. Wang, H.-F. Zhang, Phys. Rev. Lett. 110 (4) (2013) 042002, http://dx.doi.org/10.1103/PhysRevLett.110.042002, arXiv:1205.6682.
[116] N. Brambilla, H.S. Chung, A. Vairo, X.-P. Wang, Phys. Rev. D 105 (11) (2022) L111503, http://dx.doi.org/10.1103/PhysRevD.105.L111503, arXiv:2203.07778.
[117] B. Gong, J.-X. Wang, H.-F. Zhang, Phys. Rev. D 83 (2011) 114021, http://dx.doi.org/10.1103/PhysRevD.83.114021, arXiv:1009.3839.
[118] K. Wang, Y.-Q. Ma, K.-T. Chao, Phys. Rev. D 85 (2012) 114003, http://dx.doi.org/10.1103/PhysRevD.85.114003, arXiv:1202.6012.
[119] B. Gong, L.-P. Wan, J.-X. Wang, H.-F. Zhang, Phys. Rev. Lett. 112 (3) (2014) 032001, http://dx.doi.org/10.1103/PhysRevLett.112.032001, arXiv:1305.0748.
[120] H. Han, Y.-Q. Ma, C. Meng, H.-S. Shao, K.-T. Chao, Phys. Rev. Lett. 114 (9) (2015) 092005, http://dx.doi.org/10.1103/PhysRevLett.114.092005, arXiv:1411.7350.
[121] H.-F. Zhang, Z. Sun, W.-L. Sang, R. Li, Phys. Rev. Lett. 114 (9) (2015) 092006, http://dx.doi.org/10.1103/PhysRevLett.114.092006, arXiv:1412.0508.
[122] N. Brambilla, H.S. Chung, A. Vairo, X.-P. Wang, J. High Energy Phys. 03 (2023) 242, http://dx.doi.org/10.1007/JHEP03(2023)242, arXiv:2210.17345.
[123] F. Maltoni, et al., Phys. Lett. B 638 (2006) 202–208, http://dx.doi.org/10.1016/j.physletb.2006.05.010, arXiv:hep-ph/0601203.
[124] Y. Feng, J.-P. Lansberg, J.-X. Wang, Eur. Phys. J. C 75 (7) (2015) 313, http://dx.doi.org/10.1140/epjc/s10052-015-3527-1, arXiv:1504.00317.
[125] M. Butenschoen, B.A. Kniehl, Phys. Rev. Lett. 130 (4) (2023) 041901, http://dx.doi.org/10.1103/PhysRevLett.130.041901, arXiv:2207.09366.
[126] N. Brambilla, M. Butenschoen, X.-P. Wang, 2024. arXiv:2411.16384.
[127] G. Aad, et al., Phys. Rev. Lett. 108 (2012) 152001, http://dx.doi.org/10.1103/PhysRevLett.108.152001, arXiv:1112.5154.
[128] Y. Feng, B. Gong, C.-H. Chang, J.-X. Wang, Chin. Phys. C 45 (1) (2021) 013117, http://dx.doi.org/10.1088/1674-1137/abc682, arXiv:2009.03028.
[129] M. Aivazis, J.C. Collins, F.I. Olness, W.-K. Tung, Phys. Rev. D 50 (1994) 3102–3118, http://dx.doi.org/10.1103/PhysRevD.50.3102, arXiv:hep-ph/9312319.
[130] H.-S. Shao, Phys. Rev. D 102 (2020) 034023, http://dx.doi.org/10.1103/PhysRevD.102.034023, arXiv:2005.12967.
[131] Q.-M. Feng, C.-F. Qiao, Phys. Rev. D 110 (9) (2024) 094047, http://dx.doi.org/10.1103/PhysRevD.110.094047, arXiv:2405.05683.
[132] S. Dulat, T.-J. Hou, J. Gao, M. Guzzi, J. Huston, P. Nadolsky, J. Pumplin, C. Schmidt, D. Stump, C. Yuan, Phys. Rev. D 93 (3) (2016) 033006, http://dx.doi.org/10.1103/PhysRevD.93.033006, arXiv:1506.07443.
[133] S. Catani, M. Ciafaloni, F. Hautmann, Phys. Lett. B 242 (1990) 97–102, http://dx.doi.org/10.1016/0370-2693(90)91601-7.
[134] S. Catani, M. Ciafaloni, F. Hautmann, Nuclear Phys. B 366 (1991) 135–188, http://dx.doi.org/10.1016/0550-3213(91)90055-3.
[135] J.C. Collins, R.K. Ellis, Nuclear Phys. B 360 (1991) 3–30, http://dx.doi.org/10.1016/0550-3213(91)90288-9.
[136] S. Catani, F. Hautmann, Nuclear Phys. B 427 (1994) 475–524, http://dx.doi.org/10.1016/0550-3213(94)90636-X, arXiv:hep-ph/9405388.
[137] M.A. Kimber, A.D. Martin, M.G. Ryskin, Phys. Rev. D 63 (2001) 114027, http://dx.doi.org/10.1103/PhysRevD.63.114027, arXiv:hep-ph/0101348.
[138] G. Watt, A.D. Martin, M.G. Ryskin, Eur. Phys. J. C 31 (2003) 73–89, http://dx.doi.org/10.1140/epjc/s2003-01320-4, arXiv:hep-ph/0306169.
[139] G. Watt, A.D. Martin, M.G. Ryskin, Phys. Rev. D 70 (2004) 014012, http://dx.doi.org/10.1103/PhysRevD.70.014012, http://dx.doi.org/10.1103/PhysRevD.70.079902, arXiv:hep-ph/0309096;   Phys. Rev. D 70 (2004) 079902, Erratum:.
[140] M. Nefedov, Phys. Rev. D 104 (5) (2021) 054039, http://dx.doi.org/10.1103/PhysRevD.104.054039, arXiv:2105.13915.
[141] M. Hentschinski, Phys. Rev. D 104 (5) (2021) 054014, http://dx.doi.org/10.1103/PhysRevD.104.054014, arXiv:2107.06203.
[142] A.V. Lipatov, N.P. Zotov, Eur. Phys. J. C 27 (2003) 87–99, http://dx.doi.org/10.1140/epjc/s2002-01106-2, arXiv:hep-ph/0210310.
[143] B. Kniehl, D. Vasin, V. Saleev, Phys. Rev. D 73 (2006) 074022, http://dx.doi.org/10.1103/PhysRevD.73.074022, arXiv:hep-ph/0602179.
[144] M.A. Nefedov, V.A. Saleev, Phys. Rev. D 102 (2020) 114018, http://dx.doi.org/10.1103/PhysRevD.102.114018, arXiv:2009.13188.
[145] A. Arbuzov, et al., Prog. Part. Nucl. Phys. 119 (2021) 103858, http://dx.doi.org/10.1016/j.ppnp.2021.103858, arXiv:2011.15005.
[146] A. Karpishkov, M. Nefedov, V. Saleev, J. Phys. Conf. Ser. 1435 (1) (2020) 012015, http://dx.doi.org/10.1088/1742-6596/1435/1/012015.
[147] A. Colpani Serri, Y. Feng, C. Flore, J.-P. Lansberg, M.A. Ozcelik, H.-S. Shao, Y. Yedelkina, Phys. Lett. B 835 (2022) 137556, http://dx.doi.org/10.1016/j.physletb.2022.137556, arXiv:2112.05060.
[148] J.-X. Wang, Nucl. Instrum. Meth. A 534 (2004) 241–245, http://dx.doi.org/10.1016/j.nima.2004.07.094, arXiv:hep-ph/0407058.
[149] J.-P. Lansberg, M. Nefedov, M.A. Ozcelik, J. High Energy Phys. 05 (2022) 083, http://dx.doi.org/10.1007/JHEP05(2022)083, arXiv:2112.06789.
[150] J.-P. Lansberg, M. Nefedov, M.A. Ozcelik, Eur. Phys. J. C 84 (4) (2024) 351, http://dx.doi.org/10.1140/epjc/s10052-024-12588-x, arXiv:2306.02425.
[151] Y.-Q. Ma, K. Wang, K.-T. Chao, Phys. Rev. D 83 (2011) 111503, http://dx.doi.org/10.1103/PhysRevD.83.111503, arXiv:1002.3987.
[152] M. Butenschoen, B.A. Kniehl, Phys. Rev. D 107 (3) (2023) 034003, http://dx.doi.org/10.1103/PhysRevD.107.034003, arXiv:2207.09346.
[153] P. Aurenche, J.P. Guillet, M. Fontannaz, Z. Phys. C 64 (1994) 621–630, http://dx.doi.org/10.1007/BF01957771, arXiv:hep-ph/9406382.
[154] J.-W. Qiu, X.-P. Wang, H. Xing, Chin. Phys. Lett. 38 (4) (2021) 041201, http://dx.doi.org/10.1088/0256-307X/38/4/041201, arXiv:2005.10832.
[155] E.L. Berger, J. w. Qiu, X. f. Zhang, Phys. Rev. D 65 (2002) 034006, http://dx.doi.org/10.1103/PhysRevD.65.034006, arXiv:hep-ph/0107309.
[156] G.C. Nayak, J.-W. Qiu, G.F. Sterman, Phys. Rev. D 74 (2006) 074007, http://dx.doi.org/10.1103/PhysRevD.74.074007, arXiv:hep-ph/0608066.
[157] Z.-B. Kang, Y.-Q. Ma, J.-W. Qiu, G. Sterman, Phys. Rev. D 90 (3) (2014) 034006, http://dx.doi.org/10.1103/PhysRevD.90.034006, arXiv:1401.0923.
[158] Z.-B. Kang, Y.-Q. Ma, J.-W. Qiu, G. Sterman, Phys. Rev. D 91 (1) (2015) 014030, http://dx.doi.org/10.1103/PhysRevD.91.014030, arXiv:1411.2456.
[159] J.W. Qiu, K. Watanabe, 2024. in preparation.
[160] K. Lee, J.-W. Qiu, G. Sterman, K. Watanabe, EPJ Web Conf. 274 (2022) 04005, http://dx.doi.org/10.1051/epjconf/202227404005, arXiv:2211.12648.
[161] J.-W. Qiu, G.F. Sterman, Nuclear Phys. B 353 (1991) 137–164, http://dx.doi.org/10.1016/0550-3213(91)90504-Q.
[162] Y.-Q. Ma, J.-W. Qiu, H. Zhang, Phys. Rev. D 89 (9) (2014) 094029, http://dx.doi.org/10.1103/PhysRevD.89.094029, arXiv:1311.7078.

[163] Y.-Q. Ma, J.-W. Qiu, H. Zhang, Phys. Rev. D 89 (9) (2014) 094030, http://dx.doi.org/10.1103/PhysRevD.89.094030, arXiv:1401.0524.
[164] Z.-B. Kang, A. Metz, J.-W. Qiu, J. Zhou, Phys. Rev. D 84 (2011) 034046, http://dx.doi.org/10.1103/PhysRevD.84.034046, arXiv:1106.3514.
[165] P. Hinderer, M. Schlegel, W. Vogelsang, Phys. Rev. D 92 (1) (2015) 014001, http://dx.doi.org/10.1103/PhysRevD.92.014001, arXiv:1505.06415;
Phys.Rev.D 93 (2016) 119903, Erratum:.
[166] P. Hinderer, M. Schlegel, W. Vogelsang, Phys. Rev. D 96 (1) (2017) 014002, http://dx.doi.org/10.1103/PhysRevD.96.014002, arXiv:1703.10872.
[167] R. Boughezal, F. Petriello, H. Xing, Phys. Rev. D 98 (5) (2018) 054031, http://dx.doi.org/10.1103/PhysRevD.98.054031, arXiv:1806.07311.
[168] G. Abelof, R. Boughezal, X. Liu, F. Petriello, Phys. Lett. B 763 (2016) 52–59, http://dx.doi.org/10.1016/j.physletb.2016.10.022, arXiv:1607.04921.
[169] E. Moffat, W. Melnitchouk, T.C. Rogers, N. Sato, Phys. Rev. D 104 (1) (2021) 016015, http://dx.doi.org/10.1103/PhysRevD.104.016015, arXiv:2101.04664.
[170] P.L. Cho, M.B. Wise, Phys. Lett. B 346 (1995) 129–136, http://dx.doi.org/10.1016/0370-2693(94)01658-Y, arXiv:hep-ph/9411303.
[171] T. Affolder, et al., Phys. Rev. Lett. 85 (2000) 2886–2891, http://dx.doi.org/10.1103/PhysRevLett.85.2886, arXiv:hep-ex/0004027.
[172] A. Abulencia, et al., Phys. Rev. Lett. 99 (2007) 132001, http://dx.doi.org/10.1103/PhysRevLett.99.132001, arXiv:0704.0638.
[173] A. Adare, et al., Phys. Rev. D 82 (2010) 012001, http://dx.doi.org/10.1103/PhysRevD.82.012001, arXiv:0912.2082.
[174] L. Adamczyk, et al., Phys. Lett. B 739 (2014) 180–188, http://dx.doi.org/10.1016/j.physletb.2014.10.049, arXiv:1311.1621.
[175] A. Adare, et al., Phys. Rev. D 95 (2017) 092003, http://dx.doi.org/10.1103/PhysRevD.95.092003, arXiv:1612.06807.
[176] B. Abelev, et al., Phys. Rev. Lett. 108 (2012) 082001, http://dx.doi.org/10.1103/PhysRevLett.108.082001, arXiv:1111.1630.
[177] R. Aaij, et al., Eur. Phys. J. C 73 (11) (2013) 2631, http://dx.doi.org/10.1140/epjc/s10052-013-2631-3, arXiv:1307.6379.
[178] S. Chatrchyan, et al., Phys. Lett. B 727 (2013) 381–402, http://dx.doi.org/10.1016/j.physletb.2013.10.055, arXiv:1307.6070.
[179] V. Khachatryan, et al., Phys. Rev. Lett. 114 (19) (2015) 191802, http://dx.doi.org/10.1103/PhysRevLett.114.191802, arXiv:1502.04155.
[180] S. Acharya, et al., Eur. Phys. J. C 78 (7) (2018) 562, http://dx.doi.org/10.1140/epjc/s10052-018-6027-2, arXiv:1805.04374.
[181] A. Hayrapetyan, et al., Phys. Lett. B 858 (2024) 139044, http://dx.doi.org/10.1016/j.physletb.2024.139044, arXiv:2406.14409.
[182] R. Aaij, et al., Eur. Phys. J. C 74 (5) (2014) 2872, http://dx.doi.org/10.1140/epjc/s10052-014-2872-9, arXiv:1403.1339.
[183] A.M. Sirunyan, et al., Phys. Lett. B 790 (2019) 509–532, http://dx.doi.org/10.1016/j.physletb.2019.01.058, arXiv:1805.02248.
[184] D. Acosta, et al., Phys. Rev. Lett. 88 (2002) 161802, http://dx.doi.org/10.1103/PhysRevLett.88.161802.
[185] T. Aaltonen, et al., Phys. Rev. Lett. 108 (2012) 151802, http://dx.doi.org/10.1103/PhysRevLett.108.151802, arXiv:1112.1591.
[186] V.M. Abazov, et al., Phys. Rev. Lett. 101 (2008) 182004, http://dx.doi.org/10.1103/PhysRevLett.101.182004, arXiv:0804.2799.
[187] S. Chatrchyan, et al., Phys. Rev. Lett. 110 (8) (2013) 081802, http://dx.doi.org/10.1103/PhysRevLett.110.081802, arXiv:1209.2922.
[188] R. Aaij, et al., J. High Energy Phys. 12 (2017) 110, http://dx.doi.org/10.1007/JHEP12(2017)110, arXiv:1709.01301.
[189] P. Artoisenet, J.M. Campbell, F. Maltoni, F. Tramontano, Phys. Rev. Lett. 102 (2009) 142001, http://dx.doi.org/10.1103/PhysRevLett.102.142001, arXiv:0901.4352.
[190] C.-H. Chang, R. Li, J.-X. Wang, Phys. Rev. D 80 (2009) 034020, http://dx.doi.org/10.1103/PhysRevD.80.034020, arXiv:0901.4749.
[191] M. Butenschoen, B.A. Kniehl, Phys. Rev. Lett. 107 (2011) 232001, http://dx.doi.org/10.1103/PhysRevLett.107.232001, arXiv:1109.1476.
[192] S. Chekanov, et al., J. High Energy Phys. 12 (2009) 007, http://dx.doi.org/10.1088/1126-6708/2009/12/007, arXiv:0906.1424.
[193] C. Adloff, et al., Eur. Phys. J. C 25 (2002) 41–53, http://dx.doi.org/10.1007/s10052-002-1014-y, arXiv:hep-ex/0205065.
[194] M. Steder, PoS DIS 2010 (2010) 180, http://dx.doi.org/10.22323/1.106.0180.
[195] F. Yuan, K.-T. Chao, Phys. Rev. D 63 (2001) 034017, http://dx.doi.org/10.1103/PhysRevD.63.034017, arXiv:hep-ph/0008301;   Phys. Rev. D 66 (2002) 079902, Erratum:.
[196] U. D'Alesio, L. Maxia, F. Murgia, C. Pisano, S. Rajesh, Phys. Rev. D 107 (11) (2023) 114001, http://dx.doi.org/10.1103/PhysRevD.107.114001, arXiv:2301.11987.
[197] Z. Sun, H.-F. Zhang, Phys. Rev. D 96 (9) (2017) 091502, http://dx.doi.org/10.1103/PhysRevD.96.091502, arXiv:1705.05337.
[198] Z. Sun, H.-F. Zhang, Eur. Phys. J. C 77 (11) (2017) 744, http://dx.doi.org/10.1140/epjc/s10052-017-5323-6, arXiv:1702.02097.
[199] B. Gong, J.-X. Wang, Phys. Rev. Lett. 100 (2008) 232001, http://dx.doi.org/10.1103/PhysRevLett.100.232001, arXiv:0802.3727.
[200] H.-F. Zhang, Y. Feng, W.-L. Sang, Y.-P. Yan, Phys. Rev. D 99 (11) (2019) 114018, http://dx.doi.org/10.1103/PhysRevD.99.114018, arXiv:1902.09056.
[201] H.-F. Zhang, X.-M. Mo, J. High Energy Phys. 12 (2021) 168, http://dx.doi.org/10.1007/JHEP12(2021)168, arXiv:2110.10268.
[202] L.-K. Hao, F. Yuan, K.-T. Chao, Phys. Rev. Lett. 83 (1999) 4490–4493, http://dx.doi.org/10.1103/PhysRevLett.83.4490, arXiv:hep-ph/9902338.
[203] L.-K. Hao, F. Yuan, K.-T. Chao, Phys. Rev. D 62 (2000) 074023, http://dx.doi.org/10.1103/PhysRevD.62.074023, arXiv:hep-ph/0004203.
[204] F. Abe, et al., Phys. Rev. Lett. 79 (1997) 578–583, http://dx.doi.org/10.1103/PhysRevLett.79.578.
[205] T. Affolder, et al., Phys. Rev. Lett. 84 (2000) 2094–2099, http://dx.doi.org/10.1103/PhysRevLett.84.2094, arXiv:hep-ex/9910025.
[206] T. Affolder, et al., Phys. Rev. Lett. 86 (2001) 3963–3968, http://dx.doi.org/10.1103/PhysRevLett.86.3963.
[207] A. Abulencia, et al., Phys. Rev. Lett. 98 (2007) 232001, http://dx.doi.org/10.1103/PhysRevLett.98.232001, arXiv:hep-ex/0703028.
[208] A. Adare, et al., Phys. Rev. D 85 (2012) 092004, http://dx.doi.org/10.1103/PhysRevD.85.092004, arXiv:1105.1966.
[209] R. Aaij, et al., J. High Energy Phys. 11 (2012) 031, http://dx.doi.org/10.1007/JHEP11(2012)031, arXiv:1209.0282.
[210] R. Aaij, et al., Phys. Lett. B 718 (2012) 431–440, http://dx.doi.org/10.1016/j.physletb.2012.10.068, arXiv:1204.1462.
[211] S. Chatrchyan, et al., Eur. Phys. J. C 72 (2012) 2251, http://dx.doi.org/10.1140/epjc/s10052-012-2251-3, arXiv:1210.0875.
[212] G. Aad, et al., J. High Energy Phys. 07 (2014) 154, http://dx.doi.org/10.1007/JHEP07(2014)154, arXiv:1404.7035.
[213] S. Fleming, T. Mehen, Phys. Rev. D 57 (1998) 1846–1857, http://dx.doi.org/10.1103/PhysRevD.57.1846, arXiv:hep-ph/9707365.
[214] M.G. Echevarria, J. High Energy Phys. 10 (2019) 144, http://dx.doi.org/10.1007/JHEP10(2019)144, arXiv:1907.06494.
[215] S. Fleming, Y. Makris, T. Mehen, J. High Energy Phys. 04 (2020) 122, http://dx.doi.org/10.1007/JHEP04(2020)122, arXiv:1910.03586.
[216] D. Boer, C. Pisano, P. Taels, Phys. Rev. D 103 (7) (2021) 074012, http://dx.doi.org/10.1103/PhysRevD.103.074012, arXiv:2102.00003.
[217] M. Beneke, I. Rothstein, M.B. Wise, Phys. Lett. B 408 (1997) 373–380, http://dx.doi.org/10.1016/S0370-2693(97)00832-0, arXiv:hep-ph/9705286.
[218] S. Fleming, A.K. Leibovich, T. Mehen, Phys. Rev. D 68 (2003) 094011, http://dx.doi.org/10.1103/PhysRevD.68.094011, arXiv:hep-ph/0306139.
[219] S. Fleming, A.K. Leibovich, T. Mehen, Phys. Rev. D 74 (2006) 114004, http://dx.doi.org/10.1103/PhysRevD.74.114004, arXiv:hep-ph/0607121.
[220] M. Beneke, G.A. Schuler, S. Wolf, Phys. Rev. D 62 (2000) 034004, http://dx.doi.org/10.1103/PhysRevD.62.034004, arXiv:hep-ph/0001062.
[221] M.G. Echevarria, Y. Makris, I. Scimemi, J. High Energy Phys. 10 (2020) 164, http://dx.doi.org/10.1007/JHEP10(2020)164, arXiv:2007.05547.
[222] M.G. Echevarria, S.F. Romera, I. Scimemi, J. High Energy Phys. 12 (2023) 181, http://dx.doi.org/10.1007/JHEP12(2023)181, arXiv:2308.12356.
[223] M.G. Echevarria, S.F. Romera, P. Taels, J. High Energy Phys. 09 (2024) 188, http://dx.doi.org/10.1007/JHEP09(2024)188, arXiv:2407.04793.
[224] M.G. Echevarria, T. Kasemets, P.J. Mulders, C. Pisano, J. High Energy Phys. 07 (2015) 158, http://dx.doi.org/10.1007/JHEP07(2015)158, arXiv:1502.05354;   JHEP 05 (2017) 073, Erratum:.
[225] D. Boer, U. D'Alesio, F. Murgia, C. Pisano, P. Taels, J. High Energy Phys. 09 (2020) 040, http://dx.doi.org/10.1007/JHEP09(2020)040, arXiv:2004.06740.
[226] D. Boer, J. Bor, L. Maxia, C. Pisano, F. Yuan, J. High Energy Phys. 08 (2023) 105, http://dx.doi.org/10.1007/JHEP08(2023)105, arXiv:2304.09473.
[227] A. Mukherjee, S. Rajesh, Eur. Phys. J. C 77 (12) (2017) 854, http://dx.doi.org/10.1140/epjc/s10052-017-5406-4, arXiv:1609.05596.
[228] R. Kishore, A. Mukherjee, Phys. Rev. D 99 (5) (2019) 054012, http://dx.doi.org/10.1103/PhysRevD.99.054012, arXiv:1811.07495.
[229] A. Bacchetta, D. Boer, C. Pisano, P. Taels, Eur. Phys. J. C 80 (1) (2020) 72, http://dx.doi.org/10.1140/epjc/s10052-020-7620-8, arXiv:1809.02056.
[230] P. Mulders, J. Rodrigues, Phys. Rev. D 63 (2001) 094021, http://dx.doi.org/10.1103/PhysRevD.63.094021, arXiv:hep-ph/0009343.
[231] S. Meissner, A. Metz, K. Goeke, Phys. Rev. D 76 (2007) 034002, http://dx.doi.org/10.1103/PhysRevD.76.034002, arXiv:hep-ph/0703176.
[232] D. Boer, P.J. Mulders, C. Pisano, Phys. Lett. B 660 (2008) 360–368, http://dx.doi.org/10.1016/j.physletb.2008.01.021, arXiv:0712.0777.
[233] R. Sharma, I. Vitev, Phys. Rev. D C 87 (4) (2013) 044905, http://dx.doi.org/10.1103/PhysRevC.87.044905, arXiv:1203.0329.

[234] T. Matsui, H. Satz, Phys. Lett. B 178 (1986) 416–422, http://dx.doi.org/10.1016/0370-2693(86)91404-8.
[235] A. Adil, I. Vitev, Phys. Lett. B 649 (2007) 139–146, http://dx.doi.org/10.1016/j.physletb.2007.03.050, arXiv:hep-ph/0611109.
[236] R. Sharma, I. Vitev, B.-W. Zhang, Phys. Rev. C 80 (2009) 054902, http://dx.doi.org/10.1103/PhysRevC.80.054902, arXiv:0904.0032.
[237] A. Adare, et al., Phys. Rev. Lett. 111 (20) (2013) 202301, http://dx.doi.org/10.1103/PhysRevLett.111.202301, arXiv:1305.5516.
[238] U.A. Acharya, et al., Phys. Rev. C 105 (6) (2022) 064912, http://dx.doi.org/10.1103/PhysRevC.105.064912, arXiv:2202.03863.
[239] U. Acharya, et al., Phys. Rev. C 102 (1) (2020) 014902, http://dx.doi.org/10.1103/PhysRevC.102.014902, arXiv:1910.14487.
[240] S. Chatrchyan, et al., JHEP 04 (2014) 103, http://dx.doi.org/10.1007/JHEP04(2014)103, arXiv:1312.6300.
[241] A. Rothkopf, Phys. Rep. 858 (2020) 1–117, http://dx.doi.org/10.1016/j.physrep.2020.02.006, arXiv:1912.02253.
[242] A. Tumasyan, et al., Phys. Lett. B 835 (2022) 137397, http://dx.doi.org/10.1016/j.physletb.2022.137397, arXiv:2202.11807.
[243] E.G. Ferreiro, Phys. Lett. B 749 (2015) 98–103, http://dx.doi.org/10.1016/j.physletb.2015.07.066, arXiv:1411.0549.
[244] H.T. Li, Z.L. Liu, I. Vitev, Phys. Lett. B 816 (2021) 136261, http://dx.doi.org/10.1016/j.physletb.2021.136261, arXiv:2007.10994.
[245] H.T. Li, I. Vitev, Phys. Rev. Lett. 126 (25) (2021) 252001, http://dx.doi.org/10.1103/PhysRevLett.126.252001, arXiv:2010.05912.
[246] H.T. Li, Z.L. Liu, I. Vitev, Phys. Lett. B 827 (2022) 137007, http://dx.doi.org/10.1016/j.physletb.2022.137007, arXiv:2108.07809.
[247] L. Adamczyk, et al., Nature 527 (2015) 345–348, http://dx.doi.org/10.1038/nature15724, arXiv:1507.07158.
[248] A. Collaboration, et al., Nature 588 (2020) 232–238, http://dx.doi.org/10.1038/s41586-020-3001-6, arXiv:2005.11495;   Nature 590 (2021) E13.
[249] S. Acharya, et al., Phys. Rev. Lett. 127 (17) (2021) 172301, http://dx.doi.org/10.1103/PhysRevLett.127.172301, arXiv:2105.05578.
[250] X. Yao, T. Mehen, J. High Energy Phys. 02 (2021) 062, http://dx.doi.org/10.1007/JHEP02(2021)062, arXiv:2009.02408.
[251] X. Yao, T. Mehen, Phys. Rev. D 99 (9) (2019) 096028, http://dx.doi.org/10.1103/PhysRevD.99.096028, arXiv:1811.07027.
[252] X. Yao, B. Müller, Phys. Rev. D 100 (1) (2019) 014008, http://dx.doi.org/10.1103/PhysRevD.100.014008, arXiv:1811.09644.
[253] X. Yao, Internat. J. Modern Phys. A 36 (20) (2021) 2130010, http://dx.doi.org/10.1142/S0217751X21300106, arXiv:2102.01736.
[254] T. Binder, K. Mukaida, B. Scheihing-Hitschfeld, X. Yao, J. High Energy Phys. 01 (2022) 137, http://dx.doi.org/10.1007/JHEP01(2022)137, arXiv:2107.03945.
[255] B. Scheihing-Hitschfeld, X. Yao, Phys. Rev. D 108 (5) (2023) 054024, http://dx.doi.org/10.1103/PhysRevD.108.054024, arXiv:2306.13127;   Phys.Rev.D 109 (2024) 099902, Erratum:.
[256] G. Nijs, B. Scheihing-Hitschfeld, X. Yao, Phys. Rev. D 109 (9) (2024) 094043, http://dx.doi.org/10.1103/PhysRevD.109.094043, arXiv:2310.09325.
[257] S. Aid, et al., Nuclear Phys. B 472 (1996) 3–31, http://dx.doi.org/10.1016/0550-3213(96)00274-X, arXiv:hep-ex/9603005.
[258] J. Breitweg, et al., Z. Phys. C 76 (1997) 599–612, http://dx.doi.org/10.1007/s002880050583, arXiv:hep-ex/9708010.
[259] S. Chekanov, et al., Eur. Phys. J. C 27 (2003) 173–188, http://dx.doi.org/10.1140/epjc/s2002-01130-2, arXiv:hep-ex/0211011.
[260] C. Adloff, et al., Eur. Phys. J. C 25 (2002) 25–39, http://dx.doi.org/10.1007/s10052-002-1009-8, arXiv:hep-ex/0205064.
[261] S. Chekanov, et al., J. High Energy Phys. 12 (2009) 007, http://dx.doi.org/10.1088/1126-6708/2009/12/007, arXiv:0906.1424.
[262] H. Abramowicz, et al., J. High Energy Phys. 02 (2013) 071, http://dx.doi.org/10.1007/JHEP02(2013)071, arXiv:1211.6946.
[263] M.L. Mangano, A. Petrelli, Internat. J. Modern Phys. A 12 (1997) 3887–3897, http://dx.doi.org/10.1142/S0217751X97002048, arXiv:hep-ph/9610364.
[264] J.-P. Lansberg, M.A. Ozcelik, Eur. Phys. J. C 81 (6) (2021) 497, http://dx.doi.org/10.1140/epjc/s10052-021-09258-7, arXiv:2012.00702.
[265] T.-J. Hou, et al., Phys. Rev. D 103 (1) (2021) 014013, http://dx.doi.org/10.1103/PhysRevD.103.014013, arXiv:1912.10053.
[266] P.A. Zyla, et al., PTEP 2020 (8) (2020) 083C01, http://dx.doi.org/10.1093/ptep/ptaa104.
[267] M.E. Binkley, et al., Phys. Rev. Lett. 48 (1982) 73, http://dx.doi.org/10.1103/PhysRevLett.48.73.
[268] B.H. Denby, et al., Phys. Rev. Lett. 52 (1984) 795–798, http://dx.doi.org/10.1103/PhysRevLett.52.795.
[269] P. Frabetti, et al., Phys. Lett. B 316 (1) (1993) 197–206, http://dx.doi.org/10.1016/0370-2693(93)90679-C.
[270] C. Adloff, et al., Phys. Lett. B 483 (2000) 23–35, http://dx.doi.org/10.1016/S0370-2693(00)00530-X, arXiv:hep-ex/0003020.
[271] S. Chekanov, et al., Nuclear Phys. B 695 (2004) 3–37, http://dx.doi.org/10.1016/j.nuclphysb.2004.06.034, arXiv:hep-ex/0404008.
[272] S. Chekanov, et al., Phys. Lett. B 680 (2009) 4–12, http://dx.doi.org/10.1016/j.physletb.2009.07.066, arXiv:0903.4205.
[273] C. Alexa, et al., Eur. Phys. J. C 73 (6) (2013) 2466, http://dx.doi.org/10.1140/epjc/s10052-013-2466-y, arXiv:1304.5162.
[274] R. Aaij, et al., J. Phys. G 41 (2014) 055002, http://dx.doi.org/10.1088/0954-3899/41/5/055002, arXiv:1401.3288.
[275] R. Aaij, et al., J. High Energy Phys. 09 (2015) 084, http://dx.doi.org/10.1007/JHEP09(2015)084, arXiv:1505.08139.
[276] R. Aaij, et al., J. High Energy Phys. 10 (2018) 167, http://dx.doi.org/10.1007/JHEP10(2018)167, arXiv:1806.04079.
[277] C.A. Flett, J.A. Gracey, S.P. Jones, T. Teubner, J. High Energy Phys. 08 (2021) 150, http://dx.doi.org/10.1007/JHEP08(2021)150, arXiv:2105.07657.
[278] A. Aktas, et al., Eur. Phys. J. C 46 (2006) 585–603, http://dx.doi.org/10.1140/epjc/s2006-02519-5, arXiv:hep-ex/0510016.
[279] S. Bailey, T. Cridge, L.A. Harland-Lang, A.D. Martin, R.S. Thorne, Eur. Phys. J. C 81 (4) (2021) 341, http://dx.doi.org/10.1140/epjc/s10052-021-09057-0, arXiv:2012.04684.
[280] A. Shuvaev, Phys. Rev. D 60 (1999) 116005, http://dx.doi.org/10.1103/PhysRevD.60.116005, arXiv:hep-ph/9902318.
[281] A.G. Shuvaev, K.J. Golec-Biernat, A.D. Martin, M.G. Ryskin, Phys. Rev. D 60 (1999) 014015, http://dx.doi.org/10.1103/PhysRevD.60.014015, arXiv:hep-ph/9902410.
[282] R.D. Ball, et al., Eur. Phys. J. C 77 (10) (2017) 663, http://dx.doi.org/10.1140/epjc/s10052-017-5199-5, arXiv:1706.00428.
[283] S.P. Jones, A.D. Martin, M.G. Ryskin, T. Teubner, Eur. Phys. J. C 76 (11) (2016) 633, http://dx.doi.org/10.1140/epjc/s10052-016-4493-y, arXiv:1610.02272.
[284] C.A. Flett, S.P. Jones, A.D. Martin, M.G. Ryskin, T. Teubner, Phys. Rev. D 101 (9) (2020) 094011, http://dx.doi.org/10.1103/PhysRevD.101.094011, arXiv:1908.08398.
[285] C.A. Flett, S.P. Jones, A.D. Martin, M.G. Ryskin, T. Teubner, PoS LC2019 (2020) 040, http://dx.doi.org/10.22323/1.374.0040, arXiv:1912.09128.
[286] C. Flett, A. Martin, M. Ryskin, T. Teubner, Phys. Rev. D 102 (2020) 114021, http://dx.doi.org/10.1103/PhysRevD.102.114021, arXiv:2006.13857.
[287] C.A. Flett, S.P. Jones, A.D. Martin, M.G. Ryskin, T. Teubner, Phys. Rev. D 105 (3) (2022) 034008, http://dx.doi.org/10.1103/PhysRevD.105.034008, arXiv:2110.15575.
[288] C.A. Flett, S.P. Jones, A.D. Martin, M.G. Ryskin, T. Teubner, Phys. Rev. D 106 (7) (2022) 074021, http://dx.doi.org/10.1103/PhysRevD.106.074021, arXiv:2206.10161.
[289] C.A. Flett, A.D. Martin, M.G. Ryskin, T. Teubner, 2024, arXiv:2408.01128.
[290] K.J. Eskola, C.A. Flett, V. Guzey, T. Löytäinen, H. Paukkunen, Phys. Rev. C 106 (3) (2022) 035202, http://dx.doi.org/10.1103/PhysRevC.106.035202, arXiv:2203.11613.
[291] K.J. Eskola, C.A. Flett, V. Guzey, T. Löytäinen, H. Paukkunen, Phys. Rev. C 107 (4) (2023) 044912, http://dx.doi.org/10.1103/PhysRevC.107.044912, arXiv:2210.16048.
[292] S.J. Brodsky, P. Hoyer, C. Peterson, N. Sakai, Phys. Lett. B 93 (1980) 451–455, http://dx.doi.org/10.1016/0370-2693(80)90364-0.
[293] S.J. Brodsky, C. Peterson, N. Sakai, Phys. Rev. D 23 (1981) 2745, http://dx.doi.org/10.1103/PhysRevD.23.2745.
[294] R.S. Sufian, T. Liu, A. Alexandru, S.J. Brodsky, G.F. de Téramond, H.G. Dosch, T. Draper, K.-F. Liu, Y.-B. Yang, Phys. Lett. B 808 (2020) 135633, http://dx.doi.org/10.1016/j.physletb.2020.135633, arXiv:2003.01078.
[295] S.J. Brodsky, P. Hoyer, A.H. Mueller, W.-K. Tang, Nuclear Phys. B 369 (1992) 519–542, http://dx.doi.org/10.1016/0550-3213(92)90278-J.
[296] S.J. Brodsky, E. Chudakov, P. Hoyer, J.M. Laget, Phys. Lett. B 498 (2001) 23–28, http://dx.doi.org/10.1016/S0370-2693(00)01373-3, arXiv:hep-ph/0010343.
[297] S.J. Brodsky, J. Gillespie, Phys. Rev. 173 (1968) 1011–1020, http://dx.doi.org/10.1103/PhysRev.173.1011.

[298] S. Paiva, M. Nielsen, F.S. Navarra, F.O. Duraes, L.L. Barz, Modern Phys. Lett. A 13 (1998) 2715–2724, http://dx.doi.org/10.1142/S0217732398002886, arXiv:hep-ph/9610310.

[299] F.M. Steffens, W. Melnitchouk, A.W. Thomas, Eur. Phys. J. C 11 (1999) 673–683, http://dx.doi.org/10.1007/s100520050663, arXiv:hep-ph/9903441.

[300] T.J. Hobbs, J.T. Londergan, W. Melnitchouk, Phys. Rev. D 89 (7) (2014) 074008, http://dx.doi.org/10.1103/PhysRevD.89.074008, arXiv:1311.1578.

[301] J. Pumplin, H.L. Lai, W.K. Tung, Phys. Rev. D 75 (2007) 054029, http://dx.doi.org/10.1103/PhysRevD.75.054029, arXiv:hep-ph/0701220.

[302] P.M. Nadolsky, H.-L. Lai, Q.-H. Cao, J. Huston, J. Pumplin, D. Stump, W.-K. Tung, C.P. Yuan, Phys. Rev. D 78 (2008) 013004, http://dx.doi.org/10.1103/PhysRevD.78.013004, arXiv:0802.0007.

[303] S. Dulat, T.-J. Hou, J. Gao, J. Huston, J. Pumplin, C. Schmidt, D. Stump, C.P. Yuan, Phys. Rev. D 89 (7) (2014) 073004, http://dx.doi.org/10.1103/PhysRevD.89.073004, arXiv:1309.0025.

[304] P. Jimenez-Delgado, T.J. Hobbs, J.T. Londergan, W. Melnitchouk, Phys. Rev. Lett. 114 (8) (2015) 082002, http://dx.doi.org/10.1103/PhysRevLett.114.082002, arXiv:1408.1708.

[305] R.D. Ball, V. Bertone, M. Bonvini, S. Carrazza, S. Forte, A. Guffanti, N.P. Hartland, J. Rojo, L. Rottoli, Eur. Phys. J. C 76 (11) (2016) 647, http://dx.doi.org/10.1140/epjc/s10052-016-4469-y, arXiv:1605.06515.

[306] E. Hoffmann, R. Moore, Z. Phys. C 20 (1983) 71, http://dx.doi.org/10.1007/BF01577720.

[307] B.W. Harris, J. Smith, R. Vogt, Nuclear Phys. B 461 (1996) 181–196, http://dx.doi.org/10.1016/0550-3213(95)00652-4, arXiv:hep-ph/9508403.

[308] J.J. Aubert, et al., Phys. Lett. B 110 (1982) 73–76, http://dx.doi.org/10.1016/0370-2693(82)90955-8.

[309] S.J. Brodsky, A. Kusina, F. Lyonnet, I. Schienbein, H. Spiesberger, R. Vogt, Adv. High Energy Phys. 2015 (2015) 231547, http://dx.doi.org/10.1155/2015/231547, arXiv:1504.06287.

[310] S.J. Brodsky, G.I. Lykasov, A.V. Lipatov, J. Smiesko, Prog. Part. Nucl. Phys. 114 (2020) 103802, http://dx.doi.org/10.1016/j.ppnp.2020.103802, arXiv:2006.09443.

[311] R.D. Ball, A. Candido, J. Cruz-Martinez, S. Forte, T. Giani, F. Hekhorn, G. Magni, E.R. Nocera, J. Rojo, R. Stegeman, Phys. Rev. D 109 (9) (2024) L091501, http://dx.doi.org/10.1103/PhysRevD.109.L091501, arXiv:2311.00743.

[312] T. Gutierrez, R. Vogt, Nuclear Phys. B 539 (1999) 189–214, http://dx.doi.org/10.1016/S0550-3213(98)00748-2, arXiv:hep-ph/9808213.

[313] S.J. Brodsky, K.Y.-J. Chiu, J.-P. Lansberg, N. Yamanaka, Phys. Lett. B 783 (2018) 287–293, http://dx.doi.org/10.1016/j.physletb.2018.06.070, arXiv:1805.03173.

[314] J. Badier, et al., Z. Phys. C 20 (1983) 101, http://dx.doi.org/10.1007/BF01573213.

[315] P. Chauvat, et al., Phys. Lett. B 199 (1987) 304, http://dx.doi.org/10.1016/0370-2693(87)91379-7.

[316] R. Aaij, et al., Phys. Rev. Lett. 128 (8) (2022) 082001, http://dx.doi.org/10.1103/PhysRevLett.128.082001, arXiv:2109.08084.

[317] R.D. Ball, A. Candido, J. Cruz-Martinez, S. Forte, T. Giani, F. Hekhorn, K. Kudashkin, G. Magni, J. Rojo, Nature 608 (7923) (2022) 483–487, http://dx.doi.org/10.1038/s41586-022-04998-2, arXiv:2208.08372.

[318] M. Kelsey, R. Cruz-Torres, X. Dong, Y. Ji, S. Radhakrishnan, E. Sichtermann, Phys. Rev. D 104 (5) (2021) 054002, http://dx.doi.org/10.1103/PhysRevD.104.054002, arXiv:2107.05632.

[319] J. High Energy Phys. 04 (2014) 172, http://dx.doi.org/10.1007/JHEP04(2014)172, arXiv:1401.2831.

[320] Eur. Phys. J. C 75 (5) (2015) 229, http://dx.doi.org/10.1140/epjc/s10052-015-3406-9, arXiv:1412.6428.

[321] R. Aaij, et al., Phys. Lett. B 707 (2012) 52–59, http://dx.doi.org/10.1016/j.physletb.2011.12.015, arXiv:1109.0963.

[322] R. Aaij, et al., J. High Energy Phys. 06 (2017) 047, http://dx.doi.org/10.1007/JHEP06(2017)047, http://dx.doi.org/10.1007/JHEP10(2017)068. arXiv:1612.07451;   JHEP 10 (2017) 068, Erratum:.

[323] V.M. Abazov, et al., Phys. Rev. D 90 (11) (2014) 111101, http://dx.doi.org/10.1103/PhysRevD.90.111101, arXiv:1406.2380.

[324] V. Khachatryan, et al., J. High Energy Phys. 09 (2014) 094, http://dx.doi.org/10.1007/JHEP09(2014)094, arXiv:1406.0484.

[325] M. Aaboud, et al., Eur. Phys. J. C 77 (2) (2017) 76, http://dx.doi.org/10.1140/epjc/s10052-017-4644-9, arXiv:1612.02950.

[326] R. Aaij, et al., J. High Energy Phys. 06 (2012) 141, http://dx.doi.org/10.1007/JHEP06(2012)141, http://dx.doi.org/10.1007/JHEP03(2014)108. arXiv:1205.0975;   JHEP 03 (2014) 108, Addendum:.

[327] V.M. Abazov, et al., Phys. Rev. Lett. 116 (8) (2016) 082002, http://dx.doi.org/10.1103/PhysRevLett.116.082002, arXiv:1511.02428.

[328] V. Khachatryan, et al., J. High Energy Phys. 05 (2017) 013, http://dx.doi.org/10.1007/JHEP05(2017)013, arXiv:1610.07095.

[329] E. Chudakov, D. Higinbotham, C. Hyde, S. Furletov, Y. Furletova, D. Nguyen, M. Stratmann, M. Strikman, C. Weiss, R. Yoshida, PoS DIS2016 (2016) 143, http://dx.doi.org/10.22323/1.265.0143, arXiv:1608.08686.

[330] T.-J. Hou, S. Dulat, J. Gao, M. Guzzi, J. Huston, P. Nadolsky, C. Schmidt, J. Winter, K. Xie, C.P. Yuan, J. High Energy Phys. 02 (2018) 059, http://dx.doi.org/10.1007/JHEP02(2018)059, arXiv:1707.00657.

[331] V. Moos, I. Scimemi, A. Vladimirov, P. Zurita, J. High Energy Phys. 05 (2024) 036, http://dx.doi.org/10.1007/JHEP05(2024)036, arXiv:2305.07473.

[332] A. Bacchetta, V. Bertone, C. Bissolotti, G. Bozzi, M. Cerutti, F. Piacenza, M. Radici, A. Signori, J. High Energy Phys. 10 (2022) 127, http://dx.doi.org/10.1007/JHEP10(2022)127, arXiv:2206.07598.

[333] V. Bertone, I. Scimemi, A. Vladimirov, J. High Energy Phys. 06 (2019) 028, http://dx.doi.org/10.1007/JHEP06(2019)028, arXiv:1902.08474.

[334] A. Bacchetta, F. Delcarro, C. Pisano, M. Radici, A. Signori, J. High Energy Phys. 06 (2017) 081, http://dx.doi.org/10.1007/JHEP06(2017)081, http://dx.doi.org/10.1007/JHEP06(2019)051. arXiv:1703.10157;   JHEP 06 (2019) 051, Erratum:.

[335] D. Gutierrez-Reyes, S. Leal-Gomez, I. Scimemi, A. Vladimirov, J. High Energy Phys. 11 (2019) 121, http://dx.doi.org/10.1007/JHEP11(2019)121, arXiv:1907.03780.

[336] J.-P. Lansberg, C. Pisano, F. Scarpa, M. Schlegel, Phys. Lett. B 784 (2018) 217–222, http://dx.doi.org/10.1016/j.physletb.2018.08.004, arXiv:1710.01684; Phys. Lett. B 791 (2019) 420–421, Erratum:.

[337] F. Scarpa, D. Boer, M.G. Echevarria, J.-P. Lansberg, C. Pisano, M. Schlegel, Eur. Phys. J. C 80 (2) (2020) 87, http://dx.doi.org/10.1140/epjc/s10052-020-7619-1, arXiv:1909.05769.

[338] R. Aaij, et al., J. High Energy Phys. 06 (2017) 047, http://dx.doi.org/10.1007/JHEP06(2017)047, arXiv:1612.07451;   JHEP 10 (2017) 068, Erratum:.

[339] J.-P. Lansberg, H.-S. Shao, Phys. Lett. B 751 (2015) 479–486, http://dx.doi.org/10.1016/j.physletb.2015.10.083, arXiv:1410.8822.

[340] W.J. den Dunnen, J. Lansberg, C. Pisano, M. Schlegel, Phys. Rev. Lett. 112 (2014) 212001, http://dx.doi.org/10.1103/PhysRevLett.112.212001, arXiv:1401.7611.

[341] F. Dominguez, C. Marquet, B.-W. Xiao, F. Yuan, Phys. Rev. D 83 (2011) 105005, http://dx.doi.org/10.1103/PhysRevD.83.105005, arXiv:1101.0715.

[342] D. Boer, P.J. Mulders, C. Pisano, J. Zhou, J. High Energy Phys. 08 (2016) 001, http://dx.doi.org/10.1007/JHEP08(2016)001, arXiv:1605.07934.

[343] D. Boer, C. Pisano, Phys. Rev. D 86 (2012) 094007, http://dx.doi.org/10.1103/PhysRevD.86.094007, arXiv:1208.3642.

[344] J.P. Ma, J.X. Wang, S. Zhao, Phys. Rev. D 88 (1) (2013) 014027, http://dx.doi.org/10.1103/PhysRevD.88.014027, arXiv:1211.7144.

[345] R. Kishore, A. Mukherjee, M. Siddiqah, Phys. Rev. D 104 (9) (2021) 094015, http://dx.doi.org/10.1103/PhysRevD.104.094015, arXiv:2103.09070.

[346] R. Kishore, A. Mukherjee, A. Pawar, M. Siddiqah, Phys. Rev. D 106 (3) (2022) 034009, http://dx.doi.org/10.1103/PhysRevD.106.034009, arXiv:2203.13516.

[347] L.D. McLerran, R. Venugopalan, Phys. Rev. D 49 (1994) 2233–2241, http://dx.doi.org/10.1103/PhysRevD.49.2233, arXiv:hep-ph/9309289.

[348] J. Bor, D. Boer, Phys. Rev. D 106 (1) (2022) 014030, http://dx.doi.org/10.1103/PhysRevD.106.014030, arXiv:2204.01527.

[349] Y. Koike, W. Vogelsang, F. Yuan, Phys. Lett. B 659 (2008) 878–884, http://dx.doi.org/10.1016/j.physletb.2007.11.096, arXiv:0711.0636.

[350] A. Efremov, O. Teryaev, Sov. J. Nucl. Phys. 36 (1982) 140.

[351] A. Efremov, O. Teryaev, Sov. J. Nucl. Phys. 39 (1984) 962.

[352] J. w. Qiu, G.F. Sterman, Phys. Rev. Lett. 67 (1991) 2264–2267, http://dx.doi.org/10.1103/PhysRevLett.67.2264.

[353] J. w. Qiu, G.F. Sterman, Nuclear Phys. B 353 (1991) 105–136, http://dx.doi.org/10.1016/0550-3213(91)90503-P.

[354] J.-W. Qiu, G.F. Sterman, AIP Conf. Proc. 223 (1991) 249–254, http://dx.doi.org/10.1063/1.40488.

[355] L. Gamberg, Z.-B. Kang, A. Metz, D. Pitonyak, A. Prokudin, Phys. Rev. D 90 (7) (2014) 074012, http://dx.doi.org/10.1103/PhysRevD.90.074012, arXiv:1407.5078.

[356] L. Chen, H. Xing, S. Yoshida, Phys. Rev. D 108 (5) (2023) 054021, http://dx.doi.org/10.1103/PhysRevD.108.054021, arXiv:2306.12647.

[357] D.W. Sivers, Phys. Rev. D 41 (1990) 83, http://dx.doi.org/10.1103/PhysRevD.41.83.

[358] R. Kishore, A. Mukherjee, S. Rajesh, Phys. Rev. D 101 (5) (2020) 054003, http://dx.doi.org/10.1103/PhysRevD.101.054003, arXiv:1908.03698.

[359] D. Chakrabarti, R. Kishore, A. Mukherjee, S. Rajesh, Phys. Rev. D 107 (1) (2023) 014008, http://dx.doi.org/10.1103/PhysRevD.107.014008, arXiv:2211.08709.

[360] U. D'Alesio, F. Murgia, Prog. Part. Nucl. Phys. 61 (2008) 394–454, http://dx.doi.org/10.1016/j.ppnp.2008.01.001, arXiv:0712.4328.

[361] L. Gamberg, Z.-B. Kang, Phys. Lett. B 696 (2011) 109–118, http://dx.doi.org/10.1016/j.physletb.2010.11.066, arXiv:1009.1936.

[362] U. D'Alesio, F. Murgia, C. Pisano, P. Taels, Phys. Rev. D 96 (3) (2017) 036011, http://dx.doi.org/10.1103/PhysRevD.96.036011, arXiv:1705.04169.

[363] J.C. Collins, Phys. Lett. B 536 (2002) 43–48, http://dx.doi.org/10.1016/S0370-2693(02)01819-1, arXiv:hep-ph/0204004.

[364] S.J. Brodsky, D.S. Hwang, I. Schmidt, Phys. Lett. B 530 (2002) 99–107, http://dx.doi.org/10.1016/S0370-2693(02)01320-5, arXiv:hep-ph/0201296.

[365] M. Buffing, A. Mukherjee, P. Mulders, Phys. Rev. D 88 (2013) 054027, http://dx.doi.org/10.1103/PhysRevD.88.054027, arXiv:1306.5897.

[366] D. Boer, C. Lorcé, C. Pisano, J. Zhou, Adv. High Energy Phys. 2015 (2015) 371396, http://dx.doi.org/10.1155/2015/371396, arXiv:1504.04332.

[367] U. D'Alesio, C. Flore, F. Murgia, Phys. Rev. D 95 (9) (2017) 094002, http://dx.doi.org/10.1103/PhysRevD.95.094002, arXiv:1701.01148.

[368] U. D'Alesio, C. Flore, F. Murgia, C. Pisano, P. Taels, Phys. Rev. D 99 (3) (2019) 036013, http://dx.doi.org/10.1103/PhysRevD.99.036013, arXiv:1811.02970.

[369] M. Boglione, U. D'Alesio, C. Flore, J.O. Gonzalez-Hernandez, F. Murgia, A. Prokudin, Phys. Lett. B 815 (2021) 136135, http://dx.doi.org/10.1016/j.physletb.2021.136135, arXiv:2101.03955.

[370] M. Boglione, U. D'Alesio, C. Flore, J.O. Gonzalez-Hernandez, F. Murgia, A. Prokudin, Phys. Lett. B 854 (2024) 138712, http://dx.doi.org/10.1016/j.physletb.2024.138712, arXiv:2402.12322.

[371] S. Rajesh, R. Kishore, A. Mukherjee, Phys. Rev. D 98 (1) (2018) 014007, http://dx.doi.org/10.1103/PhysRevD.98.014007, arXiv:1802.10359.

[372] U. D'Alesio, L. Maxia, F. Murgia, C. Pisano, S. Rajesh, Phys. Rev. D 102 (9) (2020) 094011, http://dx.doi.org/10.1103/PhysRevD.102.094011, arXiv:2007.03353.

[373] U. D'Alesio, A. Mukherjee, F. Murgia, C. Pisano, S. Rajesh, JPS Conf. Proc. 37 (2022) 020127, http://dx.doi.org/10.7566/JPSCP.37.020127, arXiv:2203.03299.

[374] S. Frixione, M.L. Mangano, P. Nason, G. Ridolfi, Phys. Lett. B 319 (1993) 339–345, http://dx.doi.org/10.1016/0370-2693(93)90823-Z, arXiv:hep-ph/9310350.

[375] F. Yuan, Phys. Rev. D 78 (2008) 014024, http://dx.doi.org/10.1103/PhysRevD.78.014024, arXiv:0801.4357.

[376] U. D'Alesio, F. Murgia, C. Pisano, J. High Energy Phys. 09 (2015) 119, http://dx.doi.org/10.1007/JHEP09(2015)119, arXiv:1506.03078.

[377] D. Boer, W. Vogelsang, Phys. Rev. D 69 (2004) 094025, http://dx.doi.org/10.1103/PhysRevD.69.094025, arXiv:hep-ph/0312320.

[378] M. Anselmino, M. Boglione, U. D'Alesio, F. Murgia, A. Prokudin, J. High Energy Phys. 04 (2017) 046, http://dx.doi.org/10.1007/JHEP04(2017)046, arXiv:1612.06413.

[379] A.D. Martin, W.J. Stirling, R.S. Thorne, G. Watt, Eur. Phys. J. C 63 (2009) 189–285, http://dx.doi.org/10.1140/epjc/s10052-009-1072-5, arXiv:0901.0002.

[380] T. Sjostrand, S. Ask, J.R. Christiansen, R. Corke, N. Desai, P. Ilten, S. Mrenna, S. Prestel, C.O. Rasmussen, P.Z. Skands, Comput. Phys. Comm. 191 (2015) 159–177, http://dx.doi.org/10.1016/j.cpc.2015.01.024, arXiv:1410.3012.

[381] D. Kikola, M.G. Echevarria, C. Hadjidakis, J.-P. Lansberg, C. Lorcé, L. Massacrier, C.M. Quintans, A. Signori, B. Trzeciak, Few Body Syst. 58 (4) (2017) 139, http://dx.doi.org/10.1007/s00601-017-1299-x, arXiv:1702.01546.

[382] C. Aidala, et al., Phys. Rev. D 98 (1) (2018) 012006, http://dx.doi.org/10.1103/PhysRevD.98.012006, arXiv:1805.01491.

[383] S. Rajesh, U. D'Alesio, A. Mukherjee, F. Murgia, C. Pisano, SciPost Phys. Proc. 8 (2022) 017, http://dx.doi.org/10.21468/SciPostPhysProc.8.017, arXiv:2108.04866.

[384] J.C. Collins, A. Freund, Phys. Rev. D 59 (1999) 074009, http://dx.doi.org/10.1103/PhysRevD.59.074009, arXiv:hep-ph/9801262.

[385] X.-D. Ji, J. Osborne, Phys. Rev. D 58 (1998) 094018, http://dx.doi.org/10.1103/PhysRevD.58.094018, arXiv:hep-ph/9801260.

[386] M.V. Polyakov, P. Schweitzer, Internat. J. Modern Phys. A 33 (26) (2018) 1830025, http://dx.doi.org/10.1142/S0217751X18300259, arXiv:1805.06596.

[387] C. Lorcé, H. Moutarde, A.P. Trawiński, Eur. Phys. J. C 79 (1) (2019) 89, http://dx.doi.org/10.1140/epjc/s10052-019-6572-3, arXiv:1810.09837.

[388] X.-D. Ji, Phys. Rev. Lett. 78 (1997) 610–613, http://dx.doi.org/10.1103/PhysRevLett.78.610, arXiv:hep-ph/9603249.

[389] K. Kumericki, S. Liuti, H. Moutarde, Eur. Phys. J. A 52 (6) (2016) 157, http://dx.doi.org/10.1140/epja/i2016-16157-3, arXiv:1602.02763.

[390] S. Joosten, 2021. URL https://eicweb.phy.anl.gov/monte_carlo/lager.

[391] O. Gryniuk, M. Vanderhaeghen, Phys. Rev. D 94 (7) (2016) 074001, http://dx.doi.org/10.1103/PhysRevD.94.074001, arXiv:1608.08205.

[392] M. Deák, A.M. Staśto, M. Strikman, Phys. Rev. D 103 (2021) 014022, http://dx.doi.org/10.1103/PhysRevD.103.014022, URL https://link.aps.org/doi/10.1103/PhysRevD.103.014022.

[393] K.J. Eskola, C.A. Flett, V. Guzey, T. Löytäinen, H. Paukkunen, 29th International Workshop on Deep-Inelastic Scattering and Related Subjects, 2022, arXiv:2208.06806.

[394] K.J. Eskola, C.A. Flett, V. Guzey, T. Löytäinen, H. Paukkunen, Acta Phys. Pol. Su 16 (1) (2023) 1–A113, http://dx.doi.org/10.5506/APhysPolBSupp.16.1-A113, arXiv:2209.08327.

[395] K.J. Eskola, V. Guzey, T. Löytäinen, H. Paukkunen, C.A. Flett, Acta Phys. Pol. Su 16 (7) (2023) 7–A9, http://dx.doi.org/10.5506/APhysPolBSupp.16.7-A9, arXiv:2303.12630.

[396] K.J. Eskola, C.A. Flett, V. Guzey, T. Löytäinen, H. Paukkunen, PoS HardProbes 2023 (2024) 107, http://dx.doi.org/10.22323/1.438.0107, arXiv:2308.06984.

[397] K.J. Eskola, C.A. Flett, V. Guzey, T. Löytäinen, H. Paukkunen, Eur. Phys. J. C 83 (8) (2023) 758, http://dx.doi.org/10.1140/epjc/s10052-023-11927-8, arXiv:2303.03007.

[398] C.A. Flett, J.P. Lansberg, S. Nabeebaccus, M. Nefedov, P. Sznajder, J. Wagner, Phys. Lett. B 859 (2024) 139117, http://dx.doi.org/10.1016/j.physletb.2024.139117, arXiv:2409.05738.

[399] S. Meissner, A. Metz, M. Schlegel, K. Goeke, J. High Energy Phys. 08 (2008) 038, http://dx.doi.org/10.1088/1126-6708/2008/08/038, arXiv:0805.3165.

[400] S. Meissner, A. Metz, M. Schlegel, J. High Energy Phys. 08 (2009) 056, http://dx.doi.org/10.1088/1126-6708/2009/08/056, arXiv:0906.5323.

[401] C. Lorcé, B. Pasquini, J. High Energy Phys. 09 (2013) 138, http://dx.doi.org/10.1007/JHEP09(2013)138, arXiv:1307.4497.

[402] M.G. Echevarria, A. Idilbi, K. Kanazawa, C. Lorcé, A. Metz, B. Pasquini, M. Schlegel, Phys. Lett. B 759 (2016) 336–341, http://dx.doi.org/10.1016/j.physletb.2016.05.086, arXiv:1602.06953.

[403] A.V. Belitsky, X. d. Ji, F. Yuan, Phys. Rev. D 69 (2004) 074014, http://dx.doi.org/10.1103/PhysRevD.69.074014, arXiv:hep-ph/0307383.

[404] C. Lorcé, B. Pasquini, M. Vanderhaeghen, J. High Energy Phys. 05 (2011) 041, http://dx.doi.org/10.1007/JHEP05(2011)041, arXiv:1102.4704.

[405] C. Lorcé, B. Pasquini, Phys. Rev. D 84 (2011) 014015, http://dx.doi.org/10.1103/PhysRevD.84.014015, arXiv:1106.0139.

[406] C. Lorcé, B. Pasquini, X. Xiong, F. Yuan, Phys. Rev. D 85 (2012) 114006, http://dx.doi.org/10.1103/PhysRevD.85.114006, arXiv:1111.4827.

[407] Y. Hatta, Phys. Lett. B 708 (2012) 186–190, http://dx.doi.org/10.1016/j.physletb.2012.01.024, arXiv:1111.3547.

[408] C. Lorcé, Phys. Lett. B 735 (2014) 344–348, http://dx.doi.org/10.1016/j.physletb.2014.06.068, arXiv:1401.7784.

[409] C. Lorcé, B. Pasquini, Phys. Rev. D 93 (3) (2016) 034040, http://dx.doi.org/10.1103/PhysRevD.93.034040, arXiv:1512.06744.

[410] C. Lorcé, Phys. Rev. D 87 (3) (2013) 034031, http://dx.doi.org/10.1103/PhysRevD.87.034031, arXiv:1205.6483.

[411] C. Lorcé, Phys. Lett. B 719 (2013) 185–190, http://dx.doi.org/10.1016/j.physletb.2013.01.007, arXiv:1210.2581.

[412] X. Ji, X. Xiong, F. Yuan, Phys. Rev. Lett. 109 (2012) 152005, http://dx.doi.org/10.1103/PhysRevLett.109.152005, arXiv:1202.2843.

[413] E. Leader, C. Lorcé, Phys. Rep. 541 (3) (2014) 163–248, http://dx.doi.org/10.1016/j.physrep.2014.02.010, arXiv:1309.4235.

[414] K. Kanazawa, C. Lorcé, A. Metz, B. Pasquini, M. Schlegel, Phys. Rev. D 90 (1) (2014) 014028, http://dx.doi.org/10.1103/PhysRevD.90.014028, arXiv:1403.5226.

[415] K.-F. Liu, C. Lorcé, Eur. Phys. J. A 52 (6) (2016) 160, http://dx.doi.org/10.1140/epja/i2016-16160-8, arXiv:1508.00911.

[416] M. Engelhardt, Phys. Rev. D 95 (9) (2017) 094505, http://dx.doi.org/10.1103/PhysRevD.95.094505, arXiv:1701.01536.

[417] M. Engelhardt, J.R. Green, N. Hasan, S. Krieg, S. Meinel, J. Negele, A. Pochinsky, S. Syritsyn, Phys. Rev. D 102 (7) (2020) 074505, http://dx.doi.org/10.1103/PhysRevD.102.074505, arXiv:2008.03660.

[418] R. Boussarie, Y. Hatta, L. Szymanowski, S. Wallon, Phys. Rev. Lett. 124 (17) (2020) 172501, http://dx.doi.org/10.1103/PhysRevLett.124.172501, arXiv:1912.08182.

[419] Y. Hatta, B.-W. Xiao, F. Yuan, Phys. Rev. Lett. 116 (20) (2016) 202301, http://dx.doi.org/10.1103/PhysRevLett.116.202301, arXiv:1601.01585.

[420] J. Zhou, Phys. Rev. D 94 (11) (2016) 114017, http://dx.doi.org/10.1103/PhysRevD.94.114017, arXiv:1611.02397.

[421] Y. Hagiwara, Y. Hatta, B.-W. Xiao, F. Yuan, Phys. Lett. B 771 (2017) 374–378, http://dx.doi.org/10.1016/j.physletb.2017.05.083, arXiv:1701.04254.

[422] E. Iancu, A.H. Rezaeian, Phys. Rev. D 95 (9) (2017) 094003, http://dx.doi.org/10.1103/PhysRevD.95.094003, arXiv:1702.03943.

[423] Y. Hatta, Y. Nakagawa, F. Yuan, Y. Zhao, B. Xiao, Phys. Rev. D 95 (11) (2017) 114032, http://dx.doi.org/10.1103/PhysRevD.95.114032, arXiv:1612.02445.

[424] X. Ji, F. Yuan, Y. Zhao, Phys. Rev. Lett. 118 (19) (2017) 192004, http://dx.doi.org/10.1103/PhysRevLett.118.192004, arXiv:1612.02438.

[425] Y. Hagiwara, Y. Hatta, R. Pasechnik, M. Tasevsky, O. Teryaev, Phys. Rev. D 96 (3) (2017) 034009, http://dx.doi.org/10.1103/PhysRevD.96.034009, arXiv:1706.01765.

[426] S. Bhattacharya, A. Metz, J. Zhou, Phys. Lett. B 771 (2017) 396–400, http://dx.doi.org/10.1016/j.physletb.2017.05.081, arXiv:1702.04387; Phys.Lett.B 810 (2020) 135866, Erratum:.

[427] S. Bhattacharya, R. Boussarie, Y. Hatta, Phys. Rev. Lett. 128 (18) (2022) 182002, http://dx.doi.org/10.1103/PhysRevLett.128.182002, arXiv:2201.08709.

[428] M.G. Echevarria, P.A. Gutierrez Garcia, I. Scimemi, Phys. Lett. B 840 (2023) 137881, http://dx.doi.org/10.1016/j.physletb.2023.137881, arXiv:2208.00021.

[429] H. Mäntysaari, K. Roy, F. Salazar, B. Schenke, Phys. Rev. D 103 (9) (2021) 094026, http://dx.doi.org/10.1103/PhysRevD.103.094026, arXiv:2011.02464.

[430] S. Bhattacharya, A. Metz, V.K. Ojha, J.-Y. Tsai, J. Zhou, Phys. Lett. B 833 (2022) 137383, http://dx.doi.org/10.1016/j.physletb.2022.137383, arXiv:1802.10550.

[431] R. Boussarie, Y. Hatta, B.-W. Xiao, F. Yuan, Phys. Rev. D 98 (7) (2018) 074015, http://dx.doi.org/10.1103/PhysRevD.98.074015, arXiv:1807.08697.

[432] D. Boer, C. Setyadi, Phys. Rev. D 104 (7) (2021) 074006, http://dx.doi.org/10.1103/PhysRevD.104.074006, arXiv:2106.15148.

[433] H. Kowalski, L. Motyka, G. Watt, Phys. Rev. D 74 (2006) 074016, http://dx.doi.org/10.1103/PhysRevD.74.074016, arXiv:hep-ph/0606272.

[434] M.A. Shifman, A.I. Vainshtein, V.I. Zakharov, Phys. Lett. B 78 (1978) 443–446, http://dx.doi.org/10.1016/0370-2693(78)90481-1.

[435] J.F. Donoghue, Physics with Light Mesons, 1987.

[436] J.C. Collins, A. Duncan, S.D. Joglekar, Phys. Rev. D 16 (1977) 438–449, http://dx.doi.org/10.1103/PhysRevD.16.438.

[437] N.K. Nielsen, Nuclear Phys. B 120 (1977) 212–220, http://dx.doi.org/10.1016/0550-3213(77)90040-2.

[438] Y. Hatta, A. Rajan, K. Tanaka, J. High Energy Phys. 12 (2018) 008, http://dx.doi.org/10.1007/JHEP12(2018)008, arXiv:1810.05116.

[439] K. Tanaka, J. High Energy Phys. 01 (2019) 120, http://dx.doi.org/10.1007/JHEP01(2019)120, arXiv:1811.07879.

[440] X.-D. Ji, Phys. Rev. Lett. 74 (1995) 1071–1074, http://dx.doi.org/10.1103/PhysRevLett.74.1071, arXiv:hep-ph/9410274.

[441] X.-D. Ji, Phys. Rev. D 52 (1995) 271–281, http://dx.doi.org/10.1103/PhysRevD.52.271, arXiv:hep-ph/9502213.

[442] C. Lorcé, Eur. Phys. J. C 78 (2) (2018) 120, http://dx.doi.org/10.1140/epjc/s10052-018-5561-2, arXiv:1706.05853.

[443] S. Rodini, A. Metz, B. Pasquini, J. High Energy Phys. 09 (2020) 067, http://dx.doi.org/10.1007/JHEP09(2020)067, arXiv:2004.03704.

[444] A. Metz, B. Pasquini, S. Rodini, Phys. Rev. D 102 (2020) 114042, http://dx.doi.org/10.1103/PhysRevD.102.114042, arXiv:2006.11171.

[445] X. Ji, Y. Liu, Sci. China Phys. Mech. Astron. 64 (8) (2021) 281012, http://dx.doi.org/10.1007/s11433-021-1723-2, arXiv:2101.04483.

[446] X. Ji, Y. Liu, A. Schäfer, Nuclear Phys. B 971 (2021) 115537, http://dx.doi.org/10.1016/j.nuclphysb.2021.115537, arXiv:2105.03974.

[447] C. Lorcé, A. Metz, B. Pasquini, S. Rodini, J. High Energy Phys. 11 (2021) 121, http://dx.doi.org/10.1007/JHEP11(2021)121, arXiv:2109.11785.

[448] R. Gupta, S. Park, M. Hoferichter, E. Mereghetti, B. Yoon, T. Bhattacharya, Phys. Rev. Lett. 127 (24) (2021) 242002, http://dx.doi.org/10.1103/PhysRevLett.127.242002, arXiv:2105.12095.

[449] P.M. Copeland, C.-R. Ji, W. Melnitchouk, Phys. Rev. D 107 (9) (2023) 094041, http://dx.doi.org/10.1103/PhysRevD.107.094041, arXiv:2112.03198.

[450] S. Joosten, Z.E. Meziani, PoS QCDEV 2017 (2018) 017, http://dx.doi.org/10.22323/1.308.0017, arXiv:1802.02616.

[451] A. Freese, G.A. Miller, Phys. Rev. D 103 (2021) 094023, http://dx.doi.org/10.1103/PhysRevD.103.094023, arXiv:2102.01683.

[452] A. Ali, et al., Phys. Rev. Lett. 123 (7) (2019) 072001, http://dx.doi.org/10.1103/PhysRevLett.123.072001, arXiv:1905.10811.

[453] B. Duran, et al., Nature 615 (7954) (2023) 813–816, http://dx.doi.org/10.1038/s41586-023-05730-4, arXiv:2207.05212.

[454] Y. Hatta, D.-L. Yang, Phys. Rev. D 98 (7) (2018) 074003, http://dx.doi.org/10.1103/PhysRevD.98.074003, arXiv:1808.02163.

[455] Y. Hatta, A. Rajan, D.-L. Yang, Phys. Rev. D 100 (1) (2019) 014032, http://dx.doi.org/10.1103/PhysRevD.100.014032, arXiv:1906.00894.

[456] K.A. Mamo, I. Zahed, Phys. Rev. D 101 (8) (2020) 086003, http://dx.doi.org/10.1103/PhysRevD.101.086003, arXiv:1910.04707.

[457] R. Wang, J. Evslin, X. Chen, Eur. Phys. J. C 80 (6) (2020) 507, http://dx.doi.org/10.1140/epjc/s10052-020-8057-9, arXiv:1912.12040.

[458] R. Boussarie, Y. Hatta, Phys. Rev. D 101 (11) (2020) 114004, http://dx.doi.org/10.1103/PhysRevD.101.114004, arXiv:2004.12715.

[459] F. Zeng, X.-Y. Wang, L. Zhang, Y.-P. Xie, R. Wang, X. Chen, Eur. Phys. J. C 80 (11) (2020) 1027, http://dx.doi.org/10.1140/epjc/s10052-020-08584-6, arXiv:2008.13439.

[460] O. Gryniuk, S. Joosten, Z.-E. Meziani, M. Vanderhaeghen, Phys. Rev. D 102 (1) (2020) 014016, http://dx.doi.org/10.1103/PhysRevD.102.014016, arXiv:2005.09293.

[461] L. Pentchev, I.I. Strakovsky, Eur. Phys. J. A 57 (2) (2021) 56, http://dx.doi.org/10.1140/epja/s10050-021-00364-4, arXiv:2009.04502.

[462] M.-L. Du, V. Baru, F.-K. Guo, C. Hanhart, U.-G. Meißner, A. Nefediev, I. Strakovsky, Eur. Phys. J. C 80 (11) (2020) 1053, http://dx.doi.org/10.1140/epjc/s10052-020-08620-5, arXiv:2009.08345.

[463] D.E. Kharzeev, Phys. Rev. D 104 (5) (2021) 054015, http://dx.doi.org/10.1103/PhysRevD.104.054015, arXiv:2102.00110.

[464] R. Wang, W. Kou, Y.-P. Xie, X. Chen, Phys. Rev. D 103 (9) (2021) L091501, http://dx.doi.org/10.1103/PhysRevD.103.L091501, arXiv:2102.01610.

[465] X. Ji, Front. Phys. (Beijing) 16 (6) (2021) 64601, http://dx.doi.org/10.1007/s11467-021-1065-x, arXiv:2102.07830.

[466] Y. Hatta, M. Strikman, Phys. Lett. B 817 (2021) 136295, http://dx.doi.org/10.1016/j.physletb.2021.136295, arXiv:2102.12631.

[467] K.A. Mamo, I. Zahed, Phys. Rev. D 103 (9) (2021) 094010, http://dx.doi.org/10.1103/PhysRevD.103.094010, arXiv:2103.03186.

[468] Y. Guo, X. Ji, Y. Liu, Phys. Rev. D 103 (9) (2021) 096010, http://dx.doi.org/10.1103/PhysRevD.103.096010, arXiv:2103.11506.

[469] P. Sun, X.-B. Tong, F. Yuan, Phys. Lett. B 822 (2021) 136655, http://dx.doi.org/10.1016/j.physletb.2021.136655, arXiv:2103.12047.

[470] Y.-P. Xie, V.P. Goncalves, Eur. Phys. J. C 81 (7) (2021) 645, http://dx.doi.org/10.1140/epjc/s10052-021-09453-6, arXiv:2103.12568.

[471] K.A. Mamo, I. Zahed, Phys. Rev. D 104 (6) (2021) 066023, http://dx.doi.org/10.1103/PhysRevD.104.066023, arXiv:2106.00722.

[472] R. Wang, W. Kou, C. Han, J. Evslin, X. Chen, Phys. Rev. D 104 (7) (2021) 074033, http://dx.doi.org/10.1103/PhysRevD.104.074033, arXiv:2108.03550.
[473] P. Sun, X.-B. Tong, F. Yuan, Phys. Rev. D 105 (5) (2022) 054032, http://dx.doi.org/10.1103/PhysRevD.105.054032, arXiv:2111.07034.
[474] C. Han, G. Xie, W. Kou, R. Wang, X. Chen, Eur. Phys. J. A 58 (6) (2022) 105, http://dx.doi.org/10.1140/epja/s10050-022-00756-0, arXiv:2201.08535.
[475] J.M. Butterworth, J.R. Forshaw, M.H. Seymour, Z. Phys. C 72 (1996) 637–646, http://dx.doi.org/10.1007/s002880050286, arXiv:hep-ph/9601371.
[476] F.A. Ceccopieri, M. Rinaldi, Phys. Rev. D 105 (1) (2022) L011501, http://dx.doi.org/10.1103/PhysRevD.105.L011501, arXiv:2103.13480.
[477] M. Klasen, Rev. Modern Phys. 74 (2002) 1221–1282, http://dx.doi.org/10.1103/RevModPhys.74.1221, arXiv:hep-ph/0206169.
[478] C. Goebel, F. Halzen, D.M. Scott, Phys. Rev. D 22 (1980) 2789, http://dx.doi.org/10.1103/PhysRevD.22.2789.
[479] B. Humpert, Phys. Lett. B 131 (1983) 461–467, http://dx.doi.org/10.1016/0370-2693(83)90540-3.
[480] M. Mekhfi, Phys. Rev. D 32 (1985) 2371, http://dx.doi.org/10.1103/PhysRevD.32.2371.
[481] M. Mekhfi, Phys. Rev. D 32 (1985) 2380, http://dx.doi.org/10.1103/PhysRevD.32.2380.
[482] B. Humpert, R. Odorico, Phys. Lett. B 154 (1985) 211, http://dx.doi.org/10.1016/0370-2693(85)90587-8.
[483] M.L. Mangano, Z. Phys. C 42 (1989) 331, http://dx.doi.org/10.1007/BF01555875.
[484] N. Paver, D. Treleani, Nuovo Cimento A 70 (1982) 215, http://dx.doi.org/10.1007/BF02814035.
[485] T. Sjostrand, M. van Zijl, Phys. Lett. B 188 (1987) 149–154, http://dx.doi.org/10.1016/0370-2693(87)90722-2.
[486] J.R. Gaunt, J. High Energy Phys. 07 (2014) 110, http://dx.doi.org/10.1007/JHEP07(2014)110, arXiv:1405.2080.
[487] M. Diehl, J.R. Gaunt, P. Plößl, A. Schäfer, SciPost Phys. 7 (2) (2019) 017, http://dx.doi.org/10.21468/SciPostPhys.7.2.017, arXiv:1902.08019.
[488] M. Diehl, R. Nagar, J. High Energy Phys. 04 (2019) 124, http://dx.doi.org/10.1007/JHEP04(2019)124, arXiv:1812.09509.
[489] ATLAS Collaboration, J. High Energy Phys. 11 (2016) 110, http://dx.doi.org/10.1007/JHEP11(2016)110, arXiv:1608.01857.
[490] CMS, 2021.
[491] J.-P. Lansberg, H.-S. Shao, Nuclear Phys. B 900 (2015) 273–294, http://dx.doi.org/10.1016/j.nuclphysb.2015.09.005, arXiv:1504.06531.
[492] S. Chekanov, et al., Nuclear Phys. B 792 (2008) 1–47, http://dx.doi.org/10.1016/j.nuclphysb.2007.08.021, arXiv:0707.3749.
[493] M. Gluck, E. Reya, A. Vogt, Phys. Rev. D 46 (1992) 1973–1979, http://dx.doi.org/10.1103/PhysRevD.46.1973.
[494] M. Gluck, E. Reya, M. Stratmann, Phys. Rev. D 51 (1995) 3220–3229, http://dx.doi.org/10.1103/PhysRevD.51.3220.
[495] H.-S. Shao, Comput. Phys. Comm. 184 (2013) 2562–2570, http://dx.doi.org/10.1016/j.cpc.2013.05.023, arXiv:1212.5293.
[496] H.-S. Shao, Comput. Phys. Comm. 198 (2016) 238–259, http://dx.doi.org/10.1016/j.cpc.2015.09.011, arXiv:1507.03435.
[497] M. Rinaldi, F.A. Ceccopieri, Phys. Rev. D 97 (7) (2018) 071501, http://dx.doi.org/10.1103/PhysRevD.97.071501, arXiv:1801.04760.
[498] M. Rinaldi, S. Scopetta, M.C. Traini, V. Vento, J. High Energy Phys. 10 (2016) 063, http://dx.doi.org/10.1007/JHEP10(2016)063, arXiv:1608.02521.
[499] M. Rinaldi, S. Scopetta, M. Traini, V. Vento, J. High Energy Phys. 12 (2014) 028, http://dx.doi.org/10.1007/JHEP12(2014)028, arXiv:1409.1500.
[500] M. Diehl, A. Schafer, Phys. Lett. B 698 (2011) 389–402, http://dx.doi.org/10.1016/j.physletb.2011.03.024, arXiv:1102.3081.
[501] A.V. Manohar, W.J. Waalewijn, Phys. Rev. D 85 (2012) 114009, http://dx.doi.org/10.1103/PhysRevD.85.114009, arXiv:1202.3794.
[502] M. Rinaldi, S. Scopetta, M. Traini, V. Vento, Phys. Lett. B 752 (2016) 40–45, http://dx.doi.org/10.1016/j.physletb.2015.11.031, arXiv:1506.05742.
[503] G. Aad, et al., J. High Energy Phys. 04 (2014) 172, http://dx.doi.org/10.1007/JHEP04(2014)172, arXiv:1401.2831.
[504] G. Aad, et al., Eur. Phys. J. C 75 (5) (2015) 229, http://dx.doi.org/10.1140/epjc/s10052-015-3406-9, arXiv:1412.6428.
[505] R. Aaij, et al., J. High Energy Phys. 06 (2012) 141, http://dx.doi.org/10.1007/JHEP06(2012)141, arXiv:1205.0975;   JHEP 03 (2014) 108, Addendum:.
[506] V.M. Abazov, et al., Phys. Rev. D 90 (11) (2014) 111101, http://dx.doi.org/10.1103/PhysRevD.90.111101, arXiv:1406.2380.
[507] J.J. Aubert, et al., Phys. Lett. B 123 (1983) 275–278, http://dx.doi.org/10.1016/0370-2693(83)90437-9.
[508] K.J. Eskola, P. Paakkinen, H. Paukkunen, C.A. Salgado, Eur. Phys. J. C 77 (3) (2017) 163, http://dx.doi.org/10.1140/epjc/s10052-017-4725-9, arXiv:1612.05741.
[509] K. Kovarik, et al., Phys. Rev. D 93 (8) (2016) 085037, http://dx.doi.org/10.1103/PhysRevD.93.085037, arXiv:1509.00792.
[510] K.J. Eskola, P. Paakkinen, H. Paukkunen, C.A. Salgado, Eur. Phys. J. C 82 (5) (2022) 413, http://dx.doi.org/10.1140/epjc/s10052-022-10359-0, arXiv:2112.12462.
[511] A. Accardi, et al., Eur. Phys. J. A 52 (9) (2016) 268, http://dx.doi.org/10.1140/epja/i2016-16268-9, arXiv:1212.1701.
[512] H. Mäntysaari, Rep. Progr. Phys. 83 (8) (2020) 082201, http://dx.doi.org/10.1088/1361-6633/aba347, arXiv:2001.10705.
[513] T. Toll, T. Ullrich, Phys. Rev. C 87 (2) (2013) 024913, http://dx.doi.org/10.1103/PhysRevC.87.024913, arXiv:1211.3048.
[514] H. Mäntysaari, P. Zurita, Phys. Rev. D 98 (2018) 036002, http://dx.doi.org/10.1103/PhysRevD.98.036002, arXiv:1804.05311.
[515] T. Toll, T. Ullrich, Comput. Phys. Comm. 185 (2014) 1835–1853, http://dx.doi.org/10.1016/j.cpc.2014.03.010, arXiv:1307.8059.
[516] C. Alexa, et al., Eur. Phys. J. C 73 (6) (2013) 2466, http://dx.doi.org/10.1140/epjc/s10052-013-2466-y, arXiv:1304.5162.
[517] A. Aktas, et al., Phys. Lett. B 568 (2003) 205–218, http://dx.doi.org/10.1016/j.physletb.2003.06.056, arXiv:hep-ex/0306013.
[518] H. Abramowicz, et al., J. High Energy Phys. 02 (2013) 071, http://dx.doi.org/10.1007/JHEP02(2013)071, arXiv:1211.6946.
[519] S. Chekanov, et al., J. High Energy Phys. 05 (2010) 085, http://dx.doi.org/10.1007/JHEP05(2010)085, arXiv:0910.1235.
[520] T. Aaltonen, et al., Phys. Rev. Lett. 102 (2009) 242001, http://dx.doi.org/10.1103/PhysRevLett.102.242001, arXiv:0902.1271.
[521] R. Aaij, et al., J. Phys. G 40 (2013) 045001, http://dx.doi.org/10.1088/0954-3899/40/4/045001, arXiv:1301.7084.
[522] B.B. Abelev, et al., Phys. Rev. Lett. 113 (23) (2014) 232504, http://dx.doi.org/10.1103/PhysRevLett.113.232504, arXiv:1406.7819.
[523] B. Abelev, et al., Phys. Lett. B 718 (2013) 1273–1283, http://dx.doi.org/10.1016/j.physletb.2012.11.059, arXiv:1209.3715.
[524] S. Acharya, et al., Eur. Phys. J. C 81 (8) (2021) 712, http://dx.doi.org/10.1140/epjc/s10052-021-09437-6, arXiv:2101.04577.
[525] V. Khachatryan, et al., Phys. Lett. B 772 (2017) 489–511, http://dx.doi.org/10.1016/j.physletb.2017.07.001, arXiv:1605.06966.
[526] R. Aaij, et al., Phys. Rev. C 105 (3) (2022) L032201, http://dx.doi.org/10.1103/PhysRevC.105.L032201, arXiv:2108.02681.
[527] M. Abdallah, et al., Phys. Rev. Lett. 128 (12) (2022) 122303, http://dx.doi.org/10.1103/PhysRevLett.128.122303, arXiv:2109.07625.
[528] S. Afanasiev, et al., Phys. Lett. B 679 (2009) 321–329, http://dx.doi.org/10.1016/j.physletb.2009.07.061, arXiv:0903.2041.
[529] K. Tu, 2023.
[530] W. Chang, E.-C. Aschenauer, M.D. Baker, A. Jentsch, J.-H. Lee, Z. Tu, Z. Yin, L. Zheng, Phys. Rev. D 104 (11) (2021) 114030, http://dx.doi.org/10.1103/PhysRevD.104.114030, arXiv:2108.01694.
[531] M. Burkardt, Internat. J. Modern Phys. A 18 (2003) 173–208, http://dx.doi.org/10.1142/S0217751X03012370, arXiv:hep-ph/0207047.
[532] E. Aschenauer, et al., BeAGLE - Benchmark eA Generator for Leptoproduction, https://eic.github.io/software/beagle.html.
[533] L.L. Frankfurt, M.I. Strikman, D.B. Day, M. Sargsian, Phys. Rev. C 48 (1993) 2451–2461, http://dx.doi.org/10.1103/PhysRevC.48.2451.
[534] E.O. Cohen, et al., Phys. Rev. Lett. 121 (9) (2018) 092501, http://dx.doi.org/10.1103/PhysRevLett.121.092501, arXiv:1805.01981.
[535] B. Schmookler, et al., Nature 566 (7744) (2019) 354–358, http://dx.doi.org/10.1038/s41586-019-0925-9, arXiv:2004.12065.
[536] J. Rittenhouse West, Nucl. Phys. A 1029 (2023) 122563, http://dx.doi.org/10.1016/j.nuclphysa.2022.122563, arXiv:2009.06968.
[537] J. Rittenhouse West, S.J. Brodsky, G.F. de Teramond, A.S. Goldhaber, I. Schmidt, Nucl. Phys. A 1007 (2021) 122134, http://dx.doi.org/10.1016/j.nuclphysa.2020.122134, arXiv:2004.14659.
[538] H. Mäntysaari, B. Schenke, Phys. Rev. C 101 (1) (2020) 015203, http://dx.doi.org/10.1103/PhysRevC.101.015203, arXiv:1910.03297.
[539] Z. Tu, A. Jentsch, M. Baker, L. Zheng, J.-H. Lee, R. Venugopalan, O. Hen, D. Higinbotham, E.-C. Aschenauer, T. Ullrich, Phys. Lett. B 811 (2020) 135877, http://dx.doi.org/10.1016/j.physletb.2020.135877, arXiv:2005.14706.
[540] J. Altmann, et al., Eur. Phys. J. C 84 (4) (2024) 421, http://dx.doi.org/10.1140/epjc/s10052-024-12650-8, arXiv:2401.09930.

[541] J.W. Cronin, H.J. Frisch, M.J. Shochet, J.P. Boymond, R. Mermod, P.A. Piroue, R.L. Sumner, Phys. Rev. D 11 (1975) 3105–3123, http://dx.doi.org/10.1103/PhysRevD.11.3105.

[542] D. Antreasyan, J.W. Cronin, H.J. Frisch, M.J. Shochet, L. Kluberg, P.A. Piroue, R.L. Sumner, Phys. Rev. D 19 (1979) 764–778, http://dx.doi.org/10.1103/PhysRevD.19.764.

[543] U.A. Acharya, et al., Phys. Rev. C 105 (6) (2022) 064902, http://dx.doi.org/10.1103/PhysRevC.105.064902, arXiv:2111.05756.

[544] A. Airapetian, et al., Nuclear Phys. B 780 (2007) 1–27, http://dx.doi.org/10.1016/j.nuclphysb.2007.06.004, arXiv:0704.3270.

[545] S. Aronson, E. Borras, B. Odegard, R. Sharma, I. Vitev, Phys. Lett. B 778 (2018) 384–391, http://dx.doi.org/10.1016/j.physletb.2018.01.038, arXiv:1709.02372.

[546] J. w. Qiu, I. Vitev, Phys. Rev. Lett. 93 (2004) 262301, http://dx.doi.org/10.1103/PhysRevLett.93.262301, arXiv:hep-ph/0309094.

[547] J.-W. Qiu, I. Vitev, Phys. Lett. B 587 (2004) 52–61, http://dx.doi.org/10.1016/j.physletb.2004.02.065, arXiv:hep-ph/0401062.

[548] J. w. Qiu, I. Vitev, Phys. Lett. B 632 (2006) 507–511, http://dx.doi.org/10.1016/j.physletb.2005.10.073, arXiv:hep-ph/0405068.

[549] R.B. Neufeld, I. Vitev, B.-W. Zhang, Phys. Lett. B 704 (2011) 590–595, http://dx.doi.org/10.1016/j.physletb.2011.09.045, arXiv:1010.3708.

[550] Z.-B. Kang, I. Vitev, H. Xing, Phys. Rev. C 92 (5) (2015) 054911, http://dx.doi.org/10.1103/PhysRevC.92.054911, arXiv:1507.05987.

[551] Z.-B. Kang, I. Vitev, E. Wang, H. Xing, C. Zhang, Phys. Lett. B 740 (2015) 23–29, http://dx.doi.org/10.1016/j.physletb.2014.11.024, arXiv:1409.2494.

[552] Z.-B. Kang, I. Vitev, H. Xing, Phys. Rev. D 85 (2012) 054024, http://dx.doi.org/10.1103/PhysRevD.85.054024, arXiv:1112.6021.

[553] C. Adloff, et al., Eur. Phys. J. C 25 (2002) 25–39, http://dx.doi.org/10.1007/s10052-002-1009-8, arXiv:hep-ex/0205064.

[554] F.D. Aaron, et al., Eur. Phys. J. C 68 (2010) 401–420, http://dx.doi.org/10.1140/epjc/s10052-010-1376-5, arXiv:1002.0234.

[555] S. Chekanov, et al., Eur. Phys. J. C 27 (2003) 173–188, http://dx.doi.org/10.1140/epjc/s2002-01130-2, arXiv:hep-ex/0211011.

[556] F. Abe, et al., Phys. Rev. Lett. 79 (1997) 572–577, http://dx.doi.org/10.1103/PhysRevLett.79.572.

[557] D. Acosta, et al., Phys. Rev. D 71 (2005) 032001, http://dx.doi.org/10.1103/PhysRevD.71.032001, arXiv:hep-ex/0412071.

[558] 2010.

[559] V. Khachatryan, et al., Eur. Phys. J. C 71 (2011) 1575, http://dx.doi.org/10.1140/epjc/s10052-011-1575-8, arXiv:1011.4193.

[560] R. Aaij, et al., Eur. Phys. J. C 71 (2011) 1645, http://dx.doi.org/10.1140/epjc/s10052-011-1645-y, arXiv:1103.0423.

[561] J. Abdallah, et al., Phys. Lett. B 565 (2003) 76–86, http://dx.doi.org/10.1016/S0370-2693(03)00660-9, arXiv:hep-ex/0307049.

[562] P. Pakhlov, et al., Phys. Rev. D 79 (2009) 071101, http://dx.doi.org/10.1103/PhysRevD.79.071101, arXiv:0901.2775.

[563] S. Chatrchyan, et al., J. High Energy Phys. 02 (2012) 011, http://dx.doi.org/10.1007/JHEP02(2012)011, arXiv:1111.1557.

[564] G. Aad, et al., Nuclear Phys. B 850 (2011) 387–444, http://dx.doi.org/10.1016/j.nuclphysb.2011.05.015, arXiv:1104.3038.

[565] A.M. Sirunyan, et al., Phys. Lett. B 780 (2018) 251–272, http://dx.doi.org/10.1016/j.physletb.2018.02.033, arXiv:1710.11002.

[566] G. Aad, et al., Phys. Rev. D 87 (5) (2013) 052004, http://dx.doi.org/10.1103/PhysRevD.87.052004, arXiv:1211.7255.